Use of Advanced White Matter Imaging and Tractography Techniques in Neurosurgical, Neurological and Neuroanatomical Studies

Thesis submitted in accordance with the requirements of the University of Liverpool for the degree of Doctor in Medicine (Medical Imaging) by

Dr Kumar Abhinav BSc. (Hons), MBBS, FRCS (Neurosurgery)

27th January 2020

Table of Contents

Word count (abstract): 449

Word count (including references and excluding list of abbreviations, abstract, acknowledgements, appendix): 58,406. Total number of figures: 41 and tables: 14

List of Abbreviations

ADC: Apparent Diffusion Coefficient

AF: Arcuate Fasciculus

AFD: Apparent Fiber Density

ALS: Amyotrophic Lateral Sclerosis

CC: Corpus Callosum

CM: Cavernous Malformations

CN: Cranial Nerve

CSD: Constrained Spherical Deconvolution

CST: Corticospinal Tract

DSI: Diffusion Spectrum Imaging

DTI: Diffusion Tensor Imaging

FA: Fractional Anisotropy

fMRI: functional MRI

GBM: Glioblastoma Multiforme

GQI: Generalised Q-Sampling Imaging

HARDI: High Angular Resolution Diffusion Imaging

HD: Huntington's Disease

HDFT: High Definition Fiber Tractography

IOF: Inferior Occipito-Frontal Fasciculus

LMN: Lower Motor Neuron

MD: Mean Diffusivity

MdLF: Middle Longitudinal Fasciculus

MND: Motor Neurone Disease

mRS: modified Rankin Scale

ODF: Orientation Distribution Function

OR: Optic Radiation

PLS: Primary Lateral Sclerosis

QA: Quantitative Anisotropy

ROI: Regions Of Interest

ROA: Region Of Avoidance

SDF: Spin Distribution Function

SLF: Superior Longitudinal Fasciculus

SRS: Stereotactic Radiosurgery

TBSS: Tract-Based Spatial Statistics

TPC: Thalamopostcentral

UF: Uncinate Fasciculus

UMN: Upper Motor Neuron

VBA: Voxel-Based Analysis

WM: White Matter

Use of advanced white matter imaging and tractography techniques in neurosurgical, neurological and neuroanatomical studies

Kumar Abhinav

Abstract

Background: Neurological and neurosurgical applications of conventional approaches such as diffusion tensor imaging (DTI) have limitations due to the crossing fiber problem and susceptibility to partial volume effects. Advanced acquisition methods and analytical approaches have therefore, emerged.

Objectives: Using multiple studies, aims were to investigate the utility of advanced white matter imaging techniques [(High definition fiber tractography (HDFT)] and diffusion connectometry, where applicable in: a) qualitatively and quantitatively assessing the perilesional white matter tracts in neurosurgical patients with supra- and infratentorial cavernous malformations (CMs) and high grade gliomas; b) providing a prognostic quantitative marker like anisotropy values (including for defined perilesional *tract* segments) for characterising changes in the tract and predicting eventual postoperative clinical outcomes in patients with CMs; c) devising an imaging biomarker for Amyotrophic lateral sclerosis (ALS) and d) a neuroanatomical study on the depiction of cranial nerves (CNs). Use of DTI in evaluating the corticospinal tract (CST) and eventual clinical outcomes was assessed in patients with deep-seated CMs.

Methods: Imaging data was derived from healthy adults (n = 5) and patients with ALS (n = 5), CMs (n = 31; supra- and infratentorial) and brain tumours (n = 8). Atlas-based data including from the human connectome project was also used. Imaging analysis included reconstruction of diffusion spectrum imaging (DSI) data with generalised q-sampling imaging approach. Fiber tracking was performed with DSI studio with tractography using quantitative anisotropy (QA)-based generalised deterministic tracking algorithm and selection of regions of interest. Perilesional tracts were assessed qualitatively and quantitatively with the latter using mean QA values including in a novel fashion for the *perilesional* segment. Contralateral tracts were used for comparison. DTI-based tractography was also utilised in patients with

deep-seated CMs. Automated diffusion connectometry was used for studies involving patients with brainstem CMs and ALS.

Results and Conclusions: Qualitatively, HDFT could illustrate the precise spatial relationship of intracranial lesions like supra- and infratentorial CMs and high grade gliomas (including in oedematous zone) to multiple perilesional tracts in a 3-dimensional fashion, thereby optimising surgical planning by minimising injury to these tracts. Accurate tractography reconstruction of all CNs was achieved. CMs can displace and disrupt the perilesional white matter tracts with these changes supported by QA values thereby justifying the combined qualitative and quantitative approach. Observed anisotropy decreases in the perilesional segments were consistent with neural injury following haemorrhages as validated by postoperative imaging. FA values for the distal *ipsilateral CST segment* can be used for prognostication regarding postoperative functional outcomes for patients with deep CMs. Diffusion connectometry can provide longitudinal information on the CST integrity in patients with brainstem CMs and can also be used for devising imaging biomarker in ALS by identifying the affected tracts and associated patterns of progression.

Chapter 1. Introduction

1.1 Setting the scene

One of the great scientific challenges of the 21st century has been to advance our understanding of the structural-functional networks in the brain using non-invasive imaging techniques. A desire to understand these neural connections has been coupled with an eagerness to explore the nature of dysfunction occurring in these in neurological, neurosurgical, and psychiatric disorders.[1-3] White matter imaging has never been more topical, particularly in light of the recent studies aimed at developing new imaging techniques towards mapping human brain connectivity.[4-10] Nonetheless, accurate imaging of structural connectivity *in vivo* is challenging with most techniques having a limited resolution at a scale of millimeters (mm). Reliable characterisation of the connections at an axonal level requires better resolution, usually at a scale of micrometers (μm). Diffusion magnetic resonance imaging (MRI) detects microscopic changes in the diffusion pattern of water and reveals microstructural information regarding the human brain.

In this section of thesis, an overview of the most popular diffusion MRI modelling method, diffusion tensor imaging (DTI) is presented along with a discussion of its limitations. This is followed with a discussion of the methods beyond DTI, based on the contemporaneous literature search. The potential advantages of moving beyond DTI in clinical studies is discussed. In the ensuing chapters of the thesis (2-7), our preliminary experience and research work with the application of an advanced white matter imaging technique in neurosurgical, neurological and neuroanatomical studies is presented.[11-18] The individual chapters (2-7) resulting from the published manuscripts, aside from providing a general introduction, detail the specific aspects of the objectives, methods, results and conclusions as pertinent to the individual research study.[11-14,16,18,19]

1.2 Diffusion tensor imaging (DTI), applications, limitations and need for models beyond DTI

Diffusion MRI is an imaging modality, which utilises diffusion of water to characterise the structural connections in the brain at a microscopic level. The earliest work, conducted by Stejskal and Tanner[20] applied diffusion MR-sensitizing

gradients to measure diffusion coefficient and investigated structures at a microscopic level. This basic diffusion sequence then fuelled the development of diffusion MRI, further diffusion modelling methods and ultimately *in-vivo* fiber tracking and tractography using DTI. DTI[21] is a diffusion MRI analysis method, which models diffusion pattern as a Gaussian distribution.[22] The tensor model requires at least six diffusion gradient samplings to calculate the diffusion tensor. The axonal direction can be determined by the principal direction of the tensor. Based on this principal direction, the trajectories of the axonal connections can be revealed by diffusion fiber tracking. This computational approach demonstrates the axonal connections between the cortical areas.[23,24] The tensor model however cannot demonstrate the crossing fibers, and therefore, DTI-based tractography may suffer with false connections or terminations. Although DTI has been widely used in multiple studies, its major limitations have been well described. These include its inability to represent the crossing of multiple fibers[25-27] or to determine with precision their cortical and subcortical terminations.[28-31]

In addition to demonstrating axonal connections and qualitative tractography data, DTI also offers several quantitative indices to characterise the axonal integrity. These include fractional anisotropy (FA) and diffusivities,[32,33] both of which have been applied in clinical studies. FA is one of the most commonly used DTI-based quantitative measure of anisotropy[34,35] and has been applied in the evaluation of white matter integrity in multiple disease states including multiple sclerosis,[36] stroke,[37] amyotrophic lateral sclerosis (ALS),[38-40] cavernous malformations (CMs)[41] and brain tumours.[42,43] It has been suggested that the changes in FA may reflect changes in the organisation of fibers[44] with a reduction reflecting axonal fiber degeneration and myelin breakdown in the central and peripheral nervous systems.[45,46] Studies have shown that the indices derived from DTI can be affected by field strength;[47] b-value;[48] number of gradient directions; spatial resolution;[35] partial volume effect;[27,29,49,50] head motion,[51] and the crossing fiber configuration.[25,26] This can lead to the underestimation of the anisotropic values in areas with multiple crossing fibers.[27,35] Such limitations associated with DTI are accentuated in cases of clinical applications. A cerebral tumour, for example may be present with surrounding oedema and mass effect[27,43,52] with associated potential thinning of the tracts, all of which may contribute further to the partial volume effects and

misinterpretation of the data. Other DTI-derived measures include radial diffusivity, which has been shown to increase with demyelination.[53] A decrease in apparent diffusion coefficient (ADC) is correlated with the increased cellularity of brain tumours.[54,55] ADC derived from DTI, however cannot differentiate vasogenic oedema or define tumour infiltration.[56,57] Although DTI can reveal some characteristics of the white matter pathways and provide qualitative tractography data, its use as a *gold standard* diagnostic tool has been limited. One problem with DTI relates to the diffusivity being overestimated or underestimated, when axonal injury occurs with cell infiltration.[58] This therefore, limits its application in neurological conditions. To overcome the limitations of DTI-based fiber tractography and its derived indices, studies have used more complex models to resolve the crossing fibers and quantify diffusion characteristics. These endeavours have led to the development of methods beyond DTI.

1.3 Beyond DTI: technical details underpinning the advanced white matter imaging techniques

1.3.1 Literature search

PubMed was searched using keywords such as “tractography” or “fiber tracking” with search being limited to last five years. A total of 1838 papers were identified, of which studies using conventional DTI-based fiber tracking approach, resulting in 735 papers. The abstract of these papers were then scrutinised to select publications demonstrating clinical application. Methodology, engineering, and review papers were excluded. These further criteria resulted in the inclusion of 84 clinical research publications. These papers were then extensively reviewed to document their fiber resolving methods, tracking algorithms, and analytical approaches. In summary, the ball-and-stick model was the most popular method for resolving crossing fibers (57%). Diffusion spectrum imaging (DSI) was the next most popular method (15%) followed by constrained spherical deconvolution (CSD) (11%). For fiber tracking, 64% of the studies used probabilistic fiber tracking, whereas 36% used deterministic fiber tracking. The analysis was done in the majority using tract-specific analysis (58%) followed by connectivity approach (31%) and pathway visualisation (14%).

These advanced algorithms are discussed in more detail below to provide further background.

1.3.2 Fiber resolving methods

The fiber resolving methods can be categorized into the model-based and model-free methods. The analytical approaches can be categorized into voxel-based analysis (VBA); tract-specific analysis; connectivity analysis; pathway visualisation; and tract morphology analysis. It is noteworthy that a particular study may use different combinations of fiber resolving methods tracking algorithms, and analytical approaches. In the following sections, these methods using in different clinical studies are discussed.

1.3.2.1 Model-based methods

Several new diffusion methods (model-based and model-free) have been proposed to overcome the limitations of DTI. The model-based approaches use a model to describe the diffusion pattern. The parameters for these models are calculated using numerical optimisation. For example, the most popular method beyond DTI is the ball-and-sticks model.[59] The ball-and-stick model is a specific form of multiple tensors that models free diffusion (ball) and axons (sticks). The CHARM model[60] describes the diffusion pattern using a composite diffusion model.[61] Diffusion kurtosis imaging[62] models the non-Gaussian characteristics of diffusion and provides information on the pathological conditions.[63-66] Diffusion basis spectrum imaging[58] separates the effects of vasogenic oedema, cell infiltration, and axonal injury. It further provides information about the cell and fiber ratios; local oedema; and density distribution of the axonal fibers. Spherical deconvolution[67] obtains fiber orientation distribution by calibrating the signal profile of a single fiber as the model and deconvoluting the MR signals to obtain the orientation distribution. Further improvements can be achieved by CSD,[68] deconvolution with reduced background effect;[69] diffusion deconvolution;[70] and compressed sensing related estimations.[71,72] The fiber distribution obtained from the deconvolution can depict the local axonal connections and assist further fiber tracking (Figure 1). The main advantage of the model-based methods is the requirement for a fewer number of diffusion sampling

directions, thereby leading to a substantial reduction of the scanning time. The principal drawback relates to the diffusion model depending upon certain assumptions to obtain an accurate parameter.

1.3.2.2 Model-free methods

Instead of assuming a diffusion model, another emerging interest relates to the model-free approaches, which obtain empirical distribution of water diffusion by exhaustive sampling. The model-free methods use a distribution function to model the diffusion distribution. For example, q-space imaging[73] is used to estimate the ensemble *average propagator*, which is the distribution of spin displacement. To resolve the axonal direction from an average propagator, DSI[74] further integrates the radial distribution of an average propagator and calculates the orientation distribution function (ODF). This approach discards the radial information and focuses on the orientation information. The peak orientations on the ODF can be used as the fiber orientation for further fiber tracking.[75] As ODF does not contain information on the radial directions, the calculation of ODF does not necessarily require exhaustive sampling. Only the signal responses at different orientations are needed to calculate the ODF. This idea leads to the high angular resolution diffusion imaging (HARDI).[26] HARDI is a sampling strategy that acquires diffusion images using the same diffusion gradient strength. This is in contrast to the q-space imaging, which requires sampling on both different gradient strengths and directions. The simplified sampling scheme improves the feasibility of acquisition of the diffusion data. Diffusion ODF can be reconstructed from HARDI using q-ball imaging.[76,77] Despite this improvement, it is noteworthy that discarding radial information forfeits the rich information characterising the tissue structure. A more flexible approach is to allow a method to make use of the radial information while offering the orientation information. This is enabled by generalised Q-sampling imaging (GQI),[78] which offers a length parameter to switch the focus between restricted diffusion and none restricted one. GQI has been shown to improve the quality of demonstration of the crossing fibers[70,72,79] and assist diffusion MRI-based fiber tracking.[80]

1.3.3 Deterministic and probabilistic fiber tracking

Both model-based and model-free methods can provide the local fiber orientations within a voxel. The deterministic fiber tracking algorithm makes use of the local fiber orientations to delineate the whole trajectory. It starts from a seeding point and propagates along the fiber orientation until the termination criteria are met. Examples of this approach include the fiber assignment continuous tracking method[24] and streamline fiber tracking algorithm.[81] Both of these assume a single fiber orientation per voxel. With high angular resolution data, multiple fiber orientations can be resolved per voxel (Figure 2). Further, a multiple-fiber version of deterministic fiber tracking has been proposed to describe the complex connections of the fibers' geometry.[75,80,82] Despite this improvement, one major limitation in deterministic fiber tracking is the crossing-branching problem.[83] Deterministic fiber tracking prefers trajectories with less turning, thereby potentially missing the minor branches. One study showed that the percentages of false connections can range from 7% to 35%.[80] Identification of these false connections is an active research question. As opposed to deterministic fiber tracking, probabilistic fiber tracking was proposed to explore the *connection probability*. Although there are numerous versions of probabilistic fiber tracking algorithms, the probabilistic tracking routine from the FSL package is the one most commonly used.[59] In general, probabilistic fiber tracking utilises the probabilistic distribution of fiber orientations to obtain a set of trajectories connecting to a voxel. The number of fibers connecting to a voxel can be used as an index to reveal the differences in connectivity.

1.3.4 Analytical approaches

1.3.4.1 Voxel-based analysis

The diffusion indices can be analysed at the voxel level. The regions of interest (ROI) can be manually selected by experts, and the indices within the region can then be used to compute group differences. The result however, may be subjective and not easily reproducible. A more objective approach is to use the analysis paradigm of

voxel-based analysis (VBA). The mapping of the diffusion indices (for example, FA) is normalized to a stereotaxic space and statistical tests are applied to examine the significance of the group-wise differences. One should note that the transformation of direction-independent quantities such as FA and MD are straightforward. It does not require additional correction with respect to the directional information. This makes group-wise comparisons feasible with VBA. Reproducibility of this technique however, has been questioned due to the controversial effect related to the filter size.[84] The voxel-based approach further does not provide information with respect to the fiber orientations (directions), and cannot handle diffusion quantities of the crossing fibers.

1.3.4.2 Tract-specific analysis

Tract-specific analysis utilises fiber trajectories from the fiber tracking to sample the diffusion indices.[85-87] The combination of tract-specific analysis and DSI extends the analysis to regions with crossing fibers.[88,89] Although the tract-specific approach can handle the problem of crossing fibers, it is reliant upon an accurate fiber tracking method to carry out a trustworthy analysis. Due to the limitation of the crossing-branching pattern, the fiber tracking algorithm may give rise to false connections. It further has reproducibility issues, as the results are not perfectly objective. Although this analytical approach can target a specific fiber pathway and analyse its integrity, it is reliant upon the user expertise in terms of selection of ROIs and segmentation of the obtained tracts. These therefore, lead to reproducibility issues, particularly when multiple users are involved.[90-93]

1.3.4.3 Skeleton-based approach

Spatial transformation has been widely used in analysing the structural characteristics of the human brain. Its use with the diffusion data however, is much more challenging as the transformation needs to consider the rotations of the axonal directions.[94] In DTI, the spatial transformation can be handled by a Jacobian matrix to correct the rotation problem.[94,95] The spatial transformation of HARDI can also be

similarly corrected.[96] The spatial transformation for q-space imaging however, needs to consider the scaling effect at the radial direction. Another DTI-related analytical technique, tract-based spatial statistics (TBSS),[97] utilizes a mean FA skeleton. By projecting the diffusion indices to the skeleton, TBSS avoids the drawbacks of VBA, such as the smoothing and alignment issues. This enables localized statistical analysis in a stereotaxic space.[98] TBSS however, cannot reliably estimate and interpret the voxel-wise statistics at the crossing regions of fibers due to the inherent limitations associated with DTI. A recent improvement on TBSS has attempted to overcome this limitation by using the ball-and-stick model. Nonetheless, the skeleton used in TBSS assumes a single fiber orientation per voxel and does not make use of the information from the crossing fibers.

A solution to this problem is *diffusion MRI connectometry*,[99] an analytical method that uses a multiple fiber skeleton (multiple fiber orientations per voxel) to sample the diffusion quantities on ODFs. Connectometry obtains statistical validation of fiber pathways with deviant ODF quantities. Instead of mapping the entire pathway before studying their differences, connectometry initially maps the difference at each fiber orientation in a voxel. It then connects the differences using fiber tracking to reveal the entire affected pathway (Figure 3). The sampled ODF values from a normal population are used to construct a *norm*, which can then be used to test the deviant cases. Importantly, the affected tracts are revealed with information regarding the sensitivity and specificity of the findings. The specificity of the results can be controlled using the false discovery rate. The application of this methodology is demonstrated with respect to the brainstem CMs and ALS in Chapters 3 and 5 respectively.

1.4. Applications of advanced white matter imaging technique in neurosurgical and neurodegenerative disorders and neuroanatomical studies

Here, along with the pertinent literature from conventional DTI-based approaches, an account of our indicative examples of use of the advanced algorithm in neurosurgical, neurological and neuroanatomical studies is presented thereby providing further introduction to the topic. The subsequent chapters and published manuscripts explore this is much greater depth and detail.[11-15,17,18,100]

1.4.1 Applications in neurosurgical conditions (Chapters 2-4,6,7)

One of the key advantages of using advanced white matter imaging[101] had been the ability to obtain superior qualitative data in terms of depiction of multiple perilesional tracts in a three dimensional fashion around mass lesions like CMs and tumours. This greatly assisted with accurate surgical planning. The first such research study as part of the current body of the research work (Chapter 2)[12] assessed the relationship specifically of supratentorial CMs to the relevant perilesional white matter tracts. We attempted to characterise the associated changes both qualitatively (in terms of displacement or disruption) and quantitatively, using mean anisotropy index (derived from ODF). This was done both for the overall affected white matter tracts and for the specific perilesional segments in a *novel* fashion. Supratentorial CMs represented an ideal model for assessing the usefulness of an advanced white matter imaging technique in investigating perilesional tracts. By definition, CMs, within their core do not possess any intervening brain parenchyma and therefore, white matter. Use of the more conventional DTI in brainstem CMs' resection, which are surgically challenging with a higher annual average symptomatic haemorrhage rate of 2.7% to 5%[102-104] had been reported.[105-109] Only isolated case reports had described the utility of DTI with supratentorial CMs.[110,111] In our series, we demonstrated the utility of GQI-based tractography (Chapter 2) in illustrating the precise spatial relationship of CMs to multiple perilesional white matter tracts in a three dimensional fashion (Figure 4). This was helpful for surgical planning and for demonstrating associated disruption and/or displacement, both of which occurred perilesionally.[12] These changes were supported by the anisotropy index (an indirect marker of fiber integrity and organisation like FA in DTI) with the perilesional values being lower compared to the contralateral homologous segment for disruption. The reverse was true for displacement. These advantages can be demonstrated (Figure 4) using a case example of a 66-year-old right handed female with a symptomatic 10mm left parietal lobe haemorrhagic CM.[12] Due to the lesion's proximity to the sensory cortex and its potential effect on the arcuate fasciculus (AF), perilesional white matter tracts were evaluated preoperatively. Perilesionally, tractography demonstrated posterior displacement of the AF (with the lateral margin being free of these fibers); anteromedial displacement of the thalamopostcentral; and

an unaffected corticospinal tract (CST) (Figure 4). Using information from the fiber tractography, she underwent an image-guided surgical approach through the post-central sulcus for lesionectomy without any postoperative neurological deficit. Following this study, the use of advanced imaging algorithm both in a qualitative and quantitative fashion including diffusion connectometry was further explored in the brainstem CMs (Chapter 3).[16] Quantitative indices were specifically examined in an effort towards devising prognostic markers.

Limitation of DTI with respect to discerning multiple perilesional tracts is usually accentuated in the presence of a space occupying mass with its associated oedema. There is increasing emerging data regarding the utility of advanced white matter imaging techniques in mass lesions.[112-114] A study[112] evaluated the differences between GQI and DTI in the preoperative mapping of fiber tractography in peritumoral oedema of cerebral tumours. Five patients underwent 3-T MRI scans with subsequent reconstruction of the tracts using both GQI and DTI. GQI-based tractography was able to fully display the intact fibers in the oedematous zone in comparison with DTI. These tracts were found to be incomplete, missing or ruptured with DTI. Although conventional neurosurgical wisdom does not permit the resection of the oedematous zone around the cerebral neoplasms, demonstration of the fiber tracts in that zone in their correct orientation will aid surgical trajectory planning and potential tract preservation. The advantage of using advanced algorithms can be particularly demonstrated for high grade gliomas with significant associated peritumoral oedema and in close proximity to the reconstructed fiber tracts. This led to further research work as part of the current body of work whereby the application of advanced white matter imaging techniques in patients with cerebral tumours was directed towards accurately reconstructing the perilesional tracts in their anatomical entirety in the surrounding oedematous zones (Chapter 6).[14]

Despite its limitations, DTI has been an important adjunct in the resection of intracranial mass lesions including tumours,[43,115] and CMs[106,107,109] and has been widely used in clinical and research studies. Further, the short image acquisition time for DTI makes it more clinically accessible. In the current body of research work in the thesis, utility of a quantitative approach (Chapter 4) using DTI for prognostication regarding motor and functional outcomes in patients with surgically resected deep intracranial CMs was investigated.[11]

1.4.2 Application in Neurodegenerative disorders

1.4.2.1 Amyotrophic lateral sclerosis (Chapter 5)

ALS is a neurodegenerative disorder, marked by progressive failure of both upper (UMN) and lower motor neurons (LMN). LMN symptoms in ALS obscure the UMN symptoms and therefore, contribute at least partly to the potential delay in the diagnosis and subsequent treatment. Although the diagnosis of ALS is based on clinical examination and electrophysiological studies among others,[116] an imaging biomarker is potentially useful for monitoring *pathological* progression and for evaluating efficacy of treatments in future trials. Previous studies in ALS, using DTI had shown that white matter pathology, predominantly in the motor pathways, can be detected and potentially tracked longitudinally over time. This makes white matter pathology a candidate as an outcome measure for future trials. Multiple DTI[38-40,117-120] studies in ALS had therefore been carried out to investigate the involvement of the white matter tracts. The white matter pathology had been examined for potential correlation with clinical markers of progression like the revised ALS functional rating scale.[116,121] These studies relied on the DTI-based indices like FA or ADC for quantification of the observed changes in the integrity of white matter tracts, for example CST or corpus callosum. In general, these studies demonstrated a reduction in the values of FA, when compared with controls or when monitored in a longitudinal fashion[118,120,122,123] over time along the CST. These changes therefore, indirectly demonstrated the disease progression in ALS. Another noteworthy point in ALS with respect to monitoring white matter disease, is the presence of extramotoric changes. These changes have been demonstrated in multiple studies, notably so in the corpus callosum,[124] cingulum and hippocampal formation,[125] and cerebellum.[122] A previous pathological study in ALS[126] based on post-mortem examination had shown evidence of degenerating fibers in the pre-central gyrus (and CST); post-central gyrus; the adjacent frontal and parietal gyri; corpus callosum; and basal ganglia. Overall these changes suggested a multisystem neurodegenerative process, which so far using the DTI and VBA in a complementary fashion, have been elucidated to varying extents.[40,123,127,128] Although these studies have been promising in demonstrating the white matter changes in ALS, use of DTI and its associated

quantitative indices is limited as a quantitative marker in ALS. This is related to the DTI-based quantitative indices suffering with partial volume effects.[27,35] Other limitations pertinent to all tractography-based studies are also applicable including the inherent variability, particularly between observers. These are due to issues related to the ROIs chosen and the manual nature of the analysis. Changes in the imaging data in terms of the signal to noise ratio across multiple scans, is another issue affecting reproducibility.

Building upon the findings from DTI studies, our study as detailed in Chapter 5, adopted a two-step approach to evaluating white matter disease in a longitudinal fashion in ALS patients in relation to markers of clinical progression.[13] The first *primary* step involved an adaptation of the diffusion connectometry[129] analysis to identify the affected white matter tracts followed by a detailed 'tractography' approach towards the quantitative evaluation of these identified abnormal fiber pathways. This approach was tailored to test both ‘individual’ and ‘group’ data against a control population. In line with the current literature, our study[13] identified the involvement of both motoric and extramotoric white matter pathways with an illustrative example depicted in Figure 5.

1.4.2.2 Huntington's disease

Previous studies (PREDICT-HD and TRACK-HD) in Huntington’s disease (HD) patients have shown that white matter pathology can be tracked longitudinally and reliably over 12 to 24 month periods. As the white matter pathology correlates with some clinical characteristics, it is potentially a strong candidate as an outcome measure for future clinical trials.[130] DTI among other MR techniques has been previously employed in the demonstration of white matter pathology in premanifest and symptomatic HD.[131-133] The primary aim in HD has been to use DTI to develop an imaging biomarker for disease progression rather than as a diagnostic tool. Premanifest HD in this respect is of particular importance, as a reproducible marker of disease (pathological) progression in terms of an imaging biomarker will be invaluable in this group. This is related to the fact that this group has limited markers of clinical and imaging progression (as seen on standard MRI). In future, this

imaging biomarker may be used to evaluate the efficacy of novel treatments. There is further emerging evidence regarding early extrastriatal involvement in HD, including in premanifest disease,[134,135] and its correlation with measures of clinical progression.[136,137] White matter projections including corticostriatal projections, cingulum and uncinate fasciculus (UF) have been implicated in the pathophysiology of HD.[134] Other tracts of interest include corticostriatal projections [dorsolateral prefrontal cortex (DLPFC) and orbitofrontal cortex to striatum]; thalamocortical projections; callosal fibers; CST; inferior occipito-frontal fasciculus (IOF); and thalamopostcentral fibers. These can be difficult to reconstruct reliably using DTI-based tractography. These are currently being investigated in the premanifest and the manifest HD patients in a longitudinal fashion using both DTI and advanced white matter imaging techniques.

Based on the current literature largely derived from DTI and structural MRI studies, changes in the white matter seem to be present before the clinical manifestation of motor symptoms in gene-positive premanifest HD patients. With the use of advanced white matter imaging techniques, these can be evaluated over time. An example of this approach is the evaluation of quantitative parameters such as percentage changes in anisotropy and volumes for fiber tracts of interest over longitudinal scans. Changes in these parameters over longitudinal scans will indirectly track pathological progression. Similarly, tract-specific qualitative and quantitative data can be expected to deteriorate with clinical progression in early manifest HD (as defined by total functional capacity (TFC $\geq$8) and potentially correlate with measures of clinical progression. In light of this evidence, the current focus of the research community is therefore, on the longitudinal scanning of premanifest and early manifest HD patients. Cortical changes[135] including thinning in the premanifest and manifest groups, are also an additional area of evaluation with potential different patterns of cortical changes possibly providing explanations for the widespread clinical heterogeneity in HD. Possible correlation between areas of cortical thinning and white matter changes can be expected. This is based on the assumption that the anatomy of white matter degeneration should correspond to the regions of cortical gray matter atrophy.

An example of use of the advanced white matter imaging technique in HD is provided using a patient (age: 41; CAG: 42) at the premanifest stage (Figure 6), who underwent two scans six months apart. During this scan interval, the score on behavioural assessment increased from 9 to 13. There were quantitative reductions (volume and anisotropy) in multiple fiber tracts of interest bilaterally for this patient including in the genu and splenium of corpus callosum. In terms of demonstrated tracts (Figure 6), the percentage reductions in the anisotropy values were: left side [DLPFC to striatum (14.8%); CST (18%)] and right side [DLPFC to striatum (16.6%); CST (14.5%)]. Despite a decrease in the corticostriatal projections, there was no corresponding decrease in the striatal or extrastriatal subcortical nuclei volumes, as measured using the Freesurfer analysis. Although the behavioural scores changed over the scan duration, there was no evidence of motor symptoms or change in the motor scores despite a quantitative decrease in the CST bilaterally. Our experience with HD is preliminary and there are ongoing studies involving this cohort of patients however, advanced white matter imaging in conjunction with other MR-based analytical techniques, seems to be a promising tool for development as an imaging biomarker in HD.

1.4.3 Neuroanatomical studies (Chapters 6,7)

Several neuroanatomical studies, including on CST; corticostriatal projections; arcuate; MdLF; and claustrum have been facilitated with the help of GQI-based tractography.[19,79,138-140] GQI-based tractography has been found to be useful in terms of demonstrating the fiber tracts reliably along their anatomical course with accurate cortical end points.[101] The findings from the GQI-based tractography have been consistent with the neuroanatomical knowledge. With limitations associated with all tractography techniques, dissection of the white matter tracts has been immensely valuable in validating these findings and the neuroanatomical features.

All of the presented research studies in the current thesis emphasise the fact that all tractography techniques and the findings require sound neuroanatomical knowledge and validation (Chapter 2-7). Contemporary neuroanatomical studies require combination of use of imaging algorithms with cadaveric dissections for neuroanatomical validation. Previous use of advanced imaging algorithm in a

neuroanatomical structure can be demonstrated using Claustrum, which has been studied via cadaveric fiber dissection, an advanced white matter imaging technique[19] and previously with DTI. Connectivity features and the structural significance of the claustrum have been postulated to relate to consciousness; however its exact role is unknown.[141] Based on the anatomical studies, the claustrum[19] is divided into two parts: the dorsal claustrum (also referred to as compact[142,143] or insular claustrum[144-146]) and the ventral claustrum (also named fragmented,[142,143] prepiriform, amygdalar, or temporal claustrum[145,146]). The dorsal claustrum is a continuous irregular lamina of gray matter lying between the putamen (from which it is separated by the external capsule) and the insular cortex (from which it is separated by the extreme capsule) (Figure 7). The ventral claustrum consists of a group of diffuse or island-like gray masses fragmented by the UF and the IOF (Figure 7). White matter anatomy of the claustrum has been studied using the fiber microsurgical dissection technique (the Klinger technique) in the post-mortem human brains.[147] The gray matter of the short and long insular gyri is carefully removed to expose the extreme capsule and the claustrum. After removal of the dorsal extreme capsule, the fibers of the dorsal external capsule are seen to converge into and merge with the gray matter of the dorsal claustrum, forming a characteristic spoke-and-wheel pattern with its centre at the dorsal claustrum (Figure 7). The fibers of the UF (connecting orbital-frontal cortex with the medial temporal lobe and temporal pole) and IOF (connecting prefrontal to the parieto-occipital regions) traverse the most anterior and inferior parts of the claustrum to create the gray matter islands that form the ventral claustrum. Based on fiber dissection studies, the so-called dorsal external capsule seems to be mainly composed of the claustro-cortical projection system. This projection system interconnects the claustrum with multiple cortical areas. The conventional "static" conceptualization of the external capsule is therefore, replaced with a more dynamic view of the external capsule or the claustro-cortical system.[147,148] One DTI study reported on the claustro-cortical projection system in the human brain.[147] This demonstrated that the external capsule was composed of multiple fiber bundles originating from different regions and converging in the area of the dorsal claustrum. This led to the conclusion that the dorsal external capsule was mainly composed of the projection and not association fibers. Although the findings from this DTI study were exciting, the claustro-cortical fibers were not seen to be truly ending in the claustrum. These fibers were instead converging on the

claustrum with evidence of false continuation in between the fiber tracts at the level of the claustrum. With advanced white matter imaging, connectivity features of the claustrum have been demonstrated in better detail including the representation of its endpoint projection pattern onto the cerebral cortex.[19] The claustrum fiber bundles show a ribbon-like pattern, highly resembling the fiber microdissection findings (Figure 7).[19] The claustro-cortical fibers terminate at the level of the dorsal claustrum. Further analysis of the cortical terminations of the claustro-cortical fibers reveal connections with the superior and rostral middle frontal gyrus; pre-motor; primary motor; somatosensory; and posterior parietal cortex areas supporting its role in multi-model integration of the sensory and motor information.

Pertinent to the body of research work presented in this thesis, the previous successful use of advanced white matter imaging techniques in neuroanatomical studies underpins its use in all studies including in the neurosurgical and neurological conditions (Chapters 2-6). Supplementary figures in Chapter 6 showing side by side images of those derived from neuroanatomical dissection studies and tractography demonstrate the use of this technique further in neuroanatomical studies and the relevance to the surgery of brain tumours and in particular, high grade gliomas.[14]

The focus in Chapter 7 on cranial nerves is almost entirely neuroanatomical. At a preliminary level, the use of advanced imaging algorithm in the depiction of the anatomical course of cranial nerves in healthy subjects followed by its application in a select few clinical surgical cases with brain tumours is demonstrated (Chapter 7).[18] Conventional DTI has been applied to track cranial nerves with limited angular resolution. DTI tractography is unable to depict the intra-brainstem portions of these nerves. The susceptibility artifacts and partial volume averaging of complex fiber architecture with DTI further leads to poor tracking of cranial nerves. HDFT, in comparison with DTI was therefore, hypothesised to provide better localisation of cranial nerves by accurately solving and reproducing multiple crossing fibers within the brainstem. The cisternal portion of most cranial nerves were successfully tracked and visualised in each healthy subject and in atlas fiber tracking. The attempt at using the tractography to delineate cranial nerves in normal subjects and cases with brain tumours is undertaken future implications for surgical approach planning such that injury to cranial nerves during operative procedures can be minimised. From an

anatomical perspective, traditionally difficult to depict fiber bundles including the entire optic radiation, medial longitudinal fasciculus, spinal trigeminal nucleus/tract, petroclival portion of the abducens nerve, and the intra-brainstem portion of the facial nerve from the root exit zone to adjacent abducens nucleus are demonstrated and discussed in further detail in Chapter 7.

Having presented the technological advances leading up to the development of DTI and general background for the advanced techniques aimed at imaging the white matter including the rationale for using the latter technique, the subsequent chapters of the thesis will present the research findings acquired during the course of the study predominantly using the advanced white matter imaging algorithm (Chapters 2,3,5-7) and DTI (Chapter 4) and as pertinent to supratentorial CMs (Chapter 2), infratentorial and deep seated CMs (Chapters 3, 4), ALS (Chapter 5), brain tumours (Chapter 6) and cranial nerves (Chapter 7).

1.5 References

1. Akil H, Brenner S, Kandel E, et al. Medicine. The future of psychiatric research: genomes and neural circuits. *Science.* 2010;327(5973):1580-1581.
2. Akil H, Martone ME, Van Essen DC. Challenges and opportunities in mining neuroscience data. *Science.* 2011;331(6018):708-712.
3. DeFelipe J. From the connectome to the synaptome: an epic love story. *Science.* 2010;330(6008):1198-1201.
4. Williams R. The human connectome: just another 'ome? *Lancet Neurol.* 2010;9(3):238-239.
5. Van Essen DC, Ugurbil K, Auerbach E, et al. The Human Connectome Project: a data acquisition perspective. *Neuroimage.* 2012;62(4):2222-2231.
6. Van Essen DC, Ugurbil K. The future of the human connectome. *Neuroimage.* 2012;62(2):1299-1310.
7. Toga AW, Clark KA, Thompson PM, Shattuck DW, Van Horn JD. Mapping the human connectome. *Neurosurgery.* 2012;71(1):1-5.
8. Wedeen VJ, Rosene DL, Wang R, et al. The geometric structure of the brain fiber pathways. *Science.* 2012;335(6076):1628-1634.

9. Behrens TE, Johansen-Berg H, Woolrich MW, et al. Non-invasive mapping of connections between human thalamus and cortex using diffusion imaging. *Nat Neurosci.* 2003;6(7):750-757.
10. Craddock RC, Jbabdi S, Yan CG, et al. Imaging human connectomes at the macroscale. *Nat Methods.* 2013;10(6):524-539.
11. Abhinav K, Nielsen TH, Singh R, et al. Utility of a Quantitative Approach Using Diffusion Tensor Imaging for Prognostication Regarding Motor and Functional Outcomes in Patients With Surgically Resected Deep Intracranial Cavernous Malformations. *Neurosurgery.* 2019.
12. Abhinav K, Pathak S, Richardson RM, et al. Application of high-definition fiber tractography in the management of supratentorial cavernous malformations: a combined qualitative and quantitative approach. *Neurosurgery.* 2014;74(6):668-681.
13. Abhinav K, Yeh FC, El-Dokla A, et al. Use of diffusion spectrum imaging in preliminary longitudinal evaluation of amyotrophic lateral sclerosis: development of an imaging biomarker. *Frontiers in human neuroscience.* 2014;8:270.
14. Abhinav K, Yeh FC, Mansouri A, Zadeh G, Fernandez-Miranda JC. High-definition fiber tractography for the evaluation of perilesional white matter tracts in high-grade glioma surgery. *Neuro Oncol.* 2015;17(9):1199-1209.
15. Abhinav K, Yeh FC, Pathak S, et al. Advanced diffusion MRI fiber tracking in neurosurgical and neurodegenerative disorders and neuroanatomical studies: A review. *Biochim Biophys Acta.* 2014;1842(11):2286-2297.
16. Faraji AH, Abhinav K, Jarbo K, et al. Longitudinal evaluation of corticospinal tract in patients with resected brainstem cavernous malformations using high-definition fiber tractography and diffusion connectometry analysis: preliminary experience. *Journal of neurosurgery.* 2015;123(5):1133-1144.
17. Panesar SS, Abhinav K, Yeh FC, Jacquesson T, Collins M, Fernandez-Miranda J. Tractography for Surgical Neuro-Oncology Planning: Towards a Gold Standard. *Neurotherapeutics.* 2019;16(1):36-51.
18. Yoshino M, Abhinav K, Yeh FC, et al. Visualization of Cranial Nerves Using High-Definition Fiber Tractography. *Neurosurgery.* 2016;79(1):146-165.

19. Pathak S. F-MJC. *Structural and functional connectivity of the claustrum in the human brain.* 1st ed: Academic press; 2013.
20. Stejskal EO, Tanner JE. Spin Diffusion Measurements: Spin Echoes in the Presence of a Time-Dependent Field Gradient. *The Journal of Chemical Physics.* 1965;42(1):288-292.
21. Basser PJ, Mattiello J, LeBihan D. Estimation of the effective self-diffusion tensor from the NMR spin echo. *J Magn Reson B.* 1994;103(3):247-254.
22. Basser PJ. Relationships between diffusion tensor and q-space MRI. *Magn Reson Med.* 2002;47(2):392-397.
23. Conturo TE, Lori NF, Cull TS, et al. Tracking neuronal fiber pathways in the living human brain. *Proc Natl Acad Sci U S A.* 1999;96(18):10422-10427.
24. Mori S, Crain BJ, Chacko VP, van Zijl PC. Three-dimensional tracking of axonal projections in the brain by magnetic resonance imaging. *Ann Neurol.* 1999;45(2):265-269.
25. Jbabdi S, Behrens TE, Smith SM. Crossing fibres in tract-based spatial statistics. *Neuroimage.* 2010;49(1):249-256.
26. Tuch DS, Reese TG, Wiegell MR, Makris N, Belliveau JW, Wedeen VJ. High angular resolution diffusion imaging reveals intravoxel white matter fiber heterogeneity. *Magn Reson Med.* 2002;48(4):577-582.
27. Alexander AL, Hasan KM, Lazar M, Tsuruda JS, Parker DL. Analysis of partial volume effects in diffusion-tensor MRI. *Magn Reson Med.* 2001;45(5):770-780.
28. Chung HW, Chou MC, Chen CY. Principles and limitations of computational algorithms in clinical diffusion tensor MR tractography. *AJNR Am J Neuroradiol.* 2011;32(1):3-13.
29. Pasternak O, Sochen N, Gur Y, Intrator N, Assaf Y. Free water elimination and mapping from diffusion MRI. *Magn Reson Med.* 2009;62(3):717-730.
30. Liu C, Bammer R, Acar B, Moseley ME. Characterising non-Gaussian diffusion by using generalised diffusion tensors. *Magn Reson Med.* 2004;51(5):924-937.
31. Alexander DC, Barker GJ, Arridge SR. Detection and modeling of non-Gaussian apparent diffusion coefficient profiles in human brain data. *Magn Reson Med.* 2002;48(2):331-340.

32. Pierpaoli C, Basser PJ. Toward a quantitative assessment of diffusion anisotropy. *Magn Reson Med.* 1996;36(6):893-906.
33. Pierpaoli C, Jezzard P, Basser PJ, Barnett A, Di Chiro G. Diffusion tensor MR imaging of the human brain. *Radiology.* 1996;201(3):637-648.
34. Basser PJ, Pierpaoli C. Microstructural and physiological features of tissues elucidated by quantitative-diffusion-tensor MRI. *J Magn Reson B.* 1996;111(3):209-219.
35. Oouchi H, Yamada K, Sakai K, et al. Diffusion anisotropy measurement of brain white matter is affected by voxel size: underestimation occurs in areas with crossing fibers. *AJNR Am J Neuroradiol.* 2007;28(6):1102-1106.
36. Guo AC, MacFall JR, Provenzale JM. Multiple sclerosis: diffusion tensor MR imaging for evaluation of normal-appearing white matter. *Radiology.* 2002;222(3):729-736.
37. Thomalla G, Glauche V, Koch MA, Beaulieu C, Weiller C, Rother J. Diffusion tensor imaging detects early Wallerian degeneration of the pyramidal tract after ischemic stroke. *Neuroimage.* 2004;22(4):1767-1774.
38. Sach M, Winkler G, Glauche V, et al. Diffusion tensor MRI of early upper motor neuron involvement in amyotrophic lateral sclerosis. *Brain : a journal of neurology.* 2004;127(Pt 2):340-350.
39. Iwata NK, Kwan JY, Danielian LE, et al. White matter alterations differ in primary lateral sclerosis and amyotrophic lateral sclerosis. *Brain : a journal of neurology.* 2011;134(Pt 9):2642-2655.
40. van der Graaff MM, Sage CA, Caan MW, et al. Upper and extra-motoneuron involvement in early motoneuron disease: a diffusion tensor imaging study. *Brain : a journal of neurology.* 2011;134(Pt 4):1211-1228.
41. Cauley KA, Andrews T, Gonyea JV, Filippi CG. Magnetic resonance diffusion tensor imaging and tractography of intracranial cavernous malformations: preliminary observations and characterisation of the hemosiderin rim. *Journal of neurosurgery.* 2010;112(4):814-823.
42. De Belder FE, Oot AR, Van Hecke W, et al. Diffusion tensor imaging provides an insight into the microstructure of meningiomas, high-grade gliomas, and peritumoral oedema. *Journal of computer assisted tomography.* 2012;36(5):577-582.

43. Lazar M, Alexander AL, Thottakara PJ, Badie B, Field AS. White matter reorganisation after surgical resection of brain tumours and vascular malformations. *AJNR Am J Neuroradiol.* 2006;27(6):1258-1271.
44. Beaulieu C. The basis of anisotropic water diffusion in the nervous system - a technical review. *NMR Biomed.* 2002;15(7-8):435-455.
45. Beaulieu C, Does MD, Snyder RE, Allen PS. Changes in water diffusion due to Wallerian degeneration in peripheral nerve. *Magn Reson Med.* 1996;36(4):627-631.
46. Ciccarelli O, Behrens TE, Altmann DR, et al. Probabilistic diffusion tractography: a potential tool to assess the rate of disease progression in amyotrophic lateral sclerosis. *Brain : a journal of neurology.* 2006;129(Pt 7):1859-1871.
47. Huisman TA, Loenneker T, Barta G, et al. Quantitative diffusion tensor MR imaging of the brain: field strength related variance of apparent diffusion coefficient (ADC) and fractional anisotropy (FA) scalars. *Eur Radiol.* 2006;16(8):1651-1658.
48. Hui ES, Cheung MM, Chan KC, Wu EX. B-value dependence of DTI quantitation and sensitivity in detecting neural tissue changes. *Neuroimage.* 2010;49(3):2366-2374.
49. Berlot R, Metzler-Baddeley C, Jones DK, O'Sullivan MJ. CSF contamination contributes to apparent microstructural alterations in mild cognitive impairment. *Neuroimage.* 2014.
50. Metzler-Baddeley C, O'Sullivan MJ, Bells S, Pasternak O, Jones DK. How and how not to correct for CSF-contamination in diffusion MRI. *Neuroimage.* 2012;59(2):1394-1403.
51. Yendiki A, Koldewyn K, Kakunoori S, Kanwisher N, Fischl B. Spurious group differences due to head motion in a diffusion MRI study. *Neuroimage.* 2013.
52. Provenzale JM, McGraw P, Mhatre P, Guo AC, Delong D. Peritumoral brain regions in gliomas and meningiomas: investigation with isotropic diffusion-weighted MR imaging and diffusion-tensor MR imaging. *Radiology.* 2004;232(2):451-460.

53. Song SK, Sun SW, Ramsbottom MJ, Chang C, Russell J, Cross AH. Dysmyelination revealed through MRI as increased radial (but unchanged axial) diffusion of water. *Neuroimage.* 2002;17(3):1429-1436.
54. Sugahara T, Korogi Y, Kochi M, et al. Usefulness of diffusion-weighted MRI with echo-planar technique in the evaluation of cellularity in gliomas. *J Magn Reson Imaging.* 1999;9(1):53-60.
55. Gauvain KM, McKinstry RC, Mukherjee P, et al. Evaluating pediatric brain tumor cellularity with diffusion-tensor imaging. *AJR Am J Roentgenol.* 2001;177(2):449-454.
56. Kono K, Inoue Y, Nakayama K, et al. The role of diffusion-weighted imaging in patients with brain tumours. *AJNR Am J Neuroradiol.* 2001;22(6):1081-1088.
57. Zimmerman RD. Is there a role for diffusion-weighted imaging in patients with brain tumours or is the "bloom off the rose"? *AJNR Am J Neuroradiol.* 2001;22(6):1013-1014.
58. Wang Y, Wang Q, Haldar JP, et al. Quantification of increased cellularity during inflammatory demyelination. *Brain : a journal of neurology.* 2011;134(Pt 12):3590-3601.
59. Behrens TE, Woolrich MW, Jenkinson M, et al. Characterisation and propagation of uncertainty in diffusion-weighted MR imaging. *Magn Reson Med.* 2003;50(5):1077-1088.
60. Assaf Y, Basser PJ. Composite hindered and restricted model of diffusion (CHARMED) MR imaging of the human brain. *Neuroimage.* 2005;27(1):48-58.
61. Barazany D, Basser PJ, Assaf Y. In vivo measurement of axon diameter distribution in the corpus callosum of rat brain. *Brain : a journal of neurology.* 2009;132(Pt 5):1210-1220.
62. Jensen JH, Helpern JA, Ramani A, Lu H, Kaczynski K. Diffusional kurtosis imaging: the quantification of non-gaussian water diffusion by means of magnetic resonance imaging. *Magn Reson Med.* 2005;53(6):1432-1440.
63. Cheung JS, Wang E, Lo EH, Sun PZ. Stratification of heterogeneous diffusion MRI ischemic lesion with kurtosis imaging: evaluation of mean diffusion and kurtosis MRI mismatch in an animal model of transient focal ischemia. *Stroke.* 2012;43(8):2252-2254.

64. Giannelli M, Toschi N, Passamonti L, et al. Diffusion Kurtosis and Diffusion-Tensor MR Imaging in Parkinson Disease. *Radiology.* 2012;265(2):645-646.
65. Van Cauter S, Veraart J, Sijbers J, et al. Gliomas: diffusion kurtosis MR imaging in grading. *Radiology.* 2012;263(2):492-501.
66. Zhuo J, Xu S, Proctor JL, et al. Diffusion kurtosis as an in vivo imaging marker for reactive astrogliosis in traumatic brain injury. *Neuroimage.* 2012;59(1):467-477.
67. Tournier JD, Calamante F, Gadian DG, Connelly A. Direct estimation of the fiber orientation density function from diffusion-weighted MRI data using spherical deconvolution. *Neuroimage.* 2004;23(3):1176-1185.
68. Tournier JD, Calamante F, Connelly A. Robust determination of the fibre orientation distribution in diffusion MRI: non-negativity constrained super-resolved spherical deconvolution. *Neuroimage.* 2007;35(4):1459-1472.
69. Dell'acqua F, Scifo P, Rizzo G, et al. A modified damped Richardson-Lucy algorithm to reduce isotropic background effects in spherical deconvolution. *Neuroimage.* 2009;49(2):1446-1458.
70. Yeh FC, Wedeen VJ, Tseng WY. Estimation of fiber orientation and spin density distribution by diffusion deconvolution. *Neuroimage.* 2011;55(3):1054-1062.
71. Landman BA, Bogovic JA, Wan H, El Zahraa ElShahaby F, Bazin PL, Prince JL. Resolution of crossing fibers with constrained compressed sensing using diffusion tensor MRI. *Neuroimage.* 2012;59(3):2175-2186.
72. Yeh FC, Tseng WY. Sparse solution of fiber orientation distribution function by diffusion decomposition. *PLoS ONE.* 2013;8(10):e75747.
73. Callaghan PT, Xia Y. Velocity and diffusion imaging in dynamic NMR microscopy. *Journal of Magnetic Resonance.* 1991;91(2):326-352
74. Wedeen VJ, Hagmann P, Tseng WY, Reese TG, Weisskoff RM. Mapping complex tissue architecture with diffusion spectrum magnetic resonance imaging. *Magn Reson Med.* 2005;54(6):1377-1386.
75. Wedeen VJ, Wang RP, Schmahmann JD, et al. Diffusion spectrum magnetic resonance imaging (DSI) tractography of crossing fibers. *Neuroimage.* 2008;41(4):1267-1277.
76. Tuch DS. Q-ball imaging. *Magn Reson Med.* 2004;52(6):1358-1372.

77. Descoteaux M, Angelino E, Fitzgibbons S, Deriche R. Regularized, fast, and robust analytical Q-ball imaging. *Magn Reson Med.* 2007;58(3):497-510.
78. Yeh FC, Wedeen VJ, Tseng WY. Generalised q-sampling imaging. *IEEE Trans Med Imaging.* 2010;29(9):1626-1635.
79. Wang Y, Fernandez-Miranda JC, Verstynen T, Pathak S, Schneider W, Yeh FC. Rethinking the role of the middle longitudinal fascicle in language and auditory pathways. *Cereb Cortex.* 2013;23(10):2347-2356.
80. Yeh FC, Verstynen TD, Wang Y, Fernandez-Miranda JC, Tseng WY. Deterministic diffusion fiber tracking improved by quantitative anisotropy. *PLoS ONE.* 2013;8(11):e80713.
81. Basser PJ, Pajevic S, Pierpaoli C, Duda J, Aldroubi A. In vivo fiber tractography using DT-MRI data. *Magn Reson Med.* 2000;44(4):625-632.
82. Descoteaux M, Deriche R, Knosche TR, Anwander A. Deterministic and probabilistic tractography based on complex fibre orientation distributions. *IEEE Trans Med Imaging.* 2009;28(2):269-286.
83. Jbabdi S, Johansen-Berg H. Tractography: Where Do We Go from Here? . *Brain Connectivity.* 2011;1(3):169-183.
84. Jones DK, Symms MR, Cercignani M, Howard RJ. The effect of filter size on VBM analyses of DT-MRI data. *Neuroimage.* 2005;26(2):546-554.
85. Pagani E, Filippi M, Rocca MA, Horsfield MA. A method for obtaining tract-specific diffusion tensor MRI measurements in the presence of disease: application to patients with clinically isolated syndromes suggestive of multiple sclerosis. *Neuroimage.* 2005;26(1):258-265.
86. Kanaan RA, Shergill SS, Barker GJ, et al. Tract-specific anisotropy measurements in diffusion tensor imaging. *Psychiatry Res.* 2006;146(1):73-82.
87. Hua K, Zhang J, Wakana S, et al. Tract probability maps in stereotaxic spaces: analyses of white matter anatomy and tract-specific quantification. *Neuroimage.* 2008;39(1):336-347.
88. Nezamzadeh M, Wedeen VJ, Wang R, et al. In-vivo investigation of the human cingulum bundle using the optimization of MR diffusion spectrum imaging. *Eur J Radiol.* 2010;75(1):e29-36.

89. Kuo LW, Lee CY, Chen JH, et al. Mossy fiber sprouting in pilocarpine-induced status epilepticus rat hippocampus: a correlative study of diffusion spectrum imaging and histology. *Neuroimage.* 2008;41(3):789-800.
90. Besseling RM, Jansen JF, Overvliet GM, et al. Tract specific reproducibility of tractography based morphology and diffusion metrics. *PLoS ONE.* 2012;7(4):e34125.
91. Tensaouti F, Lahlou I, Clarisse P, Lotterie JA, Berry I. Quantitative and reproducibility study of four tractography algorithms used in clinical routine. *J Magn Reson Imaging.* 2011;34(1):165-172.
92. Chung HW, Chou MC, Chen CY. Principles and Limitations of Computational Algorithms in Clinical Diffusion Tensor MR Tractography. *AJNR Am J Neuroradiol.* 2010.
93. Malykhin N, Concha L, Seres P, Beaulieu C, Coupland NJ. Diffusion tensor imaging tractography and reliability analysis for limbic and paralimbic white matter tracts. *Psychiatry Res.* 2008;164(2):132-142.
94. Alexander DC, Pierpaoli C, Basser PJ, Gee JC. Spatial transformations of diffusion tensor magnetic resonance images. *IEEE Trans Med Imaging.* 2001;20(11):1131-1139.
95. Jones DK, Griffin LD, Alexander DC, et al. Spatial normalization and averaging of diffusion tensor MRI data sets. *Neuroimage.* 2002;17(2):592-617.
96. Hong X, Arlinghaus LR, Anderson AW. Spatial normalization of the fiber orientation distribution based on high angular resolution diffusion imaging data. *Magn Reson Med.* 2009;61(6):1520-1527.
97. Smith SM, Jenkinson M, Johansen-Berg H, et al. Tract-based spatial statistics: voxelwise analysis of multi-subject diffusion data. *Neuroimage.* 2006;31(4):1487-1505.
98. Smith SM, Johansen-Berg H, Jenkinson M, et al. Acquisition and voxelwise analysis of multi-subject diffusion data with tract-based spatial statistics. *Nat Protoc.* 2007;2(3):499-503.
99. Yeh FC, Tang PF, Tseng WY. Diffusion MRI connectometry automatically reveals affected fiber pathways in individuals with chronic stroke. *Neuroimage Clin.* 2013;2:912-921.

100. Yeh FC, Panesar S, Barrios J, et al. Automatic Removal of False Connections in Diffusion MRI Tractography Using Topology-Informed Pruning (TIP). *Neurotherapeutics.* 2019;16(1):52-58.
101. Fernandez-Miranda JC, Pathak S, Engh J, et al. High-definition fiber tractography of the human brain: neuroanatomical validation and neurosurgical applications. *Neurosurgery.* 2012;71(2):430-453.
102. Abla AA, Lekovic GP, Turner JD, de Oliveira JG, Porter R, Spetzler RF. Advances in the treatment and outcome of brainstem cavernous malformation surgery: a single-centre case series of 300 surgically treated patients. *Neurosurgery.* 2011;68(2):403-414; discussion 414-405.
103. Kim DS, Park YG, Choi JU, Chung SS, Lee KC. An analysis of the natural history of cavernous malformations. *Surgical neurology.* 1997;48(1):9-17; discussion 17-18.
104. Monaco EA, Khan AA, Niranjan A, et al. Stereotactic radiosurgery for the treatment of symptomatic brainstem cavernous malformations. *Neurosurgical focus.* 2010;29(3):E11.
105. Chen X, Weigel D, Ganslandt O, Buchfelder M, Nimsky C. Diffusion tensor imaging and white matter tractography in patients with brainstem lesions. *Acta neurochirurgica.* 2007;149(11):1117-1131; discussion 1131.
106. Chen X, Weigel D, Ganslandt O, Fahlbusch R, Buchfelder M, Nimsky C. Diffusion tensor-based fiber tracking and intraoperative neuronavigation for the resection of a brainstem cavernous angioma. *Surgical neurology.* 2007;68(3):285-291; discussion 291.
107. McLaughlin N, Kelly DF. Corticospinal tractography as a prognosticator for motor improvement after brainstem cavernoma resection. *British journal of neurosurgery.* 2013;27(1):108-110.
108. Royo A, Utrilla C, Carceller F. Surgical management of brainstem-expanding lesions: the role of neuroimaging. *Seminars in ultrasound, CT, and MR.* 2013;34(2):153-173.
109. Mai JC, Ramanathan D, Kim LJ, Sekhar LN. Surgical resection of cavernous malformations of the brainstem: evolution of a minimally invasive technique. *World neurosurgery.* 2013;79(5-6):691-703.

110. Jhawar S, Nadkarni T, Goel A. Giant cerebral cavernous hemangiomas: a report of two cases and review of the literature. *Turkish neurosurgery.* 2012;22(2):226-232.
111. Nimsky C, Ganslandt O, Fahlbusch R. Implementation of fiber tract navigation. *Neurosurgery.* 2007;61(1 Suppl):306-317; discussion 317-308.
112. Zhang H, Wang Y, Lu T, et al. Differences between generalised q-sampling imaging and diffusion tensor imaging in the preoperative visualization of the nerve fiber tracts within peritumoral oedema in brain. *Neurosurgery.* 2013;73(6):1044-1053; discussion 1053.
113. Kuhnt D, Bauer MH, Sommer J, Merhof D, Nimsky C. Optic radiation fiber tractography in glioma patients based on high angular resolution diffusion imaging with compressed sensing compared with diffusion tensor imaging - initial experience. *PLoS One.* 2013;8(7):e70973.
114. Bucci M, Mandelli ML, Berman JI, et al. Quantifying diffusion MRI tractography of the corticospinal tract in brain tumours with deterministic and probabilistic methods. *Neuroimage Clin.* 2013;3:361-368.
115. Zolal A, Hejcl A, Vachata P, et al. The use of diffusion tensor images of the corticospinal tract in intrinsic brain tumor surgery: a comparison with direct subcortical stimulation. *Neurosurgery.* 2012;71(2):331-340; discussion 340.
116. Brooks BR, Miller RG, Swash M, Munsat TL, World Federation of Neurology Research Group on Motor Neuron D. El Escorial revisited: revised criteria for the diagnosis of amyotrophic lateral sclerosis. *Amyotrophic lateral sclerosis and other motor neuron disorders : official publication of the World Federation of Neurology, Research Group on Motor Neuron Diseases.* 2000;1(5):293-299.
117. Graham JM, Papadakis N, Evans J, et al. Diffusion tensor imaging for the assessment of upper motor neuron integrity in ALS. *Neurology.* 2004;63(11):2111-2119.
118. Jacob S, Finsterbusch J, Weishaupt JH, Khorram-Sefat D, Frahm J, Ehrenreich H. Diffusion tensor imaging for long-term follow-up of corticospinal tract degeneration in amyotrophic lateral sclerosis. *Neuroradiology.* 2003;45(9):598-600.

119. Menke RA, Abraham I, Thiel CS, et al. Fractional anisotropy in the posterior limb of the internal capsule and prognosis in amyotrophic lateral sclerosis. *Archives of neurology.* 2012;69(11):1493-1499.
120. Nickerson JP, Koski CJ, Boyer AC, Burbank HN, Tandan R, Filippi CG. Linear longitudinal decline in fractional anisotropy in patients with amyotrophic lateral sclerosis: preliminary results. *Klinische Neuroradiologie.* 2009;19(2):129-134.
121. Cedarbaum JM, Stambler N, Malta E, et al. The ALSFRS-R: a revised ALS functional rating scale that incorporates assessments of respiratory function. BDNF ALS Study Group (Phase III). *Journal of the neurological sciences.* 1999;169(1-2):13-21.
122. Keil C, Prell T, Peschel T, Hartung V, Dengler R, Grosskreutz J. Longitudinal diffusion tensor imaging in amyotrophic lateral sclerosis. *BMC neuroscience.* 2012;13:141.
123. Sage CA, Peeters RR, Gorner A, Robberecht W, Sunaert S. Quantitative diffusion tensor imaging in amyotrophic lateral sclerosis. *Neuroimage.* 2007;34(2):486-499.
124. Filippini N, Douaud G, Mackay CE, Knight S, Talbot K, Turner MR. Corpus callosum involvement is a consistent feature of amyotrophic lateral sclerosis. *Neurology.* 2010;75(18):1645-1652.
125. Raaphorst J, de Visser M, van Tol MJ, et al. Cognitive dysfunction in lower motor neuron disease: executive and memory deficits in progressive muscular atrophy. *Journal of neurology, neurosurgery, and psychiatry.* 2011;82(2):170-175.
126. Smith MC. Nerve Fibre Degeneration in the Brain in Amyotrophic Lateral Sclerosis. *Journal of neurology, neurosurgery, and psychiatry.* 1960;23(4):269-282.
127. Rose S, Pannek K, Bell C, et al. Direct evidence of intra- and interhemispheric corticomotor network degeneration in amyotrophic lateral sclerosis: an automated MRI structural connectivity study. *Neuroimage.* 2012;59(3):2661-2669.
128. Verstraete E, Veldink JH, van den Berg LH, van den Heuvel MP. Structural brain network imaging shows expanding disconnection of the motor system in amyotrophic lateral sclerosis. *Human brain mapping.* 2013.

129. Yeh FC, Tang P.F., Tseng W.I. Diffusion MRI connectometry automatically reveals affected fiber pathways in individuals with chronic stroke. *Neuroimage: Clinical.* 2013;2:912-921.
130. Georgiou-Karistianis N, Scahill R, Tabrizi SJ, Squitieri F, Aylward E. Structural MRI in Huntington's disease and recommendations for its potential use in clinical trials. *Neuroscience and biobehavioral reviews.* 2013;37(3):480-490.
131. Rosas HD, Tuch DS, Hevelone ND, et al. Diffusion tensor imaging in presymptomatic and early Huntington's disease: Selective white matter pathology and its relationship to clinical measures. *Movement disorders : official journal of the Movement Disorder Society.* 2006;21(9):1317-1325.
132. Dumas EM, van den Bogaard SJ, Ruber ME, et al. Early changes in white matter pathways of the sensorimotor cortex in premanifest Huntington's disease. *Human brain mapping.* 2012;33(1):203-212.
133. Sritharan A, Egan GF, Johnston L, et al. A longitudinal diffusion tensor imaging study in symptomatic Huntington's disease. *Journal of neurology, neurosurgery, and psychiatry.* 2010;81(3):257-262.
134. Nopoulos PC, Aylward EH, Ross CA, et al. Cerebral cortex structure in prodromal Huntington disease. *Neurobiology of disease.* 2010;40(3):544-554.
135. Rosas HD, Hevelone ND, Zaleta AK, Greve DN, Salat DH, Fischl B. Regional cortical thinning in preclinical Huntington disease and its relationship to cognition. *Neurology.* 2005;65(5):745-747.
136. Paulsen JS, Nopoulos PC, Aylward E, et al. Striatal and white matter predictors of estimated diagnosis for Huntington disease. *Brain research bulletin.* 2010;82(3-4):201-207.
137. Tabrizi SJ, Langbehn DR, Leavitt BR, et al. Biological and clinical manifestations of Huntington's disease in the longitudinal TRACK-HD study: cross-sectional analysis of baseline data. *Lancet Neurol.* 2009;8(9):791-801.
138. Verstynen T, Jarbo K, Pathak S, Schneider W. In vivo mapping of microstructural somatotopies in the human corticospinal pathways. *Journal of neurophysiology.* 2011;105(1):336-346.
139. Jarbo K, Verstynen T, Schneider W. In vivo quantification of global connectivity in the human corpus callosum. *Neuroimage.* 2012;59(3):1988-1996.

140. Verstynen TD, Badre D, Jarbo K, Schneider W. Microstructural organisational patterns in the human corticostriatal system. *Journal of neurophysiology.* 2012;107(11):2984-2995.
141. Crick FC, Koch C. What is the function of the claustrum? *Philos T R Soc B.* 2005;360(1458):1271-1279.
142. Rae A. The connections of the claustrum. *Confinia neurologica.* 1954;14(4):211-219.
143. Rae A. The form and structure of the human claustrum. *The Journal of comparative neurology.* 1954;100(1):15-39.
144. Brand S. A serial section Golgi analysis of the primate claustrum. *Anatomy and embryology.* 1981;162(4):475-488.
145. Filimonoff I. The claustrum, its origin and development. *Journal für Hirnforschung.* 1966;8(5):503-528.
146. Morys J, Narkiewicz O, Wisniewski H. Neuronal loss in the human claustrum following ulegyria. *Brain research.* 1993;616(1-2):176-180.
147. Fernández-Miranda J, Rhoton A, Kakizawa Y, Choi C, Alvarez-Linera J. The claustrum and its projection system in the human brain: a microsurgical and tractographic anatomical study. *Journal of neurosurgery.* 2008;108(4):764-774.
148. Fernández-Miranda J, Rhoton A, Alvarez-Linera J, Kakizawa Y, Choi C, de Oliveira E. Three-dimensional microsurgical and tractographic anatomy of the white matter of the human brain. *Neurosurgery.* 2008;62(6 Suppl 3):989.

1.6 Figures

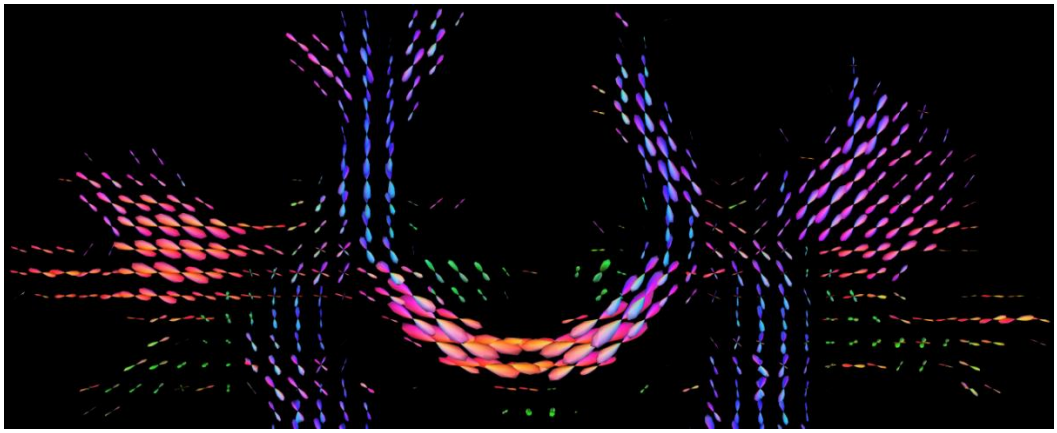

FIGURE 1. The fiber orientation distribution obtained by diffusion deconvolution. This coronal slice is positioned at the centrum semiovale with corticospinal tracts being the vertically oriented tracts. The crossing region with the corpus callosum is also demonstrated.

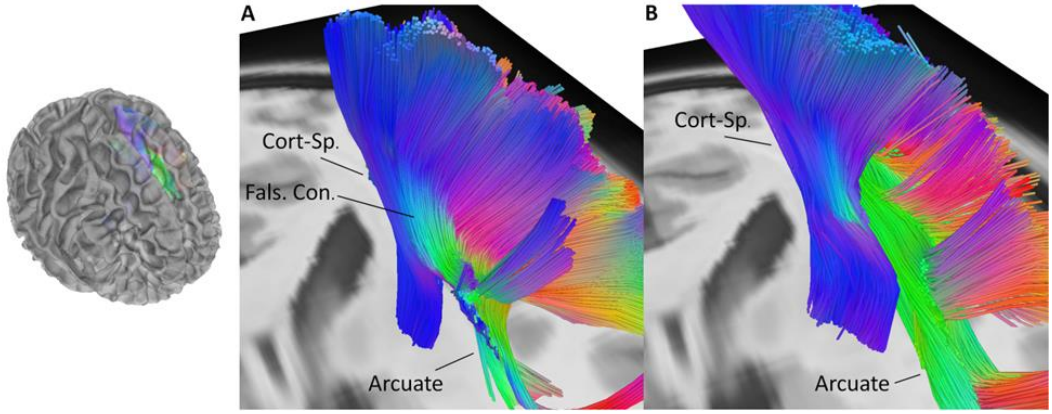

FIGURE 2. A, Diffusion tensor imaging-based tractography leads to false continuation (Fals. Con.) between the arcuate and the corticospinal (Cort-sp.) tracts in the region of their crossing. B, an advanced fiber tracking method using GQI is able to resolve this issue displaying the orientation of the arcuate in an anteroposterior direction and that of corticospinal tract in the superoinferior direction without any major false continuation. Inset image demonstrates the angle pertinent to the viewing of the fiber tracts.

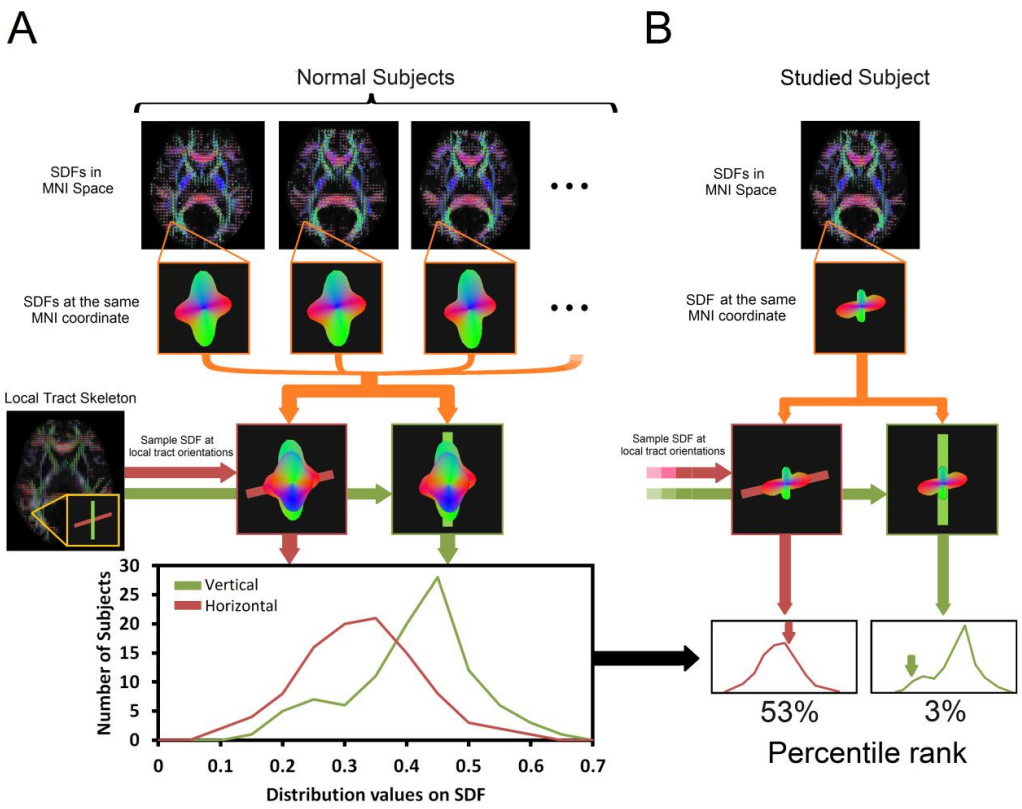

FIGURE 3. Diffusion MRI connectometry. A, the spin distribution functions (SDFs) are reconstructed in the MNI template space using q-space diffeomorphic reconstruction and sampled at the local fiber orientations to obtain the diffusion quantity of corresponding fiber. The sampled SDF values from a normal population construct a norm that can be used to test the deviant cases. B, the data of a studied study (e.g., a patient with tract damage) are reconstructed in the template space and sampled using same procedure. The sampled SDF values are compared with the norm to calculate the percentile rank for further statistical testing.

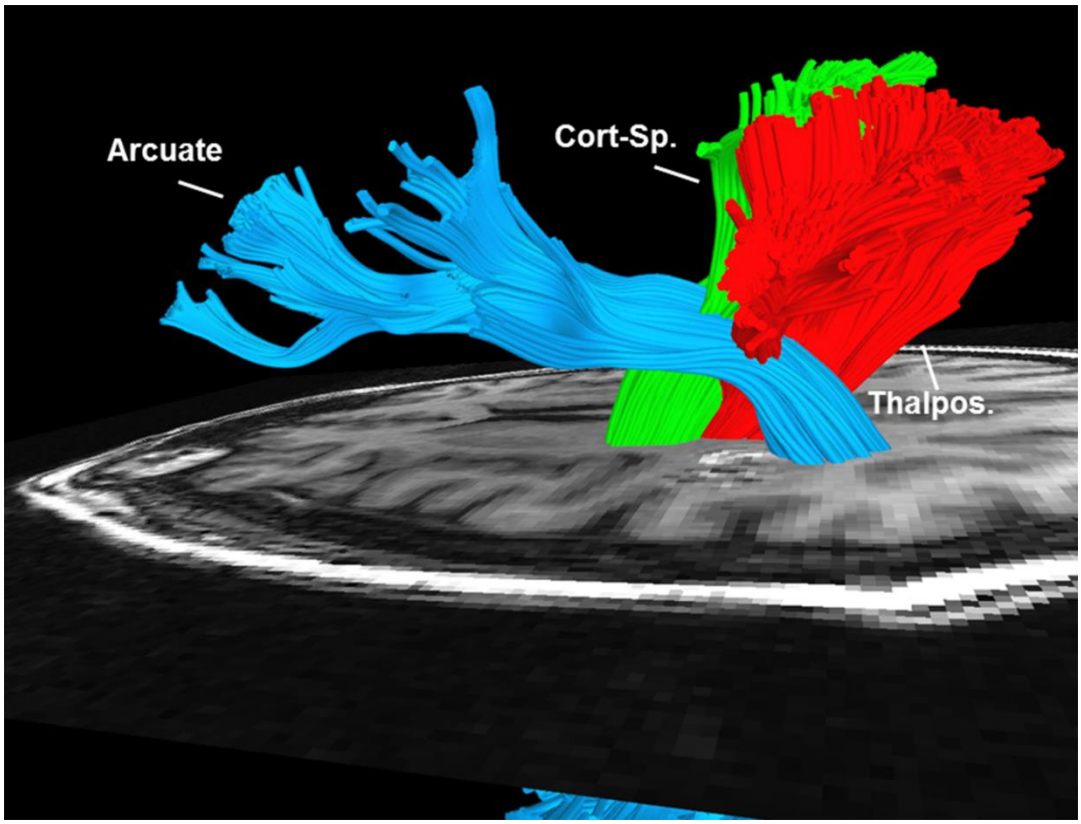

FIGURE 4. Advanced fiber tracking analysis (note MRI scan has been flipped) showed posterior displacement of the arcuate around the left parietal cavernous malformation with anteromedial displacement of the thalamopostcentral (Thalpos.) fibers with no effect on the corticospinal (Cort-Sp.) tract and with lateral margin being free of the traversing superior longitudinal fasciculus fibers, allowing a surgical approach through the post-central sulcus. Multiple crossing perilesional fibers are demonstrated.

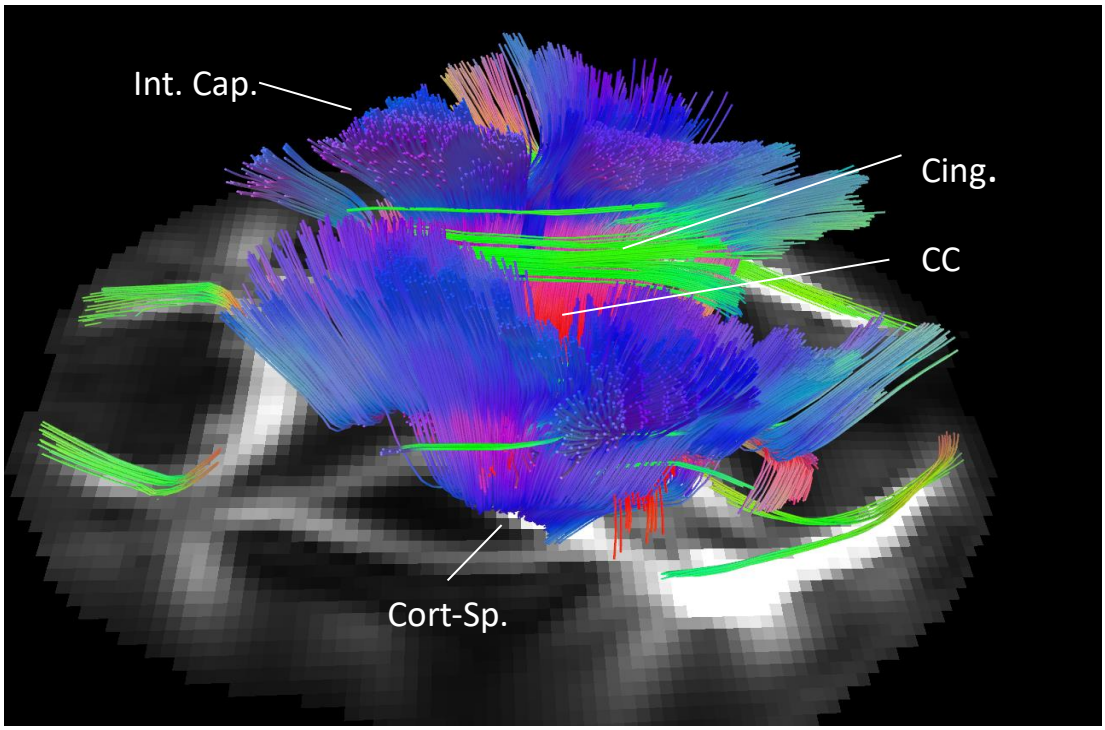

FIGURE 5. In a patient with ALS, approximately 42 months into the disease onset, there were demonstrated bilateral changes in the motoric and extramotoric pathways; involved tracts included corticospinal tract (Cort-sp.); the internal capsule (Int. Cap.); corpus callosum (CC) and cingulum (Cing.) among other tracts.

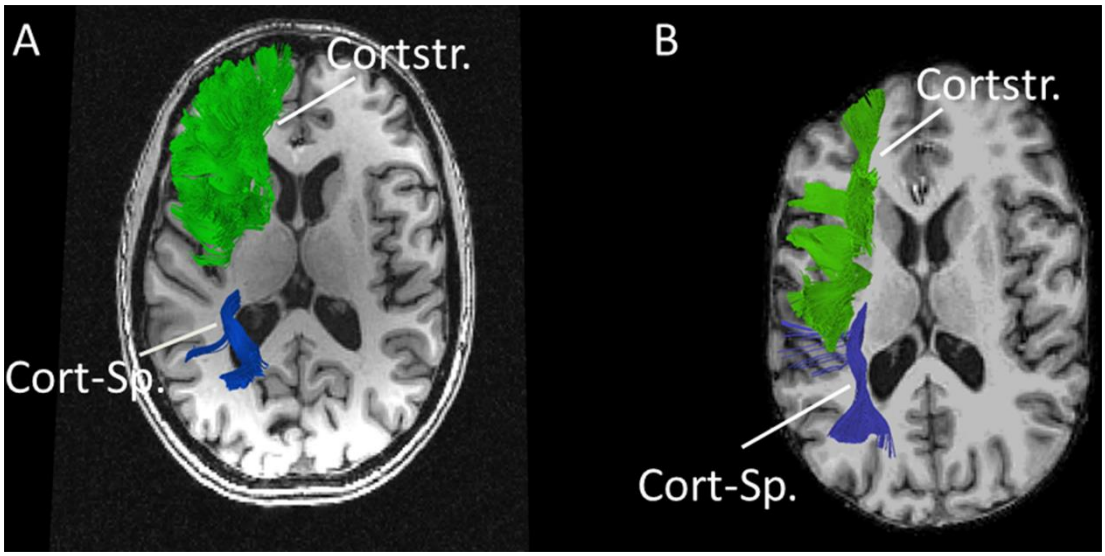

FIGURE 6. Axial MR (advanced white matter imaging) (A, earlier; B, 6 months later) of a patient with premanifest Huntington's disease demonstrating qualitative reduction in dorsolateral prefrontal cortex projections to striatum or corticostriatal (Cortstr.) projections; corticospinal (Cort-Sp.) tract (blue) is also shown.

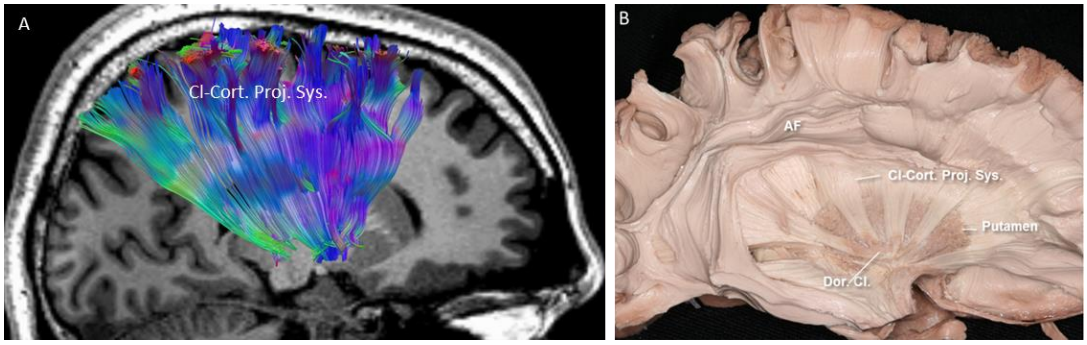

FIGURE 7. A, Reconstruction of the claustro-cortical projection system (Cl-Cort. Proj. Sys.) using advanced white matter imaging technique; these fibers form the dorsal portion of the external capsule and converge into the dorsal claustrum. B, fiber microdissection of the post-mortem human brain demonstrating the dorsal claustrum (Dor. Cl.) and the claustrocortical projection system with the latter having been partially dissected to expose the underlying putamen; arcuate fasciculus (AF).

Chapter 2: Application of High Definition Fiber Tractography (HDFT) in Management of Supratentorial Cavernous malformations: a combined qualitative and quantitative approach

Paper 1: **Abhinav K**, Pathak S, Richardson RM, Engh J, Gardner P, Yeh FC, Friedlander RM, Fernandez-Miranda JC. Application of High Definition Fiber Tractography (HDFT) in Management of Supratentorial Cavernous malformations: a combined qualitative and quantitative approach. *Neurosurgery* 2014; **74(6):**668-81.

2.1 Declaration

I led this study as first author and was responsible for devising the concept of using quantitative anisotropy (QA) for the perilesional segment (QA-based perilesional segment analysis) for evaluating tract integrity.

2.2 General introduction to and brief summary of the manuscript

At an institutional level, HDFT had been used on a preliminary basis to provide qualitative data towards complementing surgical planning for cases with cavernous malformations or intracranial tumours. This manuscript represented the effort towards examining the use of HDFT solely with respect to the supratentorial cavernous malformations (CMs). Importantly the effort was directed towards examining the quantitative data in a preliminary fashion to characterise the associated changes in the perilesional white matter (WM) tracts.

The primary objective therefore, was to investigate the use of HDFT in the management of supratentorial CMs and in characterising the relationship of these malformations to the relevant perilesional WM tracts and associated changes first qualitatively and then quantitatively with the novel imaging measure, QA. Imaging analysis was carried out by researchers blinded to the clinical details. Contralateral homologous WM tracts were used for comparison. Mean QA values were obtained for the whole WM tracts. Qualitatively affected superior longitudinal fasciculus/arcuate fibers and corticospinal tracts were further analysed with the use of mean QA values for the perilesional segments in a novel fashion. Of 10 patients, HDFT assisted with the decision-making process and the offer of surgical resection

in 2 patients, lesion approach and removal in 7 patients, and conservative management in 1 patient. Of 17 analysed WM tracts, HDFT demonstrated partial disruption in 2 tracts, complete disruption in 2 tracts, a combination of displacement and partial disruption in 1 tract, displacement only in 7 tracts, and no change in 5 tracts. Qualitative changes correlated with clinical symptoms. Mean QA values for the whole WM tracts were similar, with the exception of 1 case demonstrating complete disruption of 2 WM tracts. QA-based perilesional segment analysis was consistent with qualitative data in 5 assessed WM tracts. This preliminary study therefore, demonstrated the utility of HDFT in illustrating the precise spatial relationship of CMs to multiple WM tracts in a 3-dimensional fashion, optimizing surgical planning, and demonstrated associated disruption and/or displacement, with both seen perilesionally. In this preliminary study, these changes were supported by our quantitative marker, analogous to fractional anisotropy in DTI. The use of qualitative and quantitative data is further explored in subsequent chapters dealing with infratentorial and deep-seated CMs.

2.3 Introduction

The prevalence of cavernous malformations (CMs) is estimated to be between 0.4 to 0.9% of the population.[1, 2] with an overall rate of symptomatic haemorrhage being 0.22% to 0.7% per year.[3] Most CMs occur in the supratentorial white matter (WM) and their management can either be conservative or include microsurgical resection or radiosurgery, with the indications for their surgical resection being controversial.[4] Use of diffusion tensor imaging (DTI) in brainstem CMs' resection, which are surgically challenging with a higher annual average symptomatic haemorrhage rate of 2.7% to 5%,[5-7] has been reported[8-12] with only isolated case reports describing its utility with supratentorial CMs[13, 14] along with a further study detailing its perilesional quantitative characteristics.[15] DTI's major limitations include its inability to represent the crossing of multiple fibers or to determine with precision their cortical and subcortical termination; further it misses large tract segments resulting in multiple artifacts.[16, 17] DTI indices, e.g. fractional anisotropy (FA) suffer with partial volume effects, leading to underestimation in areas with multiple

crossing fibers.[18, 19] Despite these, DTI has been an important adjunct in the resection of tumours[20, 21] and CMs.[9, 10, 12]

Our group has demonstrated the use of an advanced WM imaging technique, High Definition Fiber Tractography (HDFT), which addresses the limitations of DTI, and is accurate in tracking fiber pathways, through complex crossings to subcortical regions and targets with subvoxel resolution.[22] HDFT relies on diffusion spectrum imaging (DSI) for acquisition;[23] generalised q-sampling imaging for fiber orientation estimation;[24] a generalised deterministic fiber tracking method[25] and other innovations.[26] We have reported its use in studies on several tracts, e.g. the middle longitudinal fascicle;[27] CST;[26] corpus callosum;[28] dorsal stream visual pathways;[29] cortico-striatal pathways[30] and in a study concerning its utility for surgical planning in a limited series of tumours and CMs.[22]

We aimed to analyse the HDFT's utility in optimizing the decision-making and management of a preliminary series of supratentorial CMs, including for surgical approach planning. We hypothesised that CMs can lead to displacement and/ or disruption in the perilesional WM tracts, which can then be demonstrated and assessed both qualitatively and quantitatively, using HDFT. We also intended to investigate the relationship of CMs to perilesional tracts, assumed to be less relevant than CST, e.g. uncinate fasciculus (UF); thalamopostcentral (TPC) fibers; non-dominant superior longitudinal fasciculus (SLF) and arcuate fasciculus (AF). We aimed to achieve these by obtaining both qualitative information with respect to perilesional fibers as well as by their quantitative evaluation using our novel imaging measure, quantitative anisotropy (QA),[24] which has not been attempted previously. QA, a measure of anisotropy of water with estimated spin density, can serve as a reliable stopping criterion for fiber tracking, essential towards demonstrating endpoint connectivity of functional regions. QA overcomes the limitations of FA in assessing the fiber integrity in areas with multiple crossing fibers, being less sensitive to partial volume effects, as demonstrated in our recent study,[25] therefore making it a more accurate quantitative measure to evaluate the relationship of the CMs to the perilesional tracts.

2.4 Patients and Methods

2.4.1 Data Collection

HDFT database was reviewed to identify evaluated patients with supratentorial CMs. Patients were prescreened for contraindications to MRI. Qualitative analysis of the HDFT data had been performed previously (not as part of our study) in order to guide the decision-making process and surgery, if applicable. The first two authors qualitatively and quantitatively analysed the HDFT data, blinded to clinical details followed by review of operative and clinical records for comparison. Intrasubject contralateral fiber tracts were used for comparison. Approval was obtained from the internal review board at the University of Pittsburgh, with all patients providing written informed consent.

2.4.2 Image Acquisition and Reconstruction

DSI data was acquired on a 3-T Tim Trio System (Siemens, Erlangen, Germany) using a 32-channel coil. A head stabiliser was utilized to prevent head motion. A 43-minute, 257-direction DSI scan with a twice-refocused spin-echo planar imaging sequence and multiple b values (repetition time = 9916 ms, echo time = 157 ms, voxel size = 2.4x 2.4x2.4 mm, field of view = 231x231 mm, maximum b-value = 7000 s/mm^2) was performed. For anatomical comparisons, we also included high-resolution anatomical imaging using a 9-minute T_1-weighted axial magnetization-prepared rapid-acquisition gradient-echo sequence (repetition time = 2110 ms, echo time = 2.63 ms, flip angle = 8 degrees, number of slices = 176, field of view = 256 x 256 mm^2, voxel size = 0.5 x 0.5 x1.0 mm^3). DSI data was reconstructed with a generalised q-sampling imaging approach.[24] The orientation distribution functions were reconstructed to 642 discrete sampling directions for each pixel and with a diffusion distance scaling parameter of 1.2.

2.4.3 Fiber Tracking and Analysis

Fiber tracking was performed with DSI-Studio.[31] Tracts were calculated using a QA-based generalised deterministic tracking algorithm.[25] Advantages of using QA over FA-aided tractography included greater accuracy in demonstrating the full extent of the fiber pathways and their termination.[25] Fiber tracking was started by randomly seeding the region of interest (ROI) and initiating tracking in the most prominent fiber's direction. Fiber progression continued with a step size of 1.2 mm, minimum fiber length of 20 mm, and a turning angle threshold of 65 degrees. For tracts' smoothing, the next directional estimate of each voxel was weighted by 20% of the previous moving direction and 80% by the incoming direction of the fiber. Tracking terminated when the relative QA for the incoming direction dropped below a preset threshold or exceeded a turning angle of 65 degrees. QA termination threshold was adjusted on a per-subject basis to ensure consistent white matter coverage in all, critical for single-subject–based tractography studies, where individual differences in coil sensitivity and diffusion signal homogeneity can vary across subjects. All streamlines were saved, and tract segmentation performed in DSI-Studio.

2.4.4 Qualitative Analysis

We described perilesional tracts as being disrupted and/or displaced or unaffected, using contralateral homologous tracts for comparison. Disruption may be partial, e.g. due to 'breakage' or thinning of fibers as seen in a cross-section or due to discontinuity in a limited segment of the tract; or complete if despite relaxation of stopping criteria, the specific tract was not seen predominantly through most or all of its course with major discontinuity. With suspected disruption, while keeping other tracking parameters constant to reduce generation of spurious tracts, we relaxed the QA threshold to identify anatomically feasible perilesional fibers. Definition of 'displacement' was strictly limited to tracts with a change of location or direction due to the lesion-related mass effect.[21]

2.4.5 Quantitative and specific tract (perilesional segment) analysis

This followed qualitative analysis. Mean QA values were obtained for the surgically relevant whole tracts on both sides. For qualitatively affected SLF/ AF and CST fibers, we further used mean QA values for the perilesional segments in a novel fashion to check for consistency with observed disruption and/ or displacement. This included calculation of mean QA values in three distinct divided regions in a tract: in the subcortical region, adjacent to the anatomical origin of the fibers (segment 1); more distally in the subcortical region (segment 2), where fibers were more organized, corresponding to the perilesional area on affected sides and finally in a distal region (segment 3). For comparison, mean QA values for three anatomically equivalent regions in the contralateral homologous tract were obtained. Ten specific tracts, including both sides in five subjects were selected due to a combination of clinical relevance and/ or anatomical proximity to the lesion as well as the feasibility of dividing them accurately. The obtained mean QA, particularly for the perilesional segments, when compared with the contralateral segments were assessed for concordance with the qualitative data either in terms of partial and/ or complete disruption, where this value was hypothesised to be lower; or with tracts with pure displacement, this value was hypothesised to be raised or at least similar. We also calculated the percentage differences between the QA values obtained for these segments (particularly for the perilesional) on the affected in relation to the unaffected side. Finally, for comparison and to establish a preliminary normal range of difference in mean QA values across three broadly similar divided segments in WM tracts between the left and right sides, we used the Carnegie Mellon University (CMU)-30 template to analyse two tracts of interest i.e. SLF and CST. The CMU-30 template[32] is a diffusion orientation distribution template averaged from the DSI data of 30 neurologically healthy volunteers using q-space diffeomorphic reconstruction.[33]

2.5 Results

Ten patients (female = 7; male = 3) were identified (Table 1). The patients' median age was 41.5 years (22-67).

2.5.1 Clinical Details (Table 1, Figures 1-6)

Patient 1

A 33-year-old right-handed female with a 16 mm CM in the right periatrial WM presented with refractory headaches and left hemibody numbness. During surveillance, she had another episode of left hemibody numbness and haemorrhage within the CM. HDFT, consistent with presentation demonstrated partial disruption of the right AF and slight medial displacement of TPC (Figure 1). She underwent an image guided right temporoparietal craniotomy and lesionectomy using endoscopic port surgery (EPS) with symptomatic resolution postoperatively. The trajectory through the non-dominant posterior superior temporal gyrus avoided the AF and TPC fibers, located posterosuperiorly and anteromedially to the lesion respectively.

Patient 2

A 50-year-old right-handed man with a 14 mm anterior left temporal CM presented with a 28-year history of refractory complex partial seizures and no preoperative deficits. A functional MRI (fMRI) showed left hemisphere dominance with Wernicke's in the posterior left superior temporal gyrus region, remote from the CM. HDFT, consistent with the fMRI demonstrated cortical (temporal) terminations of the AF, as being remote from the CM.
The patient underwent an awake left temporal craniotomy for resection of the CM and surrounding epileptogenic tissue, with cortical stimulation and had no deficit postoperatively.

Patient 3

A 53-year-old right-handed male with a left thalamic CM presented with right-sided weakness, headache and dysarthria. He underwent Gamma Knife Surgery and gradually fully recovered. He represented with another haemorrhagic event 5 years later, with the lesion, now measuring 25 mm. Neurological examination demonstrated significant dysarthria; right sided upper motor neuron (UMN) facial weakness; grade 4+/5 strength in the upper and lower extremities; and hemibody anaesthesia. He was managed conservatively and at follow-up, had not returned to his baseline with the neurological examination, as above. HDFT revealed a displaced

and partially disrupted left CST, descending anterolateral to the CM with accompanying posteromedial displacement of the left TPC (Figure 2). In view of significant preservation and anterolateral location of the CST; its risk of injury during an operative procedure and patient's neurological status, he was managed conservatively with planned surveillance.

Patient 4

A 25-year-old right-handed female presented to another institution with right facial and extremity numbness, paraesthesia and hemiparesis related to a left thalamic CM, which had bled on multiple occasions. She underwent a frontal parasagittal craniotomy and right-sided interhemispheric transcallosal contralateral approach at another institution leading to initial worsening of her paresis, followed by gradual resolution to 70-80% of normal strength.

Four years postoperatively, during surveillance for residual CM, she had another clinically relevant haemorrhage. When referred to our institution five years later, she had another symptomatic recurrence with grade 4+/5 power on the right side with an ataxic gait; significant dysmetria and lack of proprioception.

HDFT demonstrated complete disruption of the left TPC and CST, although with evidence of some of the premotor fibers continuing on towards cerebral peduncle, probably representing a case of neuroplasticity and possibly explaining her partially preserved motor function (Figure 3). In view of the patient's young age, previous haemorrhages, surgery (image-guided EPS) was offered, who has currently opted for conservative management.

Patient 5

A 67-year-old right-handed female presented with medically refractory focal seizures attributable to a 13 mm CM (Figure 4) in the left pars orbitalis region and characterised by right upper and lower limb weakness. An fMRI showed frontal language areas posterior to the lesion, at pars triangularis and opercularis and ventral premotor cortex. HDFT demonstrated the frontal origin of the AF as being posterior to the CM, consistent with the fMRI (Figure 4A-B). An image-guided left frontal craniotomy (anterior trans-sulcal approach) was used for complete lesionectomy,

with particular attention to the posterior margin. Postoperatively she had no seizures at six months follow-up.

Patient 6

A 22-year-old left-handed female presented with a 12-year history of medically refractory complex partial seizures (episodes of bad taste and/or vomiting, word finding difficulty) attributable to a 16 mm CM at superior left insula with surrounding hemosiderin. An fMRI demonstrated left hemisphere dominance with Broca's and Wernicke's in their anatomical location with no major activation along the posterior margin of the lesion. HDFT demonstrated medial deformation of a small segment of the left SLF fibers with an unaffected CST. Anterior cortical terminations of the AF on HDFT were consistent with Broca's on the fMRI. In view of her presentation and HDFT findings, she is pending an awake craniotomy involving a transsylvian-transinsular approach and language mapping.

Patient 7

A 66-year-old right-handed female presented with acute headache, difficulty with pronouncing words (words getting 'twisted') and a 10 mm left parietal lobe haemorrhagic CM. The lesion over eight months, doubled in size with MR evidence of blood products. Due to the lesion's proximity to the sensory cortex and its potential effect on the AF, she underwent HDFT and an fMRI in preparation for surgery. HDFT demonstrated posterior displacement of the AF around the lesion with the lateral margin being free of these fibers; anteromedial displacement of the TPC and an unaffected CST (Figure 4C-D). The fMRI confirmed the left hemisphere to be language dominant with Broca's in the inferior frontal gyrus. She underwent an image-guided left parietal craniotomy and an approach through the post-central sulcus for lesionectomy, using information from the HDFT. Resection of the gliotic plane was limited due to the fiber tracts' proximity. Postoperatively she had normal speech.

Patient 8

A 26-year-old right-handed woman presented with an eight-year history of a complicated migraine disorder and a 13 mm haemorrhagic CM (at least two documented episodes of bleeding on CT) within the right caudate head with mild

mass effect. She had transient ischemic symptoms (dysphasia, anomia, left-sided weakness (arm>leg), and gait dysfunction) during migrainous episodes, resistant to prophylactic medications. There was no history of seizures. HDFT demonstrated medial displacement of the fibers of anterior limb of the internal capsule. In view of her age and presentation, she underwent an image-guided right frontal craniotomy and EPS for resection of the lesion. HDFT and the MRI were used preoperatively to plan a trajectory through the superior frontal sulcus with a pre-coronal entry point. Postoperatively patient had no deficit with an MRI showing complete resection.

Patient 9

A 53-year-old man presented with repeated seizures and a CM in the left orbitofrontal region, in front of the caudate head and putamen and medial to anterior insular sulcus. The patient previously had two episodes of seizures and headaches, presumably related to the bleeding of the CM. Surgery was offered in view of repeated haemorrhagic episodes with seizures being controlled medically. Preoperative HDFT demonstrated partial disruption of the orbitofrontal segment of UF, where the lesion was anatomically located (Figure 5). Based on this information, for the lesion's resection, subfrontal route was selected to take advantage of the already established fiber damage and to avoid new disruption (Figure 5).

Patient 10

A 21-year-old lady presented with an episode of severe vertigo and light-headedness. Neurological examination was normal with an MR demonstrating a posterior right frontal 15 mm haemorrhagic CM in the subcortical WM beneath the motor cortex. After initial conservative management patient had a second symptomatic episode, leading to surgical management. HDFT demonstrated the proximity of the lesion to the CST and AF with both being on the medial side (Figure 6). Perilesionally the AF was displaced supero-medially. An image-guided craniotomy was used for excision of the CM, via an approach through the central sulcus. In the immediate post-operative period, she was noted to have minimal left facial UMN weakness with normal speech.

2.5.2 Qualitative data summary

Of 17 analysed relevant perilesional tracts, there was partial disruption in two; complete disruption in two; combination of displacement and partial disruption in one and displacement only in seven; while five tracts were unaffected (Table 1).

2.5.3 Quantitative analysis

2.5.3.1 Mean QA for the whole tract

In total, 34 tracts were evaluated bilaterally for ten patients. Mean QA of the perilesional anatomically relevant tracts (Table 2) were similar compared with the contralateral side for most subjects with the exception of patient 4, where mean QA values for the perilesional CST and TPC were 0.97 and 0.57 respectively versus 1.48 and 1.22 on the unaffected side. In this subject, there was qualitative evidence of complete disruption of CST and TPC fibers.

2.5.3.2 Specific Tract Analysis (perilesional segment)

Of 13 disrupted and/or displaced tracts on the affected side, five (SLF/AF= 3; CST= 2) (Table 3) were further analysed in five cases using mean QA values for the perilesional segment. Segment 2 represented the perilesional segment in all cases. Of note in patient 4 (Figure 3) in addition to an 85.9% drop in the perilesional segment on the affected side there was a drop in the mean QA values for segments 1 and 3 at 30.8% and 42.2% respectively, compared with the contralateral side. Similar QA-based analysis in the control group (CMU-30 template)[32] for the SLF/AF for segments 1, 2 and 3 yielded percentage differences of 9, 7.9, 3.7% respectively between the two sides (right assessed in relation to left). Similarly for CST, the percentage differences between the segments 1, 2 and 3 were 9.3, 1.3 and 7.1% respectively. The percentage differences between the mean QA of two anatomically equivalent segments for SLF/AF and CST, therefore ranged from approximately 1 to 9%. Our quantitative data (Table 3), therefore supported the qualitative data in these cases in line with our hypothesis and encouragingly the observed percentage differences in mean QA for the perilesional segments in relation to the unaffected side were outside of the range from the control group analysis.

2.5.4 Case examples demonstrating direct comparison of HDFT with DTI

This is demonstrated using patients 9 (Figure 7) and 7 (Figure 8) with results obtained by applying HDFT and DTI to the same dataset to perform an optimal comparison. The contrast of each inset image was min-max-scaled to 0 and 255 in grayscale. The FA map (Figure 7A) demonstrates decreased value in the CM, however, the mapping is noisy with the CM's location not readily discernible. The QA map (Figure 7B), on the contrary, shows clear CM location (indicated by the red arrow) with its extent readily discernible. This result suggests that the FA-based analysis may not be as accurate as the QA-based analysis used in HDFT. The ADC map (Figure 7C) shows decreased values in the CM region, but similar to the FA map, it also has a noisy profile with the CM location not clearly discernible. Sum of spin distribution function (SDF), derived from generalised q-sampling imaging,[24] has a similar physical meaning as ADC. The red arrow in SDF summation map (Figure 7D) indicates decreased intensity with the CM extent readily delineated. Generalised q-sampling imaging therefore, offers better diffusion profile, benefitting HDFT. DTI-based tractography (Figure 5F) of the UF demonstrates the partial disruption, however with missing fiber segments, compared with HDFT (Figure 5B and C). Demonstration of superiority of qualitative tractography data from HDFT is further shown (Figure 8) using patient 7. DTI-based tractography was generated using an FA threshold of 0.1, with the value for angular threshold reduced to 45 degrees, much lower than 65 degrees for HDFT, in order to avoid false continuation. HDFT accurately demonstrated perilesional crossing fibers i.e. AF and CST (Figure 8A) in contrast with DTI-based tractography (Figure 8B) showing false continuation between these two fibers despite a stricter angular threshold. This error is related to DTI assuming single fiber population with the resulting tractography suffering from false continuation at fiber crossing regions, therefore demonstrating a direct advantage of using HDFT in evaluating lesions surrounded by multiple crossing fibers.

2.6 Discussion

Most incidental supratentorial CMs can be managed conservatively. Symptomatic CMs can be considered for microsurgical resection with the indications being: progressive neurological deficit; documented episodes of recurrent bleeding; medically intractable seizures and the need to establish a tissue diagnosis.[4] A surgical decision-making analysis in cerebral CMs demonstrated a 0.4 to 2.8% combined morbidity and mortality risk for superficial lesions with surgery being more justified in younger patients.[34] In our series of 10 relatively young patients, surgical resection was offered in nine and carried out in seven. Eight patients' symptomatology were directly related to the CM; while one had a complex migraine disorder, potentially attributable to the CM[35, 36] and the other (patient 10) demonstrated displacement of the right SLF/AF, implicated in vertigo.[37]

2.6.1 Qualitative data and its implications, clinical symptomatology

In all cases, the HDFT scans provided optimal qualitative data with respect to the relevant perilesional tracts and assessed their position precisely with respect to the CMs (Figure 1-6). This facilitated decision making and appropriate surgical trajectory planning, minimizing morbidity from potential approaches. In our preliminary series, the HDFT data, when sequentially analysed with respect to qualitative and quantitative information, seemed largely consistent with the patients' symptomatology.

An advantage of using superior qualitative data lies in defining the anatomical location of the CMs in a three-dimensional manner in relation to the WM tracts. In addition to optimizing the visualization of eloquent tracts and their relationship to the CM, we also obtained good qualitative data regarding tracts, considered either non-eloquent or difficult to reconstruct in their entirety using DTI, for example UF/IOF, TPC or non-dominant AF/SLF. These principles underlying the usefulness of HDFT were illustrated by our cases; e.g. in patient 9 (Figure 5) we defined CM's location in the UF and took advantage of the established damage. In patient 7 using HDFT (Figure 4), we determined the orientation of three fiber tracts i.e. AF, TPC and CST

and associated qualitative effect in relation to the left parietal CM in a three-dimensional manner and chose a surgical route through the postcentral sulcus. In patients 1, 9, 10, the CMs' relationship to non-eloquent tracts was also examined, aimed at neural preservation and minimizing injury to the WM tracts, eloquent or non-eloquent. Non-dominant SLF may serve spatial awareness by integrating the visuospatial and audiospatial information[38] and is thought to play a role in the vestibular multimodal network including in nystagmus and vertigo.[37, 39] UF is implicated in a circuitry involved in retrieval of word form for proper names.[40]

Lazar et al., examined the use of DTI and tractography in six patients, including two with supratentorial CMs[21] using pre- and postoperative data. For most cases, the principal eigenvector colour maps were useful for identifying specific perilesional WM tracts, while in some tractography approach was used. Patterns of tract alterations described included ‘deviation’; ‘interruption’ (partial or complete) and 'degeneration'. In two with CMs, evidence of deviation of the perilesional tracts was found.[21] A further strength of our study is related to demonstrating multiple crossing fibers in the proximity to the CMs, an acknowledged limitation with DTI.[16-18, 41] We simplified the qualitative change in the WM tracts (Table 1) due to superior qualitative data obtained in terms of complex spatial relationships between multiple perilesional tracts (including nature of their change (Figure 1-6)) and CMs in a three dimensional fashion and due to lack of heterogeneity in the disease states in our study. Similar to Lazar, we found that patterns of changes in WM tracts are not exclusive and therefore, disruption to varying degrees can be associated with displacement. Interestingly, based on qualitative data regarding the affected tracts (Table 1), there was evidence of hemibody numbness or sensory disturbance in three of four with displaced or disrupted TPC fibers and evidence of motor dysfunction and qualitative changes in affected CST in two cases. Patient 4 is noteworthy due to presence of mild hemiparesis despite complete disruption of CST (Figure 3); based on our reconstructions, this could be due to a potential ‘recruitment’ phenomenon of some of the premotor fibers continuing on towards the brainstem (Figure 3), towards serving motor function. Finally, one of two patients with affected dominant SLF/AF was symptomatic with dysphasia, as was one of two with affected non-dominant SLF with vestibular symptoms. These highlight a potential correlation between qualitative data and patients’ symptomatology.

2.6.2 Quantitative data and implications

FA, a commonly used DTI measure[19, 42] has been applied in multiple conditions including multiple sclerosis,[43] stroke,[44] amyotrophic lateral sclerosis,[45-47] CMs[15] and brain tumours.[21, 48] Changes in FA may potentially reflect changes in organisation of fibers[49] with a reduction reflecting axonal degeneration and myelin breakdown.[50, 51] The major limitation with FA is linked to its underestimation in regions containing crossing fibers[19] like centrum semiovale, due to a certain degree of voxel size/shape dependent change. Such limitations are accentuated around lesions with surrounding oedema and mass effect[18, 21, 52] with potential thinning of the tracts, contributing further to partial volume effects and data's misinterpretation.

New fiber mapping techniques such as high-angular-resolution diffusion imaging[53] and DSI addressed these limitations with the latter measuring diffusion spectra and enabling resolution of intravoxel heterogeneity of diffusion, thereby resolving not the average direction, as in DTI, but a set of directions of multiple pathways or fiber orientations within a voxel.[23] We therefore used mean QA, a directionally specific quantitative measure to provide us with indirect information regarding the integrity of the whole WM tract and in certain cases with respect to the specific perilesional segment. Overall mean QA, although broadly similar for most tracts, for patient 4 represented a reduction of approximately 53% and 35% for the perilesional TPC and the CST fibers respectively, compatible with the observed complete disruption. The consistent pattern of slightly increased overall mean QA for the SLF/ AF on the left in the patient group, is probably related to the left hemisphere dominance; for the control group, this value was 4.3% higher on the left compared to right. In the control group, the observed maximum percentage difference between the two sides in the mean QA for the divided tract segments at 9% was higher than (particularly for CST) that noted in segment 2 (corresponding to the perilesional segment), where fibers were more organized. Mean QA for the perilesional segment was consistent with the qualitative data in all five assessed tracts (Table 3). In tracts with disruption with or without displacement, the drop in QA in the perilesional segment varied from approximately 24 to 85%. These cases had tract-specific symptoms, with the exception of one featuring a partially disrupted non-dominant SLF. Patient 4 with

complete left CST disruption had associated drop in the mean QA values for all segments, therefore the tract was considered ‘degenerated’[21] representing craniocaudal compromise of its integrity. In the two patients analysed similarly with displaced AF/ SLF and tract-specific symptoms, the perilesional segments' values were comparatively higher. The quantitative data regarding the perilesional segments were consistent with our hypothesis regarding its decrease or increase, while evaluating disruption or displacement respectively in an affected tract.

2.6.3 Combination of qualitative and quantitative approach, limitations and future directions

Cauley and colleagues,[15] using DTI demonstrated that WM tracts deviated around CMs with tracts passing through the peripheral hemosiderin rim, which was found to have a high FA value relative to central lesion or adjacent WM. This was thought to be related to the mass effect and ‘crowding’ of WM or to iron's susceptibility effects in the rim and its effect on the signal to noise ratio. Tract-specific information was not detailed. Our combined approach demonstrated that WM tracts around CMs may be displaced and/or disrupted to varying extent, in line with their biological behaviour, particularly so for symptomatic CMs with recurrent microhaemorrhages. The usefulness of this approach was illustrated by patient 3, where an anterolaterally displaced CST also seemed ‘qualitatively’ partially disrupted; the latter interpretation seemed more likely with the drop observed with the QA-based perilesional segment analysis, as the overall QA of the CST on both sides were very similar. The affected CST however, had functional integrity and therefore, due to the risk of injury to a compromised yet functioning tract, we managed him conservatively.

The limitations of qualitative data from DTI had led Lazar[21] to state that with mass lesions, an abnormal trajectory may be either pathological or technical in origin and be difficult to interpret. This paradigm still applies to HDFT data, while cautiously interpreting the abnormal results with a sound knowledge of the perilesional neuroanatomy. The quantitative data overall adds a further degree of ‘confidence’, due to the inherent subjectivity in qualitative data's interpretation. A comprehensive direct comparison of HDFT with DTI is outside the scope of this paper with their use, based partly at least on surgeons' and institutional preference; however in our

experience, including in the current series and as demonstrated by the case examples (Figure 7 and 8), HDFT has provided us with superior qualitative data, and further allowed us to propose and apply a quantitative analytical technique with respect to perilesional segments, at best done previously using overall FA of the tracts in DTI studies.[21]

The limitations in our study relate to a small sample size with related selection bias, as patients' underwent HDFT predominantly due to the CMs' location, and the need for further validation of QA, as a marker of white matter integrity, including in establishing its range of variability between the two sides, currently based on the 'template' analysis. This will be pertinent for AF, with a higher expected QA value on the dominant side. CMs are found at variable locations in the WM, making perilesional segments' analysis difficult, particularly for AF, which compared with CST has a wider area of origin; termination and is oriented in the anteroposterior and superoinferior directions. We, therefore aim to create an 'automated' QA profile, using multiple points in the perilesional and contralateral WM tracts to obtain a better picture of craniocaudal integrity, particularly useful for partial disruption without extensive tract compromise, including of overall QA. A further limitation pertains to the susceptibility artifact related to the CM, which may account for 'false' or 'artifactual' disruption of the WM tract, e.g. explaining partly preserved motor function in patient 4 despite CST disruption. Although craniocaudal compromise of QA beyond the perilesional segment argues against this, in order to address this, importantly for localized partial disruption without extensive tract compromise, we are performing pre- and postoperative HDFT on patients with CMs and neoplasms. We expect a 'truly' disrupted tract (partial or complete) and its associated qualitative and quantitative characteristics and related deficits to remain mostly unchanged after the lesion's removal with the reverse being true for displaced tracts.

This approach is potentially useful towards prognostication and assessing the chances of neurological recovery after surgery. In view of the preliminary accuracy of cortical termination points of HDFT,[22] we are evaluating its correlation with the functional data obtained from fMRI and with results from intraoperative WM stimulation for cerebral lesions. Further the long DSI sequence can now be improved by using a multi-band acquisitions sequence,[54] leading to substantial reduction of

scanning time to 10 to 15 minutes and additional improved patient comfort during future clinical studies without compromising accuracy.

2.7 Conclusions

In a preliminary series, we demonstrated the utility of HDFT in providing superior qualitative data with respect to spatial relationship of the CMs to the perilesional WM tracts in a three dimensional manner and further in characterising these changes in terms of disruption and/ or displacement, both of which can occur to a varying extent. These qualitative changes optimized decision making and/or surgical trajectory planning; potentially correlated with the patients' symptomatology and were further elucidated using a novel quantitative marker, highlighting the need for a combined qualitative and quantitative approach, while evaluating perilesional WM tracts.

2.8 References

1. Moriarity JL, Clatterbuck RE, Rigamonti D. The natural history of cavernous malformations. *Neurosurg Clin N Am.* Jul 1999;10(3):411-417.
2. Bertalanffy H, Benes L, Miyazawa T, Alberti O, Siegel AM, Sure U. Cerebral cavernomas in the adult. Review of the literature and analysis of 72 surgically treated patients. *Neurosurg Rev.* Mar 2002;25(1-2):1-53; discussion 54-55.
3. McLaughlin MR, Kondziolka D, Flickinger JC, Lunsford S, Lunsford LD. The prospective natural history of cerebral venous malformations. *Neurosurgery.* Aug 1998;43(2):195-200; discussion 200-191.
4. Shah M, Heros RC. *Microsurgical treatment of supratentorial lesions*. In: Awad IA, Barrow DL, eds. *Cavernous Malformations.* Park Ridge, Ill.: American Association of Neurological Surgeons; 1993; 101-116.
5. Abla AA, Lekovic GP, Turner JD, de Oliveira JG, Porter R, Spetzler RF. Advances in the treatment and outcome of brainstem cavernous malformation surgery: a single-centre case series of 300 surgically treated patients. *Neurosurgery.* Feb 2011;68(2):403-414; discussion 414-405.

6. Kim DS, Park YG, Choi JU, Chung SS, Lee KC. An analysis of the natural history of cavernous malformations. *Surg Neurol.* Jul 1997;48(1):9-17; discussion 17-18.
7. Monaco EA, Khan AA, Niranjan A, et al. Stereotactic radiosurgery for the treatment of symptomatic brainstem cavernous malformations. *Neurosurg Focus.* Sep 2010;29(3):E11.
8. Chen X, Weigel D, Ganslandt O, Buchfelder M, Nimsky C. Diffusion tensor imaging and white matter tractography in patients with brainstem lesions. *Acta Neurochir (Wien).* Nov 2007;149(11):1117-1131; discussion 1131.
9. Chen X, Weigel D, Ganslandt O, Fahlbusch R, Buchfelder M, Nimsky C. Diffusion tensor-based fiber tracking and intraoperative neuronavigation for the resection of a brainstem cavernous angioma. *Surg Neurol.* Sep 2007;68(3):285-291; discussion 291.
10. McLaughlin N, Kelly DF. Corticospinal tractography as a prognosticator for motor improvement after brainstem cavernoma resection. *Br J Neurosurg.* Feb 2013;27(1):108-110.
11. Royo A, Utrilla C, Carceller F. Surgical management of brainstem-expanding lesions: the role of neuroimaging. *Semin Ultrasound CT MR.* Apr 2013;34(2):153-173.
12. Mai JC, Ramanathan D, Kim LJ, Sekhar LN. Surgical resection of cavernous malformations of the brainstem: evolution of a minimally invasive technique. *World Neurosurg.* May-Jun 2013;79(5-6):691-703.
13. Jhawar S, Nadkarni T, Goel A. Giant cerebral cavernous hemangiomas: a report of two cases and review of the literature. *Turk Neurosurg.* 2012;22(2):226-232.
14. Nimsky C, Ganslandt O, Fahlbusch R. Implementation of fiber tract navigation. *Neurosurgery.* Jul 2007;61(1 Suppl):306-317; discussion 317-308.
15. Cauley KA, Andrews T, Gonyea JV, Filippi CG. Magnetic resonance diffusion tensor imaging and tractography of intracranial cavernous malformations: preliminary observations and characterisation of the hemosiderin rim. *J Neurosurg.* Apr 2010;112(4):814-823.
16. Alexander DC, Barker GJ. Optimal imaging parameters for fiber-orientation estimation in diffusion MRI. *NeuroImage.* Aug 15 2005;27(2):357-367.

17. Le Bihan D, Poupon C, Amadon A, Lethimonnier F. Artifacts and pitfalls in diffusion MRI. *J Magn Reson Imaging.* Sep 2006;24(3):478-488.
18. Alexander AL, Hasan KM, Lazar M, Tsuruda JS, Parker DL. Analysis of partial volume effects in diffusion-tensor MRI. *Magn Reson Med.* May 2001;45(5):770-780.
19. Oouchi H, Yamada K, Sakai K, et al. Diffusion anisotropy measurement of brain white matter is affected by voxel size: underestimation occurs in areas with crossing fibers. *AJNR Am J Neuroradiol.* Jun-Jul 2007;28(6):1102-1106.
20. Zolal A, Hejcl A, Vachata P, et al. The use of diffusion tensor images of the corticospinal tract in intrinsic brain tumor surgery: a comparison with direct subcortical stimulation. *Neurosurgery.* Aug 2012;71(2):331-340; discussion 340.
21. Lazar M, Alexander AL, Thottakara PJ, Badie B, Field AS. White matter reorganisation after surgical resection of brain tumours and vascular malformations. *AJNR Am J Neuroradiol.* Jun-Jul 2006;27(6):1258-1271.
22. Fernandez-Miranda JC, Pathak S, Engh J, et al. High-definition fiber tractography of the human brain: neuroanatomical validation and neurosurgical applications. *Neurosurgery.* Aug 2012;71(2):430-453.
23. Wedeen VJ, Hagmann P, Tseng WY, Reese TG, Weisskoff RM. Mapping complex tissue architecture with diffusion spectrum magnetic resonance imaging. *Magn Reson Med.* Dec 2005;54(6):1377-1386.
24. Yeh FC, Wedeen VJ, Tseng WY. Generalised q-sampling imaging. *IEEE Trans Med Imaging.* Sep 2010;29(9):1626-1635.
25. Yeh FC, Verstynen TD, Wang Y, Fernandez-Miranda JC, Tseng WY. Deterministic diffusion fiber tracking improved by quantitative anisotropy. *PloS one.* 2013;8(11):e80713.
26. Verstynen T, Jarbo K, Pathak S, Schneider W. In vivo mapping of microstructural somatotopies in the human corticospinal pathways. *J Neurophysiol.* Jan 2011;105(1):336-346.
27. Wang Y, Fernandez-Miranda JC, Verstynen T, Pathak S, Schneider W, Yeh FC. Rethinking the role of the middle longitudinal fascicle in language and auditory pathways. *Cereb Cortex.* Oct 2013;23(10):2347-2356.

28. Jarbo K, Verstynen T, Schneider W. In vivo quantification of global connectivity in the human corpus callosum. *NeuroImage.* Feb 1 2012;59(3):1988-1996.
29. Greenberg AS, Verstynen T, Chiu YC, Yantis S, Schneider W, Behrmann M. Visuotopic cortical connectivity underlying attention revealed with white-matter tractography. *J Neurosci.* Feb 22 2012;32(8):2773-2782.
30. Verstynen TD, Badre D, Jarbo K, Schneider W. Microstructural organisational patterns in the human corticostriatal system. *J Neurophysiol.* Jun 2012;107(11):2984-2995.
31. DSI-Studio. Available at: http://dsi-studio.labsolver.org.Accessed March 22, 2013.
32. Cognitive Axon Lab. The Carnegie Mellon University (CMU)-30 DSI template. Available at: http://www.psy.cmu.edu/~coaxlab/?page_id=305. Accessed July 30, 2013.
33. Yeh FC, Tseng WY. NTU-90: a high angular resolution brain atlas constructed by q-space diffeomorphic reconstruction. *NeuroImage.* Sep 1 2011;58(1):91-99.
34. Chang HS, Hongo K, Nakagawa H, Tsuge T. Surgical decision-making on cerebral cavernous malformations. *J Clin Neurosci.* Sep 2001;8(5):416-420.
35. Afridi S, Goadsby PJ. New onset migraine with a brain stem cavernous angioma. *J Neurol Neurosurg Psychiatry.* May 2003;74(5):680-682.
36. Sakakibara Y, Taguchi Y, Uchida K. [A case of cavernous angioma presenting as migrainous attack]. *No Shinkei Geka.* Mar 2010;38(3):287-291.
37. Spena G, Gatignol P, Capelle L, Duffau H. Superior longitudinal fasciculus subserves vestibular network in humans. *Neuroreport.* Sep 18 2006;17(13):1403-1406.
38. Fernandez-Miranda JC, Rhoton AL, Jr., Alvarez-Linera J, Kakizawa Y, Choi C, de Oliveira EP. Three-dimensional microsurgical and tractographic anatomy of the white matter of the human brain. *Neurosurgery.* Jun 2008;62(6 Suppl 3):989-1026; discussion 1026-1028.
39. Kahane P, Hoffmann D, Minotti L, Berthoz A. Reappraisal of the human vestibular cortex by cortical electrical stimulation study. *Ann Neurol.* Nov 2003;54(5):615-624.

40. Papagno C, Miracapillo C, Casarotti A, et al. What is the role of the uncinate fasciculus? Surgical removal and proper name retrieval. *Brain.* Feb 2011;134(Pt 2):405-414.
41. Fernandez-Miranda JC. Editorial: Beyond diffusion tensor imaging. *J Neurosurg.* Jun 2013;118(6):1363-1365; discussion 1365-1366.
42. Basser PJ, Pierpaoli C. Microstructural and physiological features of tissues elucidated by quantitative-diffusion-tensor MRI. *J Magn Reson B.* Jun 1996;111(3):209-219.
43. Guo AC, MacFall JR, Provenzale JM. Multiple sclerosis: diffusion tensor MR imaging for evaluation of normal-appearing white matter. *Radiology.* Mar 2002;222(3):729-736.
44. Thomalla G, Glauche V, Koch MA, Beaulieu C, Weiller C, Rother J. Diffusion tensor imaging detects early Wallerian degeneration of the pyramidal tract after ischemic stroke. *NeuroImage.* Aug 2004;22(4):1767-1774.
45. Sach M, Winkler G, Glauche V, et al. Diffusion tensor MRI of early upper motor neuron involvement in amyotrophic lateral sclerosis. *Brain.* Feb 2004;127(Pt 2):340-350.
46. Iwata NK, Kwan JY, Danielian LE, et al. White matter alterations differ in primary lateral sclerosis and amyotrophic lateral sclerosis. *Brain.* Sep 2011;134(Pt 9):2642-2655.
47. van der Graaff MM, Sage CA, Caan MW, et al. Upper and extra-motoneuron involvement in early motoneuron disease: a diffusion tensor imaging study. *Brain.* Apr 2011;134(Pt 4):1211-1228.
48. De Belder FE, Oot AR, Van Hecke W, et al. Diffusion tensor imaging provides an insight into the microstructure of meningiomas, high-grade gliomas, and peritumoral oedema. *J Comput Assist Tomogr.* Sep-Oct 2012;36(5):577-582.
49. Beaulieu C. The basis of anisotropic water diffusion in the nervous system - a technical review. *NMR Biomed.* Nov-Dec 2002;15(7-8):435-455.
50. Beaulieu C, Does MD, Snyder RE, Allen PS. Changes in water diffusion due to Wallerian degeneration in peripheral nerve. *Magn Reson Med.* Oct 1996;36(4):627-631.

51. Ciccarelli O, Behrens TE, Altmann DR, et al. Probabilistic diffusion tractography: a potential tool to assess the rate of disease progression in amyotrophic lateral sclerosis. *Brain.* Jul 2006;129(Pt 7):1859-1871.
52. Provenzale JM, McGraw P, Mhatre P, Guo AC, Delong D. Peritumoral brain regions in gliomas and meningiomas: investigation with isotropic diffusion-weighted MR imaging and diffusion-tensor MR imaging. *Radiology.* Aug 2004;232(2):451-460.
53. Tuch DS, Reese TG, Wiegell MR, Makris N, Belliveau JW, Wedeen VJ. High angular resolution diffusion imaging reveals intravoxel white matter fiber heterogeneity. *Magn Reson Med.* Oct 2002;48(4):577-582.
54. Sotiropoulos SN, Jbabdi S, Xu J, et al. Advances in diffusion MRI acquisition and processing in the Human Connectome Project. *NeuroImage.* Oct 15 2013;80:125-143.

2.9.1 Figures

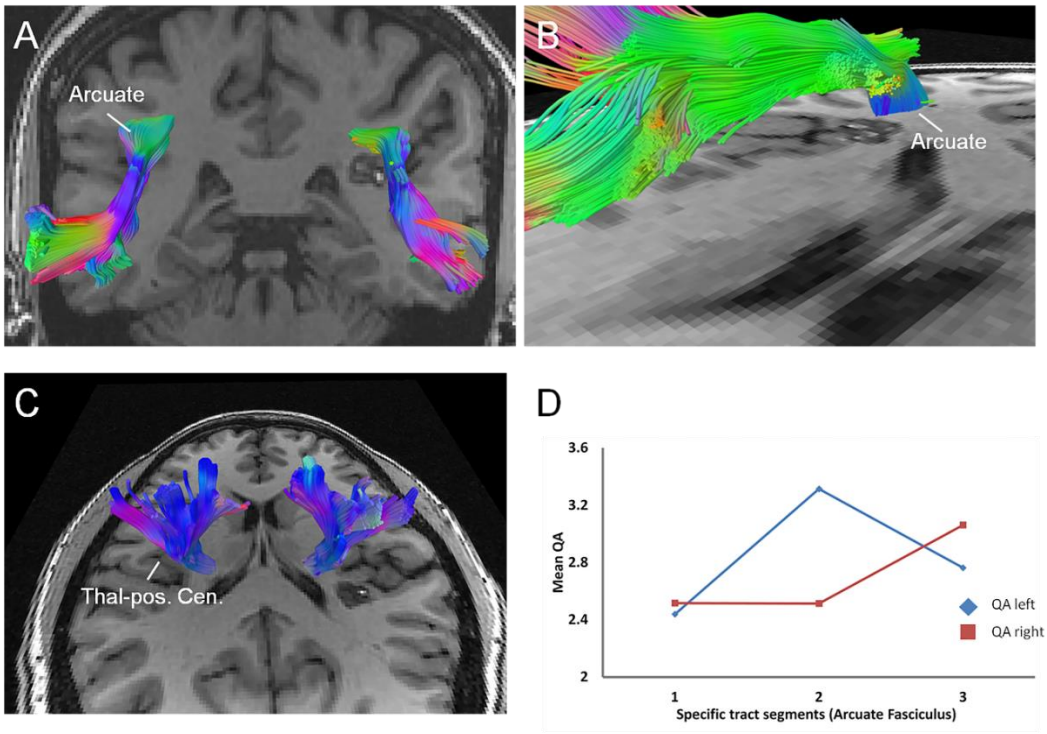

FIGURE 1. High Definition Fiber Tractography analysis in patient 1 demonstrated (note MRI scans have been flipped) **A**, partial disruption of the right arcuate fasciculus (AF) around the right periatrial CM, seen in relation to the left AF. **B**, a closer view showing the partial disruption of the right arcuate. **C**, medial displacement of the right thalamopostcentral (Thal-pos.Cen.) fibers, in relation to the contralateral tract. **D,** quantitative analysis, including comparison of the mean quantitative anisotropy values for three segments of AF bilaterally, demonstrated a reduction in the value for the right perilesional segment or 'segment 2', compared with the left, supporting disruption.

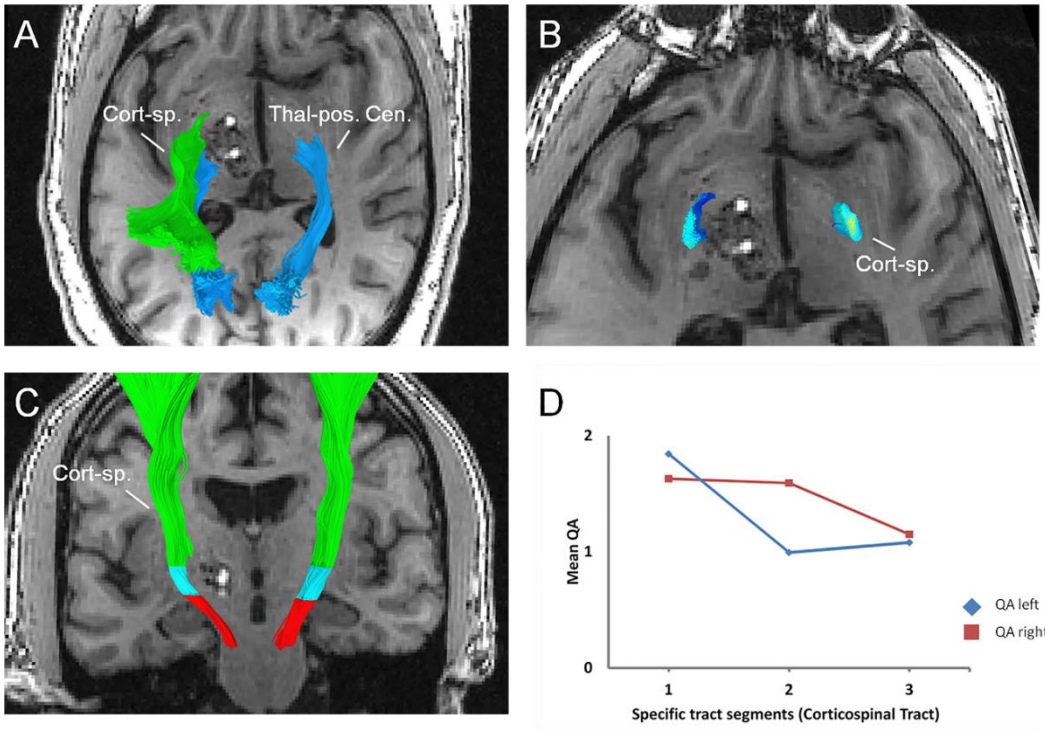

FIGURE 2. High Definition Fiber Tractography (HDFT) analysis in patient 3 (note MRI scans have been flipped) with a left thalamic cavernous malformation (CM). **A,** HDFT revealed an anterolaterally displaced and partially disrupted left corticospinal (Cort-sp.) tract, adjacent to the CM with further accompanying posteromedial displacement of the left thalamopostcentral (Thal-pos.Cen.) fibers in relation to the contralateral side. **B**, quantitative anisotropy (QA) representation (local index map) of the perilesional Cort-sp. segment with medial fibers, closer to the CM with lower values (darker blue) suggesting disruption and those more lateral with a higher value (lighter blue), implying potential displacement. **C**, representative division of the Cort-sp. tract into three segments for the perilesional QA-based analysis (segment 1: green; segment 2: blue; segment 3: red). **D,** quantitative analysis, including comparison of the mean QA values for three segments of the Cort-sp. tracts bilaterally, demonstrated a reduction in the value for the left perilesional segment or 'segment 2', compared to the right, suggesting disruption.

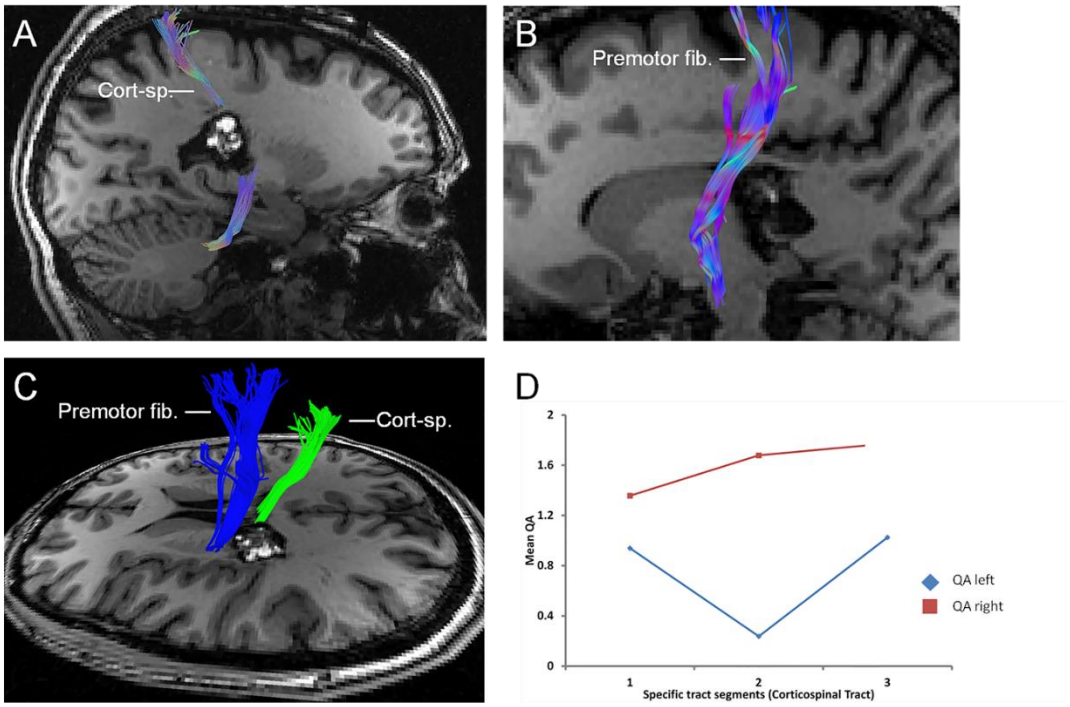

FIGURE 3. A, High Definition Fiber Tractography analysis in patient 4 (note MRI scans have been flipped) with a left thalamic cavernous malformation (CM). **A,** complete disruption with major discontinuity in left corticospinal (Cort-sp.) tract in relation to the CM, as seen on a sagittal slice. **B,** premotor fibers (fib.), anterior to the CM, continuing on towards the brainstem, and potentially serving motor function. **C,** orientation of the Cort-sp. tract and the premotor fibers in relation to each other, as seen on an axial MRI slice. **D,** quantitative analysis (mean quantitative anisotropy-based perilesional segment analysis) of the Cort-sp. tracts bilaterally, demonstrated a reduction in the value for all three segments of the left Cort-sp. tract, with marked decrease noted for the perilesional segment, representing overall craniocaudal compromise.

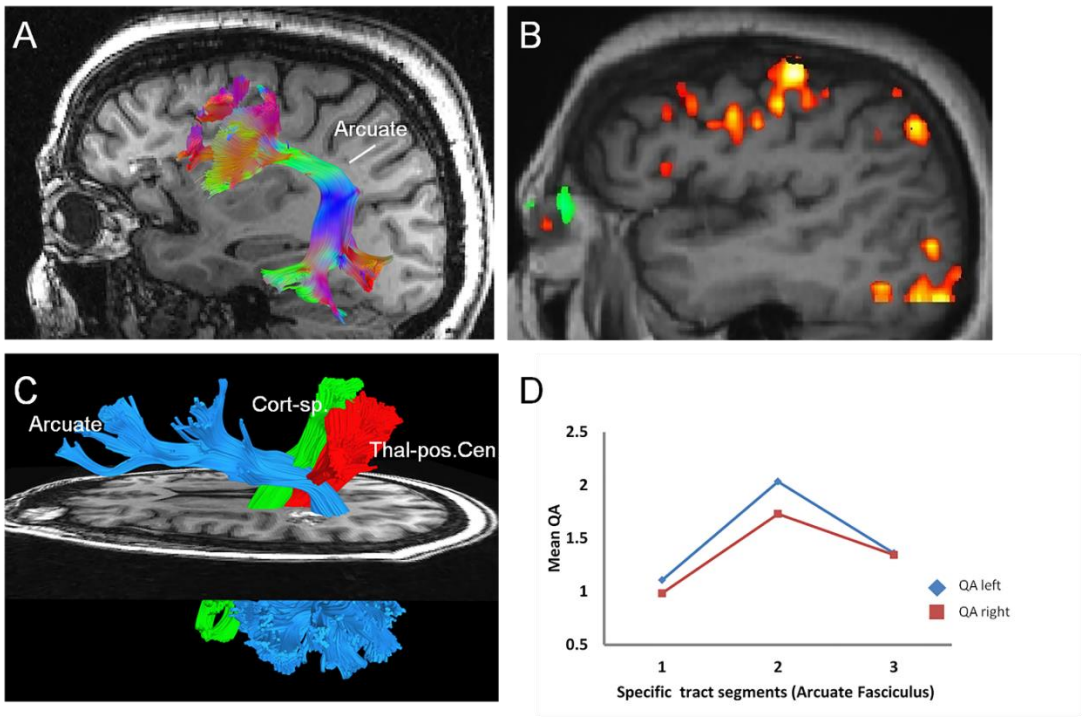

FIGURE 4. A, High Definition Fiber Tractography (HDFT) analysis in patient 5 demonstrated frontal origin of the arcuate fasciculus (AF) in the pars triangularis area in relation to the cavernous malformation (CM) located in the pars orbitalis. **B,** functional MRI in the same patient showed frontal language areas posterior to the lesion, at pars triangularis and opercularis and ventral premotor cortex, consistent with the HDFT. **C,** HDFT analysis in patient 7 (note MRI scan has been flipped) showed posterior displacement of the arcuate around the left parietal CM with anteromedial displacement of the thalamopostcentral (Thal-pos.Cen.) fibers with no effect on the corticospinal (Cort-sp.) tract and with lateral margin being free of the traversing superior longitudinal fasciculus fibers, allowing a surgical approach through post-central sulcus. **D,** quantitative analysis, including comparison of the mean quantitative anisotropy values for three segments of the AF bilaterally in patient 7, demonstrated an increase in the value for the left perilesional segment or 'segment 2', compared to the right, supporting displacement.

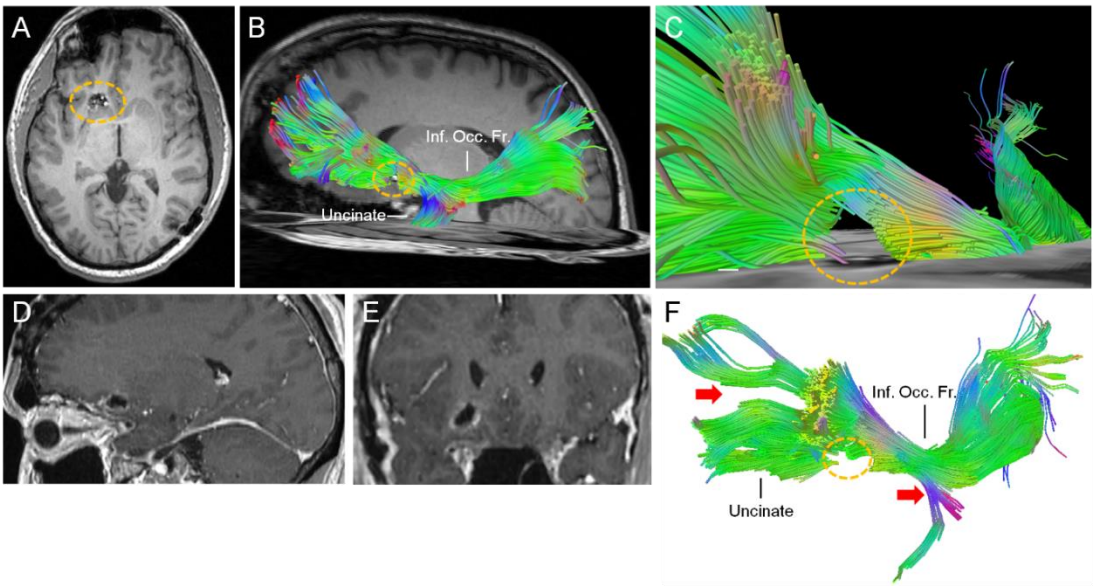

FIGURE 5. A, an axial MR slice (note MRI scans have been flipped) demonstrating a cavernous malformation (CM) in patient 9 in the left orbitofrontal region, adjacent to the caudate head. **B,** High Definition Fiber Tractography (HDFT) demonstrating partial disruption of the left orbitofrontal segment of the uncinate fasciculus in relation to the CM with inferior occipito-frontal (Inf. Occ. Fr.) fasciculus, being directed posteriorly towards temporal and the occipital lobes. **C,** a close-up view of the partial disruption of the left orbitofrontal segment of the UF. **D,** post-operative sagittal and **E,** coronal MRI showing resection of the CM via a subfrontal route, taking advantage of the existing fiber damage. **F,** Diffusion tensor imaging-based tractography demonstrating partial disruption of the left orbitofrontal segment of the UF in relation to the CM with Inf. Occ. Fr., being directed posteriorly towards temporal and the occipital lobes; in comparison with HDFT (Figure 5B and C), qualitatively superior part of the orbitofrontal segment (arrow) and proximal part of the temporal segment of the UF (arrow), in particular are thinner with missing fibers.

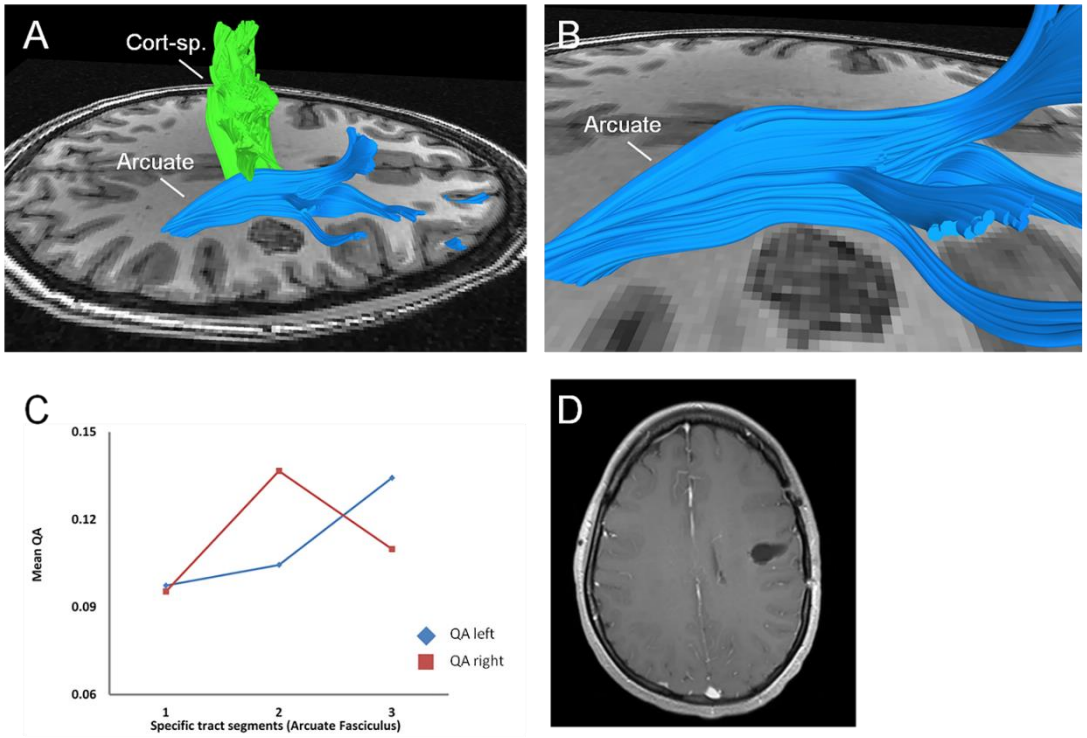

FIGURE 6. A, High Definition Fiber Tractography analysis in patient 10 (note MRI scans have been flipped) displayed the spatial relationship of a cavernous malformation (CM) in the right subcortical white matter, underlying the motor cortex to the corticospinal (Cort-sp.) tract and arcuate fasciculus (AF) fibers with both being on the medial side. **B,** close-up view showing the medial displacement of the arcuate around the right CM. **C,** quantitative analysis with comparison of the mean quantitative anisotropy values for three segments of the AF bilaterally, demonstrated an increase in the value for the right perilesional segment or 'segment 2', compared to the left, supporting displacement. **D,** post-operative MRI showing complete excision via an approach, directed through the central sulcus.

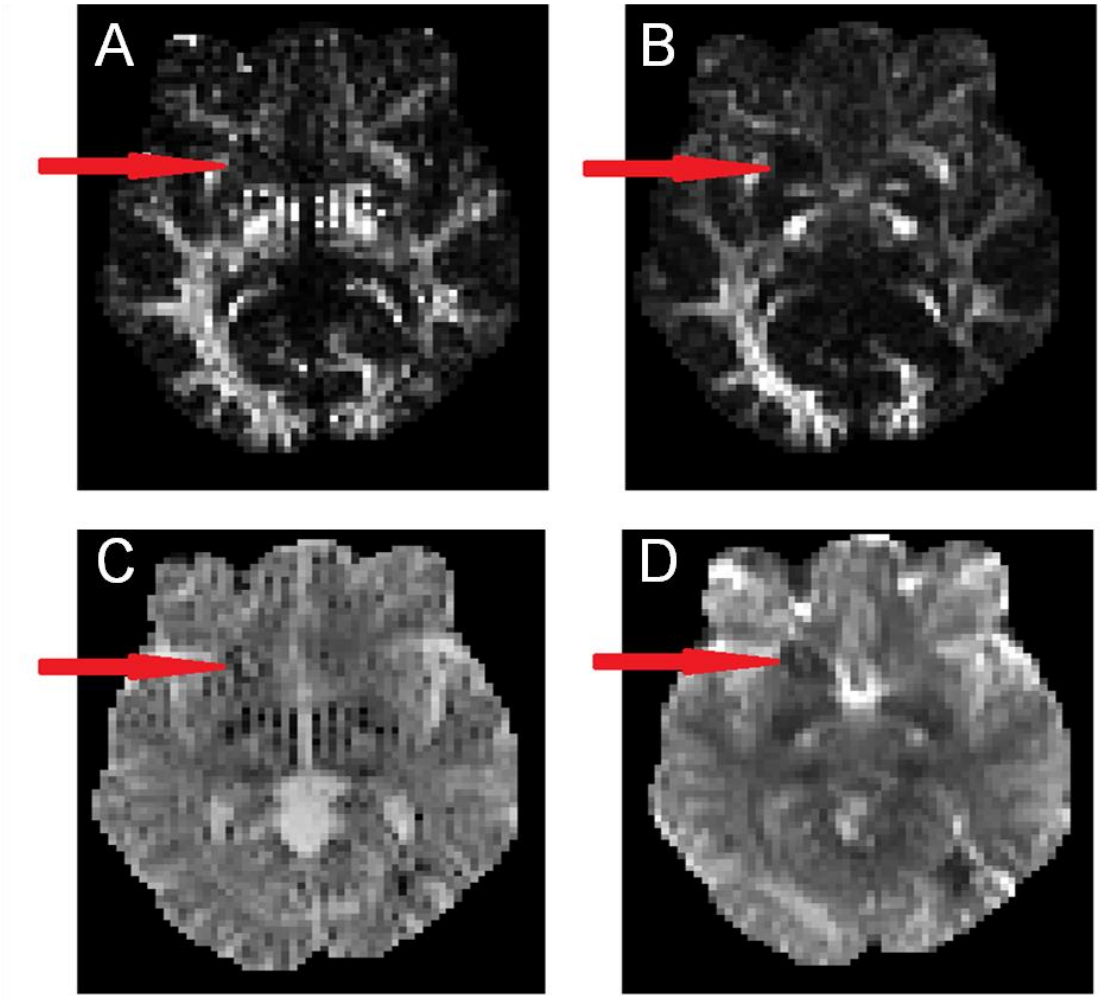

FIGURE 7. Comparison of diffusion tensor imaging and High Definition Fiber Tractography analysis in patient 9, using the same dataset. **A,** The FA map has a noisier profile and the anisotropy decrease in the cavernous malformation (CM) is not readily visible (arrow). **B,** The QA map demonstrates a clearer anisotropy decrease (arrow) in and around the CM. **C,** The ADC map also shows a noisy profile of decreased values in the CM (arrow). **D**, The sum of spin distribution function, derived from generalised q-sampling imaging demonstrates decreased values (arrow) in the CM, which is overall clearer than ADC map.

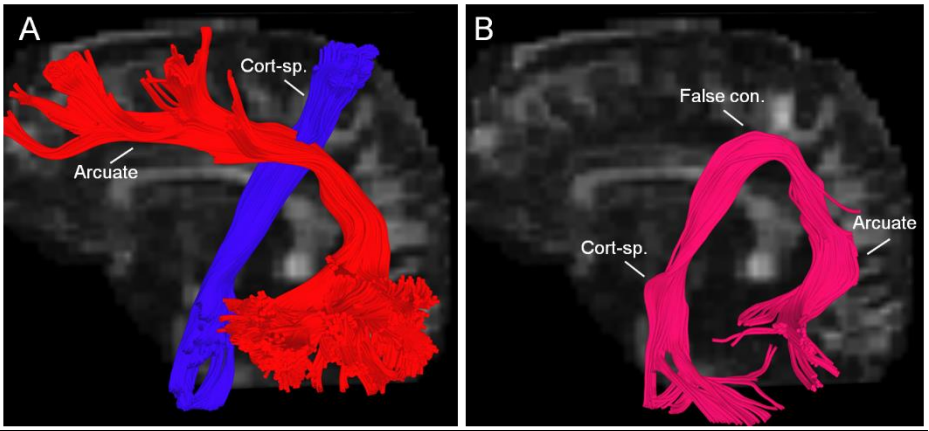

FIGURE 8. Comparison of qualitative data from diffusion tensor imaging (DTI) and High Definition Fiber Tractography (HDFT) analysis in patient 7 with a left parietal cavernous malformation, using the same dataset. **A,** HDFT accurately demonstrated perilesional crossing fibers i.e. arcuate and corticospinal (Cort-sp.) tracts. **B,** In contrast, DTI-based tractography showed false continuation (False con.) between these two fibers despite a stricter angular threshold.

2.9.2 Tables

TABLE 1. Clinical details and characteristics of analysed white matter tracts of interest of patients with cavernous malformations

Patient number	Sex	Age	Location (Side)	Clinical Summary	Tracts of interest	Qualitative information	Management
1 (Figure 1)	F	33	Periatrial (R)	H/A; left hemibody numbness	a) AF/ SLF* b) TPC	a) Partial disruption b) Displacement (slight medial)	Surgical Resection (EPS)
2	M	50	Temporal (L)	Refractory partial seizures	AF/SLF	Unaffected	Surgical resection
3 (Figure 2)	M	53	Thalamus (L)	H/A; right hemiparesis and hemibody anaesthesia	a) CST* b) TPC	a) Displacement (A/L) and partial disruption b) Displacement (P/M)	Conservative
4 (Figure 3)	F	25	Thalamus (L)	Right UMN facial weakness; hemiparesis; diminished proprioception; ataxia	a) CST* b) TPC	a) Complete disruption b) Complete disruption	Offered surgical management (EPS)
5 (Figure 4)	F	67	Pars orbitalis (L)	Simple partial seizures	AF/SLF	Unaffected	Surgical resection
6	F	22	Superior to insula (L)	Complex partial seizures	a) AF/ SLF b) CST	a) Displacement (medial) (for a small fiber segment) b) Unaffected	Offered surgical resection (awake)
7 (Figure 4)	F	66	Parietal (L sensory cortex)	H/A; mild expressive dysphasia	a)AF/ SLF* b) TPC c) CST	a) Displacement (posterior) b) Displacement (A/M) c) Unaffected	Surgical resection
8	F	26	Caudate (R)	Complex migraine	Anterior Limb of IC	Displacement (medial)	Surgical resection (EPS)
9 (Figure 5)	M	53	Orbitofrontal (L)	Seizures	UF/IOF	Partial Disruption	Surgical resection
10 (Figure 6)	F	21	Frontal (R motor cortex)	Light-headedness; vertigo	a) AF/ SLF* b) CST	a) Displacement (S/M) b) Unaffected	Surgical resection

(H/A: headache; AF: arcuate fasciculus; SLF: superior longitudinal fasciculus; TPC: thalamopostcentral; EPS: endoscopic port surgery; CST: corticospinal tract; A/L: anterolateral; P/M: posteromedial; A/M: anteromedial; IC: internal capsule; UF: uncinate fasciculus; IOF: inferior occipito-frontal fasciculus; S/M: superomedial) *: Tracts undergoing further perilesional segment analysis

TABLE 2: Mean QA values of analysed tracts of interest

Patient number (affected side)	Tracts of Interest	Mean QA±SD (Right)	Mean QA±SD (Left)
1 (Right)	AF/SLF TPC	2.68±0.95 2.51±0.87	2.70±0.82 2.53±0.89
2 (Left)	AF/SLF	1.22±0.37	1.50±0.40
3 (Left)	CST TPC	1.43± 0.52 1.26±0.41	1.43±0.65 1.44±0.60
4 (Left)	CST TPC	1.48±0.60 1.22±0.54	0.97±0.31 0.57±0.40
5 (Left)	AF/SLF	1.80±0.65	1.98±0.61
6 (Left)	AF/SLF CST	0.08±0.03 0.16±0.05	0.10±0.04 0.15±0.05
7 (Left)	AF/SLF TPC CST	1.28±0.55 1.24±0.43 1.70±0.68	1.29±0.55 1.25±0.41 1.79±0.77
8 (Right)	Anterior Limb of IC	1.13±0.42	1.15±0.53
9 (Left)	UF/IOF	0.08±0.03	0.09±0.03
10 (Right)	AF/SLF CST	0.10±0.04 0.17±0.07	0.12±0.03 0.18±0.08

(QA: quantitative anisotropy; SD: standard deviation; AF: arcuate fasciculus; SLF: superior longitudinal fasciculus; TPC: thalamopostcentral; CST: corticospinal tract; IC: internal capsule; UF: uncinate fasciculus; IOF: inferior occipito-frontal fasciculus)

TABLE 3: Mean QA values and specific tract analysis (perilesional segment)

Patient number (affected side)	**Qualitative change**	**Tracts of interest**	**Mean QA (segment 1)**	**Mean QA (segment 2)***	**Mean QA (segment 3)**	**Percentage difference (perilesional segment)****
1 (R) (Figure 1)	Partial disruption	R AF/ SLF L AF/SLF	2.52 2.43	2.51 3.32	3.06 2.76	24.2% drop
3 (L) (Figure 2)	Displacement and partial disruption	R CST L CST	1.63 1.84	1.59 0.99	1.15 1.08	37.5% drop
4 (L) (Figure 3)	Complete disruption	R CST L CST	1.36 0.94	1.68 0.24	1.77 1.03	85.9% drop
7 (L) (Figure 4)	Displacement	R AF/SLF L AF/SLF	0.98 1.11	1.73 2.04	1.35 1.36	17.6% increase
10 (R) (Figure 6)	Displacement	R AF/SLF L AF/SLF	0.10 0.10	0.14 0.11	0.11 0.13	30.8% increase

(QA: quantitative anisotropy; R: right; AF: arcuate fasciculus; SLF: superior longitudinal fasciculus; L: left; CST: corticospinal tract) *: perilesional segment on the affected side; **: calculated for the perilesional segment in relation to the unaffected side.

Chapter 3: Longitudinal evaluation of corticospinal tract in patients with surgically resected brainstem cavernous malformations using High Definition Fiber Tractography and diffusion connectometry analysis: preliminary experience

Paper 2: Faraji A*, **Abhinav K***, Jarbo K, Yeh FC, Shin SS, Pathak SK, Hirsch B, Schneider W, Fernandez-Miranda JC, Friedlander RM. Longitudinal evaluation of corticospinal tract in patients with surgically resected brainstem cavernous malformations using High Definition Fiber Tractography and diffusion connectometry analysis: preliminary experience. Journal of Neurosurgery 2015; 5:1-12. (*: equal contributors)

3.1 Declaration

I was the lead first author with respect to this manuscript and was instrumental in devising and further developing the concept of application of quantitative anisotropy (QA)-based perilesional segment analysis and of diffusion connectometry for the first time in longitudinal evaluation of corticospinal tract (CST) in patients with surgically resected *brainstem* cavernous malformations (CMs). Overall, I contributed extensively towards the writing, literature search, figures, study design, data analysis and interpretation.

3.2 Introduction to and brief summary of the manuscript and relation to previous work

Having investigated the use of advanced white matter (WM) imaging techniques/ high definition fiber tractography (HDFT) in supratentorial CMs, the emphasis was now diverted towards further examining the quantitative as well as the qualitative data in patients with brainstem/ infratentorial CMs. Importantly, this data was examined in a longitudinal fashion and in relation to patients' symptomatology in an effort directed towards devising a potential *prognostic model*.

Brainstem CMs are challenging due to a higher symptomatic haemorrhage rate and potential morbidity associated with their surgical resection. The latter is linked to their highly eloquent location in terms of perilesional WM tracts. We aimed to

preoperatively define the relationship of CMs to the perilesional corticospinal tracts (CST) by obtaining qualitative and quantitative data using HDFT. This was similar to the model used with the supratentorial CMs and as discussed in Chapter 2. These data were examined postoperatively by using longitudinal scans and in relation to patients' symptomatology. The extent of involvement of the CST was further evaluated longitudinally using the automated 'diffusion connectometry' analysis. This was the first application of the automated connectometry analysis technique in a neurosurgical condition. The details underlying this methodology are discussed further in the chapter. Fiber tractography was performed with diffusion spectrum imaging (DSI)-Studio using a QA-based generalised deterministic tracking algorithm. Qualitatively and in line with classification with supratentorial CMs, CST was classified as being disrupted and/or displaced. Quantitative analysis involved obtaining mean QA values for the CST and its perilesional and nonperilesional segments. The contralateral homologous CST was used for comparison. Diffusion connectometry analysis included comparison of patients' data with a template from 90 normal subjects. Three patients with symptomatic pontomesencephalic haemorrhagic cavernous malformations and varying degrees of hemiparesis were identified. The mean follow-up period was 37.3 months. Qualitatively, CST was partially disrupted and displaced in all. Direction of the displacement was different in each case and progressively improved corresponding with the patient's neurological status. No patient experienced neurological decline due to surgical resection. The perilesional mean QA percentage decreases supported tract disruption and decreased further over the follow-up period (Case 1: 26% to 49%; Case 2: 35% to 66%; Case 3: 63% to 78%). Diffusion connectometry demonstrated rostrocaudal involvement of the CST consistent with the quantitative data.

Based upon the findings from this study, we concluded that the haemorrhagic brainstem CMs can disrupt and displace perilesional WM tracts with the latter occurring in unpredictable directions. The inability to predict the direction of displacement based upon the anatomical paradigm alone, requires the use of tractography to accurately define the spatial relationship of WM tracts to the malformation such that the surgical entry point can be optimised towards minimising morbidity and improving neurological outcomes. Observed anisotropy decreases in the perilesional segments were consistent with neural injury following haemorrhagic

insults. We concluded that a model using these values in different CST segments can be used to longitudinally monitor its craniocaudal integrity. Diffusion connectometry was deemed to be a complementary approach providing longitudinal information on the rostrocaudal involvement of the CST. The significance of this relates to the ability to predict whether one may recover from weakness (e.g. a stroke-like condition) over a period of time.

3.3 Introduction

Cavernous malformations (CMs) are angiographically occult lesions with an estimated prevalence of 0.4 to 0.8% in the general population.[1,2] Most CMs occur in the supratentorial white matter (WM) with the indications for their surgical resection being controversial.[3] Roughly 9 to 35% of CMs are located in the brainstem[4] and are believed to have higher symptomatic bleeding rates than those in the supratentorial compartment. The estimated bleeding and re-bleeding rates for brainstem CMs range from 0.5 to 6% and 5 to 60% per patient-year respectively.[4-7] The management of brainstem CMs remains challenging due to a high degree of potential morbidity and mortality with and without treatment and specifically due to the eloquence of the perilesional anatomy. Resection is fraught with significant rates of permanent neurologic deterioration including for brainstem CMs reaching the pial surface.[5,8] The increased surgical morbidity is partly due to uncertainty regarding the precise location of the affected WM tracts. Preoperative identification of these tracts in their accurate spatial orientation may lead to a safer surgical corridor to reduce any potential morbidity.

Use of diffusion tensor imaging (DTI) in brainstem CMs' resection with a higher annual average symptomatic haemorrhage rate of 2.7 to 5%,[8-10] has been reported.[11-16] Its limitations include its inability to represent the crossing of multiple fibers or to determine with precision their cortical and subcortical termination.[17,18] DTI indices, e.g. fractional anisotropy (FA) suffer with partial volume effects, leading to underestimation in areas with multiple crossing fibers.[19,20] Despite these, DTI has been an important adjunct in the resection of tumours[21,22] and CMs.[12,13,15,16]

High Definition Fiber Tractography (HDFT), an advanced WM imaging technique, addresses some of the limitations of DTI. HDFT is accurate in tracking fiber

pathways, through complex crossings to subcortical regions and targets.[23] HDFT relies on diffusion spectrum imaging (DSI) for acquisition;[24] generalised q-sampling imaging for fiber orientation estimation, and a generalised deterministic fiber tracking method.[25] We have reported its use in studies on several WM tracts;[26-30] and in a study concerning its utility for surgical planning for space-occupying lesions.[23] Of direct relevance to this report, the utility of HDFT was recently reported in characterising changes in the perilesional WM and in guiding surgical planning in patients with supratentorial CMs using a combined qualitative and quantitative approach.[31]

In this report, we aimed to highlight the utility of HDFT in providing qualitative data with respect to accurately outlining the spatial orientation of the perilesional CST around the brainstem CMs. We demonstrate the usefulness of this information in guiding the surgical resection of haemorrhagic pontomesencephalic CMs while minimizing injury to the motor tracts.[23,32] We further aimed to characterise the perilesional changes in the CST quantitatively using quantitative anisotropy (QA) in line with our previously outlined methodology.[31] This methodology focused on evaluating the integrity of *the perilesional segment* of an affected tract using QA.[31] QA overcomes the limitations of FA in assessing the fiber integrity in areas with multiple crossing fibers being less sensitive to partial volume effects, as demonstrated in our recent study.[25]

The resistance of QA to multiple crossing fibers also enabled us to aim to indirectly ascertain the craniocaudal integrity of the affected CST by obtaining quantitative information with respect to three rostrocaudal segments (perilesional; proximal and distal to the lesion). We longitudinally monitored the qualitative and quantitative tractography data aiming to indirectly assess the craniocaudal integrity of an affected tract over time.

Finally, due to limitations associated with tractography-based studies and to validate our findings, we obtained longitudinal qualitative information regarding the involvement of CST by adaptation of our so-called *diffusion connectometry* approach.[33] This automated approach permitted comparison of our patients' data with a template created from the imaging data of normal healthy subjects to identify the affected tracts. It identifies tracts with decreased or increased connectivity in the *affected* individuals (e.g., in patients with brainstem CMs) compared with a *normal* population. The conventional tractography approach relies on choosing regions of

interest (ROI) according to the defined tracts of interest (e.g., CST) before comparing the difference making it vulnerable to reproducibility issues. Diffusion connectometry overcomes these problems as it is an automated technique not involving manual selection of the ROIs and finds the local differences in the diffusion distribution without initiating fiber tracking making it a more robust approach for detecting any real difference in the connectivity. Further details regarding the basic methodology and its adaptation to analyse the longitudinal data can be referred to in our studies on stroke and amyotrophic lateral sclerosis patients.[33,34] It is noteworthy that this is the first report using connectometry analysis in the evaluation of a lesional pathology.

3.4 Methods

3.4.1 Patient Descriptions

All three patients were screened to rule out any contraindications to the longitudinal MR imaging (MRI) scans. Consent was obtained in accordance with the University of Pittsburgh's Institutional Review Board. Analysis of the data was performed blinded to their clinical details. Senior author (RMF) performed the resection of the CM for all cases.

3.4.2 Image Acquisition and Reconstruction

DSI data was acquired on a 3-T Tim Trio System (Siemens, Erlangen, Germany) using a 32-channel coil. A head stabilizer prevented head motion. A 43-minute, 257-direction DSI scan with a twice-refocused spin-echo planar imaging sequence and multiple b values (repetition time = 9916 ms, echo time = 157 ms, voxel size = 2.4x 2.4x2.4 mm, field of view = 231x231 mm, maximum b-value = 7000 s/mm^2) was performed. For anatomical comparisons, we included high-resolution anatomical imaging using a 9-minute T_1-weighted axial magnetization-prepared rapid-acquisition gradient-echo sequence (repetition time = 2110 ms, echo time = 2.63 ms, flip angle = 8 degrees, number of slices = 176, field of view = 256 x 256 mm^2, voxel size = 0.5 x 0.5 x1.0 mm^3). DSI data was reconstructed with a generalised q-

sampling imaging approach. The orientation distribution functions were reconstructed to 642 discrete sampling directions for each pixel and with a diffusion distance scaling parameter of 1.2.

3.4.3 Tractography-based approach: Fiber tracking

DSI-Studio (dsi-studio.labsolver.org) was used to visualize the left and right CST from the DSI datasets using a generalised deterministic tractography method.[25] A whole brain seeding approach using multiple, single-slice ROI and region of avoidance (ROA) masks was implemented. For CST reconstruction, two ROIs were drawn in the axial plane to cover the WM of medulla and the posterior limb of the internal capsule just superior to the midbrain in each hemisphere. Each mask was drawn on a generalised fractional anisotropy map in tissue unaffected by the lesion or the resection procedure. These ROIs were kept constant across all subjects and the longitudinal scans. An ROA was drawn over the corpus callosum (CC) at the sagittal midline to eliminate the false continuation of CST fibers to the contralateral hemisphere. DSI-studio provides a default QA threshold to enable tractography. This default threshold can be adjusted to optimize the white matter coverage. This threshold was then kept constant across the longitudinal scans for the individual subject for depicting the CST. Fiber tracking was initiated from the whole brain seed using all orientations present within a voxel until 20,000 streamlines were detected. In order to maximize the detection of CST, the following parameters were kept constant across all subjects and the longitudinal scans: maximum turning angle of 90 degrees; step size of 0.5 mm; smoothing = 0.8; and a length constraint of 100-200 mm. All fibers terminating outside the precentral gyrus were deleted. In our experience, using a high turning angle allows a better depiction of the CST fibers originating from the lateral aspect of the precentral gyrus.

3.4.4 Tractography-based approach: Qualitative analysis

We described the CST as being disrupted and/or displaced using the contralateral homologous CST for comparison.[31] 'Disruption' may be partial, e.g., due to 'breakage' or thinning of fibers as seen in a cross-section or due to discontinuity in a

limited segment of the tract; or complete if the tract was not seen through most or all of its course. Definition of 'displacement' was strictly limited to a change of location or direction in the affected tract due to the lesion-related mass effect.[22] The qualitative changes were monitored longitudinally.

3.4.5 Tractography-based approach: Quantitative analysis

This followed qualitative analysis and was also carried out in a longitudinal fashion. Mean QA values were obtained for the whole CST on both sides (Table 1). We further used mean QA values for the *perilesional segments* (Supplemental table, Table 2) to check for consistency with the observed qualitative change, as outlined in our previous study (see Supplemental content) on supratentorial CMs.[31]

3.4.6 Diffusion connectometry approach

In this study, we applied diffusion MRI connectometry analysis[34] to evaluate the affected *motoric* tracts in relation to normal subjects. The diffusion data of each subject is reconstructed in a common stereotaxic space using the q-space diffeomorphic reconstruction.[35] The data of the brainstem CM patients was compared with that of 90 normal subjects (NTU-90; mean age: 33 years).[35] A percentile threshold of 5% was used to identify fiber orientations with substantial decrease in diffusion. Deterministic fiber tracking was used to connect these orientations. The length threshold allows differentiation of meaningful findings from random variations.[33,34] Normal subjects may have false-positive affected tracts due to the noise in the diffusion-weighted images, resulting in fragmentation of the tracts. In affected patients e.g., with brainstem CMs the true connectivity difference will continue along the fiber pathways forming *longer affected tracts*. Using length as an index (length threshold), the difference between the random effect and true connectivity difference is statistically tested. The determination of this threshold is a trade-off between sensitivity and specificity with findings becoming more specific with a higher threshold. Based upon our previous studies[33,34] and the current aim to detect changes in the CST, a length threshold of 40 mm was used, resulting in a false discovery rate (FDR) of 0.12 (Figure 1). This means that approximately 12% of the

affected tracts may be identified as being falsely affected. In order to track the longitudinal data, we used the same length threshold and therefore, the FDR to examine the subsequent scan.[33] We hypothesised that any demonstrated change with respect to the visualized affected tracts was real and therefore, an indirect marker of deterioration or improvement in those tracts in patients with brainstem CMs.

These qualitative changes were represented using the MNI T1-weighted template. The affected tracts, as demonstrated by the connectometry, only reveal the *affected segments* of the entire tract which were confirmed to be CST based on their anatomical location and using the 'tracts to ROI' function in the DSI-Studio. Using this function, the end points of the affected segments were projected on to the cortical gyri to confirm their origin from the precentral gyrus. We also examined the segments of the affected CST and their change, as revealed by the connectometry in relation to the quantitative data for the specific CST segments from the tractography-based analysis.

3.5 Results

3.5.1 Case details and tractography-based qualitative data: Patients 1, 2 and 3 (Figs. 2-6; Table 2)

Patient 1

A 24-year-old female experienced a haemorrhage from a left pontomesencephalic CM, and was admitted to another institution with a dense right upper and lower extremity hemiparesis, a right gaze preference, and speech apraxia. Two weeks later, the patient clinically deteriorated and was emergently transferred to our institution. On examination, the patient was fully oriented with a moderate speech apraxia, right facial droop, diplopia upon left lateral gaze, and right-sided tongue deviation. Her strength, as assessed by the British Medical Research Council (MRC) scale, was 5/5 in both the left upper and lower limbs. In the right upper limb, the strength was recorded as 4/5 in the proximal right upper extremity and 0/5 with a trace of finger flexion in the distal right upper extremity. In the right lower limb, her proximal strength was 4/5, while distally she was 1/5. Examination also revealed dysmetria (finger-to-nose testing) and hyperreflexia. There were no sensory deficits.

MRI demonstrated a haemorrhagic CM (Figure 2) in the anterolateral pons with extension into the middle cerebral peduncle and midbrain asymmetrically with left-sided predominance. Pre-operative HDFT (Figs. 2A, 6A) indicated partial disruption and posterior displacement of the left CST fibers. A left-anterior subtemporal transtentorial approach after an extradural anterior petrosectomy was performed.[36] The anterolateral surface of the midbrain revealed a subtle yellow stain which was chosen as the entry point to avoid the perilesional CST fibers with their known posterior displacement. A minimal opening was made into the midbrain to evacuate the hematoma and resect the CM.

Her immediate post-operative examination revealed improved: CN IV and VI palsies with resolving diplopia; facial droop; and dysarthria. Her strength was 4/5 in the proximal right upper extremity and improved to 1/5 with a trace of finger flexion in the distal right upper extremity. In the right lower extremity, her proximal strength was 4/5, while distally she improved to 2/5. Sensory exam was normal. Postoperative MRI was correlated with a three-week post-operative HDFT study to evaluate the impact of surgical resection on the CST (Figure 2B), which demonstrated reduced displacement. At six months follow-up, there was improvement in the patient's neurological status corresponding with the resolution of displacement of the CST on the HDFT (Figure 2C). A neurological examination revealed a slight facial droop; 4+/5 strength in the right upper limb and the proximal right lower limb; 0/5 strength in dorsiflexion and 3/5 in plantarflexion in the distal right lower limb. The patient was independent with her activities of daily living (ADL). Additionally, she was a skilled right-handed artist prior to the haemorrhage and had regained the ability to draw at the last follow-up. Four years and two months following resection of the CM, there is no evidence of recurrence or rehaemmorhage.

Case details and tractography-based qualitative data: Patient 2

A 20-year-old male presented with a one-week history of left-sided headache as well as right-sided weakness and paraesthesias. On examination, he was fully orientated. Left CN IV, VI, and VII palsies were observed with decreased sensation (to light touch) in the right CN V2 distribution. There were no sensory or motor deficits in the left upper and lower limbs. In the right upper and lower limbs, examination revealed increased tone; 4/5 strength; and decreased sensation to light touch. The patient also had mild urinary retention. MRI indicated the presence of a left-sided

posterolateral pontomesencephalic haemorrhagic CM**.** HDFT indicated anteromedial displacement (across the anterior surface of the pons) and partial disruption of the left CST (Figs. 3A, 6B). An apical petrosectomy and a left sided subtemporal transtentorial approach was performed to resect the CM. Using the image guidance and the information from the tractography, the surgical entry point was made along the posterolateral aspect of the pons to resect the haemorrhagic CM. His immediate post-operative examination revealed only a partial left CN VI palsy with resolving diplopia. His strength had improved to 4+/5 in the right upper and right lower extremities. Sensation to all modalities was normal. An immediate post-operative HDFT study demonstrated improvement in the configuration of the left CST with some residual displacement (Figs. 3B, 6B). Over the next three months, his strength remained stable in the right upper and lower limbs at 4+/5 along with complete resolution of his double vision. One year after surgery, he had full strength and was independent with his ADLs. Three years and two months following resection of the CM there is no evidence of recurrence or rehaemmorhage.

Case details and tractography-based qualitative data: Patient 3

A 22-year-old female presented with headache and transient left hemibody paraesthesia and dysesthesias. CT brain demonstrated a 2 cm by 2 cm right thalamic hematoma with mass effect with a negative angiographic workup. One week later, the patient experienced acute onset left leg weakness, which resolved over several hours. MRI demonstrated a resolving hematoma without any conclusive aetiology. Due to the potential surgical morbidity and symptomatic resolution, she was managed conservatively with planned radiological surveillance.

A three-month follow-up MRI demonstrated a 1.7 cm thalamic hematoma extending into the cerebral peduncle with evidence of hemosiderin deposition consistent with a CM. HDFT revealed a laterally displaced and partially disrupted CST (Figs. 4A, 5A, 6). The patient was treated with stereotactic radiosurgery (SRS) in light the lesion's location and her stable neurological condition.

A month after SRS, she had a further mild symptomatic thalamic haemorrhage. Three months after SRS, the patient represented with increasing headache; left hemibody paraesthesia; and distal left lower extremity weakness. CT imaging demonstrated a new 5 cc haemorrhage of the CM with perilesional oedema extending into the right posterior limb of the internal capsule. A solumedrol taper was initiated,

and the patient's weakness resolved though with persistent mild hemibody paraesthesias. A full year since her initial presentation, the patient presented again with increasing headaches and left upper and lower extremity weakness. On examination, the patient was fully orientated. There was evidence of left CNIII and VII palsies; grade 4/5 strength in both the left upper and lower limbs, and decreased sensation to light touch over the left hemibody. CT demonstrated a persistent right-sided thalamic and mesencephalic CM with increased perilesional oedema. A corresponding HDFT (Figs. 4B, 5B) revealed further displacement and deformation of the CST with fibers visualized across the lateral aspect of the haemorrhagic CM. Given her multiple haemorrhagic episodes and deteriorating neurological examination, surgical intervention was strongly recommended.

One week later while considering surgery, the patient's left upper limb strength acutely deteriorated to 4/5 proximally and 0/5 distally. Her left lower limb strength remained 4+/5. A further HDFT (Figs. 4C, 5C) and MRI revealed an increase in the size of the CM-associated haemorrhage with continued displacement of the CST along the posterolateral aspect of the lesion. The patient underwent an image-guided right subtemporal approach to resect the mesencephalic CM. Hemosiderin-stained tissue and hematoma were readily encountered at the anterolateral portion of the mesencephalus. Using the information from the HDFT, an anterior pial opening was made to prevent injury to the posterolaterally displaced CST. Her immediate post-operative examination revealed a partial left CN III palsy and slight left CN VII palsy; grade 1/5 strength in the left upper and 4/5 in the left lower limbs; and decreased sensation to all modalities in the left hemibody. Immediate post-operative MRI and HDFT (Figure 4D) demonstrated complete resection of the CM and improvement in the displacement of the right CST respectively. The patient had continuing neurological improvement, such that she was ambulating with a cane at one-month post-surgery. At the four-month post-operative follow-up, examination revealed complete resolution of the CN deficits and grade 4/5 strength in the left lower limb and proximal upper limb. Distally in the left upper limb her finger extensors were 2/5 and distal flexors were 3/5. The patient was independent with her ADLs and ambulating without an aid. Two years following surgery there is no evidence of rehaemorrhage or recurrence of the CM. Another HDFT scan (Figure 4E) revealed complete resolution of the displacement of the partially disrupted CST, corresponding with her improved neurological status.

3.5.2 Relevant scans for the tractography-based quantitative data and diffusion connectometry approach

The quantitative data and the diffusion connectometry approach-based results are presented with respect to the following HDFT scans for three patients: patient 1 (1, immediate preoperative; 2, three weeks after surgery; 3, six months after surgery); patient 2 (1, immediate preoperative; 2, in the immediate phase after surgery) and patient 3 (1, one year prior to surgery; 3, in the immediate preoperative phase; 4, in the immediate postoperative phase; 5, four months following surgery).

3.5.3 Tractography-based quantitative data: mean Quantitative anisotropy values for the whole CST

Overall mean QA values (Table 1) were generally noted to be lower for the CST on the affected side for all patients. At the initial HDFT scan, the percentage difference in the QA values between the two sides were found to be outside the normal difference range obtained from the template data for all patients. Specifically for patient 1, there was a further drop in the values postoperatively followed by its stabilization at six months follow-up. For patient 2, the differences in the QA values across the two scans were relatively stable. In patient 3, the difference was higher at the baseline followed by its deterioration in the immediate preoperative phase (scan 3). Following surgery and over the follow-up period, the difference in the values between the two sides remained relatively stable for patient 3.

3.5.4 Tractography-based quantitative data: percentage differences in mean Quantitative anisotropy values for the CST segments

In all patients (Table 2, Supplemental Table), the percentage differences (drop) in the mean QA values for the perilesional segments in relation to the unaffected side were higher or outside the range from the control group analysis. This was true across the longitudinal data and was also largely applicable to the non-perilesional segments. Further deterioration in these values were noted for the tract segments over time particularly so for the perilesional and the distal segment. Of note, there was no

improvement in the observed drop for the perilesional segment after resection of the lesion and removal of the blood products.

3.5.5 Diffusion connectometry approach-based qualitative results

In all patients, the affected CST as revealed by the automated connectometry analysis corresponded appropriately to the lesional side. For patient 1, the connectometry analysis at the first scan (preoperative) revealed the affected segment of the CST (Figure 7A) as being predominantly caudal, approximating predominantly to the level of the lesion and to a small distal segment beyond the lesion. At the second scan, three weeks after surgery (Figure 7A) the CST was affected more rostrally with the most caudal segment now not seen as being affected. At the third scan, six months after surgery, there was extension in the involvement of the CST in the craniocaudal direction (Figure 7A). With patient 2, the connectometry analysis of both the pre- and postoperative scans demonstrated a similar rostrocaudal extent of involvement of the CST (Figure 7B). Affected overall segment of the CST as demonstrated approximated to the level of the lesion and segments both proximal and distal to the lesion. In patient 3 with a thalamomesencephalic lesion, both the preoperative (scans 1 and 3, Figure 7C) and the first postoperative scan (scan 4, Figure 7D) demonstrated extensive rostrocaudal involvement of the CST with changes also being observed in the body of the CC. These changes were also present at the last scan four months after surgery (Figure 7D) with the rostral CST on the contralateral side also seen as being affected.

3.6 Discussion

3.6.1 Brainstem cavernous malformations in general

Brainstem CMs have a high degree of morbidity and mortality associated with both their natural history and treatment. Unlike brainstem CMs, supratentorial CMs without a history of prior bleeding have only a 0.6% per year risk of haemorrhage.[10] In a recent study evaluating the haemorrhage risks of untreated brainstem CMs, the annual haemorrhage rates in patients initially presenting with haemorrhage and focal neurological deficits was 15.9%.[6]

Patients with brainstem CMs can be managed conservatively or treated with either radiosurgery[10] and/or surgical resection. Although the risk of postoperative rehaemorrhage following surgery was reduced to 2.0% per year in one series, high rates of new post-surgical deficits are routinely reported.[4,5,37] Despite advances in the microsurgical techniques, in a large single centre-series of 260 adult patients with surgically treated brainstem CMs, 53% of the patients developed new or worsening neurological symptoms postoperatively with these neurological deficits being permanent in 36%.[8] This is not surprising in light of the eloquent perilesional WM.

In cases presenting with acutely symptomatic haemorrhagic brainstem CM, operative resection[15] may be the most effective treatment strategy to address the mass effect and reduce the risk of further symptomatic haemorrhage and associated worsening of the neurological deficit.

3.6.2 Tractography-based qualitative data and implications

DTI studies[11-16] in general, have qualitatively demonstrated the orientation of the eloquent WM tracts (deviated and partially interrupted) around the brainstem CMs for planning the surgical trajectory. A recent study [16] using DTI-based tractography, retrospectively analysed the pre- and postoperative visualization of the CST and sensory tracts in 23 cases. The improvement in visualization was associated with the patients' neurological status. Consistent with other reports,[11,31] CMs had caused a combination of displacement, thinning, or interruption of the fiber tracts.
In our cases, the qualitative data (Figs. 2-6, Table 2) precisely outlined the spatial orientation of the affected CST. Surgical trajectory was chosen based on the direction of the displacement of the fibers, which occurred in a different direction (Figure 6) for each patient (patient 1: posterior; patient 2: anterior; patient 3: initially lateral and then posterolateral after several haemorrhagic events). Consistent with other studies and our previous findings from the supratentorial CM study, we found a combination of displacement and partial disruption occurring in the CST adjacent to the brainstem CMs.[11,31] The presence and improvement of motor deficits correlated with the observed displacement in the CST and its improvement over time respectively (Table 2). Accurate depiction of the perilesional CST including in the oedematous zone

using HDFT is linked in part to the QA being less sensitive to partial volume effects.[25,38]

The surgical planning in our studies[23,31,39] for mass lesions has been based upon the principle of avoidance of damage to the displaced tracts as a result of the initial surgical trajectory or eventual lesionectomy. This is related to the hypothesis that displaced tracts even though functionally compromised, retain the ability to recover following removal of the mass effect leading to resolution of the associated neurological deficits over time, as demonstrated here. The surgical approach is therefore, modified to obviate the risks associated with the resection. Our current approach with respect to the partially disrupted WM tracts is similar in terms of preventing further injury. Neurological deficits attributable to the disruption however, may not resolve entirely after the lesionectomy.

3.6.3 Tractography-based quantitative data and implications

It is noteworthy that the CST segments in the brainstem as well as in the subcortical region adjacent to their origin are subject to crossing fiber conditions making QA an appropriate quantitative index for their assessment.

The lower values for mean QA for the affected CST (Table 1) is likely consistent with repeated haemorrhagic episodes in patients with brainstem CMs and the consequent disruption of the tracts. Overall QA may be unable to detect lesser degrees of changes in specific segments of the tract without a craniocaudal compromise.[31] An example of the latter is patient 3 with a more rostral (thalamic) CM and multiple haemorrhagic episodes prior to surgery.

In order to characterise longitudinal changes in the craniocaudal integrity of the CST, we used the specific segments' analysis. Majority of the values (Table 2) represented a compromise of both the perilesional and the non-perilesional segments. The highest drop in the QA value for the perilesional segment was unsurprisingly noted for patient 3 with a history of multiple haemorrhagic episodes over a year prior to the surgical intervention. Patients 1 and 2 however, underwent surgical resection soon after the initial presentation with symptomatic haemorrhage.

These changes (Table 2, Supplemental Table) longitudinally evolved predominantly in the perilesional segment and the segment distal to the lesion (segment 3). Further drops in the mean QA values in the most caudal segment (patients 1 and 3) are potentially consistent with Wallerian degeneration occurring over months.[40-42] Acute compromise of the fiber tract integrity for example, due to hematoma may be evident using FA within days of the event[43] with further changes due to Wallerian degeneration being observed within months.[40] It is noteworthy that the perilesional drops in the QA values either deteriorated or stayed stable over the follow-up period and after the removal of the CM and associated haemorrhagic products. The susceptibility effects from the paramagnetic molecules, such as deoxyhaemoglobin, are known to affect the quantitative results leading to artifactual signal loss.[44] Although the susceptibility artifact cannot be completely excluded, the persistence or worsening of the drops in the perilesional QA values over longitudinal scans points against a major contribution from this phenomenon to our results.
In a previous study,[43] involving 17 patients with intracerebral haemorrhage (ICH), FA ratios (hematoma side/ contralateral side) were calculated at the level of the hematoma (basal ganglia and/ or thalamus) in the CST. DTI was performed within five days after the onset of ICH. FA ratio, measured shortly after the ICH, correlated well with the motor functional outcome at three months. The study suggested a potential prognostic role for FA in determining patients' eventual motor outcome. FA was not measured in other segments of the CST due to the difficulty of underestimation of FA in areas with multiple crossing fibers. In our small series, despite improvement in their neurological status over time all patients were noted to have some residual deficit at the last follow-up (Table 2).

3.6.4 Diffusion connectometry approach-based results and implications

The results from the connectometry analysis (Figure 6) were consistent with the quantitative analysis of the specific CST segments. The changes in the rostrocaudal involvement of the CST approximately corresponded to the changes in the QA values for the perilesional and non-perilesional segments. Interestingly in patient 3, the body of the CC was observed as being affected. These retrograde changes could be potentially attributable to the previously described progressive degenerative trans-synaptic effect observed in patients with subcortical stroke involving the pyramidal

tract.[45] Progressive decrease in the FA ratios of the callosal motor fibers correlating with the FA ratios of the pyramidal tract have been demonstrated in this patient group using a DTI study and thought to be a morphological correlate of transcallosal disinhibition.[45] It is unclear whether the rostral changes in patient 3 in the contralateral CST at the last follow-up represent a compensatory phenomenon or a potential weakness of our analytical technique. Further longitudinal data acquisition in a larger series will clarify the relevance of these retrograde changes.

3.6.5 Tractography versus diffusion connectometry approach; general limitations, and future directions

Both these approaches provide complementary information with individual limitations and potentially different applications. Tractography-based approach provides important qualitative data for surgical trajectory planning, as demonstrated here and in our previous studies with supratentorial CMs and tumours.[23,31,39] The tractography-based quantitative data is derived from comparisons with the contralateral homologous normal tract within the same subject. This could be a potential limitation in the brainstem in the setting of a large mass lesion. Another limitation pertinent to demonstrating the utility of the intrasubject tractography data for surgical planning is the lack of a control group including patients treated without the information from HDFT. A comparison group may potentially better elucidate the utility of HDFT. The obvious difficulty relates to the reported high morbidity associated with the surgical resection of brainstem CMs.[8]

The tractography-based approach is reliant upon the user expertise in terms of selection of ROIs and segmentation of the tracts. These therefore, lead to reproducibility issues, particularly when multiple users are involved.[46-49] In order to improve this, the key emphasis at our centre remains the use of anatomically valid and consistent ROIs. The tractography parameters are defined and kept constant for the specific tracts. Automated diffusion connectometry analysis is a better approach in terms of reproducibility. In the setting of mass lesions, an abnormal trajectory of a fiber may be either technical in origin or be real.[22,31] Despite the improved ability of the advanced techniques[50,51] to depict WM tracts in the perilesional oedematous zone, a careful interpretation of the qualitative data should be carried out with a

sound knowledge of the loco-regional neuroanatomy to facilitate safer surgical planning. Relevant to the quantitative analysis in the longitudinal studies is the variability in the parameters, such as QA, that can occur across the scan sessions. In order to ascertain this and the normal range of differences in anisotropy values that can exist between sides (left versus right) related to hemisphere dominance, we are currently scanning normal subjects on multiple occasions. Establishing these parameters will assist further with interpretation of the quantitative findings in longitudinal studies.

It is noteworthy that the connectometry analysis is not reliant upon the contralateral homologous tract. The results are therefore, not completely equivalent to the intrasubject tractography-based analysis. The qualitative data using this approach is also not directly useful for surgical approach planning.

Despite the longitudinal nature of our current study, an obvious limitation is the small sample size. Despite our previous studies involving HDFT and intracranial mass lesions,[23,31,38,39] the preliminary nature of the findings make it necessary to exercise caution while interpreting the qualitative and quantitative data for surgical trajectory planning and characterising changes in the perilesional WM for neurological prognostication respectively.[23,31] By acquiring more data longitudinally in patients with mass lesions, we are further validating the prognostic potential of a combination of these approaches. The impact of larger lesional pathologies like tumours on the connectometry analysis also needs further evaluation.

The tractography-based data in combination with connectometry data is being evaluated longitudinally for correlation with tract-specific neurological symptoms and eventual clinical outcomes. It will be crucial to identify a threshold for decrease in the anisotropy values for the perilesional and/or the non-perilesional segment that may correlate with neurological recovery or a permanent deficit. This will move the paradigm beyond the correlation of potential visualization of affected tracts with the eventual neurological outcome.

3.7 Conclusions

Haemorrhagic brainstem CMs can disrupt and displace the perilesional CST with the latter occurring in unpredictable directions. Tractography-based information can be used to longitudinally monitor the craniocaudal integrity of CST and detect potential Wallerian degeneration. Diffusion connectometry analysis can provide complementary longitudinal information on the extent of rostrocaudal involvement of CST. Although the excellent outcome of these three patients cannot be absolutely predicated upon the use of this novel technology in this preliminary series, HDFT is clearly an important adjunct for the precise delineation of the critical WM tracts to optimize the surgical entry point and removes one aspect of uncertainty in the surgical management of such complex and risky lesions.

3.8 References

1. Abla AA, Spetzler RF. Brainstem Cavernoma Surgery: The State of the Art. *World Neurosurg.* 2012.
2. Barrow DL, Schuette AJ. Cavernous malformations: a paradigm for progress. *Clin Neurosurg.* 2011;58:27-41.
3. Shah M HR. *Microsurgical treatment of supratentorial lesions.* Park Ridge, Ill.: : American Association of Neurological Surgeons; 1993.
4. Porter RW, Detwiler PW, Spetzler RF, et al. Cavernous malformations of the brainstem: experience with 100 patients. *J Neurosurg.* 1999;90(1):50-58.
5. Lekovic GP, Gonzalez LF, Khurana VG, Spetzler RF. Intraoperative rupture of brainstem cavernous malformation. Case report. *Neurosurg Focus.* 2006;21(1):e14.
6. Li D, Hao SY, Jia GJ, Wu Z, Zhang LW, Zhang JT. Haemorrhage risks and functional outcomes of untreated brainstem cavernous malformations. *J Neurosurg.* 2014;121(1):32-41.
7. Chen L, Zhao Y, Zhou L, Zhu W, Pan Z, Mao Y. Surgical strategies in treating brainstem cavernous malformations. *Neurosurgery.* 2011;68(3):609-620; discussion 620-601.

8. Abla AA, Lekovic GP, Turner JD, de Oliveira JG, Porter R, Spetzler RF. Advances in the treatment and outcome of brainstem cavernous malformation surgery: a single-centre case series of 300 surgically treated patients. *Neurosurgery.* 2011;68(2):403-414; discussion 414-405.
9. Kim DS, Park YG, Choi JU, Chung SS, Lee KC. An analysis of the natural history of cavernous malformations. *Surgical neurology.* 1997;48(1):9-17; discussion 17-18.
10. Monaco EA, Khan AA, Niranjan A, et al. Stereotactic radiosurgery for the treatment of symptomatic brainstem cavernous malformations. *Neurosurg Focus.* 2010;29(3):E11.
11. Chen X, Weigel D, Ganslandt O, Buchfelder M, Nimsky C. Diffusion tensor imaging and white matter tractography in patients with brainstem lesions. *Acta neurochirurgica.* 2007;149(11):1117-1131; discussion 1131.
12. Chen X, Weigel D, Ganslandt O, Fahlbusch R, Buchfelder M, Nimsky C. Diffusion tensor-based fiber tracking and intraoperative neuronavigation for the resection of a brainstem cavernous angioma. *Surgical neurology.* 2007;68(3):285-291; discussion 291.
13. McLaughlin N, Kelly DF. Corticospinal tractography as a prognosticator for motor improvement after brainstem cavernoma resection. *British journal of neurosurgery.* 2013;27(1):108-110.
14. Royo A, Utrilla C, Carceller F. Surgical management of brainstem-expanding lesions: the role of neuroimaging. *Seminars in ultrasound, CT, and MR.* 2013;34(2):153-173.
15. Mai JC, Ramanathan D, Kim LJ, Sekhar LN. Surgical resection of cavernous malformations of the brainstem: evolution of a minimally invasive technique. *World Neurosurg.* 2013;79(5-6):691-703.
16. Ulrich NH, Kockro RA, Bellut D, et al. Brainstem cavernoma surgery with the support of pre- and postoperative diffusion tensor imaging: initial experiences and clinical course of 23 patients. *Neurosurgical review.* 2014;37(3):481-492.
17. Alexander DC, Barker GJ. Optimal imaging parameters for fiber-orientation estimation in diffusion MRI. *NeuroImage.* 2005;27(2):357-367.

18. Le Bihan D, Poupon C, Amadon A, Lethimonnier F. Artifacts and pitfalls in diffusion MRI. *Journal of magnetic resonance imaging : JMRI.* 2006;24(3):478-488.
19. Alexander AL, Hasan KM, Lazar M, Tsuruda JS, Parker DL. Analysis of partial volume effects in diffusion-tensor MRI. *Magnetic resonance in medicine : official journal of the Society of Magnetic Resonance in Medicine / Society of Magnetic Resonance in Medicine.* 2001;45(5):770-780.
20. Oouchi H, Yamada K, Sakai K, et al. Diffusion anisotropy measurement of brain white matter is affected by voxel size: underestimation occurs in areas with crossing fibers. *AJNR American journal of neuroradiology.* 2007;28(6):1102-1106.
21. Zolal A, Hejcl A, Vachata P, et al. The use of diffusion tensor images of the corticospinal tract in intrinsic brain tumor surgery: a comparison with direct subcortical stimulation. *Neurosurgery.* 2012;71(2):331-340; discussion 340.
22. Lazar M, Alexander AL, Thottakara PJ, Badie B, Field AS. White matter reorganisation after surgical resection of brain tumours and vascular malformations. *AJNR American journal of neuroradiology.* 2006;27(6):1258-1271.
23. Fernandez-Miranda JC, Pathak S, Engh J, et al. High-definition fiber tractography of the human brain: neuroanatomical validation and neurosurgical applications. *Neurosurgery.* 2012;71(2):430-453.
24. Wedeen VJ, Hagmann P, Tseng WY, Reese TG, Weisskoff RM. Mapping complex tissue architecture with diffusion spectrum magnetic resonance imaging. *Magnetic resonance in medicine : official journal of the Society of Magnetic Resonance in Medicine / Society of Magnetic Resonance in Medicine.* 2005;54(6):1377-1386.
25. Yeh FC, Verstynen TD, Wang Y, Fernandez-Miranda JC, Tseng WY. Deterministic diffusion fiber tracking improved by quantitative anisotropy. *PloS one.* 2013;8(11):e80713.
26. Jarbo K, Verstynen T, Schneider W. In vivo quantification of global connectivity in the human corpus callosum. *NeuroImage.* 2012;59(3):1988-1996.

27. Verstynen TD, Badre D, Jarbo K, Schneider W. Microstructural organisational patterns in the human corticostriatal system. *Journal of neurophysiology.* 2012;107(11):2984-2995.
28. Wang Y, Fernandez-Miranda JC, Verstynen T, Pathak S, Schneider W, Yeh FC. Rethinking the role of the middle longitudinal fascicle in language and auditory pathways. *Cerebral cortex.* 2013;23(10):2347-2356.
29. Verstynen T, Jarbo K, Pathak S, Schneider W. In vivo mapping of microstructural somatotopies in the human corticospinal pathways. *Journal of neurophysiology.* 2011;105(1):336-346.
30. Greenberg AS, Verstynen T, Chiu YC, Yantis S, Schneider W, Behrmann M. Visuotopic cortical connectivity underlying attention revealed with white-matter tractography. *The Journal of neuroscience : the official journal of the Society for Neuroscience.* 2012;32(8):2773-2782.
31. Abhinav K, Pathak S, Richardson RM, et al. Application of high-definition fiber tractography in the management of supratentorial cavernous malformations: a combined qualitative and quantitative approach. *Neurosurgery.* 2014;74(6):668-680; discussion 680-661.
32. Fernandez-Miranda JC, Rhoton AL, Jr., Alvarez-Linera J, Kakizawa Y, Choi C, de Oliveira EP. Three-dimensional microsurgical and tractographic anatomy of the white matter of the human brain. *Neurosurgery.* 2008;62(6 Suppl 3):989-1026; discussion 1026-1028.
33. Abhinav K, Yeh FC, El-Dokla A, et al. Use of diffusion spectrum imaging in preliminary longitudinal evaluation of amyotrophic lateral sclerosis: development of an imaging biomarker. *Frontiers in human neuroscience.* 2014;8:270.
34. Yeh FC, Tang PF, Tseng WY. Diffusion MRI connectometry automatically reveals affected fiber pathways in individuals with chronic stroke. *NeuroImage Clinical.* 2013;2:912-921.
35. Yeh FC, Tseng WY. NTU-90: a high angular resolution brain atlas constructed by q-space diffeomorphic reconstruction. *NeuroImage.* 2011;58(1):91-99.
36. MacDonald JD, Antonelli P, Day AL. The anterior subtemporal, medial transpetrosal approach to the upper basilar artery and ponto-mesencephalic junction. *Neurosurgery.* 1998;43(1):84-89.

37. Konovalov A, Samii M, Porter RW, et al. Brainstem cavernoma. *Surgical neurology.* 2000;54(6):418-421.
38. Abhinav K, Yeh FC, Pathak S, et al. Advanced diffusion MRI fiber tracking in neurosurgical and neurodegenerative disorders and neuroanatomical studies: A review. *Biochimica et biophysica acta.* 2014;1842(11):2286-2297.
39. Fernandez-Miranda JC, Engh JA, Pathak SK, et al. High-definition fiber tracking guidance for intraparenchymal endoscopic port surgery. *J Neurosurg.* 2010;113(5):990-999.
40. McDonald CR, Hagler DJ, Jr., Girard HM, et al. Changes in fiber tract integrity and visual fields after anterior temporal lobectomy. *Neurology.* 2010;75(18):1631-1638.
41. Pierpaoli C, Barnett A, Pajevic S, et al. Water diffusion changes in Wallerian degeneration and their dependence on white matter architecture. *NeuroImage.* 2001;13(6 Pt 1):1174-1185.
42. Wieshmann UC, Symms MR, Clark CA, et al. Wallerian degeneration in the optic radiation after temporal lobectomy demonstrated in vivo with diffusion tensor imaging. *Epilepsia.* 1999;40(8):1155-1158.
43. Yoshioka H, Horikoshi T, Aoki S, et al. Diffusion tensor tractography predicts motor functional outcome in patients with spontaneous intracerebral haemorrhage. *Neurosurgery.* 2008;62(1):97-103; discussion 103.
44. Dorenbeck U, Schlaier J, Bretschneider T, Schuierer G, Feuerbach S. Diffusion-weighted imaging with calculated apparent diffusion coefficient in intracranial haemorrhagic lesions. *Clinical imaging.* 2005;29(2):86-93.
45. Radlinska BA, Blunk Y, Leppert IR, Minuk J, Pike GB, Thiel A. Changes in callosal motor fiber integrity after subcortical stroke of the pyramidal tract. *Journal of cerebral blood flow and metabolism : official journal of the International Society of Cerebral Blood Flow and Metabolism.* 2012;32(8):1515-1524.
46. Besseling RM, Jansen JF, Overvliet GM, et al. Tract specific reproducibility of tractography based morphology and diffusion metrics. *PloS one.* 2012;7(4):e34125.
47. Tensaouti F, Lahlou I, Clarisse P, Lotterie JA, Berry I. Quantitative and reproducibility study of four tractography algorithms used in clinical routine. *Journal of magnetic resonance imaging : JMRI.* 2011;34(1):165-172.

48. Chung HW, Chou MC, Chen CY. Principles and Limitations of Computational Algorithms in Clinical Diffusion Tensor MR Tractography. *AJNR American journal of neuroradiology.* 2010.
49. Malykhin N, Concha L, Seres P, Beaulieu C, Coupland NJ. Diffusion tensor imaging tractography and reliability analysis for limbic and paralimbic white matter tracts. *Psychiatry Res.* 2008;164(2):132-142.
50. Zhang H, Wang Y, Lu T, et al. Differences between generalised q-sampling imaging and diffusion tensor imaging in the preoperative visualization of the nerve fiber tracts within peritumoral oedema in brain. *Neurosurgery.* 2013;73(6):1044-1053; discussion 1053.
51. Kuhnt D, Bauer MH, Sommer J, Merhof D, Nimsky C. Optic radiation fiber tractography in glioma patients based on high angular resolution diffusion imaging with compressed sensing compared with diffusion tensor imaging - initial experience. *PloS one.* 2013;8(7):e70973.

3.9.1 Figures

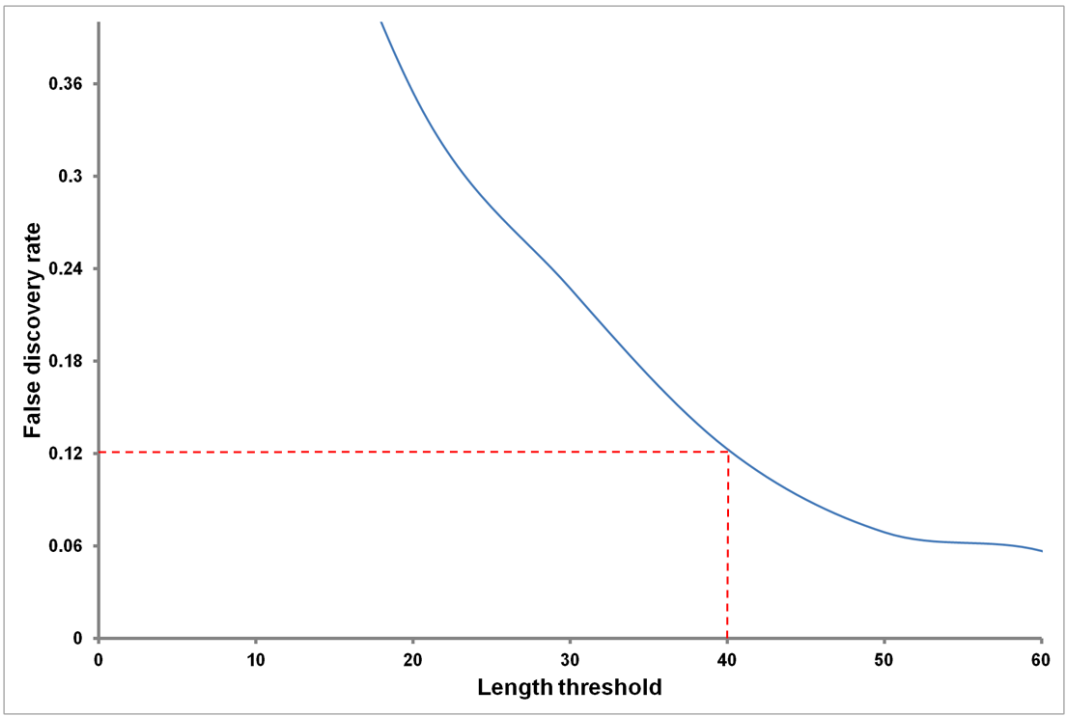

FIGURE 1. Length threshold in relation to the false discovery rate (FDR). A length threshold of 40 mm was chosen corresponding to an FDR of 0.12 (denoted by the red dotted line).

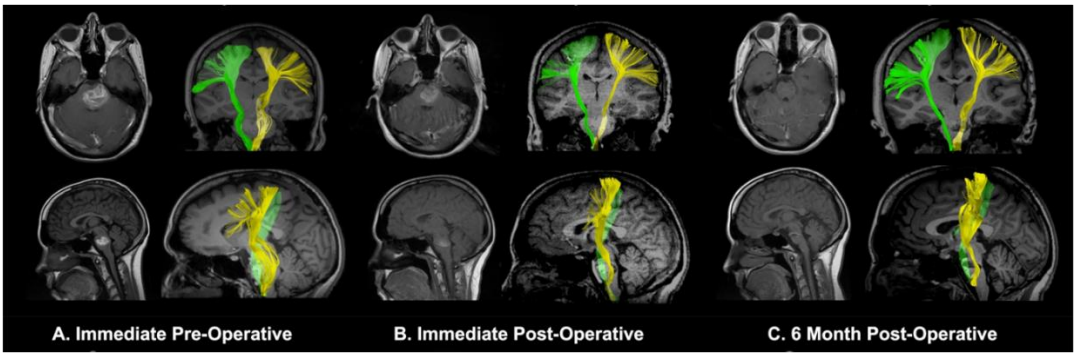

FIGURE 2. Longitudinal High definition fiber tractography reconstruction of the corticospinal tract (CST) in patient 1 with a left-sided pontomesencephalic cavernous malformation. Immediate pre-operative (A), immediate post-operative (B), and six-month post-operative (C) scans demonstrate improvement in the displacement of the CST on the lesional side (yellow) in relation to the CST on the unaffected side (green) during the postoperative and the follow-up period.

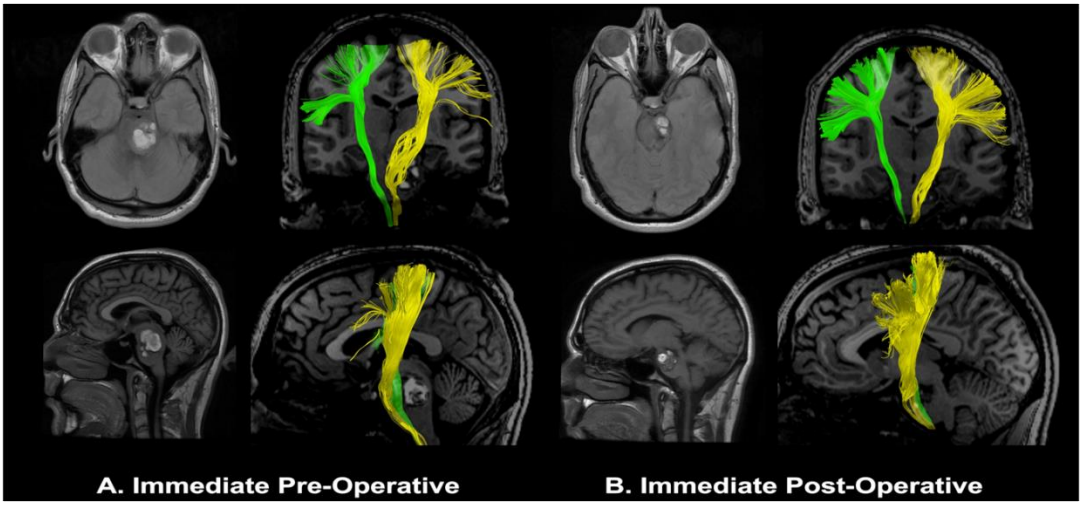

FIGURE 3. Pre- and postoperative High definition fiber tractography reconstruction of the corticospinal tract (CST) in patient 2 with a left-sided pontomesencephalic cavernous malformation. Immediate preoperative (A) and postoperative (B) tractography of the CST show an improvement in the configuration (displacement) of the perilesional CST (yellow) in relation to the contralateral CST (green) after the resection of the cavernous malformation.

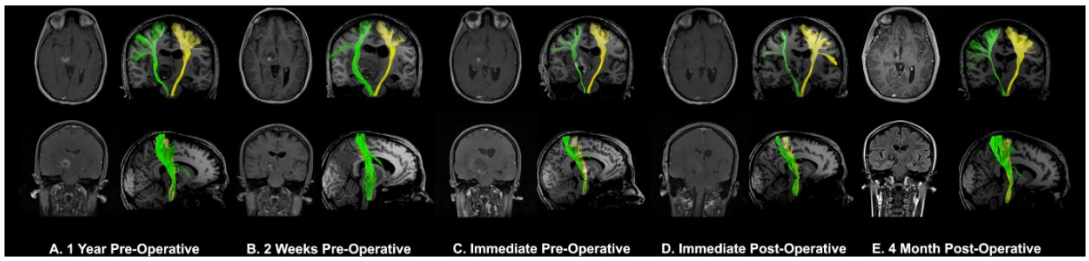

FIGURE 4. Longitudinal High definition fiber tractography (HDFT) reconstruction of the corticospinal tract (CST) in patient 3 with a right-sided thalamomesencephalic cavernous malformation (CM). (A-C): Preoperative HDFT reconstructions of the CST demonstrate a displaced and partially disrupted perilesional CST (green) in relation to the CM. There is worsening of the displacement between the first (A) and the second (B) HDFT scans. In the immediate postoperative phase (D) and the follow-up period (E), there is an improvement in the configuration of the previously displaced CST in relation to the unaffected CST (yellow).

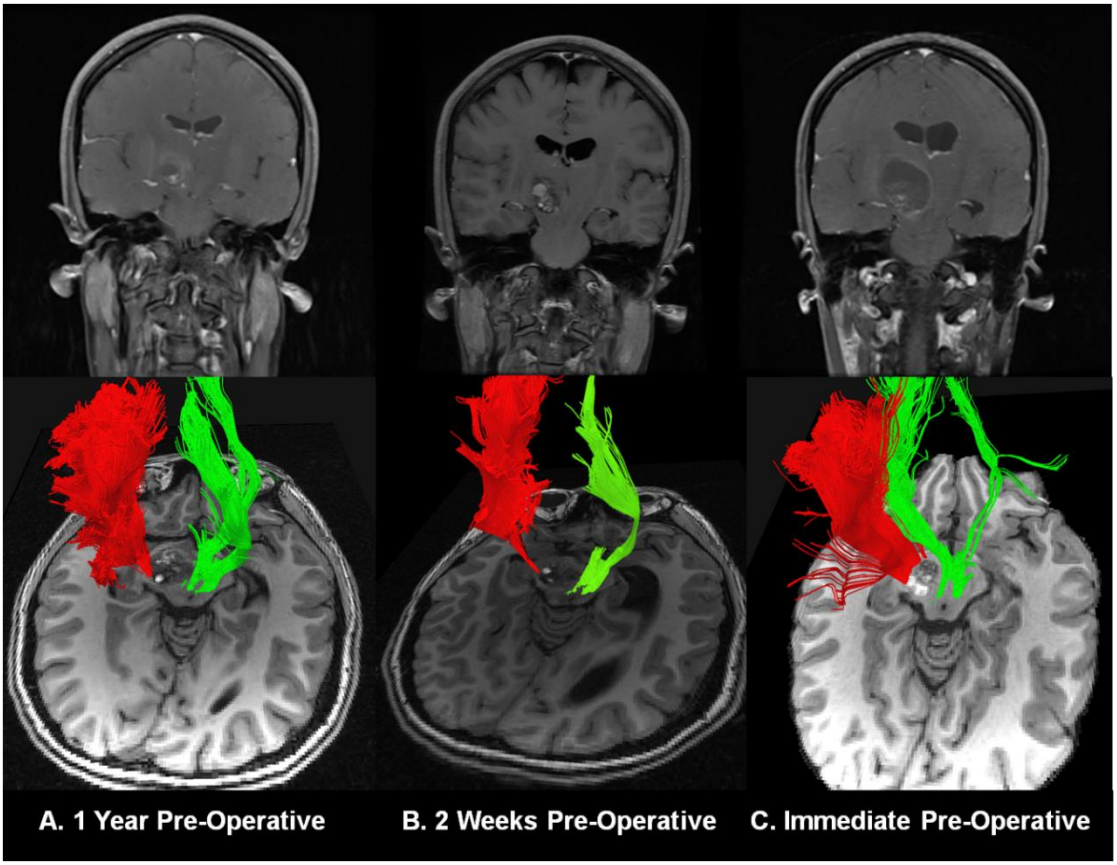

FIGURE 5. Longitudinal preoperative High definition fiber tractography (HDFT) reconstruction of the perilesional tracts in Patient 3 with a right-sided thalamomesencephalic cavernous malformation (CM) (represented using axial MR slices). (A-C): Preoperative HDFT reconstructions of the corticospinal tracts (CST) demonstrate a laterally and partially disrupted perilesional CST (red) in relation to the CM. There is progressive worsening of the fiber configuration with the immediate preoperative scan (C) demonstrating posterolateral displacement of the CST. This led to selection of an anterior trajectory to resect the CM and to minimize any injury to the CST. In relation to the CM, medially located superior cerebellar peduncle and medial lemniscus (green) fibers are also demonstrated.

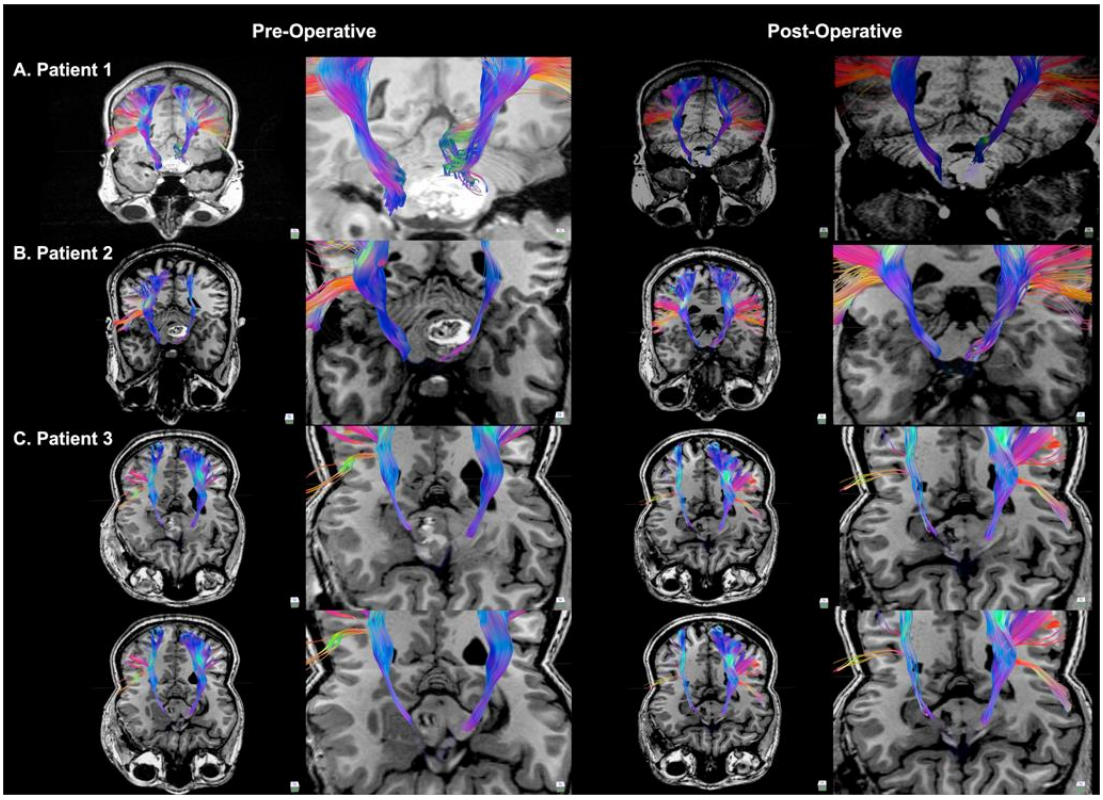

FIGURE 6. Demonstration of deformation of the pre- and postoperative corticospinal tracts (CST) in relation to the cavernous malformation (magnified views) using the High definition fiber tractography. The direction of displacement of CST was different for the three cases. Patient 1 (A) had a posteriorly displaced left CST; patient 2 (B) had an anteromedially displaced left CST; and patient 3 had a laterally displaced right CST in relation to the lesion.

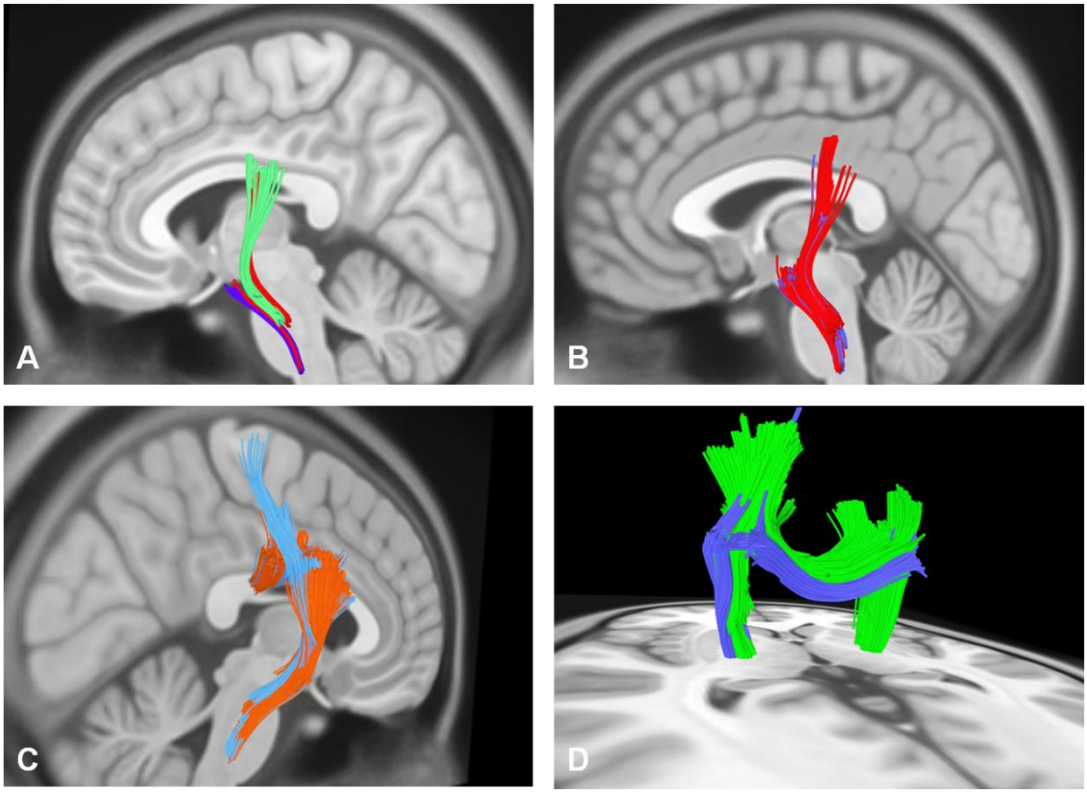

FIGURE 7. Diffusion connectometry analysis approach in patient 1 (A), patient 2 (B) and patient 3 (C-D). For patient 1 (A) with a left-sided pontomesencephalic cavernous malformation (CM) the connectometry analysis at the first scan (preoperative, blue) revealed the affected segment of the CST as being predominantly caudal, approximating to the level of the lesion with the second scan (three weeks after surgery, green) indicating a more rostral involvement. At the third scan (six months after surgery, red), there was an increase in the extent of the involvement of CST in the craniocaudal direction. For patient 2 with a left-sided pontomesencephalic CM, the connectometry analysis of both the immediate pre- (blue) and postoperative (red) scans demonstrated similar rostrocaudal involvement of the CST. In patient 3 with a right-sided thalamomesencephalic lesion (C-D), both the preoperative [C, blue (1 year preoperative); orange (immediate preoperative)] and the first postoperative scan (D) (blue, immediate postoperatively) demonstrated extensive rostrocaudal involvement of the CST with further changes in the body of the corpus callosum (medially coursing fibers). At the last scan four months after surgery (D, green), rostral CST on the contralateral side was also seen as being involved.

3.9.2 Tables

TABLE 1: Overall mean quantitative anisotropy values for the corticospinal tract over longitudinal scans

Patient number (affected side)	Scan number (stage)	Time period	Mean QA ± S.d. (R)	Mean QA ± S.d. (L)	Percentage (%) drop (QA)*
1 (L)	1 (preop.) 2 (postop.) 3 (postop.)	Immediate 3 weeks 6 months	0.16±0.08 0.17±0.08 0.15±0.06	0.14±0.08 0.12±0.06 0.10±0.06	12.83% 26.57% 28.47%
2 (L)	1 (preop.) 2 (postop.)	Immediate Immediate	0.19±0.08 0.21±0.09	0.14±0.08 0.14±0.08	27.24% 35.29%
3 (R)	1 (preop.) 3 (preop.) 4 (postop.) 5 (postop.)	1 year Immediate Immediate 4 months	0.07±0.04 0.05±0.03 0.05±0.03 0.05±0.03	0.10±0.05 0.10±0.03 0.10±0.05 0.11±0.05	35.87% 52.46% 52.32% 55.70%

(L: left; preop.: preoperative; postop.: postoperative; QA: quantitative anisotropy; R: right; S.d.: standard deviation; *: calculated for the affected side in relation to the unaffected side)

TABLE 2: Qualitative change and percentage drops* in the mean quantitative anisotropy values for the corticospinal tract segments over longitudinal scans in relation to the motor findings

Patient number (affected side)	Scan number (stage)	Seg. 1 (proximal)	Seg. 2 (perilesional)	Seg. 3 (distal)	Qualitative change	Limb motor findings
1 (L)	1 (imm. preop.) 2 (3 weeks postop.) 3 (6 months postop.)	8.44 26.84 24.17	26.38 28.12 48.70	32.89 20.16 45.59	(1) Partial disruption and displacement (post.) (2) Partial disruption and reduced displacement (post.) (3) Partial disruption only	(1) RUL (4/5 proximal & 0/5 distal) & RLL (4/5 proximal & 1/5 distal) (2) RUL (4/5 proximal and 1/5 distal) & RLL (4/5 proximal and 2/5 distal) (3) RUL (4+/5) & RLL (4+/5 proximal & 3/5 distal)
2 (L)	1 (imm. preop.) 2 (imm. postop.)	22.68 22.42	34.70 65.72	31.62 48.38	(1) Partial disruption and displacement (A/M) (2) Partial disruption with residual displacement	(1) RUL & RLL (4/5) (2) RUL & RLL (4+/5)
3 (R)	1 (1 year preop) 3 (imm. preop.) 4 (imm. postop.) 5 (4 months postop.)	14.68 45.06 44.66 46.06	63.39 77.70 76.62 78.52	42.20 42.77 27.94 66.87	(1) Partial disruption and displacement (lat.) (3)Partial disruption and displacement (P/L) (4) Partial disruption and improving displacement (5) Partial disruption only	(1) None (3) LUL (4/5 proximal & 0/5 distal) & LLL (4+/5) (4) LUL (1/5) & LLL (4/5) (5) LUL (4/5 proximal & 2-3/5 distal) & LLL (4/5)

(A/M: anteromedial; imm.: immediate; lat.: lateral; L: left; LL: lower limb; preop.: preoperative; postop.: postoperative; post.: posterior; P/L: posterolateral; R: right; Seg.: segment; UL: upper limb; *: calculated for the affected segments in relation to the unaffected segments)

TABLE 3: Changes in the Quantitative anisotropy values over the longitudinal scans for three segments of corticospinal tract on the affected and unaffected sides.

Patient number (affected side)	Scan number (stage)	Mean QA (Segment 1)	Mean QA (Segment 2)*	Mean QA (Segment 3)
1 (L)	1 (imm. preop.) 2 (3 weeks postop.) 3 (6 months postop.)	L(0.18);R(0.20) L(0.15);R(0.21) L(0.13);R(0.17)	L(0.08);R(0.11) L(0.08);R(0.11) L(0.05);R(0.11)	L(0.06);R(0.09) L(0.08);R(0.10) L(0.05);R(0.10)
2 (L)	1 (imm. preop.) 2 (imm. postop.)	L(0.18);R(0.23) L(0.18);R(0.23)	L(0.12);R(0.19) L(0.07);R(0.21)	L(0.08);R(0.12) L(0.06);R(0.11)
3 (R)	1 (1 year preop.) 3 (imm. preop.) 4 (imm. postop.) 5 (4 months postop.)	L(0.10);R(0.09) L(0.11);R(0.06) L(0.11);R(0.06) L(0.12); R(0.06)	L(0.12);R(0.05) L(0.12); R(0.03) L(0.12);R(0.03) L(0.14); R(0.03)	L(0.08);R(0.04) L(0.05);R(0.03) L(0.06);R(0.04) L(0.07); R(0.02)

(L: left; preop.: preoperative; postop.: postoperative; QA: quantitative anisotropy; R: right; *: represents the perilesional segment on the affected side with segment 1 and 3 being proximal and distal to the lesion respectively.)

Chapter 4: Utility of a quantitative approach using diffusion tensor imaging for prognostication regarding motor and functional outcomes in patients with surgically resected deep intracranial cavernous malformations.

Paper 3: **Abhinav K,** Nielsen TH, Singh R, Weng Y, Han SS, Iv M, Steinberg GK. Utility of a quantitative approach using diffusion tensor imaging for prognostication regarding motor and functional outcomes in patients with surgically resected deep intracranial cavernous malformations. *Neurosurgery* 2019 July 30 [Epub ahead of print]

4.1 Declaration

I was the first author with respect to this manuscript and was instrumental in the conception and design of the study and its completion with the radiology team. Overall I contributed extensively towards the writing, literature search, figures, study design, data analysis and interpretation.

4.2 Introduction to and brief summary of the manuscript in relation to the previous work

Based upon the findings from the previous study, we concluded that the haemorrhagic brainstem cavernous malformations (CMs) can disrupt and displace perilesional white matter (WM) tracts with the latter occurring in unpredictable directions. The inability to predict the direction of displacement based using the anatomical paradigm alone, requires the use of tractography to accurately define the spatial relationship of WM tracts to the malformation such that the surgical entry point can be optimised towards minimising morbidity and improving neurological outcomes. The derived qualitative data was therefore, indispensable towards optimising the surgical entry point for these CMs including as demonstrated in Chapter 2 for the supratentorial CMs. At a quantitative level, we had further applied the anisotropy based perilesional segment model in assessing the integrity of the WM tracts. We concluded that a model using these values in different CST segments could be potentially used to longitudinally monitor its craniocaudal integrity with diffusion connectometry being a potential complementary approach. A fundamental

objective was therefore to assess whether using these quantitative markers may predict extent of recovery from a haemorrhage or weakness (e.g. a stroke-like condition) over a period of time.

Despite the use of advanced WM imaging algorithm in these patients with relatively rare conditions, one of the major limitation in the previous study (Chapter 3) was the limited number of patients. In the current study, we therefore, applied a similar perilesional segment-based anisotropy model, however in a larger cohort of patients with deep seated CMs in eloquent locations. Importantly, we were able to relate the preoperative anisotropy values to both the pre- and postoperative motor examination and eventual functional outcomes using the modified Rankin scale (mRS) score. The latter was a first endeavour in terms of our research effort. Another notable difference here was the use of diffusion tractography imaging (DTI) data rather than the advanced WM imaging algorithm. Despite the use of a more conventional imaging algorithm, the completeness of the preoperative imaging data in addition to postoperative clinical examination and functional outcomes provided an invaluable opportunity to explore the validity of the model as discussed in the previous chapters.

DTI data evaluating the corticospinal tract (CST) was therefore, examined in relation to motor and functional outcomes in patients with surgically resected deep CMs. Perilesional CST was characterised as disrupted, displaced or normal. Mean fractional anisotropy (FA) values were obtained for whole ipsilateral CST and in three regions: subcortical (proximal), perilesional, and distally, as discussed in previous chapters. Mean FA values in anatomically equivalent regions in the contralateral CST were obtained. Clinical and radiological data were collected independently. Multivariable regression analysis was used for statistical analysis.

18 patients [brainstem (15) and thalamus/basal ganglia (3); median follow-up: 270 days] were identified over two years. The CST was identified preoperatively as disrupted (6), displaced (8), and normal (4). Five of 6 patients with disruption had weakness. Higher preoperative mean FA values for distal ipsilateral CST segment were associated with better preoperative lower ($p<0.001$) and upper limb ($p=0.004$) and postoperative lower ($p=0.005$) and upper limb ($p<0.001$) motor examination. Preoperative mean FA values for distal ipsilateral CST segment ($p=0.001$) and contralateral perilesional CST segment ($p<0.001$) were negatively associated with

postoperative mRS scores; therefore, higher FA values for these variables were associated with lower mRS scores and therefore, better performance status for the patients.

Lower preoperative mean FA values for overall and defined CST segments, potentially indicating compromised integrity of the tracts, corresponded to worse patient pre- and postoperative motor examination and/or functional status. FA value for the distal ipsilateral CST segment had prognostic potential with respect to clinical outcomes.

4.3. Introduction

Cavernous malformations (CMs) have an estimated prevalence of 0.4%–0.8%[1,2] with approximately 9%–35% located in the brainstem.[3] The estimated haemorrhage and rehaemorrhage rates for brainstem CMs are high ranging from 0.5% to 6% and 5% to 60% per patient-year, respectively.[3,4] Deep seated (including thalamic or basal ganglia) CMs have high rebleeding rates, up to 31.5%/patient per year.[5]

Resection of brainstem CMs is associated with significant risks of permanent neurological deterioration.[6] Precise location of the affected white matter tracts including the corticospinal tract (CST) is difficult to ascertain preoperatively. Diffusion tensor imaging (DTI) characterises the orientation of these tracts preoperatively to enable safe resection of the brainstem CMs.[7-14] Quantitative DTI data with respect to patients' motor examination or eventual functional status, however, has not been systematically evaluated.[15] We previously outlined a methodology using quantitative anisotropy (QA) to characterise the perilesional changes in the CST and evaluate its integrity.[9,16,17]

In this study of patients with surgically resected deep CMs, we evaluated the ability of preoperative fractional anisotropy (FA) values for overall and defined segments of the CST on the lesional and non-lesional side to predict pre- and postoperative motor examination and eventual functional outcomes. In those with postoperative DTI, we also assessed the quantitative data in relation to postoperative motor examination and eventual functional status.

4.4 Methods

4.4.1 Clinical data acquisition

Patients undergoing resection of deep CMs (basal ganglia/thalamic and brainstem) with DTI were identified retrospectively over two years at a single academic institution. Patients without DTI were excluded. Appropriate institutional review and patient consent were obtained. Collected information included pre- and postoperative upper and lower limb motor examination (obtained in the inpatient or clinic setting) as graded by the British Medical Research Council and modified Rankin scale (mRS) score at the final follow-up. Clinical data was collected by two authors blinded to radiological data.

4.4.2 Imaging acquisition

Majority of brain MRIs were performed on multiple 3 Tesla scanners (MR750 or 750W; GE Healthcare, Milwaukee, WI, USA; 8-channel head coil). Four were performed on a 1.5 Tesla scanner (Signa; GE Healthcare, Milwaukee, WI, USA). Each MRI included three-dimensional axial brain volume imaging with array spatial sensitivity encoding technique acceleration of 2 (ASSET 2), three-dimensional axial T1-weighted inversion-recovery spoiled gradient recalled echo and DTI. DTI was acquired with one image with a *b* value of 0 second/mm^2 and 30 isotropically distributed diffusion directions with a *b* value of 1000 second/mm^2. At 3T, DTI parameters were: TR/TE=8,000-8500 ms/61 ms, slice thickness/gap=2 mm/0 mm, matrix=128x128mm, field of view=250 mm. A subset of patients were scanned on a wide bore 3T scanner with the following parameters: TR/TE=9,965-13,000 ms/72 ms, slice thickness/gap=2.5 mm/0 mm, matrix=96x96mm, field of view=250 mm. Diffusion parameters at 1.5T were: TR/TE=10,000-17,000.

4.4.3 Imaging analysis and fiber tracking

Fiber tractography was performed in a semi-automated manner using commercially available DTI software (version 3.1.0.172457, InVivo DynaSuite Neuro, Gainseville, FL, USA) using a deterministic algorithm. The software automatically generated FA and colour FA images from the raw DTI. Placement of the region of interest (ROI) involved agreement between a student experienced in tractography and a board-certified neuro-radiologist with significant DTI expertise. Both were blinded to clinical data.

4.4.4 Quantitative analysis

Mean FA values were obtained for the CST in both hemispheres using a previous methodology based on QA.[9,16] FA values were obtained by first manually placing ROIs around the CST on colour FA images and then recording the ROI value (mean FA value) on the superimposed FA map. Mean FA values were obtained in three divided regions in the CST (Figure 1): proximal to the lesion (e.g. posterior limb of the internal capsule with a pontine or midbrain lesion) (proximal), at the level of CM and within 3 mm of the lesion where the CST was best seen on the colour FA map (perilesional), and distal to the lesion (e.g. medulla with a pontine or midbrain lesion) (distal), typically where CST fibers were condensed. For thalamic and basal ganglia CMs, the posterior corona radiata and upper pons were considered proximal and distal respectively. For medullary CMs, the pons and lower ventral medulla/ cervicomedullary junction were considered proximal and distal respectively.

The CST segment on coronal images was also interrogated as this represented maximal visual representation of the tract on a single two-dimensional image slice (overall). For comparison, mean FA values for the anatomically equivalent regions in the contralateral homologous tract were also obtained. For perilesional tracts difficult to visualize because of disruption, ROIs were placed in the expected location of the tract based upon seeding the tract above (proximal) and below (distal) the lesion as well as the contralateral tract.

Percentage differences were calculated between the FA values obtained for the perilesional segments and the overall CST on the lesional or ipsilateral side and the FA values for the homologous segments on the non-lesional or contralateral side. The corresponding FA values from the homologous segments on the contralateral

side were used for normalization of FA values for the perilesional segment and overall CST on the ipsilateral side using the equation: [(contralateral side FA value-ipsilateral side FA value)*100/ contralateral side FA value]. For patients with disruption this percentage difference was hypothesised to be larger, while with pure displacement the difference was expected to be minimal.

4.4.5 Qualitative analysis

Fiber tracking was initiated by seeding select manually placed ROIs. Tracking maximized visual representation of the CST and minimized erroneous adjacent tracts, using a minimum FA threshold of 0.05 and a maximum curvature threshold of 0.4. Perilesional tract was characterised as disrupted, displaced or normal using contralateral homologous tract for comparison. Disruption may occur with displacement and may be partial ("breakage" or thinning of fibers as seen in a cross section or due to discontinuity in a limited tract segment) or complete (tract not seen through most or all of its course with major discontinuity). Displacement applied to tracts with a change of direction due to mass effect.

4.4.6 Statistical analysis

Descriptive analysis

Preoperative patient characteristics were described including in relation to the preoperative qualitative radiological features. Median and inter-quantile range (IQR) were reported for continuous variables that were not normally distributed.

Multivariable linear regression

Multivariable linear regression analysis evaluated association between pre- and postoperative motor scores in upper and lower limbs (outcome variables) and the preoperative quantitative radiological variables. For each pair of the motor score and quantitative radiological characteristic, a multivariable linear regression model was

used with motor score as the dependent and radiological feature as the independent variable. Stepwise selection method identified additional covariates needing adjustment. Anatomical location of the CMs, pial presentation and number of haemorrhages, age at treatment preoperatively were included as covariates in the full model. A similar analysis evaluated association between the preoperative quantitative radiological features and mRS at the final follow-up. Cranial neuropathy was included as a further candidate variable for adjustment in addition to those outlined above. Estimates from the optimal models with the lowest Akaike information criterion that adjusted for a subgroup of covariates in the candidate list by stepwise model selections were presented. To adjust for multiple comparisons, a Bonferroni correction was applied using alpha=0.001 (=0.05/50) as the final value for determining statistical significance. Additional multivariable analysis explored the association between postoperative radiological quantitative features and postoperative upper and lower limb motor scores and mRS at the final follow-up.

Sensitivity Analysis

The robustness of our model was checked by sensitivity analysis. In order to check the robustness of our model, sensitivity analysis was conducted by performing: a) a set of linear regressions to predict the pre- and postoperative motor scores and mRS at follow-up visit in relation to pre- and postoperative quantitative radiological features without adjusting for other variables, and 2) Spearman's rank correlation test for pre- and postoperative quantitative radiological parameters in relation to pre and postoperative motor and mRS scores at the final follow-up.

4.5 Results

4.5.1 Baseline preoperative patient characteristics

Eighteen patients (8 females, 10 males) were included. Mean age at treatment was 47 years (SD = 17.2). Of 18, 9 were in the pons, 4 in the mesencephalon, 2 in medulla, and 3 in the thalamus/ basal ganglia. CMs had a pial presentation in 13 (72%) patients. Eleven (61%) had more than one haemorrhage preoperatively. Thirteen

(72%) patients had preoperative cranial neuropathy. In terms of the upper limb motor examination, 2 had grade 0-1 while 16 had grade 4-5 strength. In terms of the lower limb examination, 5 patients had grade 4 strength while 13 had grade 5 (Table 1). Median duration from surgery to the postoperative neurological examination (corresponding to the postoperative DTI) was 138 days [interquartile range (iqr): 203]. Median follow-up duration from surgery to the final mRS score was 270 days (iqr: 426).

4.5.2 Qualitative characteristics of corticospinal tract preoperatively and its relationship to baseline neurological motor examination

Of 18 ipsilateral CSTs, 6 were disrupted, 8 displaced and 4 normal. Of 6 patients with disrupted CST, there was weakness in upper limb in 5 and lower limb in 4 (Table 1). 7 of 8 patients with displaced CST had a normal upper and lower limb neurological examination (Table 1). Four patients with qualitatively characterised *normal* CST had normal upper and lower limb examination (Table 1).

4.5.3 Preoperative qualitative data in relationship to quantitative data

With respect to the percentage difference in FA for perilesional CST segment in relation to the contralateral side, mean values were 15% for all; 10.2% for normal, 5.3% for displaced and 31.3% for disrupted (Figure 2). These values represented a percentage decrease in FA values for the perilesional segment in relation to the contralateral side. This value was highest for the disrupted tracts. Similarly with respect to the percentage difference for the overall tract in relation to the contralateral side, mean values were 5.6% for all, 2.9% for normal, 4.5% for displaced, and 8.9% for disrupted tracts. The observed percentage decrease was again greatest for disrupted tracts (Figure 2).

4.5.4 Preoperative quantitative data in relation to pre- and postoperative motor scores (Table 2, Figure 3)

Of different variables, FA values for overall CST ipsilateral to the lesion was found to be significantly associated with preoperative upper and lower limb examination ($p<0.001$). This parameter also correlated with the postoperative upper ($p<0.05$) and lower limb examination ($p=0.002$). FA values for the distal CST segment ipsilateral to the lesion was also significantly associated with the preoperative lower limb and postoperative upper limb motor examination ($p<0.001$). Practically an increase in the FA value of distal CST segment ipsilateral to the lesion by 0.07 was associated with an increase in the postoperative motor score of the upper limb by one unit (Table 2). An association was also observed with the preoperative upper limb ($p=0.004$) and the postoperative lower limb ($p=0.005$) motor examination. Ipsilateral FA parameters for the perilesional and proximal segments were also associated with preoperative upper and lower limb examination and postoperative upper limb examination (Table 2, Figure 3). Percentage difference or decrease in the overall FA values for the ipsilateral CST was negatively associated with the preoperative upper ($p=0.015$) and lower ($p=0.044$) examination and with postoperative upper limb ($p=0.004$) examination. This was also observed for the percentage difference in the perilesional segments for the CST segments ipsilateral to the lesion in relation to the preoperative upper ($p=0.003$) and lower ($p=0.02$) limb examination and to postoperative upper limb ($p=0.006$) examination. A greater noted percentage difference in these FA parameters on the ipsilateral or lesional side relative to the contralateral side therefore, led to a poorer neurological examination pre- and postoperatively. Higher FA values for the overall CST contralateral to the lesion was significantly associated with better preoperative upper ($p<0.001$) limb examination. Similar association was also observed for the preoperative lower ($p=0.003$) limb and the postoperative upper limb ($p=0.002$) examination. Higher FA values for the contralateral proximal CST segment (homologous to the ipsilateral proximal CST segments) was also significantly associated with better pre- and postoperative upper limb examination ($p<0.001$). Similar association was also observed with the preoperative lower ($p=0.016$) limb examination.

4.5.5 Preoperative quantitative data in relation to eventual performance status

Multiple parameters (Table 3, Figure 4) were negatively correlated with the eventual mRS score for the patients. Key were FA values for: ipsilateral distal segment ($p=0.001$) and contralateral perilesional segment (segment of the CST homologous to the perilesional segment on the normal side; $p<0.001$). Higher FA values for these parameters were associated with a lower mRS score and thereby, a better performance status.

4.5.6 Postoperative patient neurological and functional status

At the last documented examination, with respect to the lower limbs, 14 patients had grade 5 strength; 3 grade 4 while 2 had grade 1. With respect to the upper limb, 13 patients had grade 5 strength and 2 grade 4. One patient each (total of 3) had grade 2, 1 and 0 strength. At the last documented follow-up, median mRS for 18 patients was 2 (0-4). The number of patients (indicated in the brackets) in the different mRS categories were as follows: 0 (1); 1 (4); 2 (7); 3 (5) and 4 (1).

4.5.7 Postoperative quantitative data in relation to postoperative motor scores and eventual functional outcomes

In 9 patients with postoperative imaging, FA values for the following were positively associated with postoperative upper limb examination (Supplemental Digital Content 3: Table 1): ipsilateral proximal ($p=0.007$) and contralateral proximal ($p=0.002$) CST segments. FA values for the following were negatively associated with the postoperative upper limb examination: percentage difference for the overall CST (lesional side; $p=0.003$) and the contralateral perilesional segment (normal side; $p=0.041$). No variables were associated with postoperative mRS at final follow-up (Table 4).

4.5.8 Changes in qualitative features from pre- to postoperative period and relationship to the neurological examination

Of 9 patients with postoperative DTI, CST configuration changed from displaced to normal in 4. In the remaining 5, there was no change in the CST configuration from the pre- to postoperative stage (disrupted in 2; normal in 3). For 3 of 4 patients with change in configuration from displaced to normal CST, the examination remained unchanged and normal. For the other, there was a neurological improvement postoperatively (grade 4 preoperatively in the upper and lower limbs to grade 4 and 5 in upper and lower limbs respectively). The examination worsened for one patient with disrupted CST at the pre- and postoperative stage (from grade 4 to 2 in the upper and lower limbs). Weakness remained unchanged for another patient with disrupted CST at baseline and postoperative stage (grade 0 and 4 in the upper and lower limbs respectively). The examination remained normal in 3 patients with normal CST at the pre- and postoperative stage.

4.5.9 Changes in quantitative features of radiological data from pre- to postoperative period

The mean percentage difference in perilesional FA values for the CST segments (in relation to the contralateral homologous segment) changed from pre- to postoperative period as follows: 17.5% to 12.5% (for all 9 patients; change (improvement) by 5%); 13.2% to 9.9% (for 4 patients with configuration changing from displaced to normal; change (improvement) by 3.3%); 36.3% to 32.9% (for 2 patients with disrupted tracts; change (improvement) by 3.4%) and 10.7% to 2.2% (for 3 patients with normal tract configuration; change (improvement) by 8.5%). With respect to the mean percentage difference in the FA values for the whole CST on the *ipsilateral* side in relation to the contralateral CST, the change from the pre- to postoperative period was: 9.3% to 8.1% (for all 9 patients; change (improvement) by 1.2%); 4.8% to 2.9% (for 4 patients with configuration changing from displaced to normal; change (improvement) by 1.9%); 27.6% to 25.2% (for 2 patients with disrupted tracts; change (improvement) by 2.4%) and 3.2% to 3.7% (for 3 patients with normal tracts; change (worsening) by 0.5%). In general, the observed decrease in the mean percentage difference implied that the FA values on the ipsilateral side improved, becoming closer to the normal side postoperatively.

4.6 Discussion

A recent randomized controlled trial demonstrated the utility of qualitative DTI data in reducing morbidity associated with resecting brainstem CMs.[14] At one year, the mean mRS score and percentage of patients with worsened motor deficits were significantly lower in the DTI than in the control group. Preoperative CST score based upon qualitative characteristics was negatively associated with preoperative motor function. This score was not significantly related to motor score at a year. Quantitative DTI data was not examined in relation to clinical outcomes.[14] Another study did not confirm the role of decreased FA values at the lesion level in predicting a poor prognosis.[15]

4.6.1 Implication of pre- and postoperative qualitative DTI data and its association with the neurological examination

Most patients with disrupted and displaced CST had abnormal and normal preoperative motor neurological examination respectively, while all with *normal* CST had a normal examination. This remained true in nine with postoperative DTI where patients with neurological weakness had disrupted CST. Interestingly, the change in configuration from displacement to normal was associated with normalization of examination in one patient. Qualitative data remained consistent from the pre- to postoperative phase after removal of the CMs. Disruption, consistent with other studies, was associated with neural weakness.[9,14,16] Interpretation of qualitative data is however, prone to variability[14] leading to our approach towards confirming morphological features quantitatively[9,16,17] and towards correlating the latter rather than qualitative data with motor examination.

4.6.2 Relationship of qualitative data to quantitative data pre- and postoperatively

Percentage difference for FA values for the perilesional segment was highest for disrupted tracts with these values being lower for displaced or normal tracts. These findings imply neural injury at the lesional level.[9,15,16] Similar trend was observed for the percentage difference for the FA values for the overall CST. For those with postoperative DTI, the change in percentage difference in the FA values suggested a trend towards normalization of the affected tract. Susceptibility effects from paramagnetic molecules (deoxyhaemoglobin) can affect quantitative results leading to artifactual signal loss.[18] The finding that the percentage difference in FA values remained relatively stable in those with postoperative imaging (carried out more than 4 months on average postoperatively) argues against a major contribution from this phenomenon.

4.6.3 Preoperative quantitative data, its relationship to neurological examination and functional outcomes and implications for prognostication

FA values for ipsilateral overall CST and distal CST segment in particular, demonstrated a positive relationship with both the pre- and postoperative motor examination. FA values for the distal CST segments, in particular was significantly associated with the postoperative motor examination. Negative association was observed between percentage decreases for FA values for the overall and perilesional segments in relation to the pre- and postoperative motor examination. Among others (Table 3), higher FA values for the distal CST segments were also associated with lower postoperative mRS at the final follow-up implying a better functional status. Negative direction of these associations further validates our model. With most patients having suffered multiple haemorrhages preoperatively, changes in the distal CST segments are noteworthy and potentially consistent with Wallerian degeneration occurring over months.[19-21] Acute compromise of the tract integrity may be evident using FA within days[22] with further changes due to Wallerian degeneration being observed over months.[21] Changes in the distal CST segment therefore, may better predict the postoperative motor examination and functional status and be of greater

prognostic significance. Furthermore, the fibers in the distal CST are more condensed in comparison to subcortical fibers. Although the FA values for the distal CST segments were most informative, FA values for both distal and proximal segments (Table 2, Figure 3) had a stronger association with the pre- and postoperative motor examination in comparison with the FA values for the perilesional segments. This is consistent with another study where the rostral and caudal diffusion parameters provided more information on integrity of the CST compared with morphological study alone.[15]

4.6.4 Implication of observed association between contralateral quantitative parameters and motor examination and functional outcomes

A noteworthy observation was the positive association between the FA values for contralateral overall CST and proximal segments with the pre- and postoperative motor examination (Table 2, Figure 3). Further, a negative association was seen between the contralateral FA values (perilesional, proximal and distal segments) and the eventual mRS score. Contralateral associations including in the rostral segment may represent a compensatory physiological phenomenon, similar to that observed in our previous longitudinal study relating to brainstem CMs.[9] Rostral changes on the normal side may be morphological correlate of transcallosal disinhibition such as shown in patients with pyramidal stroke.[23] Another contributory factor may be the proximity of multiple fibers including the contralateral CST in brainstem making it difficult to completely exclude any effect beyond that observed using DTI. This is particularly applicable for a few patients in our study with CMs close to the midline (Table 1). It is noteworthy that CMs relatively close to the midline were eccentric to one side such that the laterality of affected CST could be clearly established.

4.6.5 Limitations and future directions

FA being susceptible to partial volume effects, is underestimated in areas with multiple crossing fibers and oedema.[24-26] No significant perilesional oedema was

observed in our cohort. A small proportion were scanned on a 1.5 T scanner with implication for variability in the quantitative indices; use of control like contralateral CST would have partly mitigated this. Postoperative DTI was only available in half of the patients, likely accounting for lack of significant observed association between majority of postoperative quantitative parameters and clinical outcomes. Validity of multivariable analysis in a small number of postoperative patients is compromised. Current findings including those relating to the contralateral quantitative parameters will require further validation in a larger cohort. A composite score accounting for changes in other motoric tracts may have better prognostic potential.

4.7 Conclusions

In this preliminary model, we demonstrated the utility of using preoperative FA values of overall CST and its specific segments in predicting patient pre- and postoperative neurological motor examination and/or eventual functional status. Higher FA values for the distal CST segments ipsilateral to the lesion was particularly notable for its prognostic potential and was associated with better eventual motor and functional outcomes in patients undergoing surgery for deep CMs.

4.8 References

1. Barrow DL, Schuette AJ. CMss: a paradigm for progress. *Clin Neurosurg.* 2011;58:27-41.
2. Abla AA, Spetzler RF. Brainstem cavernoma surgery: the state of the art. *World neurosurgery.* 2013;80(1-2):44-46.
3. Porter RW, Detwiler PW, Spetzler RF, et al. CMs of the brainstem: experience with 100 patients. *Journal of neurosurgery.* 1999;90(1):50-58.
4. Li D, Hao SY, Jia GJ, Wu Z, Zhang LW, Zhang JT. Haemorrhage risks and functional outcomes of untreated brainstem CMss. *Journal of neurosurgery.* 2014;121(1):32-41.

5. Pandey P, Westbroek EM, Gooderham PA, Steinberg GK. CMs of brainstem, thalamus, and basal ganglia: a series of 176 patients. *Neurosurgery.* 2013;72(4):573-589; discussion 588-579.
6. Abla AA, Lekovic GP, Turner JD, de Oliveira JG, Porter R, Spetzler RF. Advances in the treatment and outcome of brainstem CMs surgery: a single-centre case series of 300 surgically treated patients. *Neurosurgery.* 2011;68(2):403-414; discussion 414-405.
7. Chen X, Weigel D, Ganslandt O, Buchfelder M, Nimsky C. Diffusion tensor imaging and white matter tractography in patients with brainstem lesions. *Acta neurochirurgica.* 2007;149(11):1117-1131; discussion 1131.
8. Chen X, Weigel D, Ganslandt O, Fahlbusch R, Buchfelder M, Nimsky C. Diffusion tensor-based fiber tracking and intraoperative neuronavigation for the resection of a brainstem cavernous angioma. *Surg Neurol.* 2007;68(3):285-291; discussion 291.
9. Faraji AH, Abhinav K, Jarbo K, et al. Longitudinal evaluation of corticospinal tract in patients with resected brainstem CMss using high-definition fiber tractography and diffusion connectometry analysis: preliminary experience. *Journal of neurosurgery.* 2015;123(5):1133-1144.
10. Januszewski J, Albert L, Black K, Dehdashti AR. The Usefulness of Diffusion Tensor Imaging and Tractography in Surgery of Brainstem CMss. *World neurosurgery.* 2016;93:377-388.
11. Ulrich NH, Kockro RA, Bellut D, et al. Brainstem cavernoma surgery with the support of pre- and postoperative diffusion tensor imaging: initial experiences and clinical course of 23 patients. *Neurosurgical review.* 2014;37(3):481-491; discussion 492.
12. McLaughlin N, Kelly DF. Corticospinal tractography as a prognosticator for motor improvement after brainstem cavernoma resection. *British journal of neurosurgery.* 2013;27(1):108-110.
13. Mai JC, Ramanathan D, Kim LJ, Sekhar LN. Surgical resection of CMss of the brainstem: evolution of a minimally invasive technique. *World neurosurgery.* 2013;79(5-6):691-703.
14. Li D, Jiao YM, Wang L, et al. Surgical outcome of motor deficits and neurological status in brainstem CMss based on preoperative diffusion tensor

imaging: a prospective randomized clinical trial. *Journal of neurosurgery.* 2019;130:286-301.

15. Yao Y, Ulrich NH, Guggenberger R, Alzarhani YA, Bertalanffy H, Kollias SS. Quantification of Corticospinal Tracts with Diffusion Tensor Imaging in Brainstem Surgery: Prognostic Value in 14 Consecutive Cases at 3T Magnetic Resonance Imaging. *World neurosurgery.* 2015;83(6):1006-1014.
16. Abhinav K, Pathak S, Richardson RM, et al. Application of high-definition fiber tractography in the management of supratentorial CMss: a combined qualitative and quantitative approach. *Neurosurgery.* 2014;74(6):668-680; discussion 680-661.
17. Abhinav K, Yeh FC, Pathak S, et al. Advanced diffusion MRI fiber tracking in neurosurgical and neurodegenerative disorders and neuroanatomical studies: A review. *Biochimica et biophysica acta.* 2014;1842(11):2286-2297.
18. Dorenbeck U, Schlaier J, Bretschneider T, Schuierer G, Feuerbach S. Diffusion-weighted imaging with calculated apparent diffusion coefficient in intracranial haemorrhagic lesions. *Clin Imaging.* 2005;29(2):86-93.
19. Wieshmann UC, Symms MR, Clark CA, et al. Wallerian degeneration in the optic radiation after temporal lobectomy demonstrated in vivo with diffusion tensor imaging. *Epilepsia.* 1999;40(8):1155-1158.
20. Pierpaoli C, Barnett A, Pajevic S, et al. Water diffusion changes in Wallerian degeneration and their dependence on white matter architecture. *NeuroImage.* 2001;13(6 Pt 1):1174-1185.
21. McDonald CR, Hagler DJ, Jr., Girard HM, et al. Changes in fiber tract integrity and visual fields after anterior temporal lobectomy. *Neurology.* 2010;75(18):1631-1638.
22. Yoshioka H, Horikoshi T, Aoki S, et al. Diffusion tensor tractography predicts motor functional outcome in patients with spontaneous intracerebral haemorrhage. *Neurosurgery.* 2008;62(1):97-103; discussion 103.
23. Radlinska BA, Blunk Y, Leppert IR, Minuk J, Pike GB, Thiel A. Changes in callosal motor fiber integrity after subcortical stroke of the pyramidal tract. *J Cereb Blood Flow Metab.* 2012;32(8):1515-1524.
24. Le Bihan D, Poupon C, Amadon A, Lethimonnier F. Artifacts and pitfalls in diffusion MRI. *J Magn Reson Imaging.* 2006;24(3):478-488.

25. Alexander AL, Hasan KM, Lazar M, Tsuruda JS, Parker DL. Analysis of partial volume effects in diffusion-tensor MRI. *Magn Reson Med.* 2001;45(5):770-780.
26. Oouchi H, Yamada K, Sakai K, et al. Diffusion anisotropy measurement of brain white matter is affected by voxel size: underestimation occurs in areas with crossing fibers. *AJNR Am J Neuroradiol.* 2007;28(6):1102-1106.

4.9.1 Figures

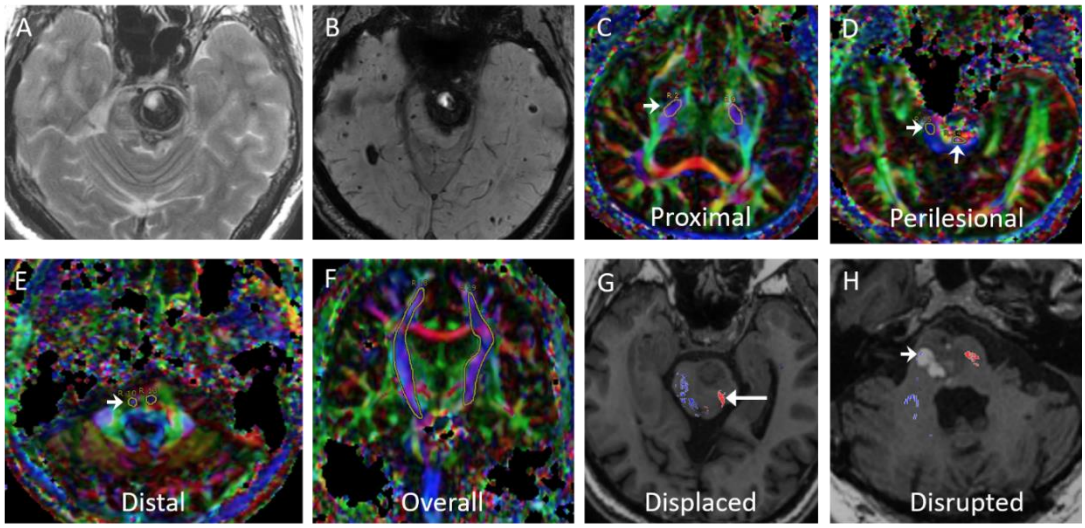

FIGURE 1. Region of interests (ROIs) methodology for quantitative analysis and examples of qualitative analysis. Axial T2-weighted (A) and susceptibility-weighted (B) images show a large cavernous malformation in the left pons. ROIs (small white arrows, C-E) were manually placed in the expected location of the corticospinal tract (CST) in both hemispheres at 3 locations relative to the cavernous malformation: proximal (C), at the level of (D), and distal (E) to the lesion. ROIs were also placed around the CST on a coronal image to evaluate the maximal visual representation of the tract on a single two-dimensional image slice (F). In this subject, the left CST (small white arrow) was described as being "displaced" by the cavernous malformation relative to the contralateral tract (G). (H) shows an example of a "disrupted" right CST (small white arrow) in another subject. For (G) and (H), colours were assigned as follows: blue=right CST and red=left CST.

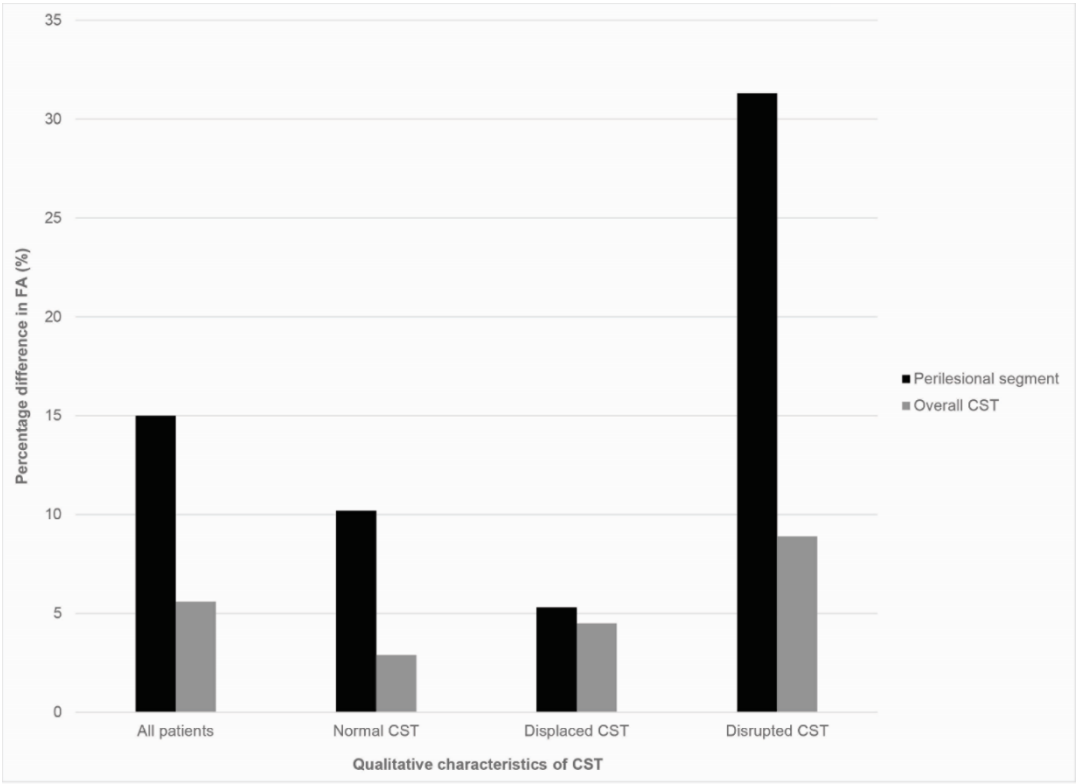

FIGURE 2. Preoperative qualitative features of the corticospinal tract (CST) in relation to the quantitative parameters [mean percentage difference in fractional anisotropy (FA) of the perilesional segment of the affected side in relation to the normal side (black); mean percentage difference in FA of the overall CST on the affected side in relation to the normal side (grey)].

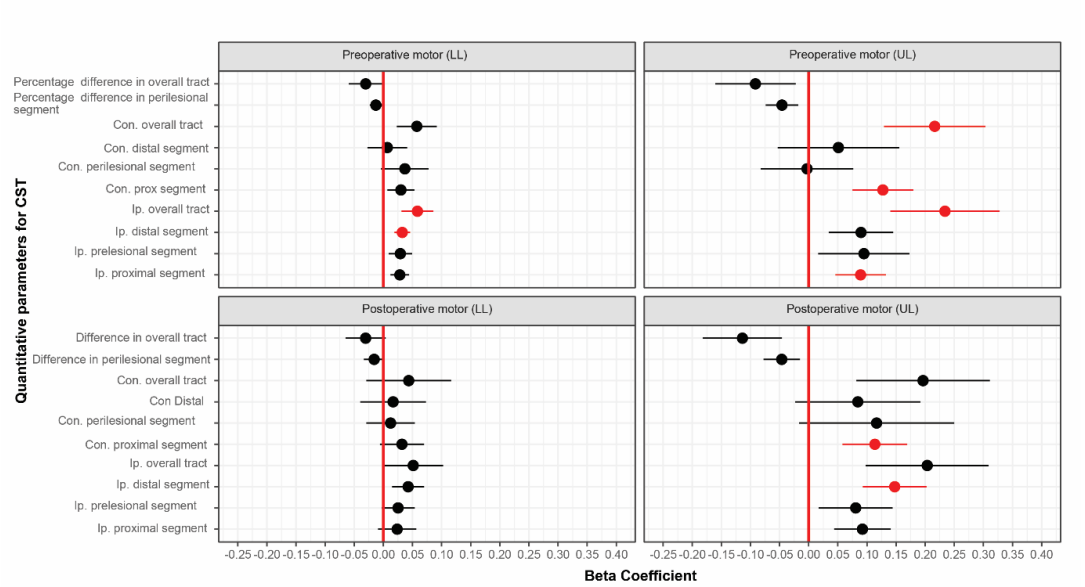

FIGURE 3. Forest plot summarizing the results of the multivariable linear regression analysis evaluating adjusted relationship between preoperative quantitative variables and pre- and postoperative motor strength in the upper and lower limbs (n=18; corresponding to Table 2). For each of the quantitative parameter [standardized FA (calculated as 100* FA with a range of 0-100) and percentage difference in overall tract or perilesional segment], a stepwise regression was performed. Each parameter was included as one independent variable in the model and the following candidate covariates were included in the full model for model selection and adjustment: preoperative location of the cavernous malformation, pial presentation, number of haemorrhages and the age at treatment. The results represented the estimates from optimal models that were adjusted for selected covariates in the candidate list with the lowest Akaike information criterion. Horizontal lines (black) represented the point estimates and 95% confidence intervals of the beta-coefficients (alpha=0.05); horizontal lines in red represented the variables that are significant at a value of $p<0.001$ after Bonferoni correction [Con.: contralateral; FA: fractional anisotropy; Ip.: ipsilateral; UL: upper limb; LL: lower limb; beta-coefficient was estimated from the regression model].

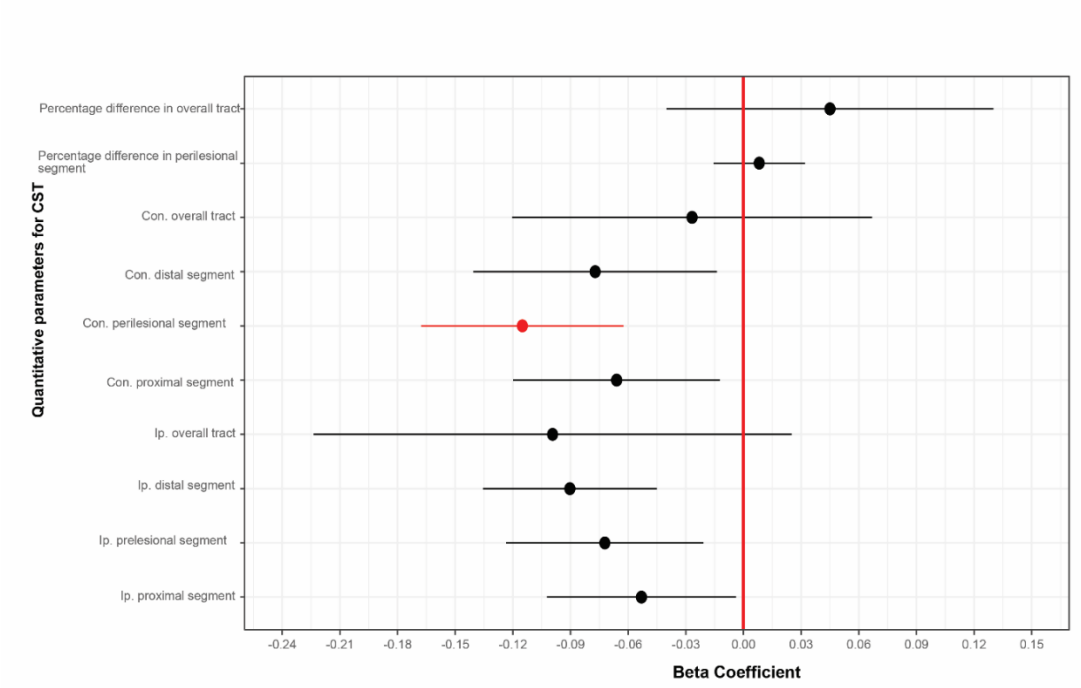

FIGURE 4. Forest plot summarizing the multivariable linear regressions analysis evaluating adjusted relationships between preoperative quantitative variables and the modified Rankin scale score at final follow-up (n=18; corresponding to Table 3). For each of the quantitative parameter [standardized FA (calculated as 100* FA with a range of 0-100) and percentage difference in overall tract or perilesional segment], a stepwise regression was performed. Each parameter was included as one independent variable in the model and the following candidate covariates were included in the full model for model selection and adjustment: preoperative location of the cavernous malformation, pial presentation, number of haemorrhages, age at treatment and cranial neuropathy. The results represented the estimates from optimal models that were adjusted for selected covariates in the candidate list with the lowest Akaike information criterion. Horizontal lines (black) represented the point estimates and 95% confidence intervals of the beta-coefficients (alpha=0.05); horizontal lines in red represented the variables that are significant at a value of $p<0.001$ after Bonferoni correction [Con.: contralateral; FA: fractional anisotropy; Ip.: ipsilateral; UL: upper limb; LL: lower limb; beta-coefficient was estimated from the regression model].

4.9.2 Tables

TABLE 1. Overall preoperative patient characteristics and in relation to qualitative features of the Corticospinal tract

Patient characteristics	ALL (n=18)		Displaced (n=8)		Disrupted (n=6)		Normal (n=4)	
Sex, n(%)								
Female	8	44.4%	4	50.0%	3	50.0%	1	25.0%
Male	10	55.6%	4	50.0%	3	50.0%	3	75.0%
Age, mean(sd)	47	17.2	43	12.5	56	23.4	41	12.8
Location, n(%)								
Medulla [R(1); midline to L(1)]	2	11.1%	2	25.0%	0	0.0%	0	0.0%
Mesencephalon [L(1); R(3)]	4	22.2%	1	12.5%	0	0.0%	3	75.0%
Pons [L(3); R(4); midline to L(1); midline to R(1)]	9	50.0%	4	50.0%	5	83.3%	0	0.0%
Thalamus/ Basal ganglia [L(3)]	3	16.7%	1	12.5%	1	16.7%	1	25.0%
Pial presentation, n(%)								
No	13	72.2%	5	62.5%	6	100.0%	2	50.0%
Yes	5	27.8%	3	37.5%	0	0.0%	2	50.0%
Number of haemorrhages, n(%)								
1	7	38.9%	3	37.5%	1	16.7%	3	75.0%
2	8	44.4%	3	37.5%	4	66.7%	1	25.0%
3	1	5.6%	1	12.5%	0	0.0%	0	0.0%
>3	2	11.1%	1	12.5%	1	16.7%	0	0.0%
Cranial Nerve Neuropathy, n(%)								
No	5	27.8%	2	25.0%	1	16.7%	2	50.0%
Yes	13	72.2%	6	75.0%	5	83.3%	2	50.0%
Motor strength (UL), n(%)								
0	1	5.6%	0	0.0%	1	16.7%	0	0.0%
1	1	5.6%	0	0.0%	1	16.7%	0	0.0%
4	4	22.2%	1	12.5%	3	50.0%	0	0.0%
5	12	66.7%	7	87.5%	1	16.7%	4	100.0%
Motor strength (LL), n(%)								
4	5	27.8%	1	12.5%	4	66.7%	0	0.0%
5	13	72.2%	7	87.5%	2	33.3%	4	100.0%
Days from surgery to postoperative examination, median (IQR)	138	203	118	149	165	100	206	264
Days from surgery to final follow-up for mRS score, median (IQR)	270	426	442	640	255	316	246	184

(IQR: interquartile range; L: left; LL: lower limbs; mRS: modified Rankin Scale; R: right; sd: standard deviation; UL: upper limbs)

TABLE 2. Multivariable linear regression analysis evaluating adjusted relationship between preoperative quantitative variables and pre- and postoperative motor strength (n=18)

Quantitative parameters for CST (FA)	Preop. motor (LL)[1]				Preop. motor (UL)[1]				Postop. Motor (LL)[1]				Postop. Motor (UL)[1]			
	Estimate	Lower CI	Upper CI	P. value	Estimate	Lower CI	Upper CI	P. value	Estimate	Lower CI	Upper CI	P. value	Estimate	Lower CI	Upper CI	P value
Percentage difference in overall tract	-0.030	-0.060	-0.001	0.044*	-0.091	-0.161	-0.022	0.015*	-0.030	-0.065	0.004	0.079	-0.114	-0.182	-0.046	0.004*
Percentage difference in perilesional segment	-0.013	-0.023	-0.002	0.020*	-0.046	-0.074	-0.018	0.003*	-0.016	-0.034	0.002	0.077	-0.046	-0.078	-0.015	0.006*
Con. overall tract	0.057	0.023	0.092	0.003*	0.216	0.129	0.304	0.000**	0.044	-0.029	0.116	0.222	0.196	0.082	0.311	0.002*
Con. distal segment	0.007	-0.027	0.041	0.678	0.051	-0.053	0.156	0.315	0.017	-0.040	0.073	0.540	0.084	-0.023	0.192	0.115
Con. perilesional segment	0.037	-0.004	0.078	0.071	-0.003	-0.082	0.077	0.940	0.012	-0.029	0.054	0.536	0.117	-0.017	0.250	0.079
Con. proximal segment	0.030	0.007	0.053	0.016*	0.127	0.075	0.180	0.000**	0.032	-0.006	0.070	0.095	0.114	0.058	0.169	0.001**
Ip.overall tract	0.058	0.031	0.086	0.001**	0.234	0.140	0.328	0.000**	0.051	0.000	0.103	0.050*	0.204	0.098	0.309	0.002*
Ip.distal segment	0.032	0.019	0.046	0.000**	0.090	0.034	0.145	0.004*	0.043	0.015	0.070	0.005*	0.148	0.093	0.202	0.000**
Ip.perilesional segment	0.029	0.009	0.049	0.009*	0.095	0.016	0.173	0.024*	0.025	-0.003	0.054	0.080	0.081	0.017	0.144	0.018*
Ip.proximal segment	0.028	0.012	0.044	0.003*	0.089	0.046	0.132	0.001**	0.024	-0.009	0.057	0.147	0.092	0.044	0.141	0.001**

[1]For each of the quantitative parameter [standardized FA (calculated as 100* FA with a range of 0-100) and percentage difference in overall tract or perilesional segment], a stepwise regression was performed. Each parameter was included as one independent variable in the model and the following candidate covariates were included in the full model for model selection and adjustment: preoperative location of the cavernous malformation, pial presentation, number of haemorrhages and the age at treatment. The results in this table represented the estimates from optimal models that were adjusted for selected covariates in the candidate list with the lowest Akaike information criterion. *: significance at $p<0.05$; **: significance at $p<0.001$ after Bonferoni correction. (CI: confidence interval; Con.: contralateral; FA: fractional anisotropy; Ip.: ipsilateral; UL: upper limb; LL: lower limb; preop.: preoperative; postop.: postoperative)

TABLE 3. Multivariable linear regressions analysis evaluating adjusted relationships between preoperative quantitative variables and the modified Rankin scale score at final follow-up (n=18)

Quantitative parameters for CST (FA)	mRS score at final follow-up[1]			
	Estimate	Lower CI	Upper CI	P. Value
Percentage difference in overall tract	0.045	-0.040	0.130	0.251
Percentage difference in perilesional segment	0.008	-0.016	0.032	0.472
Con. overall tract	-0.027	-0.120	0.067	0.552
Con. distal segment	-0.077	-0.141	-0.014	0.020*
Con. perilesional segment	-0.115	-0.168	-0.062	0.001**
Con. proximal segment	-0.066	-0.120	-0.012	0.021*
Ip. overall tract	-0.099	-0.224	0.025	0.103
Ip. distal segment	-0.090	-0.136	-0.045	0.001*
Ip. perilesional segment	-0.072	-0.124	-0.021	0.013*
Ip. proximal segment	-0.053	-0.102	-0.004	0.037*

[1]For each of the quantitative parameter [standardized FA (calculated as 100* FA with a range of 0-100) and percentage difference in overall tract or perilesional segment], a stepwise regression was performed. Each parameter was included as one independent variable in the model and the following candidate covariates were included in the full model for model selection and adjustment: preoperative location of the cavernous malformation, pial presentation, number of haemorrhages, age at treatment and cranial neuropathy. The results in this table represented the estimates from optimal models that were adjusted for selected covariates in the candidate list with the lowest Akaike information criterion. *: significance at $p<0.05$; **: significance at $p<0.001$. (CI: confidence interval; Con.: contralateral; FA: fractional anisotropy; Ip.: ipsilateral; mRS: modified Rankin scale; UL: upper limb; LL: lower limb; preop.: preoperative; postop.: postoperative)

Table 4. Multivariable linear regressions analysis evaluating the adjusted relationship between postoperative quantitative variables and postoperative motor strength and follow-up modified Rankin scale scores (n=9)

Quantitative parameters for CST (FA)	Postop. motor (LL)[1]				PostOp. motor (UL)[1]				mRS score at final follow-up[2]			
	Estimate	Lower CI	Upper CI	P. Value	Estimate	Lower CI	Upper CI	P. Value	Estimate	Lower CI	Upper CI	P. Value
Ip. proximal segment	0.030	-0.036	0.096	0.317	0.113	0.052	0.174	0.007 *	0.085	-0.274	0.444	0.204
Ip. perilesional segment	0.086	-0.006	0.178	0.062	0.070	-0.139	0.278	0.287	0.005	-0.049	0.060	0.806
Ip. distal segment	0.078	-0.006	0.163	0.065	0.074	-0.190	0.339	0.350	0.009	-0.066	0.083	0.766
Ip. overall tract	0.029	-0.067	0.124	0.498	-0.103	-1.313	1.106	0.748	0.023	-0.094	0.141	0.614
Con. proximal segment	0.050	-0.048	0.147	0.267	0.187	0.095	0.278	0.002 *	0.113	-1.584	1.809	0.554
Con. perilesional segment	-0.902	-5.467	3.662	0.241	-0.661	-1.256	-0.066	0.041 *	-0.045	-0.111	0.020	0.134
Con. distal segment	-0.348	-3.521	2.826	0.397	-0.260	-2.061	1.541	0.317	-0.123	-0.346	0.100	0.090
Con. overall tract	-1.169	-3.304	0.965	0.091	-0.789	-3.534	1.956	0.170	-0.085	-0.182	0.013	0.073
Percentage difference in perilesional segment	-0.058	-0.566	0.451	0.387	-0.036	-0.448	0.376	0.466	-0.004	-0.029	0.021	0.688
Percentage difference in overall tract	-0.024	-0.087	0.040	0.409	-0.115	-0.174	-0.055	0.003 *	-0.057	-0.278	0.164	0.383

For each of the quantitative parameter [standardized FA (calculated as 100* FA with a range of 0-100) and percentage difference in overall tract or perilesional segment], a stepwise regression was performed. Each quantitative parameter was included as one independent variable in the model and the following candidate covariates were included in the full model for model selection and adjustment: preoperative location of the cavernous malformation, pial presentation, number of haemorrhages and age at treatment.[1] In addition to the listed covariates, presence of cranial neuropathy was also included in the model for mRS score at final follow-up.[2] The results in this table represented the estimates from optimal models that were adjusted for selected covariates in the candidate list with the lowest Akaike information criterion. *: significance at $p<0.05$. (CI: confidence interval; Con.: contralateral; FA: fractional anisotropy; Ip.: ipsilateral; mRS: modified Rankin scale; UL: upper limb; LL: lower limb; postop.: postoperative)

Chapter 5: Use of diffusion spectrum imaging in longitudinal evaluation of amyotrophic lateral sclerosis: development of an imaging biomarker

Paper 4: Abhinav K, Yeh FC, El-Dokla A, Ferrando LM, Chang YF, Lacomis D, Friedlander RM, Fernandez-Miranda JC. Use of diffusion spectrum imaging in longitudinal evaluation of amyotrophic lateral sclerosis: development of an imaging biomarker. *Frontiers in Human Neuroscience* 2014; 29(8):270

5.1 Declaration

I was the lead first author with respect to this manuscript and in conjunction with the second author was instrumental in the application of diffusion connectometry in the longitudinal evaluation of amyotrophic lateral sclerosis (ALS). Overall I contributed extensively towards the writing, literature search, figures, study design, data analysis and interpretation.

5.2 Introduction to and brief summary of the manuscript and relation to the previous work

Having investigated the use of advanced white matter (WM) imaging technique/ high definition fiber tractography (HDFT) in supratentorial and infratentorial CMs, including the use of diffusion connectomerty in particular, a fully automated technique in the longitudinal evaluation of integrity of the WM tracts, in the latter, the emphasis was now diverted towards further examining the quantitative as well as the qualitative data in patients with ALS. Diffusion connectometry, being an automated method reduced the variability issues surrounding placement of regions of interest and the standardization of quantitative anisotropy. The imaging and research focus was both on neurosurgical and neurological disorders, particularly the neurodegenerative disorders. One of the primary focus of the research community in neurodegenerative disorders like ALS or Huntington's disease has been to devise an imaging biomarkers that can then be used to assess efficacy of potential novel therapeutic trials in the future.

We hypothesised that changes in the WM were present in ALS beyond the motor tracts, and that the affected pathways and associated pattern of disease progression

could be tracked longitudinally using automated diffusion connectometry analysis. Connectometry analysis, based on diffusion spectrum imaging overcomes the limitations of a conventional tractography approach and diffusion tensor imaging. The identified affected WM tracts can then be assessed in a targeted fashion qualitatively and quantitatively, using HDFT and changes in our quantitative markers over time, and be potentially correlated with clinical progression. We illustrated these principles towards developing an imaging biomarker, applicable towards demonstrating individual progression, by presenting results for five ALS patients, including with documented longitudinal data in two. Preliminary analysis demonstrated a number of changes bilaterally and asymmetrically in motoric and extramotoric white matter pathways including in limbic system possibly explaining the basis of cognitive symptoms in ALS. In two with longitudinal data, the white matter changes were less extensive at baseline with evidence of spread of disease in a frontal pattern with relative sparing of fibers from postcentral gyrus, consistent with the known pathology in ALS.

5.3 Introduction

Amyotrophic lateral sclerosis (ALS) is a neurodegenerative disorder, marked by progressive failure of both upper (UMN) and lower motor neurons (LMN). LMN symptoms in ALS may obscure the UMN symptoms, contributing at least partly to the potential delay in diagnosis and the subsequent treatment. This has therefore led to a search for an imaging biomarker, useful for diagnostic and monitoring purposes for evaluating efficacy of treatments in future trials. Previous diffusion tensor imaging (DTI) studies have shown white matter pathology in ALS, predominantly in the motor pathways. Further these studies have shown that DTI can be used longitudinally to track pathology over time, making white matter pathology a candidate as an outcome measure in future trials. DTI [1-7] studies in ALS have therefore been carried out to investigate the involvement of the white matter tracts and their potential correlation with clinical markers of progression like the revised ALS functional rating scale (ALSFRS-R).[8,9] These studies have relied on DTI-based indices, like fractional anisotropy (FA) or apparent diffusion coefficient (ADC) for quantification of the observed changes in the integrity of white matter tracts, for example corticospinal tract (CST) or corpus callosum (CC). In general, these studies

have demonstrated a reduction in the values of FA, when compared to controls or when carried out in a longitudinal fashion[3,5,10,11] over time along the CST. These studies have therefore, indirectly demonstrated disease progression in ALS. FA is a commonly used DTI-derived quantitative measure of anisotropy[12,13] and has been applied in the evaluation of white matter integrity in multiple neurological disease states including multiple sclerosis[14] and stroke.[15] It has been suggested that the changes in FA may reflect changes in organisation of fibers[16] with a reduction reflecting axonal fiber degeneration and myelin breakdown in the central and peripheral nervous system.[17,18]

A noteworthy point in the ALS pathology with respect to longitudinally monitoring white matter disease, in addition to that present in the CST is the presence of extramotoric changes. These extramotoric changes have been demonstrated in multiple studies, including in CC;[19] cingulum and hippocampal formation[20] and cerebellum.[10] A pathological study in ALS[21] based on post-mortem examination of seven patients, showed evidence of degenerating fibers in the pre-central gyrus (and CST), post-central gyrus and in the adjacent frontal and parietal gyri, CC and basal ganglia. These changes suggest a multisystem neurodegenerative process. DTI and voxel based analysis (VBA) have been used in a complementary fashion to elucidate these changes to varying extents.[7,11,22,23] Although these studies have been promising in demonstrating white matter changes in ALS, DTI is acknowledged to have major limitations. These limitations include its inability to represent the crossing of multiple fibers; it further misses large segments of tracts and results in multiple artifacts.[24,25] The indices derived from it, for example FA have been shown to suffer from the partial volume effects leading to their underestimation in regions containing crossing fibers.[13,26] This therefore, limits the use of FA as a quantitative marker in ALS. Other limitations pertinent to all tractography-based studies, are the inherent variability, particularly between observers in the tracts due to issues related to the regions of interest (ROI) chosen and the manual nature of the analysis. Further there are changes in the imaging data in terms of signal to noise ratio across multiple scans in longitudinal studies. VBA addresses some of these limitations; however it does not provide directional information in terms of the specific tracts involved. Due to these limitations, new fiber mapping techniques were developed such as high-angular-resolution diffusion imaging (HARDI)[27] and diffusion spectrum imaging

(DSI). DSI measures diffusion spectra and enables resolution of intravoxel heterogeneity of diffusion. This results in the resolution of a set of directions of multiple pathways or fiber orientations within a voxel[28] in contrast to the average direction in DTI.

Our group has developed and demonstrated the use of an advanced white matter imaging technique, the so-called High Definition Fiber Tractography (HDFT). HDFT addresses the limitations associated with DTI, and is accurate in tracking white fiber pathways in the brain through complex fiber crossings to subcortical regions and targets with subvoxel resolution.[29] HDFT relies on DSI for acquisition;[28] generalised q-sampling imaging for fiber orientation estimation;[30] multiple intravoxel sampling; and other innovations in tractography.[31] HDFT approach has facilitated innovative studies on the structural connectivity of several fiber tracts such as the middle longitudinal fascicle;[32] CST;[31] CC;[33] dorsal stream visual pathways[34] and the corticostriatal pathways.[35] Application of HDFT has enabled us to replicate several known neuroanatomical features, including claustrum, thalamic nuclei segmentation and multiple fiber crossings at the centrum semiovale.[29] Ongoing trials at our institution are examining its application in evaluating white fiber pathology in other diseases, for example cavernomas and brain tumours with promising preliminary results.[29] Quantitative anisotropy (QA) is our novel quantitative imaging measure related to our white matter imaging technique. QA is a measure of anisotropy of water with estimated spin density. QA serves as a reliable stopping criterion for fiber tracking and is essential towards demonstrating endpoint connectivity of functional regions.[30,36] It overcomes some of the limitations of FA in assessing the fiber integrity in areas with multiple crossing fibers, and is less sensitive to partial volume effects, as demonstrated in our recent study.[36] As a directionally specific quantitative measure, it therefore, seems ideally placed to assess fiber integrity in multiple areas including motoric and extramotoric white matter pathways in longitudinal studies in ALS patients.

Our specific hypotheses are as follows: changes in the white matter are present in ALS patients beyond the motor tracts; compromise of structural integrity of the white matter tracts can be demonstrated qualitatively and be indirectly measured by our imaging quantitative markers; and finally progression in affected white matter tracts

correlates with clinical progression. Accordingly, our specific aim is to identify and track the affected motoric and extramotoric white matter pathways and patterns of their progression longitudinally in a reliable manner, using automated diffusion connectometry analysis. We will then aim to further longitudinally evaluate identified affected white matter tracts qualitatively and quantitatively, using HDFT and a targeted tractography approach. The latter will enable us to examine potential correlation between associated quantitative parameters, such as changes in QA and/ or volume and clinical deterioration in ALS patients over time, for example as measured by ALSFRS-R. Overall aim using this methodology is to establish a reproducible imaging biomarker, which can identify and track progression of white matter changes in ALS patients.

5.4 Methods

5.4.1 Clinical inclusion Criteria and evaluation

A total of 20 patients, predominantly with ALS, including the diagnostic categories, as defined by the revised El-Escorial criteria[9] of clinically definite; probable; probable-laboratory supported and possible ALS will be included in addition to a smaller subset with primary lateral sclerosis (PLS).[37] Over a period of two years, these patients will undergo three scans, six months apart longitudinally. Corresponding to each scan session, the patients will also undergo extensive clinical evaluation and scoring including that of ALSFRS-R,[9] frontotemporal dementia assessment, forced vital capacity (FVC) and Ashworth spasticity scale as part of an ALS multidisciplinary clinic. Clinical evaluation will be carried out by two neurologists, with specialist interest in neuromuscular disorders. 20 age-matched neurologically normal controls will also be scanned three times in a similar fashion, in order to contribute to the matched template file for comparison for diffusion connectometry analysis. The data acquired from scanning the controls will also allow a direct matched comparison for targeted tractography in terms of changes in QA and/ or volume for specific affected fiber tracts of interest, as identified by the

connectometry analysis. Approval has been obtained from the institutional review board (IRB#: REN12100240 / PRO09010491).

5.4.2 Two-step approach towards evaluating white matter disease in ALS

We propose and have currently adopted a two-step approach to evaluating white matter disease in a longitudinal fashion in ALS patients with the first *primary* step involving diffusion connectometry[38] analysis to identify the affected white matter tracts followed by a detailed tractography approach towards the evaluation of these identified abnormal fiber pathways. Diffusion connectometry[38] is a fully automatic method for examining fiber tracts. It uses the diffusion MRI data of normal subjects as a norm to statistically examine pathways with deviant or abnormal connectivity in affected individuals. We have previously demonstrated its utility in seven patients with chronic stroke and compared the results with lesions shown on T_2-weighted images; ADC and FA maps as well as clinical manifestations. The results were noteworthy in demonstrating that the affected tracts revealed by connectometry corresponded well with the stroke lesions, as shown by the T_2-weighted images and in revealing the entire affected tracts.[38] Overall it is a way to identify tracts with decreased or increased connectivity with the central paradigm being tracking the difference. The conventional tractography approach relies on defining tracts before comparing the difference, thereby making it vulnerable to issues related to crossing and branching patterns, reliability and reproducibility. Diffusion connectometry overcomes these problems by finding the local difference in diffusion distribution first without initiating fiber tracking. This therefore, filters out regions without a substantial difference, leaving only pertinent affected regions for further analysis. This approach is more robust due to a number of reasons: a) high chance of detecting any real difference, as the analysis relies on analysing the difference in diffusion pattern, close to the signal level of the scan; b) the entire process is fully automated, therefore related variability from manual selection of the ROI is eliminated and finally the obtained results can be statistically tested using the length of the affected tracks as a threshold, as described later. Further details regarding this methodology can be referred to in the stroke study, as here we present the adaptation of this methodology towards evaluating white matter disease longitudinally in ALS.[38]

Diffusion connectometry approach can be tailored to test both individual and group data against a control population. Results from this approach can then be examined further using a targeted tractography approach.

5.4.3 Imaging Data

Image Acquisition and Reconstruction

DSI data is acquired on a 3T Tim Trio System (Siemens, Erlangen, Germany) using a 32-channel coil. A head stabilizer is utilized to prevent head motion. A 43-minute, 257-direction DSI scan with a twice-refocused spin-echo planar imaging sequence and multiple b values (repetition time = 9916 ms, echo time = 157 ms, voxel size = 2.4x 2.4x2.4 mm, field of view = 231x231 mm, maximum b-value = 7000 s/mm^2) is performed. For anatomical comparisons, we also include a high-resolution anatomical imaging using a 9-minute T_1-weighted axial magnetization-prepared rapid-acquisition gradient-echo sequence (repetition time = 2110 ms, echo time = 2.63 ms, flip angle = 8 degrees, number of slices = 176, field of view = 256 x 256 mm^2, voxel size = 0.5 x 0.5 x1.0 mm^3). In this study, we discarded any dataset that had head motion greater than one voxel deviation across the long scanning time (by comparing the first b0 and last b0 image). For this preliminary study, we only selected patients, who tolerated the scanning time well.

DSI data is reconstructed with a generalised q-sampling imaging[30] approach. The orientation distribution functions were reconstructed to 642 discrete sampling directions for each pixel and with a diffusion distance scaling parameter of 1.2. This means that the resulting reconstructed orientation distribution function can cover 1.2 standard deviations of the free water diffusion distance in the underlying voxel (measured in micrometers). The acquisition parameters, as described here are being used for our ALS patients currently. Similar acquisition parameters are being used for acquiring the control data in order to create a more accurate matched template file. Acquisition parameters for the template file, used for the connectometry analysis for the preliminary results, as presented here were detailed in previous publications, including in its previous use in the stroke study.[38,39] The normal template, used for the current analysis (DSI studio: http://dsi-studio.labsolver.org) was derived from the

DSI data of 90 neurologically normal subjects.[39]

Step 1: Diffusion Connectometry Analysis[38]

Reconstructing spin distribution functions in a common space

The diffusion data of each subject is reconstructed in a common stereotaxic space using q-space diffeomorphic reconstruction (QSDR),[39] a method that satisfies the conservation of diffusible spins and can be applied to diffusion datasets. QSDR uses diffusion signals to calculate the spin distribution function (SDF). The DSI data of a studied subject, for example an ALS patient is also reconstructed by QSDR to obtain the SDFs in the MNI space. Further details regarding the reconstruction of SDF in a common space can be found in our original methodology paper.[38]

Constructing the affected tracks

To demonstrate the segment of the tracks that are affected by ALS, we performed fiber tracking on the local tract orientations with a percentile rank lower than 5 (Figures 2-5), where local tract orientations with diffusion quantities (SDF values) lower than 5th percentile rank are plotted with directional colours (red: left-right, green: anterior-posterior, blue: superior-inferior), and tracks propagate along those local tract orientations. The tracking is conducted using a deterministic fiber tracking algorithm in the DSI Studio. The tracking begins from each local fiber orientation as seeds and propagates until no orientation is found in the propagation direction. A maximum turning angle of 60 degrees is used with a step size of 1 mm (i.e., half of the spatial resolution in the template space). The obtained trajectories, termed the affected tracks can be used to reveal the pathways with decreased connectivity. It is noteworthy that only local tract orientations with substantial loss in diffusion quantities are tracked. The affected tracks reveal only affected segments of the entire track pathways.

Length of affected tracks

We used the length of affected tracks (unit in voxel distance) to differentiate meaningful findings from random variations. The rationale behind it is that normal population may have false-positive affected tracks due to noise in diffusion weighted images, but its effect tends to appear randomly in space, resulting in fragmentation of the affected tracks. As a result, the distribution of the length of the affected tracks (termed length distribution) will be exponential since the concatenation of randomly distributed local tract orientations can be viewed as a Poisson process.[38] In contrast, the true connectivity difference in patient group will continue along fiber pathways and form longer affected tracks. Using length as an index, the difference between random effect and true connectivity difference can be differentiated and statistically tested. We can select the affected tracks with length greater than a threshold (termed length threshold) as positive findings because these trajectories are most likely related to the disease. A higher length threshold may filter out most of the false discoveries but may not be sensitive enough to detect subtle difference. The determination of the length threshold is a trade-off between sensitivity and specificity. To determine a reasonable value, we can quantify the Type 1 error of a length threshold using false discovery rate (FDR).

Adaptation of the original methodology and calculation of false discovery rate

The calculation of FDR requires the length distribution calculated from a group of subjects. In a previous study[38] and here with the preliminary results, we obtained the affected tracks of each patient by comparing his/her data with those of 90 normal subjects.[39] The length of affected tracks in all patients is accounted to obtain the empirical length distributions for the patient group. Similarly, we can treat normal subjects as patients and apply the same analysis to each of them by comparing his/her data with those of the other 89 normal subjects to obtain the empirical length distribution for the normal population. The difference in the affected tracts between patient and normal subject groups can be used to calculate the FDR of our findings in the ALS patients [38]. With respect to the preliminary data presented here (Figure 1), using a 5^{th} percentile ranking, we regarded any affected track with length > 24 mm as related to ALS, giving us an FDR of 0.16. This means that 16% of the affected tracks

may be false discoveries. Length threshold and the FDR provide a quantitative measurement of sensitivity/specificity of a finding, and for ALS, we will continue to explore this to establish an optimal threshold, particularly in future, in relation to our matched control dataset. In order to track longitudinal data, we used the same FDR and length threshold in a novel fashion to examine the subsequent scan, with the hypothesis that any demonstrated progression in the affected tracts is real and therefore, an indirect marker of disease progression.

Step 2: HDFT and targeted fiber tractography

Fiber Tracking Analysis

For the HDFT data, fiber tracking is performed with DSI Studio. Tracts are generated with the use of an orientation distribution function–streamlined version of the Fiber Assignment by Continuous Tracking (FACT) algorithm.[30,40] Fiber tracking is initiated by randomly seeding the ROI and initiating tracking in the direction of the most prominent fiber. Fiber progression continues with a step size of 1.2 mm, minimum fiber length of 20 mm, and turning angle threshold of 65 degrees. For smoothing of the tracts, the next directional estimate of each voxel is weighted by 20% of the previous moving direction and 80% by the incoming direction of the fiber. The tracking terminates when the relative QA for the incoming direction drops below a preset threshold or exceeds a turning angle of 65 degrees. The QA termination threshold is adjusted on a per-subject basis, so that the threshold allows consistent white matter coverage in all subjects. This is critical for single-subject–based tractography studies in which individual differences in coil sensitivity and diffusion signal homogeneity can vary across subjects. After tracking, all streamlines are saved and tract segmentation performed in DSI Studio. The QA threshold is kept constant across the longitudinal scans for the same subject. Mean QA and volumes (voxel wise) are then obtained for affected fiber tracts of interest, identified from connectometry analysis for both hemispheres. This is followed by calculation of percentage changes in QA and volume across longitudinal scans in order to obtain quantitative data with respect to progression in order to enable potential correlation with markers of clinical progression. Obtained data will also be evaluated

qualitatively in terms of obvious 'thinning' of the tracts in a cross-section or discontinuity in a tract segment.

5.5 Results

We present our preliminary results with respect to five patients recruited so far in our ongoing study. According to the revised El-Escorial criteria,[9] two have probable ALS; two have probable ALS (laboratory supported) and the other one has possible ALS with predominantly UMN signs. Two patients have been scanned longitudinally, while the other three have had a baseline scan only with planned longitudinal scans in the future.

5.5.1 Step 1: Diffusion MRI connectometry analysis

In order to track progression with longitudinal data in patients 1 and 2, and for current non-longitudinal data in 3, 4 and 5 we chose a length threshold of 24 mm (corresponding to 12 voxels), thus giving us an FDR of 0.16 (Figure 1) for the observed affected tracts. This threshold was kept constant across longitudinal scans to detect progressive changes with disease evolution.

Patient 1

Results are presented for this 48-year-old patient with a diagnosis of probable laboratory supported ALS (limb-onset; predominant LMN involvement) with respect to two scans acquired approximately one year apart. His symptoms started about 30 months before the baseline scan with widespread fasciculations and left hand weakness. He has no family history of neurological disease. Diffusion connectometry analysis revealed the changes predominantly at the baseline in posterior part of the CC (Figure 2A). A year later (Figure 2B-C), these changes had progressed to include the fibers in the posterior limb of the internal capsule (IC) predominantly, CST and frontal fibers coursing towards the brainstem; cingulum and other areas. These changes were consistent with multisystem neurodegeneration and frontal progression with disease evolution. The patient's ALSFRS-R score decreased from 45 to 32 during this interval. Cortical end points of the involved fiber tracts

confirmed relative sparing of the postcentral gyrus and associated sensory fibers (Figure 2D), consistent with known ALS pathology.

Patient 2

Imaging results for this 62-year-old male patient with probable ALS (bulbar onset with predominant bulbar involvement) with respect to two scans carried out approximately six months apart are presented. His symptoms started with dysarthria. The disease duration at the time of the baseline scan was 12 months. He has no family history of neurological disorders. At baseline (Figure 3A), the affected white matter tracts were predominantly the anterior and posterior parts of the CC and parts of the CST bilaterally. CST was involved more caudally than in patient 1. At the second scan, six months later (Figure 3B-C), the changes in white matter were more extensive involving the CC; corticostriatal fibers; fibers in the posterior limb of IC, including CST and the frontal fibers coursing towards the brainstem; cingulum and parts of the superior longitudinal (SLF) and inferior occipito-frontal fasciculi (IOF) bilaterally. These findings were more pronounced on the left side. Over the scan interval, his ALSFRS-R score dropped from 44 to 43. Cortical terminations of the affected fibers, as in patient 1 showed frontal progression with disease evolution (Figure 3D).

Patient 3

This 62-year-old male patient with probable ALS (limb onset), has undergone a single scan, so far 24 months into his disease onset, characterised by left hand weakness and foot drop. He has no family history of neurological disorders. The baseline scan demonstrated extensive involvement of the CC; CST; SLF; IOF and cingulum bilaterally. The changes were more pronounced on the right. There was also evidence of involvement of left superior cerebellar peduncle (Figure 4). ALSFRS-R score at baseline scan was 43.

Patient 4

A 62-year-old with probable ALS- laboratory supported (limb onset with predominant UMN involvement) was 38 months into her disease onset at her baseline scan. ALSFRS-R score was 40 at the time of the baseline scan. Her initial

symptoms were clumsiness of the left foot and leg. There was no family history of ALS, but mother had Alzheimer's disease. Diffusion connectometry analysis (Figure 5A) demonstrated changes in motoric and extramotoric tracts. As observed with other patients, changes were seen bilaterally (right>left) in CST, CC, cingulum, parts of SLF and IOF (Figure 5A).

Patient 5

A 74-year-old female has possible ALS (bulbar onset with predominant UMN signs and bulbar involvement). Her symptoms started about 27 months before the baseline scan with dysarthria. She has no family history of neurological diseases. Baseline scan demonstrated similar changes, as in patient 4 with more pronounced involvement of the tracts on the right side. There was however a greater rostro-caudal involvement of the CST, with associated involvement of the cerebellar outflow tracts bilaterally (Figure 5B).

5.5.2 Step 2: Targeted fiber tracking using HDFT of affected tracts from diffusion connectometry

Using patients 1 and 2 with longitudinal scans, we calculated the changes in QA and volumes for selected major white matter tracts, affected through majority of their course and as identified from the connectometry analysis (Table 1). As an example for patient 1, we selected CST for closer evaluation using changes in QA and volume over one-year scan interval. With similar tracking parameters and QA threshold for the two scans, there was progressive compromise of the CST bilaterally (Figure 6, right CST). This was seen qualitatively by presence of discontinuity in its caudal part and quantitatively by percentage decreases in QA for the left and right at 25% and 28% respectively and associated percentage volume reductions at 5% and 41% respectively.

5.6 Discussion

In her paper published in 1960,[21] Smith aimed to study the degeneration of myelinated fiber tracts in ALS. She demonstrated wider extramotor involvement, including frontal cortex in addition to the CST and CC. Further involvement of fibers projecting to the thalami and basal ganglia were also noted. In this remarkable early study[21] pathological involvement of both motoric and extramotoric white matter pathways in ALS was highlighted. We can now demonstrate these patterns in vivo using MR-based tractography techniques. White matter involvement is a subject of investigation in both longitudinal and non-longitudinal DTI studies in ALS towards assessing its use as a diagnostic tool, including in distinguishing between different phenotypes based on UMN versus LMN involvement and in monitoring progression.

Longitudinal studies, although lacking in general are useful towards demonstrating the time course and nature of progression of pathology in ALS. A longitudinal study involving 24 subjects with ALS demonstrated a decrease in the FA in the CST and frontal areas on a second scan, obtained 6 months later.[10] The progressive FA decrease along the CST correlated with disease duration and the decrease in ASLFRS-R.[10] Similarly, another study with six months follow-up showed DTI abnormalities extending into bilateral frontal lobes.[41] Another longitudinal study [7] examined the three phenotypes i.e. ALS, PLS and progressive muscular atrophy (PMA) within the motor neuron disease (MND) spectrum. This study assessed the upper- and extra-motoneuron white matter involvement shortly after diagnosis by comparing DTI data of the different cohorts to those of healthy controls and directly between the disease phenotypes. Follow-up data was also acquired 6 months later to evaluate FA changes over time. Diffusion tensor tractography of the CST and whole-brain VBA was utilized to ascertain the white matter involvement in MND. VBA demonstrated white matter involvement to varying extents in different phenotypes although in quite similar anatomical locations. In general, FA reductions were found to be most extensive in PLS with the observation of both upper motor and extra-motoneuron involvement in all phenotypes of MND shortly after diagnosis. VBA was more sensitive in detecting longitudinal changes than tractography of the CST. VBA was also thought to be particularly valuable in the evaluation of motor and

extra-motor white matter involvement in the early symptomatic MND, and in monitoring the spread of pathology over time.[7] We have focused our current efforts towards monitoring and establishing the nature of disease progression in the white matter via a longitudinal study. In the future, we will aim to assess its use as a diagnostic tool with potential value in distinguishing different MND phenotypes.

5.6.1 Current findings and relevance of preliminary data

Based on preliminary results presented here, including in two patients with longitudinal scans, we demonstrate a number of features, consistent with pathological studies[21] including presence of disease in the motor pathways,[6,42-44] IC and CC.[19] Beyond the motor system, we demonstrate changes in the limbic pathways;[10,45] spread of the disease frontally[10,46] and potential involvement of the cerebellum.[10,47] Cerebellar involvement has been implicated in previous functional studies.[48,49] Involvement of the CC, connecting orbitofrontal and frontal cortices, is not surprising in ALS and has been deemed to be a fairly consistent feature.[19] Similarly involvement of frontal white matter and cingulum may contribute to the cognitive symptoms, recognized in ALS patients.[10,20,45,50] Cerebellar outflow tract involvement as seen in patient 5 has been postulated[10,48,49] to be potentially related to functional compensation; however the exact relevance of its altered connectivity and structural impairment is unclear. Although cerebellar signs are lacking in most ALS patients, previous pathological[51] and functional MRI studies have suggested cerebellar involvement. The implication of cerebellar involvement is with respect to functional compensation in ALS being reliant on existing mechanisms rather than development of new synapses.[49]

Functional correlation in this initial dataset is difficult owing to a small current size, however in both patients 1 and 2 with longitudinal scans and evidence of imaging progression of white matter disease, there was decline in an already compromised ALSFRS-R score. This was more pronounced in patient 1 with a longer interval between the scans. It is noteworthy that patient 2, in comparison with other cases demonstrated less extensive changes on the baseline scan. This is likely related to the first scan being undertaken earlier in the disease course. The future data will shed light on a potential correlation between observed imaging changes and rate of

decrease in ALSFRS-R scores, including with respect to baseline values for functional scores in relation to the initial scan. Patient 2, for example with less extensive imaging changes had a similar functional score to patient 5 with widespread white matter involvement, as seen on the connectometry analysis. Potential explanations for this include the difficulty of correlating observed changes in the UMN with ALSFRS-R, a composite score relying on multiple neuronal pathways and LMN and the qualitative nature of information derived from connectometry analysis. Another explanation pertains to the heterogeneity in potential functional compensation between ALS patients with similar possible disease burden. These partly explain a further need to validate the findings from connectometry analysis with targeted tractography approach, so that quantitative markers, for example changes in QA may be examined in relation to functional scores. Another finding needing future investigation is asymmetry of radiological changes, as demonstrated here and its potential correlation with the clinical findings and the side of disease onset. This is observed in both patients 3 and 4 with more extensive imaging changes on the right side on their baseline scan with a contralateral site of disease onset.

5.6.2 Limitations, future experimental plan and directions

Another methodology, apparent fiber density (AFD)[52] compares the difference in fiber orientation distribution and uses a clustering approach to group voxels with significant differences. Since the clustering is voxel-based, it cannot handle the differences coming from different fibers within the same voxel. The clustering algorithm will indiscriminately cluster them, even if the differences are unrelated. Connectometry avoids this problem, as it is fiber-based, and the difference in multiple fibers is considered separately using a fiber skeleton. Further AFD is based on spherical deconvolution method, which is limited to HARDI and has been shown to be subject to CSF contamination. Connectometry method can make use of both the DSI and HARDI data, and the partial volume effect can be handled using the spin density information.

The limitation in the current study pertains to a small sample size. The primary purpose however, was to test the feasibility of our previously presented analytical

method[38] adapted to test the longitudinal data in ALS. In this respect, the current study presents preliminary results, as more imaging data is acquired. The 40-minutes DSI scan can now be replaced by multi-band DSI sequence,[53] which takes less than 10 minutes to acquire half sphere 101-directions DSI. This will dramatically improve the clinical applicability of this method, particularly for patients with neurodegenerative disorders. We are currently in the process of deploying this sequence for scanning new patients.

In addition to the previously mentioned details and to examining relationship between clinical and imaging progression on connectometry analysis, we will corroborate the findings from connectometry analysis by performing targeted analysis of the affected tracts beyond CST for example, cingulum or thalamopostcentral fibers. We will therefore, aim to further identify tracts, that may be preferentially affected and calculate the changes in the associated quantitative markers. The changes in these will be correlated with the rate of disease progression, for example drop in ALSFRS-R scores with change in CST or decline in ALS cognitive behavioural screen with change in cingulum. An important future consideration relates to scanning controls for purposes as outlined. Specifically we will need to establish a normal range of expected variability in QA and/ or volumes for fiber tracts of interest between scan sessions for comparison with observed changes in affected fibers. Although with disease progression, a decrease in mean QA will be expected for a specific fiber tract of interest, the increase as observed for a few tracts (Table 1) can be either explained by the variability in QA across scan sessions or potential functional compensation of the remaining fibers. This remains to be elucidated further in the future.

One of the endeavours associated with DTI in ALS has been evaluation of its use as a diagnostic tool and as an aid enabling discrimination between different MND phenotypes. A recent meta-analysis[54] concluded that the discriminatory capability of DTI to make a diagnosis of ALS is only modest and that there were no significant differences in the diagnostic test accuracy summary estimates with respect to MRI field strength or brain location. Potential reasons may be the clinico-pathological heterogeneity in ALS and use of group studies, with these issues becoming more pertinent in the context of different MND phenotypes. Although there is increasing

evidence that the different MND phenotypes lie within a spectrum[7,55] with overlapping white matter abnormalities, the anatomical location and the extent of these changes vary, making group comparisons difficult. This partly explains our reasons for focusing on the ALS patients and at least initially examining individual progression, including its nature, extent and distribution using connectometry analysis. Having established these, we will in future, embark upon studies applicable towards diagnosing and differentiating between different MND phenotypes. This could be achieved, for example by using the varying anatomical (rostro-caudal) and quantitative involvement of CST as a guide.

In conclusion, we propose an innovative method and present preliminary results, using DSI in longitudinal evaluation of white matter pathology in ALS in an endeavour towards developing an imaging biomarker to monitor disease progression. We ultimately hope that the imaging biomarker upon completion of current proposed study, can be validated and be used in future trials towards evaluating efficacy of novel therapies in slowing or reversing disease progression with or without associated documented deterioration in clinical measures.

5.7 References

1. Graham JM, Papadakis N, Evans J, et al. Diffusion tensor imaging for the assessment of upper motor neuron integrity in ALS. *Neurology.* 2004;63(11):2111-2119.
2. Iwata NK, Kwan JY, Danielian LE, et al. White matter alterations differ in primary lateral sclerosis and amyotrophic lateral sclerosis. *Brain.* 2011;134(Pt 9):2642-2655.
3. Jacob S, Finsterbusch J, Weishaupt JH, Khorram-Sefat D, Frahm J, Ehrenreich H. Diffusion tensor imaging for long-term follow-up of corticospinal tract degeneration in amyotrophic lateral sclerosis. *Neuroradiology.* 2003;45(9):598-600.
4. Menke RA, Abraham I, Thiel CS, et al. Fractional anisotropy in the posterior limb of the internal capsule and prognosis in amyotrophic lateral sclerosis. *Arch Neurol.* 2012;69(11):1493-1499.

5. Nickerson JP, Koski CJ, Boyer AC, Burbank HN, Tandan R, Filippi CG. Linear longitudinal decline in fractional anisotropy in patients with amyotrophic lateral sclerosis: preliminary results. *Klin Neuroradiol.* 2009;19(2):129-134.
6. Sach M, Winkler G, Glauche V, et al. Diffusion tensor MRI of early upper motor neuron involvement in amyotrophic lateral sclerosis. *Brain.* 2004;127(Pt 2):340-350.
7. van der Graaff MM, Sage CA, Caan MW, et al. Upper and extra-motoneuron involvement in early motoneuron disease: a diffusion tensor imaging study. *Brain.* 2011;134(Pt 4):1211-1228.
8. Cedarbaum JM, Stambler N, Malta E, et al. The ALSFRS-R: a revised ALS functional rating scale that incorporates assessments of respiratory function. BDNF ALS Study Group (Phase III). *J Neurol Sci.* 1999;169(1-2):13-21.
9. Brooks BR, Miller RG, Swash M, Munsat TL, World Federation of Neurology Research Group on Motor Neuron D. El Escorial revisited: revised criteria for the diagnosis of amyotrophic lateral sclerosis. *Amyotroph Lateral Scler Other Motor Neuron Disord.* 2000;1(5):293-299.
10. Keil C, Prell T, Peschel T, Hartung V, Dengler R, Grosskreutz J. Longitudinal diffusion tensor imaging in amyotrophic lateral sclerosis. *BMC Neurosci.* 2012;13:141.
11. Sage CA, Peeters RR, Gorner A, Robberecht W, Sunaert S. Quantitative diffusion tensor imaging in amyotrophic lateral sclerosis. *Neuroimage.* 2007;34(2):486-499.
12. Basser PJ, Pierpaoli C. Microstructural and physiological features of tissues elucidated by quantitative-diffusion-tensor MRI. *J Magn Reson B.* 1996;111(3):209-219.
13. Oouchi H, Yamada K, Sakai K, et al. Diffusion anisotropy measurement of brain white matter is affected by voxel size: underestimation occurs in areas with crossing fibers. *AJNR Am J Neuroradiol.* 2007;28(6):1102-1106.
14. Guo AC, MacFall JR, Provenzale JM. Multiple sclerosis: diffusion tensor MR imaging for evaluation of normal-appearing white matter. *Radiology.* 2002;222(3):729-736.

15. Thomalla G, Glauche V, Koch MA, Beaulieu C, Weiller C, Rother J. Diffusion tensor imaging detects early Wallerian degeneration of the pyramidal tract after ischemic stroke. *Neuroimage.* 2004;22(4):1767-1774.
16. Beaulieu C. The basis of anisotropic water diffusion in the nervous system - a technical review. *NMR Biomed.* 2002;15(7-8):435-455.
17. Beaulieu C, Does MD, Snyder RE, Allen PS. Changes in water diffusion due to Wallerian degeneration in peripheral nerve. *Magn Reson Med.* 1996;36(4):627-631.
18. Ciccarelli O, Behrens TE, Altmann DR, et al. Probabilistic diffusion tractography: a potential tool to assess the rate of disease progression in amyotrophic lateral sclerosis. *Brain.* 2006;129(Pt 7):1859-1871.
19. Filippini N, Douaud G, Mackay CE, Knight S, Talbot K, Turner MR. Corpus callosum involvement is a consistent feature of amyotrophic lateral sclerosis. *Neurology.* 2010;75(18):1645-1652.
20. Raaphorst J, de Visser M, van Tol MJ, et al. Cognitive dysfunction in lower motor neuron disease: executive and memory deficits in progressive muscular atrophy. *J Neurol Neurosurg Psychiatry.* 2011;82(2):170-175.
21. Smith MC. Nerve Fibre Degeneration in the Brain in Amyotrophic Lateral Sclerosis. *J Neurol Neurosurg Psychiatry.* 1960;23(4):269-282.
22. Rose S, Pannek K, Bell C, et al. Direct evidence of intra- and interhemispheric corticomotor network degeneration in amyotrophic lateral sclerosis: an automated MRI structural connectivity study. *Neuroimage.* 2012;59(3):2661-2669.
23. Verstraete E, Veldink JH, van den Berg LH, van den Heuvel MP. Structural brain network imaging shows expanding disconnection of the motor system in amyotrophic lateral sclerosis. *Hum Brain Mapp.* 2013.
24. Le Bihan D, Poupon C, Amadon A, Lethimonnier F. Artifacts and pitfalls in diffusion MRI. *J Magn Reson Imaging.* 2006;24(3):478-488.
25. Alexander DC, Barker GJ. Optimal imaging parameters for fiber-orientation estimation in diffusion MRI. *Neuroimage.* 2005;27(2):357-367.
26. Alexander AL, Hasan KM, Lazar M, Tsuruda JS, Parker DL. Analysis of partial volume effects in diffusion-tensor MRI. *Magn Reson Med.* 2001;45(5):770-780.

27. Tuch DS, Reese TG, Wiegell MR, Makris N, Belliveau JW, Wedeen VJ. High angular resolution diffusion imaging reveals intravoxel white matter fiber heterogeneity. *Magn Reson Med.* 2002;48(4):577-582.
28. Wedeen VJ, Hagmann P, Tseng WY, Reese TG, Weisskoff RM. Mapping complex tissue architecture with diffusion spectrum magnetic resonance imaging. *Magn Reson Med.* 2005;54(6):1377-1386.
29. Fernandez-Miranda JC, Pathak S, Engh J, et al. High-definition fiber tractography of the human brain: neuroanatomical validation and neurosurgical applications. *Neurosurgery.* 2012;71(2):430-453.
30. Yeh FC, Wedeen VJ, Tseng WY. Generalised q-sampling imaging. *IEEE Trans Med Imaging.* 2010;29(9):1626-1635.
31. Verstynen T, Jarbo K, Pathak S, Schneider W. In vivo mapping of microstructural somatotopies in the human corticospinal pathways. *J Neurophysiol.* 2011;105(1):336-346.
32. Wang Y, Fernandez-Miranda JC, Verstynen T, Pathak S, Schneider W, Yeh FC. Rethinking the role of the middle longitudinal fascicle in language and auditory pathways. *Cereb Cortex.* 2013;23(10):2347-2356.
33. Jarbo K, Verstynen T, Schneider W. In vivo quantification of global connectivity in the human corpus callosum. *Neuroimage.* 2012;59(3):1988-1996.
34. Greenberg AS, Verstynen T, Chiu YC, Yantis S, Schneider W, Behrmann M. Visuotopic cortical connectivity underlying attention revealed with white-matter tractography. *J Neurosci.* 2012;32(8):2773-2782.
35. Verstynen TD, Badre D, Jarbo K, Schneider W. Microstructural organisational patterns in the human corticostriatal system. *J Neurophysiol.* 2012;107(11):2984-2995.
36. Yeh FC, Verstynen TD, Wang Y, Fernandez-Miranda JC, Tseng WY. Deterministic diffusion fiber tracking improved by quantitative anisotropy. *PLoS One.* 2013;8(11):e80713.
37. Gordon PH, Cheng B, Katz IB, et al. The natural history of primary lateral sclerosis. *Neurology.* 2006;66(5):647-653.
38. Yeh FC, Tang P.F., Tseng W.I. Diffusion MRI connectometry automatically reveals affected fiber pathways in individuals with chronic stroke. *Neuroimage: Clinical.* 2013;2:912-921.

39. Yeh FC, Tseng WY. NTU-90: a high angular resolution brain atlas constructed by q-space diffeomorphic reconstruction. *Neuroimage.* 2011;58(1):91-99.
40. Basser PJ, Pajevic S, Pierpaoli C, Duda J, Aldroubi A. In vivo fiber tractography using DT-MRI data. *Magn Reson Med.* 2000;44(4):625-632.
41. Senda J, Kato S, Kaga T, et al. Progressive and widespread brain damage in ALS: MRI voxel-based morphometry and diffusion tensor imaging study. *Amyotroph Lateral Scler.* 2011;12(1):59-69.
42. Sage CA, Van Hecke W, Peeters R, et al. Quantitative diffusion tensor imaging in amyotrophic lateral sclerosis: revisited. *Hum Brain Mapp.* 2009;30(11):3657-3675.
43. Iwata NK, Aoki S, Okabe S, et al. Evaluation of corticospinal tracts in ALS with diffusion tensor MRI and brainstem stimulation. *Neurology.* 2008;70(7):528-532.
44. Ellis CM, Simmons A, Jones DK, et al. Diffusion tensor MRI assesses corticospinal tract damage in ALS. *Neurology.* 1999;53(5):1051-1058.
45. Sarro L, Agosta F, Canu E, et al. Cognitive functions and white matter tract damage in amyotrophic lateral sclerosis: a diffusion tensor tractography study. *AJNR Am J Neuroradiol.* 2011;32(10):1866-1872.
46. Ellis CM, Suckling J, Amaro E, Jr., et al. Volumetric analysis reveals corticospinal tract degeneration and extramotor involvement in ALS. *Neurology.* 2001;57(9):1571-1578.
47. Kassubek J, Unrath A, Huppertz HJ, et al. Global brain atrophy and corticospinal tract alterations in ALS, as investigated by voxel-based morphometry of 3-D MRI. *Amyotroph Lateral Scler Other Motor Neuron Disord.* 2005;6(4):213-220.
48. Konrad C, Jansen A, Henningsen H, et al. Subcortical reorganisation in amyotrophic lateral sclerosis. *Exp Brain Res.* 2006;172(3):361-369.
49. Schoenfeld MA, Tempelmann C, Gaul C, et al. Functional motor compensation in amyotrophic lateral sclerosis. *J Neurol.* 2005;252(8):944-952.
50. Abrahams S, Leigh PN, Goldstein LH. Cognitive change in ALS: a prospective study. *Neurology.* 2005;64(7):1222-1226.

51. Swash M, Scholtz CL, Vowles G, Ingram DA. Selective and asymmetric vulnerability of corticospinal and spinocerebellar tracts in motor neuron disease. *J Neurol Neurosurg Psychiatry.* 1988;51(6):785-789.
52. Raffelt D, Tournier JD, Rose S, et al. Apparent Fibre Density: a novel measure for the analysis of diffusion-weighted magnetic resonance images. *Neuroimage.* 2012;59(4):3976-3994.
53. Sotiropoulos SN, Jbabdi S, Xu J, et al. Advances in diffusion MRI acquisition and processing in the Human Connectome Project. *Neuroimage.* 2013;80:125-143.
54. Foerster BR, Dwamena BA, Petrou M, et al. Diagnostic accuracy of diffusion tensor imaging in amyotrophic lateral sclerosis: a systematic review and individual patient data meta-analysis. *Acad Radiol.* 2013;20(9):1099-1106.
55. Agosta F, Galantucci S, Riva N, et al. Intrahemispheric and interhemispheric structural network abnormalities in PLS and ALS. *Hum Brain Mapp.* 2013.

5.8.1 Figures

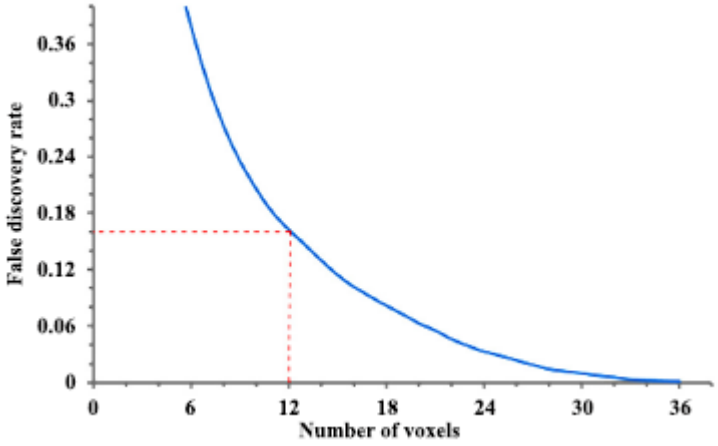

FIGURE 1. Length threshold as defined by number of voxels in relation to the 'false discovery rate (FDR)' (each voxel = 2mm). A length threshold of 24 mm corresponding to 12 voxels was chosen, therefore leading to an FDR of 0.16.

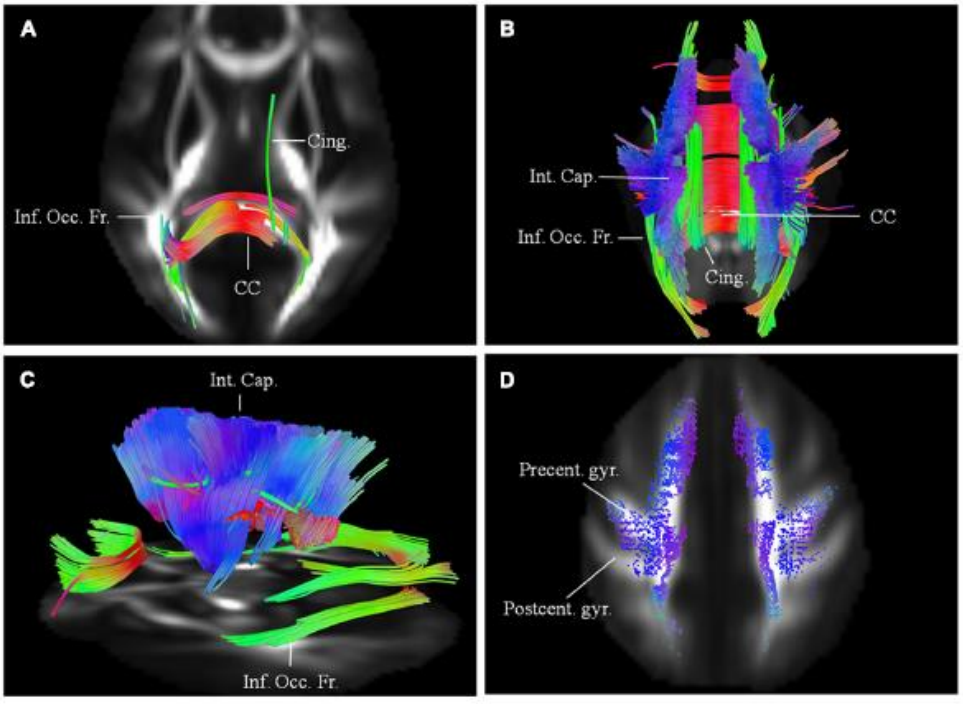

FIGURE 2. (A) Baseline diffusion connectometry analysis for patient 1, demonstrated the affected areas as being inferior occipito-frontal fasciculus (Inf. Occ. Fr.), cingulum (Cing.) and posterior part of the corpus callosum (CC) **(B)** (posterior view) and **(C)** (lateral view) a year later, extensive changes are now

evident bilaterally in the corpus callosum; cinguli and posterior limb of the internal capsule (Int. Cap.) and in parts of inferior occipito-frontal fasciculi. **(D)** Cortical end-points of the affected fiber tracts at the time of the second scan demonstrate involvement of fibers originating from precentral gryus (Precent. gyr.) and frontal areas with relative sparing of postcentral gyrus (Postcent. gyr.).

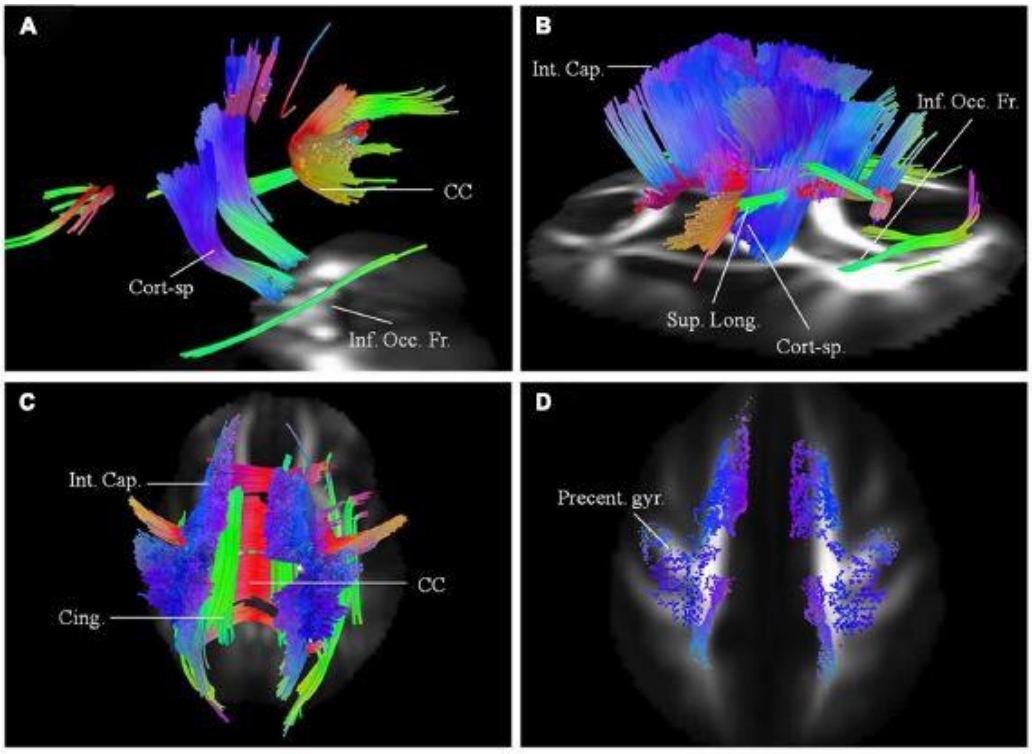

FIGURE 3. (A) Baseline diffusion connectometry analysis for patient 2, demonstrated the affected areas as being parts of the corpus callosum (CC), corticospinal (Cort-sp.) tracts and inferior occipito-frontal (Inf. Occ. Fr.) fasciculi bilaterally. **(B)** (left lateral view) and **(C)** (posterior view) six months later shows extensive bilateral changes now involving corticospinal tracts, frontal fibers coursing towards the brainstem in the posterior limb of the internal capsule (Int. Cap.); cinguli (Cing.); superior longitudinal (Sup. Long.) and inferior occipito-frontal fasciculi. **(D)** Cortical end points for the second scan display predominant involvement of fibers originating from the precentral gyrus (Precent. gyr.) and frontal areas.

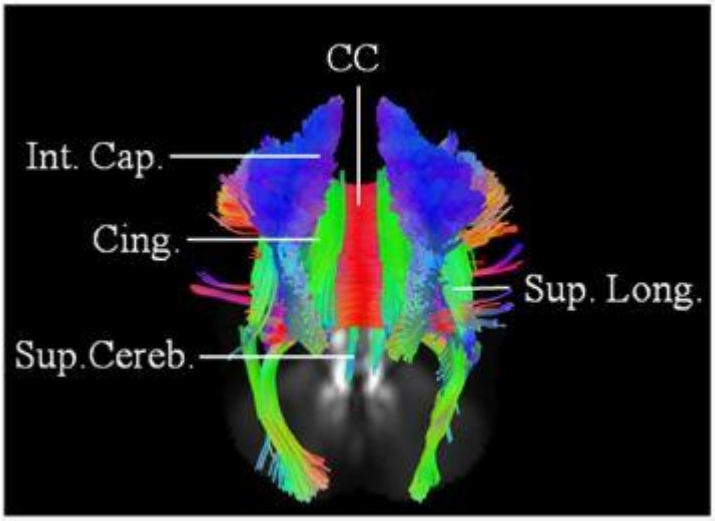

FIGURE 4. Baseline scan (posterior view) in patient 3, demonstrating evidence of extensive motoric and extramotoric changes in the white matter tracts ([corpus callosum (CC); internal capsule (IC); Superior longitudinal (Sup. Long.) fasciculus; Cingulum (Cing.)] with changes being more pronounced on the right; also noted was involvement of the left superior cerebellar peduncle (Sup. Cereb.).

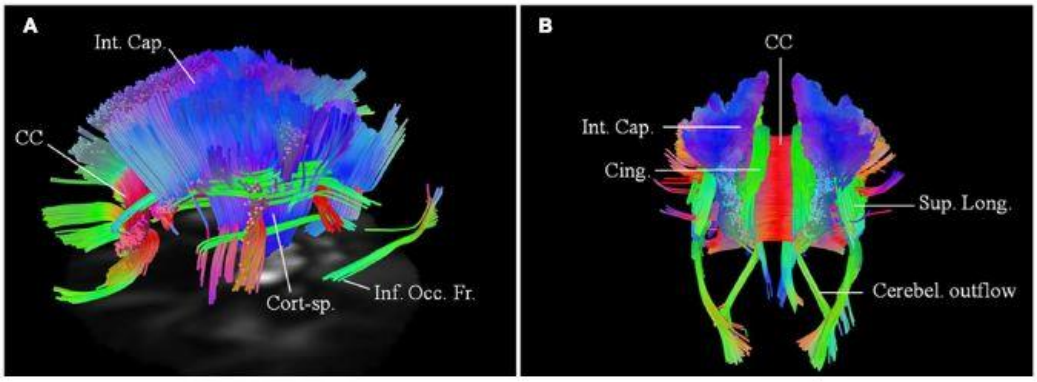

FIGURE 5. Baseline scans in patients 4 **(A,** left lateral view**)** and 5 **(B,** posterior view**)** demonstrating bilateral changes in the motoric and extramotoric pathways, being more pronounced on the right. Bilateral involvement of the cerebellar outflow tracts (Cerebel. outflow) was noted in patient 5. Bilaterally involved tracts in both included corpus callosum (CC); corticospinal tract (Cort-sp.); frontal fibers in the posterior limb of the internal capsule (Int. Cap.) coursing towards the brainstem; cinguli (Cing.) and parts of superior longitudinal (Sup. Long.) and inferior occipito-frontal (Inf. Occ. Fr.) fasciculi.

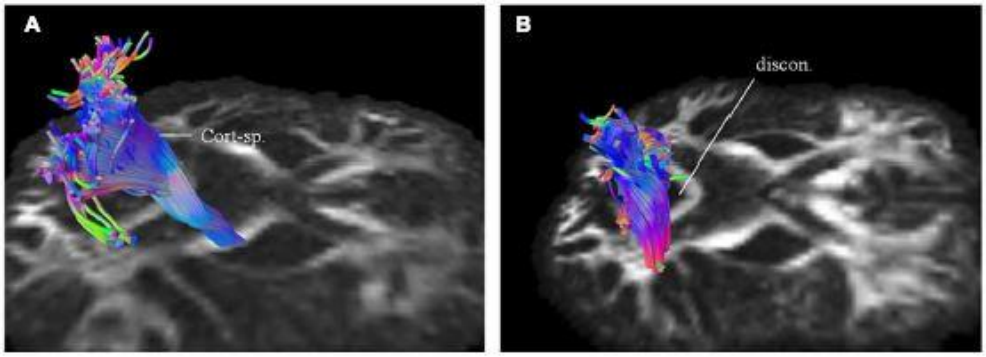

FIGURE 6. Targeted fiber tracking in patient 1 demonstrated evidence of progressive compromise of the right corticospinal tract (Cort-sp.) between the baseline scan **(A)** and the subsequent scan **(B)**, a year later, on which discontinuity (discon.) in the caudal segment was noted.

5.8.2 Table

TABLE 1: Changes in quantitative markers in two patients with longitudinal scans for major affected white matter tracts, as identified by the connectometry analysis

Patient number (scan interval)	Percentage changes‡ in quantitative markers	Affected major white matter tracts				
		L CST	R CST	CC	L Cingulum	R Cingulum
1 (12 months)	QA	25	28	20	23	16*
	Volume	5	41	86	73	71
2 (6 months)	QA	15	17	5*	4	8*
	Volume	61	72	67	78	39

(‡: the percentage changes denote a decrease in all cases except those denoted by asterisk (*), where an increase was noted; CST: corticospinal tract; CC: corpus callosum; L: left; R: right; QA: quantitative anisotropy)

Chapter 6: High Definition Fiber Tractography for the evaluation of perilesional white matter tracts in high grade glioma surgery

Paper 5: **Abhinav K,** Yeh FC, Mansouri A, Zadeh G, Fernandez-Miranda JC. High Definition Fiber Tractography for the evaluation of perilesional white matter tracts in high grade glioma surgery. *Neuro-Oncology* 2015; 17(9):1199-209

6.1 Declaration

I was the lead author with respect to this manuscript and was instrumental in the preliminary application of high definition fiber tractography (HDFT) for evaluation of perilesional white matter (WM) tracts in high grade glioma surgery. Overall, I contributed extensively towards the writing, literature search, figures, study design, data analysis and interpretation.

6.2 Introduction to and brief summary of the manuscript and relation to prior work

This study represented a switch in the direction from quantitative aspects of the advanced WM imaging towards evaluating its use in a qualitative fashion in high grade glioma surgery. As discussed in the previous chapters, we proved the utility of HDFT in demonstrating multiple crossing WM fibers in a three dimensional fashion around both supra- and infratentorial cavernous malformations such that optimal surgical trajectory could be devised towards avoiding injury to these fibers. At an institutional level, HDFT had been used on a preliminary basis to provide qualitative data towards complementing surgical planning for intracranial tumours. The following manuscript and work represents a more formal effort in this direction and also towards anatomically demonstrating the *named* normal WM tracts in the brain that are commonly encountered in neurosurgical procedures.

Conventional WM imaging approaches such as diffusion tensor imaging (DTI) have been used to preoperatively identify the location of the affected WM tracts in patients with intracranial tumours in order to maximize the extent of resection and potentially reduce postoperative morbidity. DTI as discussed in previous chapters, suffers with limitations, which include its inability to resolve multiple crossing fibers and its

susceptibility to partial volume effects. The latter is particularly applicable in the oedematous zones around high grade lesions and as such, has been explored in further detail in the manuscript. This resulted in more advanced WM imaging algorithms. In this paper, we illustrated the application of HDFT, which in our preliminary experience had enabled accurate depiction of perilesional tracts in a three-dimensional manner in multiple anatomical compartments, including in oedematous zones around high grade gliomas. Using case examples of patients with glioblastoma multiforme, we demonstrated the utility of this technique in permitting accurate surgical planning. In the manuscript, we also discussed future directions regarding the role of these techniques in surgery for gliomas.

6.3 Introduction

Diffusion magnetic resonance imaging (MRI) is an imaging modality utilizing diffusion of water to characterise microscopic structures in the brain. It provides a non-invasive way to estimate diffusivity or 'diffusion coefficient', which quantifies the speed of diffusion of water in tissues. A lower diffusion coefficient may be due to increased cellularity that restricts diffusion, whereas a high diffusion coefficient may indicate free water diffusion in an oedematous condition. The diffusion coefficient estimated using diffusion MRI is often called "apparent" diffusion coefficient (ADC)[1] since it measures the *ensemble* diffusion coefficients appearing from the underlying complex biological environment. The diffusion can be highly incoherent in the brain tissue. Studies have shown correlation between ADC and tumour cellularity[2-4] indicating its potential as a disease biomarker.

It is noteworthy that ADC may not be the same at all directions. To model this anisotropic diffusion, a model-based approach called diffusion tensor imaging (DTI)[5] was introduced. It models diffusion as a Gaussian distribution thereby allowing for a quick estimation of the diffusivity at all directions. Several indices were developed based on the tensor model. Fractional anisotropy (FA) measures how diffusivity differs in different directions.[6,7] Higher anisotropy values suggest organized diffusion of water down the axons in a certain direction for example, as may occur with fibers

in the corpus callosum. A higher FA value therefore, indicates good fiber integrity.[8] Mean diffusivity (MD) is an average measurement of the diffusivity based on DTI. Many studies have used MD as a way to measure ADC and correlated it with tumour cellularity.[9-15]

In addition to ADC and FA measurements, the axonal directions derived from the tensor can be used to track the fiber pathways creating diagrams or reconstructions termed 'tractography'. DTI-based tractography has been used in multiple studies, including in those pertaining to the intracranial mass lesions.[16-18]

Tractography can provide qualitative and quantitative information regarding potentially affected white matter (WM) tracts around an intracranial lesion. The qualitative information refers to the reconstruction of the WM tracts around an intracranial lesion which for example, can be visually analysed to see obvious discontinuity or change in the direction of the tracts to select the safest operative trajectory to the lesion.[19] Quantitative information refers to indices like FA and ADC which can be evaluated for a perilesional area in relation to the contralateral homologous unaffected area in the brain. The changes in quantitative indices from DTI such as, FA, may reflect changes in the integrity of fibers,[8] whereas ADC of tumours may indicate differences in their cellularity.[13]

The tractography data from DTI is meant to facilitate maximal tumour resection while minimizing postoperative deficit, as a greater extent of resection (EOR) is associated with an improved survival time in patients with glioblastoma multiforme (GBM).[20,21] Despite its widespread clinical use, DTI and diffusivity-based measurements have several limitations. A tensor model cannot describe *multiple fibers condition* and therefore, the estimation of the axonal direction is inaccurate in the crossing fiber regions.[22,23] As mentioned above, the diffusivity measured by diffusion MRI is an *average* measurement of the underlying diffusion environment. This implies that the partial inclusion of fast or slow diffusion will change the ADC. A simple tensor model cannot effectively distinguish between these heterogeneous components (in terms of the speed of diffusion) within a voxel leading to the so-called 'partial volume effect'.[23] An example of this effect is a cerebral tumour with surrounding oedema which can have increased or decreased ADC within the lesion (not specific to the cellularity of the tumour).[18,23,24] Similarly, the indices derived

from DTI, such as FA, can be affected by the crossing fiber conditions or partial volume effects[23,25,26] in the oedematous zone around the gliomas. The underestimated FA can therefore, lead to premature termination of the fiber tracking and potential incomplete reconstruction of a perilesional tract.

These limitations compromise the utility of DTI in the evaluation of oedematous WM around the high grade gliomas, which is potentially detrimental to the surgical goal of achieving maximal tumour resection while minimizing any postoperative deficit.[20,21] Advanced WM imaging techniques such as High definition fiber tractography (HDFT), are needed to achieve this surgical goal. Advanced WM imaging techniques overcome the limitations of DTI-based fiber tractography by using: a) a model-free approach to resolve the crossing fibers and b) a density-based (as opposed to diffusivity-based) index like quantitative anisotropy (QA) that is more resistant to the partial volume effects.[27,28] Density-based indices measure the *quantity* of water that is undergoing diffusion through the WM tracts rather than the velocity of diffusion.[28]

In this article we initially review the clinical use of DTI with cerebral neoplasms. This is followed by a discussion of recent preliminary studies in this patient group involving comparison of the qualitative tractography data in the perilesional oedematous zones derived from the advanced WM imaging techniques with that from the conventional DTI. We also demonstrate the application of HDFT in cerebral neoplasms by presenting illustrative cases. In particular, we show its utility with respect to obtaining accurate qualitative data for the perilesional WM tracts around GBMs located in multiple anatomical compartments. We also discuss future directions with respect to the role of HDFT including in the resection of low-grade gliomas (LGG).

6.4 Diffusion tensor imaging and cerebral neoplasms

Owing to its practicability and short acquisition time, DTI is the standard tool in most institutions for the preoperative assessment of perilesional WM tracts around gliomas.[29] The data from DTI can be incorporated into the neuronavigation devices

which guides safe surgical resection and potentially minimizes the postoperative morbidity.[30] Similarly, DTI has been used as a research tool in evaluating the perilesional zone around the gliomas, particularly to distinguish infiltration from oedema. These studies have relied on the reduction in FA in these zones with the assumption that this is attributable to both increased extracellular water and axonal disorganisation caused by infiltration of the tumour beyond its detectable margin.[24,31,32] A previous study had demonstrated reduction in the FA values beyond the oedematous zone in the normal appearing WM area adjacent to the gliomas, implying potential tumoral infiltration.[24] Although the reduction in FA may be helpful for potentially delineating the tumour margins, DTI has not been used in the clinical setting to this effect. Further the difficulty in depicting WM tracts accurately in the perilesional area around gliomas using DTI[33] is related to this decrease in the anisotropy. This is unsurprising as tractography reconstructions or the qualitative data are derived from quantitative measures of anisotropy such as, FA.

The limitations of DTI particularly with respect to the crossing and kissing fibers restrict its use in the evaluation of tumours located close to anatomically complex fiber bundles, for example optic radiation (OR),[34] and thereby reduce its overall utility in different anatomical compartments.

6.5 Qualitative data from advanced white matter imaging techniques and perilesional white matter tracts around gliomas

6.5.1 Beyond diffusion tensor imaging

To overcome these limitations of DTI, more complex models have been developed and discussed in the recent review papers.[27,35,36] These techniques, categorized into model-free and model-based methods, aim to resolve the crossing fibers and quantify diffusion characteristics. The model-based methods assume a diffusion model to derive orientation-related or diffusivity-related parameters.[37] These parameters may facilitate fiber tracking and further quantitative analysis. The model-free methods use an orientation distribution function (ODF) to describe the diffusion distribution. The peak orientations on the ODF can be used as the fiber orientation for further fiber

tracking.[38] ODF estimation requires signal responses at different diffusion sampling directions. This leads to the high angular resolution diffusion imaging (HARDI),[22] a sampling strategy that acquires diffusion images using the multiple diffusion sampling directions (usually > 100) at the same diffusion gradient strength. Another ODF estimation approach makes use of both multiple diffusion sampling directions and gradient strengths. This is enabled by methods such as diffusion spectrum imaging (DSI)[39,40] and generalised Q-sampling imaging (GQI).[41] GQI has been shown to improve the depiction of crossing fibers[42-44] and provide directional and quantitative information about the crossing fibers. It is not surprising therefore, that the advanced WM imaging techniques are being increasingly applied in the evaluation of perilesional WM tracts around gliomas.[33,34,45,46]

6.5.2 Recent literature

Three recent research papers are noteworthy in demonstrating advantages of advanced WM imaging algorithms in the depiction of perilesional WM tracts around gliomas, while carrying out a comparison with DTI.[33,34,45] Zhang et al., demonstrated the differences between GQI-based tractography and DTI in the preoperative mapping of WM tracts in the peritumoral oedema in 5 patients. They demonstrated that the GQI-based tractography could fully display the existing intact fibers in the oedematous zone in comparison with DTI, where the same fiber tracts were incomplete, missing or ruptured.[33] In at least one of the cases, *missing* fibers, as seen on DTI in the oedematous zone *reappeared* after the lesionectomy and resolution of the oedema.[33] This indicated that the *missing* fibers were not visualized due to partial volume artifact rather than true axonal loss. In contrast GQI, being less susceptible to partial volume effect, may faithfully reveal the tract integrity.

In another study, HARDI-compressed sensing (CS) technique-based fiber tractography was compared with DTI in the evaluation of WM tracts around gliomas located in the language-related areas in 6 patients,[45] two of which were patients with GBMs. Using the HARDI-CS algorithm, more compact language fiber bundles were demonstrated compared with DTI in all cases. Specifically in 3 cases, HARDI-CS was able to demonstrate fiber bundles in the orientations consistent with the neuroanatomical knowledge in the oedematous peritumoral region, which could not

be visualized with DTI. Ability of DTI to demonstrate the proper curvature of the tract was also compromised in 4 cases. The use of HARDI-CS-based tractography was advocated for larger tumours with significant peritumoral oedema. An additional advantage was related to a shorter acquisition time for this sequence at 15 minutes per patient, making it more clinically accessible.[45] A further study from the same group compared HARDI-CS with DTI-based tractography of the OR in 8 patients with temporal lobe gliomas.[34] Four of the eight patients had GBM. The OR was displayed more conclusively compared to DTI in all patients. This advantage was highlighted for high grade glioma cases with significant perilesional oedema, larger size or closer proximity to the reconstructed tract.[34] These preliminary studies demonstrate the advantages of using advanced techniques for evaluating WM tracts around high grade gliomas associated with significant oedema. This is particularly applicable for cases requiring reconstruction of complex fiber bundles like the OR or the arcuate fasciculus (AF).

6.5.3 Application of High definition fiber tractography with gliomas

General information

HDFT[46] addresses the limitations of DTI by using DSI for acquisition;[39] GQI for fiber orientation estimation;[41] a generalised deterministic fiber tracking method[28] and other innovations.[47] We have reported its use in anatomical studies on several tracts including CST,[47] middle longitudinal fascicle,[43] and AF[48] and in clinical studies concerning its utility for surgical planning for tumours and CMs.[19,46] One of the key advantages of using HDFT has been the ability to obtain accurate qualitative data in terms of reconstruction of multiple perilesional WM tracts in a three dimensional fashion around mass lesions, which assisted in accurate surgical planning.[19,46] The accuracy of the reconstructed perilesional WM tracts in the perilesional zone is evaluated in light of their consistency with the known loco-regional neuroanatomy. In a recent study,[19] the utility of HDFT was demonstrated through illustration of the precise spatial relationship of CMs to multiple perilesional WM tracts, which was helpful for surgical trajectory planning. We further showed the occurrence of

disruption and/or displacement around the CMs.[19] These changes were supported by the QA, which is an anisotropy index derived from the ODF.

The extent of perilesional oedema associated with gliomas is greater than that with CMs leading to further diffusion disturbance, as observed with DTI. In our clinical experience, however, this greater extent of perilesional oedema has not been prohibitive with respect to obtaining accurate qualitative tractography data for surgical planning. This is demonstrated by case examples below of application of HDFT with GBMs located in multiple anatomical compartments, including for reconstruction of complex fiber bundles. Potential explanations relate to the QA, which serves as a reliable stopping criterion for fiber tracking and therefore, accurately demonstrates endpoint connectivity in between cortical and subcortical regions.[33] QA, as a directionally specific quantitative measure overcomes some of the limitations of FA and therefore DTI, in demonstrating multiple crossing fibers. This is linked to QA being less sensitive than FA to partial volume effects, as demonstrated in our recent study.[28] Similarly, in perilesional oedematous zones, its resistance to partial volume effects leads to better qualitative tractography data.

Illustrative Cases with Glioblastoma multiforme (also see Supplementary Figures S1-4 demonstrating depiction of WM tracts via fiber dissection and HDFT reconstructions in non-pathological brains)

Motor system (also see Supplementary Figure S1)

Case 1

A 54-year-old male presented with complaints of right upper extremity weakness; numbness and a single partial seizure. On examination, he was found to have minimal weakness in his right upper and lower limbs. MRI of the brain demonstrated a left frontoparietal lesion around the central sulcus, located predominantly in the postcentral gyrus (Figure 1). HDFT was used to preoperatively demonstrate the location of the anteriorly displaced CST in the perilesional oedematous zone. The tumour was resected via an image-guided left frontoparietal craniotomy and

cortical/subcortical mapping of the motor tract. Postoperatively the patient had no neurological deficits.

Case 2

A 67-year-old female presented with a recent history of worsening right side hemiparesis leading to difficulty with ambulation. A decade ago, she had suffered a middle cerebral artery territory infarction leading to longstanding hemiparesis. MRI of the brain demonstrated a left sided basal ganglia mass. Preoperative HDFT showed an anteromedially displaced CST coursing through the perilesional area (Figure 2). The lesion was resected via an image guided left frontotemporoparietal craniotomy with adjunctive use of intraoperative electrical stimulation of the motor fibers. Consistent with the HDFT, the electrical stimulation in the anteromedial and deeper aspect of the tumour led to a positive response for the internal capsule. A residual cuff of tumour was left along this margin to avoid worsening her motor function. Postoperatively her neurological function was stable.

Visual System (also see Supplementary Figure S2)

Case 3

A 65-year-old male presented with a history of confusion and visual disturbance (left-sided incongrous homonymous hemianopia). MRI of the brain revealed a right-sided parieto-occipital lesion. A preoperative HDFT demonstrated medially and inferiorly displaced OR in the perilesional oedematous area. The tumour was resected via an image-guided right parieto-occipital craniotomy with particular attention to the deeper, medial and inferior aspects of the tumour adjacent to the atrium, where the OR was identified preoperatively. Postoperatively the visual field deficit improved (Figure 3) corresponding to the improvement in the configuration of the OR.

Language system (also see Supplementary Figure S3)

Case 4

A 69-year-old female presented with speech difficulty and confusion lasting several weeks. On examination, she had mild expressive dysphasia. MRI brain (Figure 4) revealed a left-sided insular lesion extending to the fronto-orbital opercula and left temporal lobe with associated perilesional oedema and contrast enhancement. Preoperative HDFT was performed to identify the cortical endpoints of the AF both at the frontal and temporal regions (Figure 4). Interestingly, both the uncinate and inferior fronto-occipital fascicles were not visualized due to potential disruption by the tumour. Given the degree of mass effect, perilesional swelling as well as the potential length of surgery, a decision was made to not perform intraoperative language mapping. The patient underwent an image-guided left fronto-temporal craniotomy involving wide opening of the sylvian fissure and identification of the lateral lenticulostriate arteries. Most of the tumour, including its temporal lobe extension, was removed through a trans-sylvian approach. Additionally, a small corticotomy was made in the left fronto-orbital region to remove the fronto-orbital extension. The location of the entry point was based on the preoperative information from the HDFT study, which had identified the frontal origin of AF as being posterior to the area of the corticotomy. Postoperatively there was no worsening of her speech.

Limbic system (also see Supplementary Figure S4)

Case 5

A 68-year-old male presented with a history of cognitive disturbances and left-sided hemineglect syndrome lasting several weeks. Examination revealed a left-sided hemineglect syndrome. MRI of the brain showed a posterior right cingulate (Figure 5) lesion extending towards the isthmus and the parahippocampal gyrus. HDFT demonstrated disruption of the posterior right cingulum; inferolateral displacement of the forceps major; and lateral displacement of the OR in the oedematous area. An image-guided posterior interhemispheric approach was performed to resect the tumour involving the cingulate gyrus and the medial aspect of the encysted atrium.

Lateral aspect of the atrium and the adjacent OR were carefully preserved. Postoperatively there was marked improvement in the patient's hemineglect syndrome.

6.6 Limitations and future directions

6.6.1 Limitations

All tractography studies have reproducibility issues, at least in part due to their reliance on the user expertise in terms of selection of the regions of interest and segmentation of the obtained tracts. Although automated techniques may reduce this bias, manual tractography still remains the best approach for demonstrating the orientation of the affected perilesional WM tracts for surgical trajectory planning. Qualitative data from tractography-based studies with DTI or advanced WM imaging techniques needs interpretation with a sound knowledge of fiber tract anatomy.[18,19] In the setting of mass lesions, this is paramount, as an abnormal trajectory of a fiber may be either technical in origin or be real.[18] A criticism has been the scanning time with the advanced techniques. A current trend in the diffusion field is to use fast scanning sequences,[49] which has substantially reduced the scanning time to 10 to 15 minutes. Despite this reduction, the scanning time may limit its extensive use in the clinical setting and lead to a potential compromise of the accuracy related to possible patient discomfort or movement.

It is noteworthy that experience with advanced WM imaging techniques is preliminary in both the research and the clinical areas. The majority of the experience has been acquired with DTI. Even with conventional DTI, its use in the clinical setting, for example in the resection of a neoplasm, is dependent upon its availability and preference of the institution and the surgeon.

A recent review assessed whether image-guided surgery including DTI-neuronavigation among other modalities offered any advantage in terms of improving the EOR or reducing adverse events in high grade glioma surgery.[50] Data

was examined with respect to 238 patients undergoing surgery with the aid of DTI-neuronavigation. Although the extent of resection was increased with DTI-neuronavigation, the evidence was judged as being very low quality using the GRADE criteria.[50] There was no clear evidence of improvement in overall survival using DTI-neuronavigation. Overall there was poor evidence that DTI-neuronavigation increased the percentage of patients with high grade glioma that had a complete tumour resection as evaluated by the post-operative MRI. There was similarly a theoretical concern regarding the reporting of adverse events in the examined studies.[50] This highlights the need for evaluation of the utility of tractography-based data from the DTI or advanced WM imaging techniques in surgery for gliomas using well-designed studies.

6.6.2 Future directions

In order to reduce the subjectivity of interpretation of qualitative data, the use of a combined qualitative and quantitative approach may be helpful,[19] which was validated in CMs using overall and perilesional mean QA for the affected tracts. Our current approach in an ongoing study involves application of a similar methodology to characterise the changes in the perilesional WM tracts around high grade gliomas. This approach can potentially provide information on the integrity of a fiber tract of interest with possible implications for prognostication and neurological recovery. Currently diffusion phantom studies are also being carried out to develop more robust quantitative metrics, which may better characterise the morphology of the perilesional WM tracts adjacent to gliomas in the future.

Beyond the surgical planning, the utility of HDFT in terms of reducing adverse events associated with a potentially increased EOR will need further evaluation. In view of the preliminary accuracy of cortical termination points from HDFT,[46] its correlation with the functional MRI[19] data and with results from the intraoperative WM stimulation for cerebral lesion, is being examined at our institution. This will pave the way for a potential clinical study where in cohort of patients with GBM the data from HDFT-based tractography may be used to guide the surgical resection without intraoperative subcortical WM stimulation. The outcome will need

evaluation in terms of assessment of potential morbidity associated with the surgical resection and the EOR. The obvious difficulty in setting up well-designed clinical studies in this respect relate to the patient outcome being dependent upon multiple factors including the eloquence of the perilesional anatomy.

The application of data derived from the advanced WM imaging techniques to enable maximal safe resection of LGGs will also need to be explored. Increasing the EOR in LGGs has been shown to improve overall survival and malignant progression-free survival.[51] Traditional imaging modalities used for pre- and intraoperative surgical guidance have typically utilized FLAIR sequences. Currently, cortical and subcortical stimulation mapping is an invaluable intraoperative tool for maximizing the EOR and maintaining functional integrity.[52-54] Awaiting further studies, HDFT may be used in combination with subcortical stimulation to potentially maximize the EOR while preserving neural function.

A further potential future application may be the application of advanced WM imaging techniques in distinguishing infiltration from oedema around gliomas. Most of the current focus has been directed towards obtaining tractography reconstructions for the WM tracts around these lesions to enable safer surgical planning. With increasing application of HDFT and other such imaging techniques, in future, the quantitative measures will need validation in terms of their ability to distinguish reliably between unaffected WM tracts from the affected and potentially infiltrated tracts.

6.7 Conclusion

In this article we have briefly mentioned the clinical use of DTI with cerebral neoplasms. Recent preliminary studies in this patient group using advanced WM imaging techniques have demonstrated the superiority of the qualitative WM tractography data in the perilesional oedematous zone relative to the information from the conventional DTI. The ability to demonstrate neuronatomically complex fiber bundles in the perilesional oedematous zone around high grade gliomas in a three-dimensional manner using HDFT, is clearly useful in neurosurgery. Future

studies will need to be correlated with functional imaging modalities and intraoperative white matter stimulation.

6.8 References

1. Le Bihan D, Breton E, Lallemand D, Grenier P, Cabanis E, Laval-Jeantet M. MR imaging of intravoxel incoherent motions: application to diffusion and perfusion in neurologic disorders. *Radiology.* 1986;161(2):401-407.
2. Kono K, Inoue Y, Nakayama K, et al. The role of diffusion-weighted imaging in patients with brain tumours. *AJNR Am J Neuroradiol.* 2001;22(6):1081-1088.
3. Lyng H, Haraldseth O, Rofstad EK. Measurement of cell density and necrotic fraction in human melanoma xenografts by diffusion weighted magnetic resonance imaging. *Magn Reson Med.* 2000;43(6):828-836.
4. Sugahara T, Korogi Y, Kochi M, et al. Usefulness of diffusion-weighted MRI with echo-planar technique in the evaluation of cellularity in gliomas. *J Magn Reson Imaging.* 1999;9(1):53-60.
5. Basser PJ, Mattiello J, LeBihan D. Estimation of the effective self-diffusion tensor from the NMR spin echo. *J Magn Reson B.* 1994;103(3):247-254.
6. Pierpaoli C, Basser PJ. Toward a quantitative assessment of diffusion anisotropy. *Magn Reson Med.* 1996;36(6):893-906.
7. Pierpaoli C, Jezzard P, Basser PJ, Barnett A, Di Chiro G. Diffusion tensor MR imaging of the human brain. *Radiology.* 1996;201(3):637-648.
8. Beaulieu C. The basis of anisotropic water diffusion in the nervous system - a technical review. *NMR Biomed.* 2002;15(7-8):435-455.
9. Jenkinson MD, du Plessis DG, Smith TS, Brodbelt AR, Joyce KA, Walker C. Cellularity and apparent diffusion coefficient in oligodendroglial tumours characterised by genotype. *J Neurooncol.* 2010;96(3):385-392.
10. Yamashita Y, Kumabe T, Higano S, Watanabe M, Tominaga T. Minimum apparent diffusion coefficient is significantly correlated with cellularity in medulloblastomas. *Neurol Res.* 2009;31(9):940-946.

11. Yoshikawa MI, Ohsumi S, Sugata S, et al. Relation between cancer cellularity and apparent diffusion coefficient values using diffusion-weighted magnetic resonance imaging in breast cancer. *Radiat Med.* 2008;26(4):222-226.
12. Sadeghi N, D'Haene N, Decaestecker C, et al. Apparent diffusion coefficient and cerebral blood volume in brain gliomas: relation to tumor cell density and tumor microvessel density based on stereotactic biopsies. *AJNR Am J Neuroradiol.* 2008;29(3):476-482.
13. Humphries PD, Sebire NJ, Siegel MJ, Olsen OE. Tumours in pediatric patients at diffusion-weighted MR imaging: apparent diffusion coefficient and tumor cellularity. *Radiology.* 2007;245(3):848-854.
14. Hayashida Y, Hirai T, Morishita S, et al. Diffusion-weighted imaging of metastatic brain tumours: comparison with histologic type and tumor cellularity. *AJNR Am J Neuroradiol.* 2006;27(7):1419-1425.
15. Yamasaki F, Kurisu K, Satoh K, et al. Apparent diffusion coefficient of human brain tumours at MR imaging. *Radiology.* 2005;235(3):985-991.
16. Cauley KA, Andrews T, Gonyea JV, Filippi CG. Magnetic resonance diffusion tensor imaging and tractography of intracranial cavernous malformations: preliminary observations and characterisation of the hemosiderin rim. *J Neurosurg.* 2010;112(4):814-823.
17. De Belder FE, Oot AR, Van Hecke W, et al. Diffusion tensor imaging provides an insight into the microstructure of meningiomas, high-grade gliomas, and peritumoral oedema. *J Comput Assist Tomogr.* 2012;36(5):577-582.
18. Lazar M, Alexander AL, Thottakara PJ, Badie B, Field AS. White matter reorganisation after surgical resection of brain tumours and vascular malformations. *AJNR Am J Neuroradiol.* 2006;27(6):1258-1271.
19. Abhinav K, Pathak S, Richardson RM, et al. Application of high-definition fiber tractography in the management of supratentorial cavernous malformations: a combined qualitative and quantitative approach. *Neurosurgery.* 2014;74(6):668-681.
20. Sanai N, Polley MY, McDermott MW, Parsa AT, Berger MS. An extent of resection threshold for newly diagnosed glioblastomas. *J Neurosurg.* 2011;115(1):3-8.

21. McGirt MJ, Chaichana KL, Gathinji M, et al. Independent association of extent of resection with survival in patients with malignant brain astrocytoma. *J Neurosurg.* 2009;110(1):156-162.
22. Tuch DS, Reese TG, Wiegell MR, Makris N, Belliveau JW, Wedeen VJ. High angular resolution diffusion imaging reveals intravoxel white matter fiber heterogeneity. *Magn Reson Med.* 2002;48(4):577-582.
23. Alexander AL, Hasan KM, Lazar M, Tsuruda JS, Parker DL. Analysis of partial volume effects in diffusion-tensor MRI. *Magn Reson Med.* 2001;45(5):770-780.
24. Provenzale JM, McGraw P, Mhatre P, Guo AC, Delong D. Peritumoral brain regions in gliomas and meningiomas: investigation with isotropic diffusion-weighted MR imaging and diffusion-tensor MR imaging. *Radiology.* 2004;232(2):451-460.
25. Metzler-Baddeley C, O'Sullivan MJ, Bells S, Pasternak O, Jones DK. How and how not to correct for CSF-contamination in diffusion MRI. *NeuroImage.* 2012;59(2):1394-1403.
26. Pasternak O, Sochen N, Gur Y, Intrator N, Assaf Y. Free water elimination and mapping from diffusion MRI. *Magn Reson Med.* 2009;62(3):717-730.
27. Abhinav K, Yeh FC, Pathak S, Friedlander RM, Fernandez-Miranda JC. Advanced diffusion MRI fiber tracking in neurosurgical and neurodegenerative disorders and neuroanatomical studies: A review. *Biochimica et biophysica acta.* 2014.
28. Yeh FC, Verstynen TD, Wang Y, Fernandez-Miranda JC, Tseng WY. Deterministic diffusion fiber tracking improved by quantitative anisotropy. *PLoS One.* 2013;8(11):e80713.
29. Nimsky C, Ganslandt O, Hastreiter P, et al. Preoperative and intraoperative diffusion tensor imaging-based fiber tracking in glioma surgery. *Neurosurgery.* 2005;56(1):130-137; discussion 138.
30. Kuhnt D, Bauer MH, Becker A, et al. Intraoperative visualization of fiber tracking based reconstruction of language pathways in glioma surgery. *Neurosurgery.* 2012;70(4):911-919; discussion 919-920.
31. Lu S, Ahn D, Johnson G, Cha S. Peritumoral diffusion tensor imaging of high-grade gliomas and metastatic brain tumours. *AJNR Am J Neuroradiol.* 2003;24(5):937-941.

32. Sternberg EJ, Lipton ML, Burns J. Utility of diffusion tensor imaging in evaluation of the peritumoral region in patients with primary and metastatic brain tumours. *AJNR Am J Neuroradiol.* 2014;35(3):439-444.
33. Zhang H, Wang Y, Lu T, et al. Differences between generalised q-sampling imaging and diffusion tensor imaging in the preoperative visualization of the nerve fiber tracts within peritumoral oedema in brain. *Neurosurgery.* 2013;73(6):1044-1053; discussion 1053.
34. Kuhnt D, Bauer MH, Sommer J, Merhof D, Nimsky C. Optic radiation fiber tractography in glioma patients based on high angular resolution diffusion imaging with compressed sensing compared with diffusion tensor imaging - initial experience. *PLoS One.* 2013;8(7):e70973.
35. Le Bihan D. Apparent Diffusion Coefficient and Beyond: What Diffusion MR Imaging Can Tell Us about Tissue Structure. *Radiology.* 2013;268(2):318-322.
36. Tournier JD, Mori S, Leemans A. Diffusion tensor imaging and beyond. *Magn Reson Med.* 2011;65(6):1532-1556.
37. Zhang H, Schneider T, Wheeler-Kingshott CA, Alexander DC. NODDI: practical in vivo neurite orientation dispersion and density imaging of the human brain. *Neuroimage.* 2012;61(4):1000-1016.
38. Wedeen VJ, Wang RP, Schmahmann JD, et al. Diffusion spectrum magnetic resonance imaging (DSI) tractography of crossing fibers. *NeuroImage.* 2008;41(4):1267-1277.
39. Wedeen VJ, Hagmann P, Tseng WY, Reese TG, Weisskoff RM. Mapping complex tissue architecture with diffusion spectrum magnetic resonance imaging. *Magn Reson Med.* 2005;54(6):1377-1386.
40. Kuo LW, Chen JH, Wedeen VJ, Tseng WY. Optimization of diffusion spectrum imaging and q-ball imaging on clinical MRI system. *NeuroImage.* 2008;41(1):7-18.
41. Yeh FC, Wedeen VJ, Tseng WY. Generalised q-sampling imaging. *IEEE Trans Med Imaging.* 2010;29(9):1626-1635.
42. Yeh FC, Tseng WY. Sparse solution of fiber orientation distribution function by diffusion decomposition. *PLoS ONE.* 2013;8(10):e75747.

43. Wang Y, Fernandez-Miranda JC, Verstynen T, Pathak S, Schneider W, Yeh FC. Rethinking the role of the middle longitudinal fascicle in language and auditory pathways. *Cereb Cortex.* 2013;23(10):2347-2356.
44. Yeh FC, Wedeen VJ, Tseng WY. Estimation of fiber orientation and spin density distribution by diffusion deconvolution. *NeuroImage.* 2011;55(3):1054-1062.
45. Kuhnt D, Bauer MH, Egger J, et al. Fiber tractography based on diffusion tensor imaging compared with high-angular-resolution diffusion imaging with compressed sensing: initial experience. *Neurosurgery.* 2013;72 Suppl 1:165-175.
46. Fernandez-Miranda JC, Pathak S, Engh J, et al. High-definition fiber tractography of the human brain: neuroanatomical validation and neurosurgical applications. *Neurosurgery.* 2012;71(2):430-453.
47. Verstynen T, Jarbo K, Pathak S, Schneider W. In vivo mapping of microstructural somatotopies in the human corticospinal pathways. *J Neurophysiol.* 2011;105(1):336-346.
48. Fernandez-Miranda JC, Wang Y, Pathak S, Stefaneau L, Verstynen T, Yeh FC. Asymmetry, connectivity, and segmentation of the arcuate fascicle in the human brain. *Brain Struct Funct.* 2014.
49. Sotiropoulos SN, Jbabdi S, Xu J, et al. Advances in diffusion MRI acquisition and processing in the Human Connectome Project. *Neuroimage.* 2013;80:125-143.
50. Barone DG, Lawrie TA, Hart MG. Image guided surgery for the resection of brain tumours. *The Cochrane database of systematic reviews.* 2014;1:CD009685.
51. Smith JS, Chang EF, Lamborn KR, et al. Role of extent of resection in the long-term outcome of low-grade hemispheric gliomas. *J Clin Oncol.* 2008;26(8):1338-1345.
52. Gras-Combe G, Moritz-Gasser S, Herbet G, Duffau H. Intraoperative subcortical electrical mapping of optic radiations in awake surgery for glioma involving visual pathways. *J Neurosurg.* 2012;117(3):466-473.
53. Khan OH, Herbet G, Moritz-Gasser S, Duffau H. The role of left inferior fronto-occipital fascicle in verbal perseveration: a brain electrostimulation mapping study. *Brain Topogr.* 2014;27(3):403-411.

54. Matsuda R, Moritz-Gasser S, Duvaux S, Fernandez Coello A, Martinoni M, Duffau H. The persistent crucial role of the left hemisphere for language in left-handers with a left low grade glioma: a stimulation mapping study. *Acta Neurochir (Wien).* 2014;156(4):661-670; discussion 670.

6.9.1 Figures

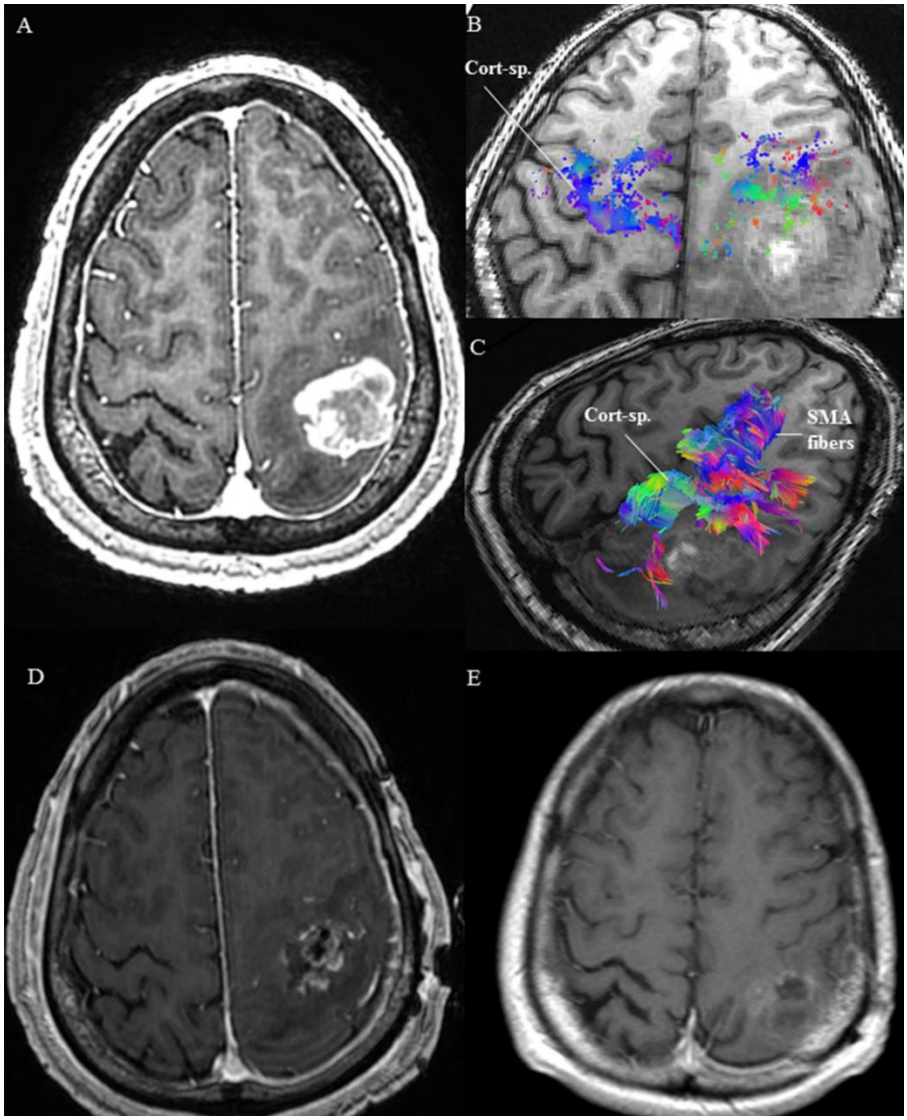

FIGURE 1. (A) MRI of the brain in Case 1 demonstrated a contrast-enhancing lesion in the left postcentral gyrus with associated perilesional oedema. (B) Preoperative HDFT revealed an anteriorly displaced corticospinal (Cort-sp.) tract, compared with the contralateral side and as demonstrated by the cortical end points of the tract. (C) Preoperative HDFT was used to demonstrate the corticospinal and supplementary motor area (SMA) fibers coursing adjacent to the lesion in the oedematous zone. (D) Early postoperative MRI of the brain with contrast demonstrated a resection cavity in the postcentral gyrus limited anteriorly due to the location of the precentral gyrus and preoperatively identified displaced corticospinal tracts. (E) A delayed follow-up MRI after chemoradiotherapy shows evidence of resolution of some of the postoperative residual tumour.

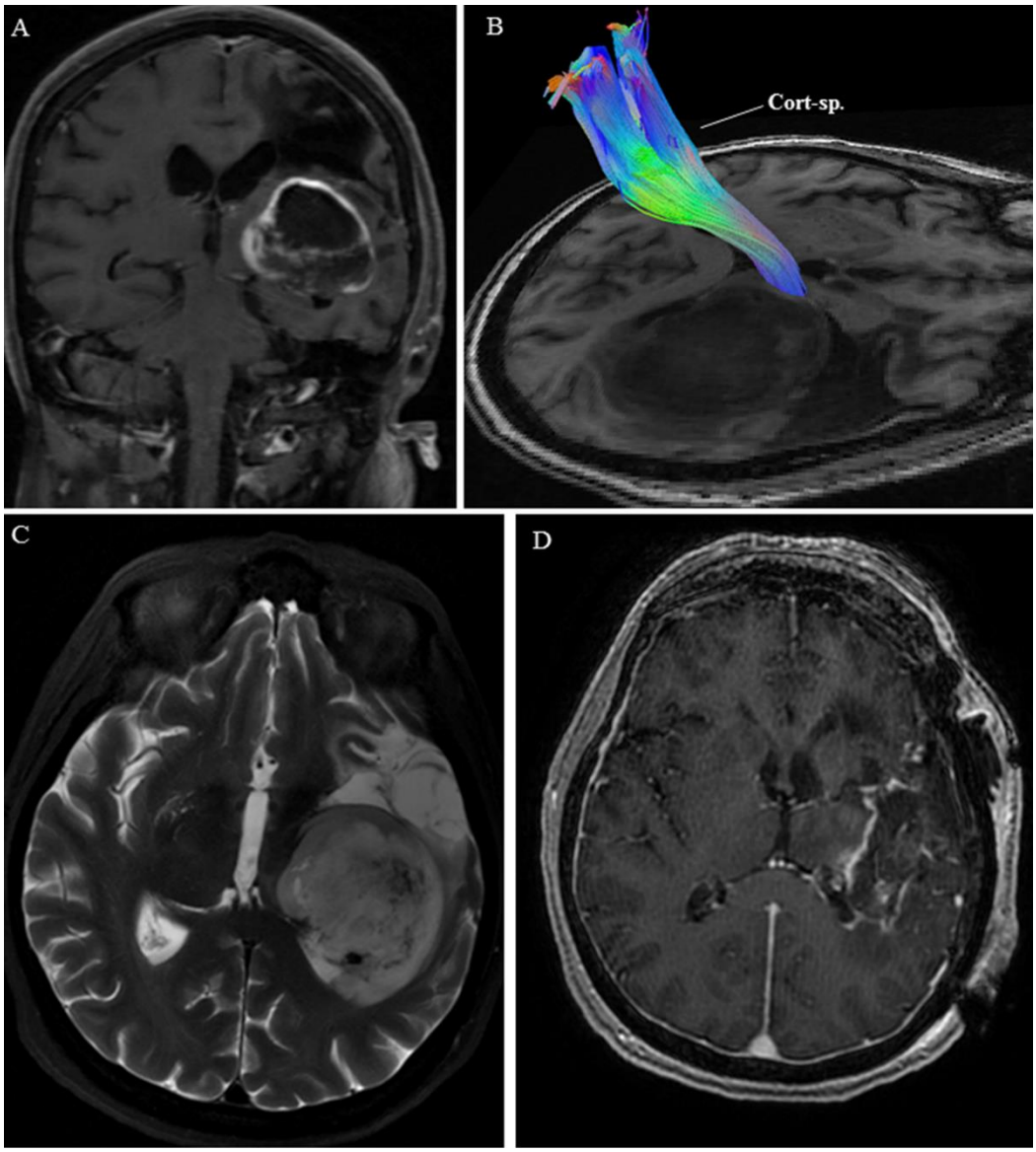

FIGURE 2. (A) MRI of the brain in Case 2 demonstrated a left-sided contrast enhancing basal ganglia mass with evidence of a previous middle cerebral artery territory infarction. (B) Preoperative HDFT revealed a displaced corticospinal tract (Cort-sp.) in the perilesional area. (C) T2-weighted MRI of the brain further delineated the tumour. (D) Postoperative contrast-enhanced MRI showed a residual cuff of tumour along the margin adjacent to the corticospinal tract and the thalamus.

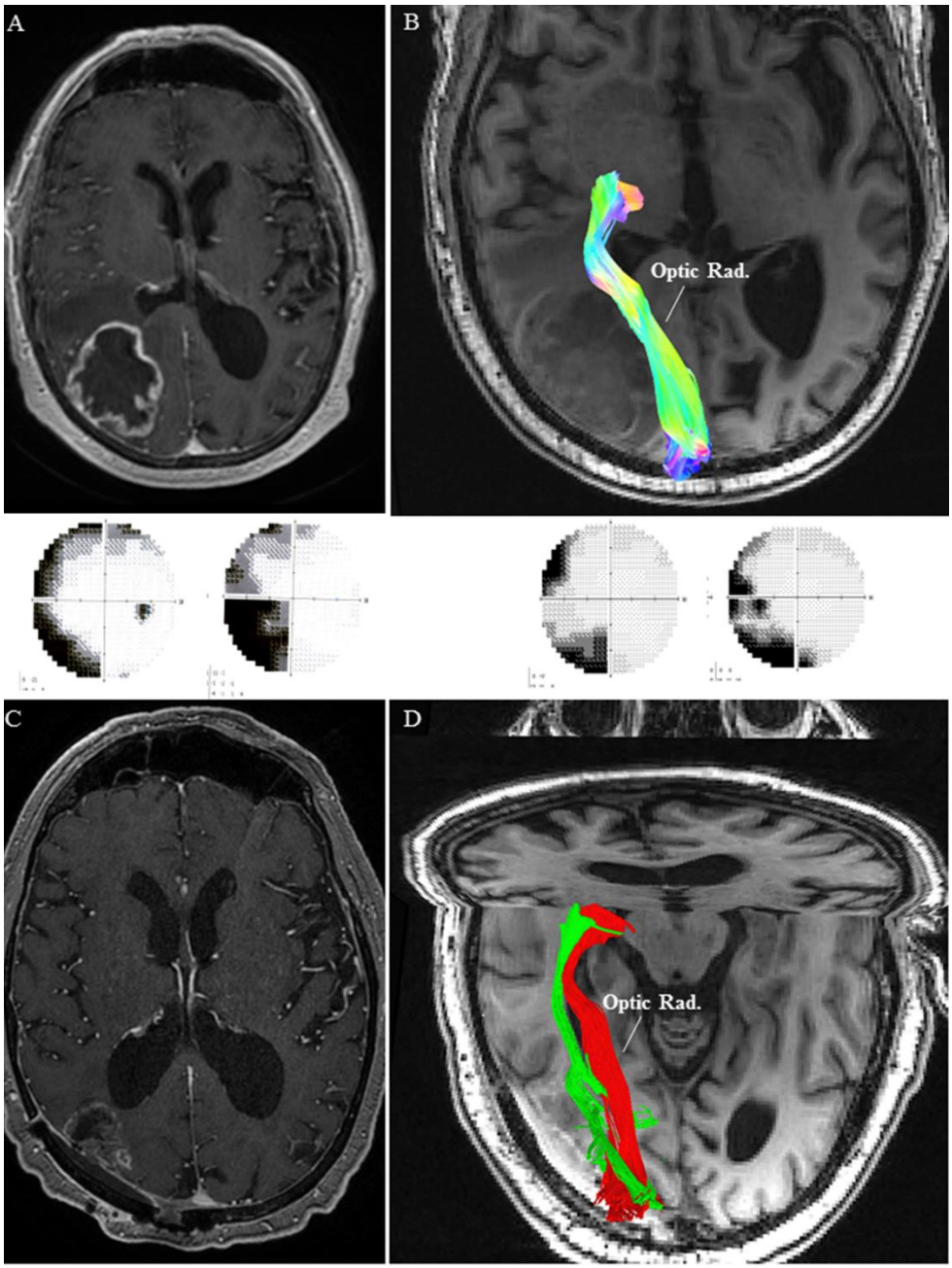

FIGURE 3. (A) MRI of the brain in Case 3 demonstrated a right-sided contrast enhancing parieto-occipital lesion leading to left sided homonymous hemianopia (panel below). (B) Preoperative HDFT showed medially and inferiorly displaced optic radiation (Optic Rad.) in the perilesional oedematous area. (C) Postoperative MRI with contrast confirmed an adequate resection with a small residual on the medial margin adjacent to the optic radiation. (D) Postoperative HDFT confirmed the improvement in the configuration of the displaced optic radiation (red: preoperative; green: postoperative). This was accompanied by an improvement in the visual field deficit (panel above).

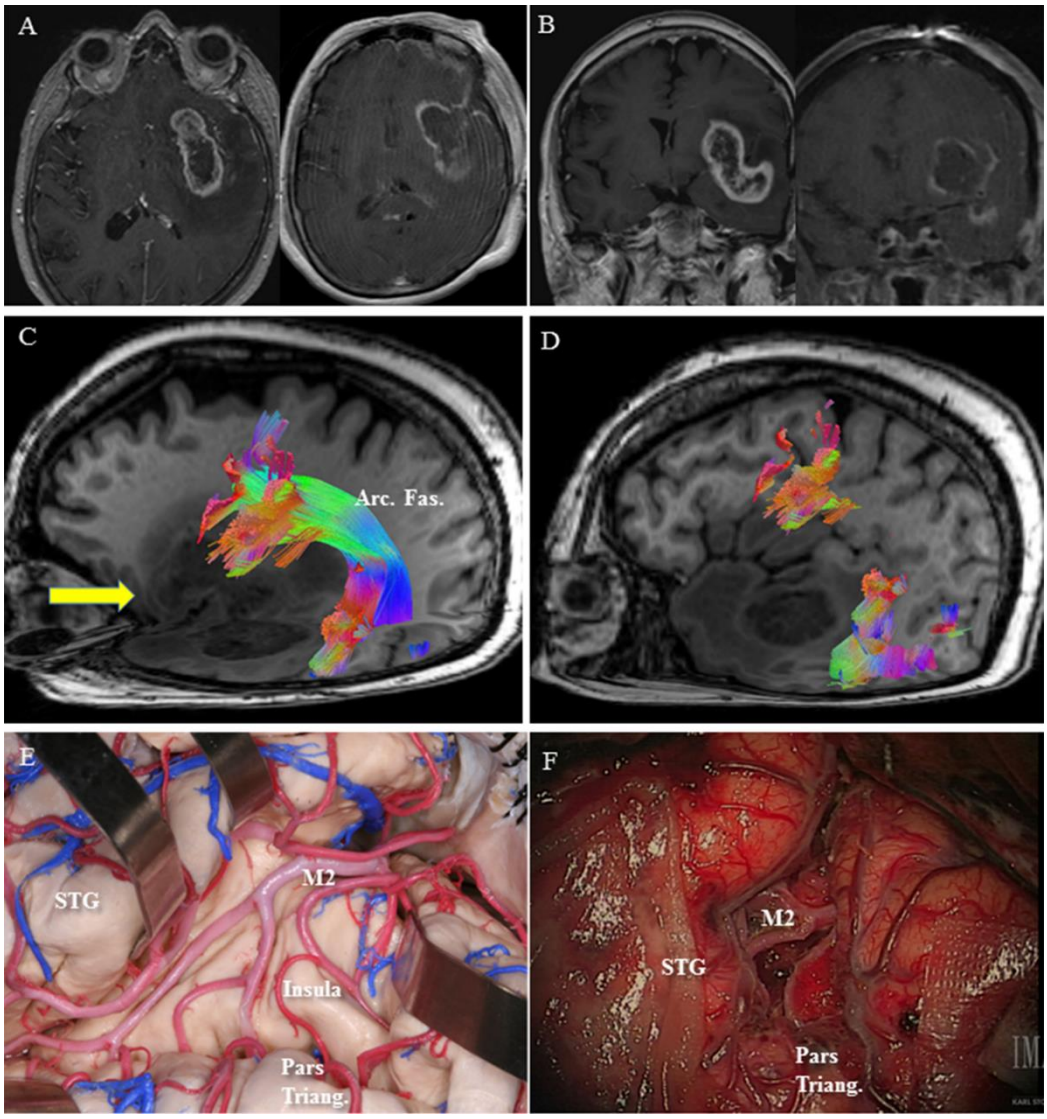

Figure 4. (A, axial) and (B, coronal) Preoperative MRI with contrast in case 4 demonstrated an enhancing left insular lesion with extension into the fronto-orbital operculum and the temporal lobe. (C) Pre-operative HDFT demonstrated the arcuate fasciculus (Arc. Fas.) coursing through the perilesional oedematous area. Arrow (yellow) represents the site of the corticotomy in the frontal operculum. (D) Frontal termination of the arcuate fibers was identified in the pars opercularis, precentral gyrus and middle frontal gyrus using HDFT and to help with the decision-making regarding the site of corticotomy in the frontal operculum. (E) A representative anatomical view in a cadaveric specimen shows the insula with overlying M2 branches of the middle cerebral artery and the location of the pars triangularis (Pars triang.) and the superior temporal gyrus (STG). (F) A comparable intraoperative view is presented after debulking of the tumour in between the M2 branches. The location of the pars triangularis (Pars triang.) is demonstrated.

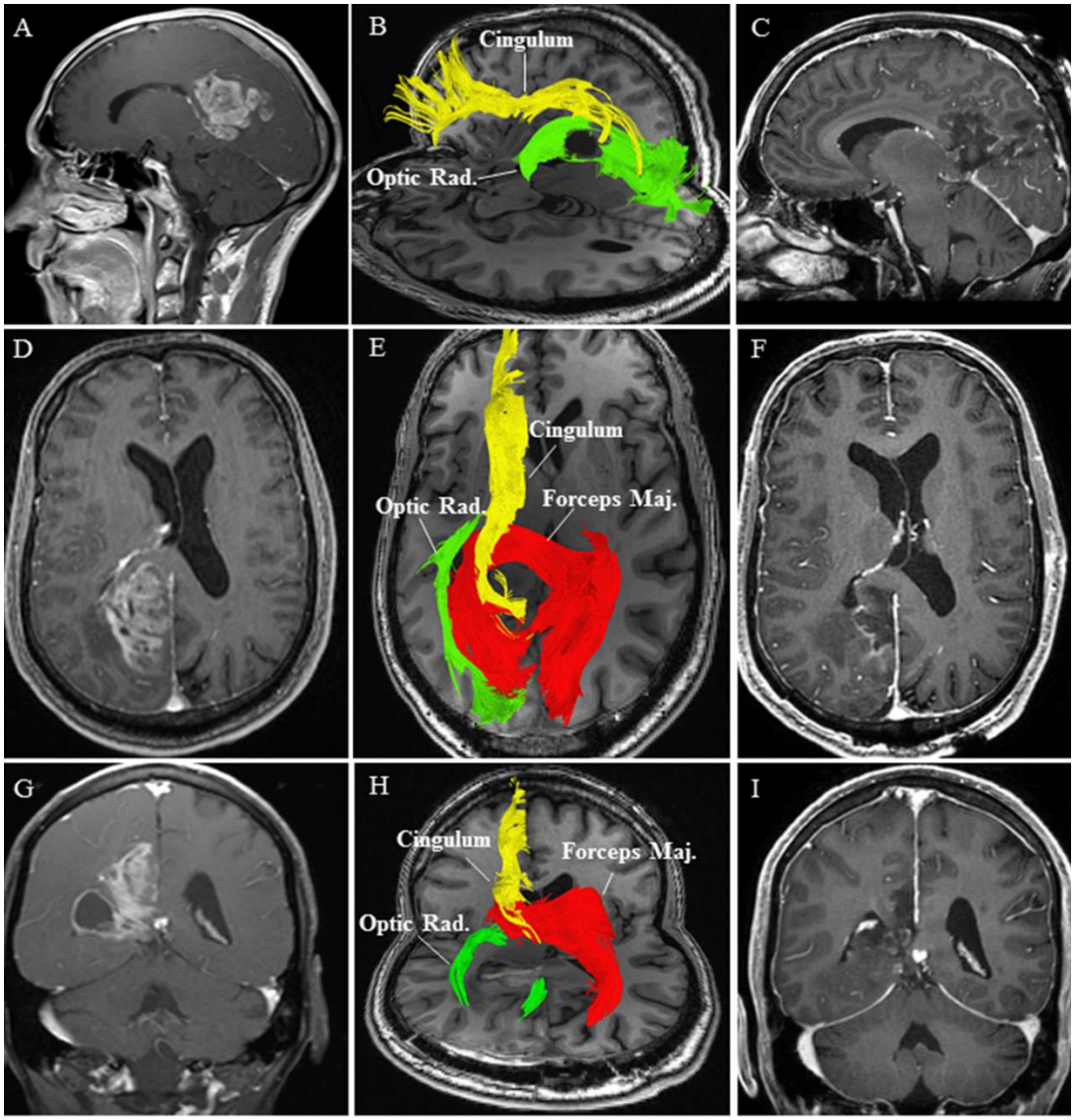

FIGURE 5. (A, sagittal); (D, axial) and (G, coronal) Preoperative MRI with contrast revealed a right-sided enhancing posterior cingulate lesion with an encysted atrium (G). (B, sagittal) and (E, axial) Preoperative HDFT characterised the qualitative changes in the perilesional white matter [cingulum, forceps major (Forceps Maj.) and optic radiations (Optic Rad.)]. (H) Postoperative HDFT demonstrated the disruption in the forceps major (Forceps Maj.) due to the surgical trajectory through this potentially infiltrated fiber bundle. (C, sagittal); (F, axial) and (I, coronal) Post-operative MRI with contrast demonstrates the resection cavity in the posterior cingulum with resolution of the tumour cyst.

6.9.2 Supplementary Figures

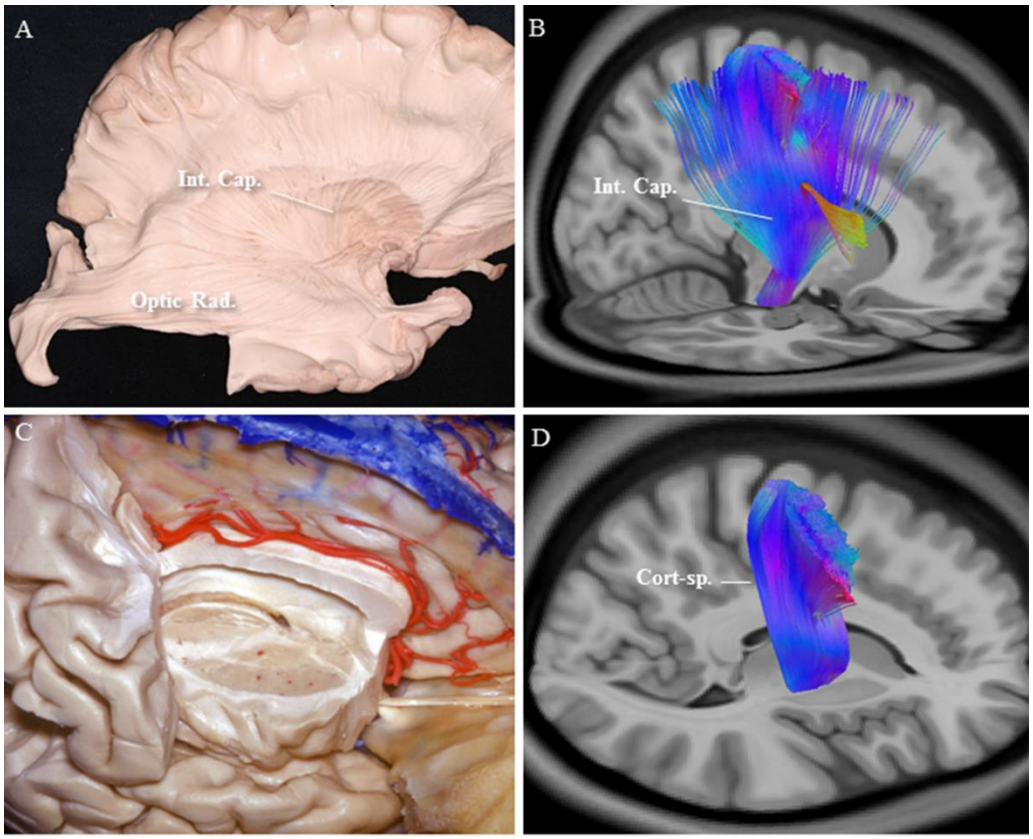

FIGURE S1. (A) Fiber-microdissection of the brain demonstrates the internal capsule (Int. Cap.) following removal of the lentiform nucleus. Optic radiation (Optic Rad.) is shown in the retrolenticular part of the internal capsule. (B) HDFT reconstruction of the internal capsule is demonstrated in a normal subject. (C) Internal capsule (superior, middle and inferior frontal gyri have been removed) is shown in a cadaveric specimen. (D) Reconstruction of the corticospinal tract (Cort-sp.) in normal subject using HDFT demonstrates its position in the posterior limb of the internal capsule.

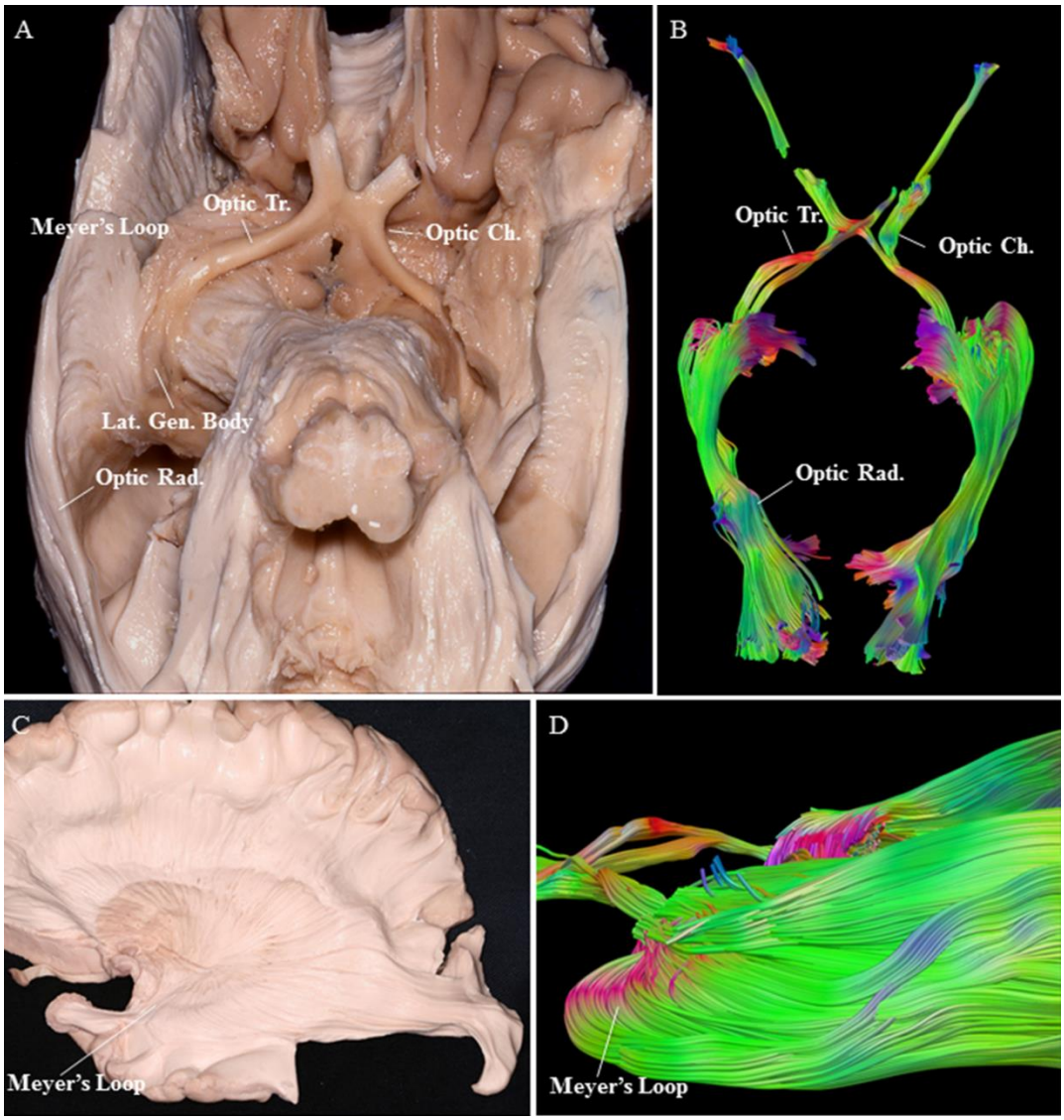

FIGURE S2. (A) Fiber-microdissection of the brain (inferior surface) demonstrates the visual pathway from the optic chiasm (Optic Ch.) to the optic tract (Optic Tr.) and the radiations (Optic Rad.). Meyer's loop is also shown looping anteriorly and laterally from the lateral geniculate body (Lat. Gen. Body). (B) A corresponding HDFT reconstruction of the visual pathway replicates the neuroanatomical features from the fiber dissection. (C) Meyer's loop is demonstrated in the sublenticular part of the internal capsule. (D) A corresponding HDFT reconstruction represents the Meyer's loop.

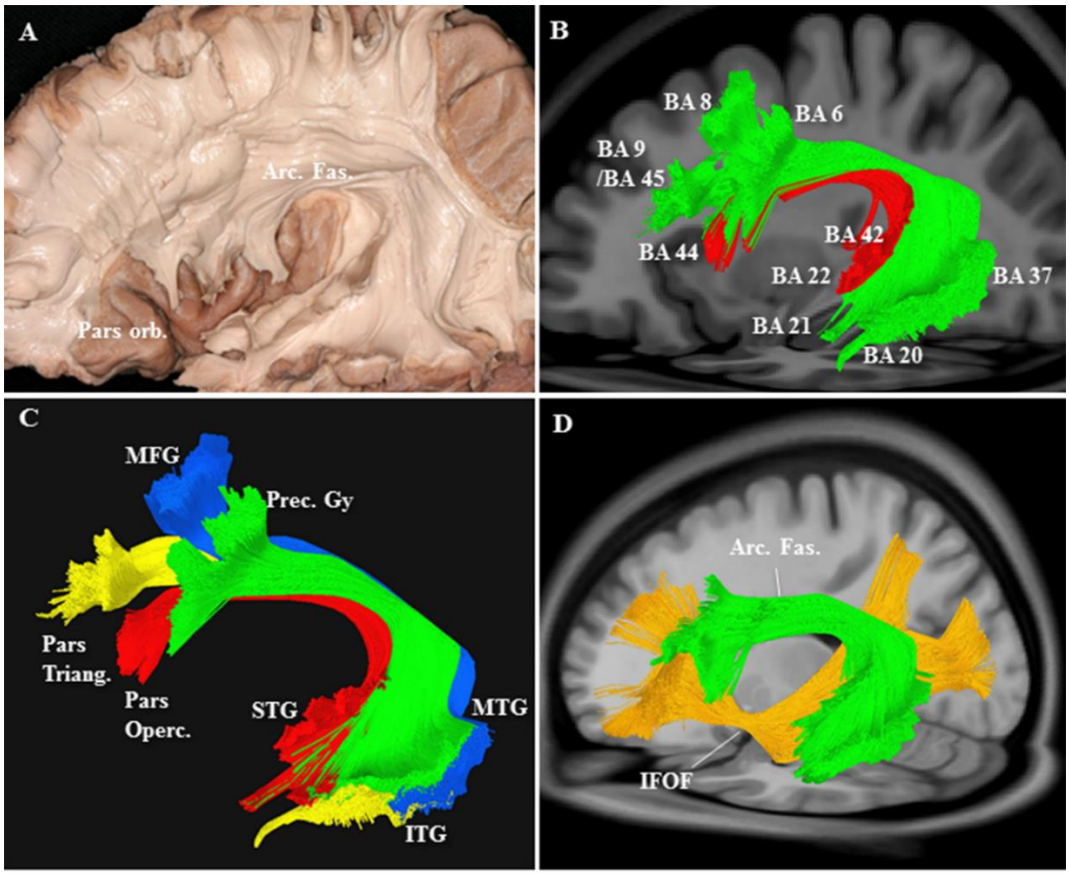

FIGURE S3. (A) Fiber-microdissection demonstrates the location of the arcuate fasciculus (Arc. Fas.) arching around the outer edges of the insula. Pars orbitalis (Pars orb.) in the inferior frontal gyrus is intact. (B) HDFT reconstruction of the arcuate fasciculus shows the inner pathway (red) corresponding to the primary language pathway and interconnecting the pars opercularis (BA44) and most ventral portion of precentral gyrus (BA6) with superior temporal gyrus (BA22) and rostral middle temporal gyrus (BA21). The outer pathway (green) interconnects ventral precentral gyrus (BA6), caudal middle frontal gyrus (BA6 and BA8), and dorsal pars triangularis/dorsal prefrontal cortex (BA45 and BA9) with middle and inferior temporal gyri (BA21–BA20–BA37) and corresponds to the supplementary language pathway. (C) Arcuate fasciculus has four different cortical areas of termination in the frontal lobe, as seen in this HDFT reconstruction [precentral gyrus (Prec. Gy, green); middle frontal gyrus (MFG, blue); pars opercularis (Pars Operc., red); and pars triangularis (Pars Triang., yellow)]. The termination of the arcuate in the temporal lobe is also shown [superior temporal gyrus (STG); middle temporal gyrus (MTG) and inferior temporal gyrus (ITG)]. (D) HDFT reconstruction shows the arcuate fasciculus (Arc. Fas.) and the orientation of the inferior fronto-occipital fasciculus (IFOF) with the latter being implicated in the semantic pathway.

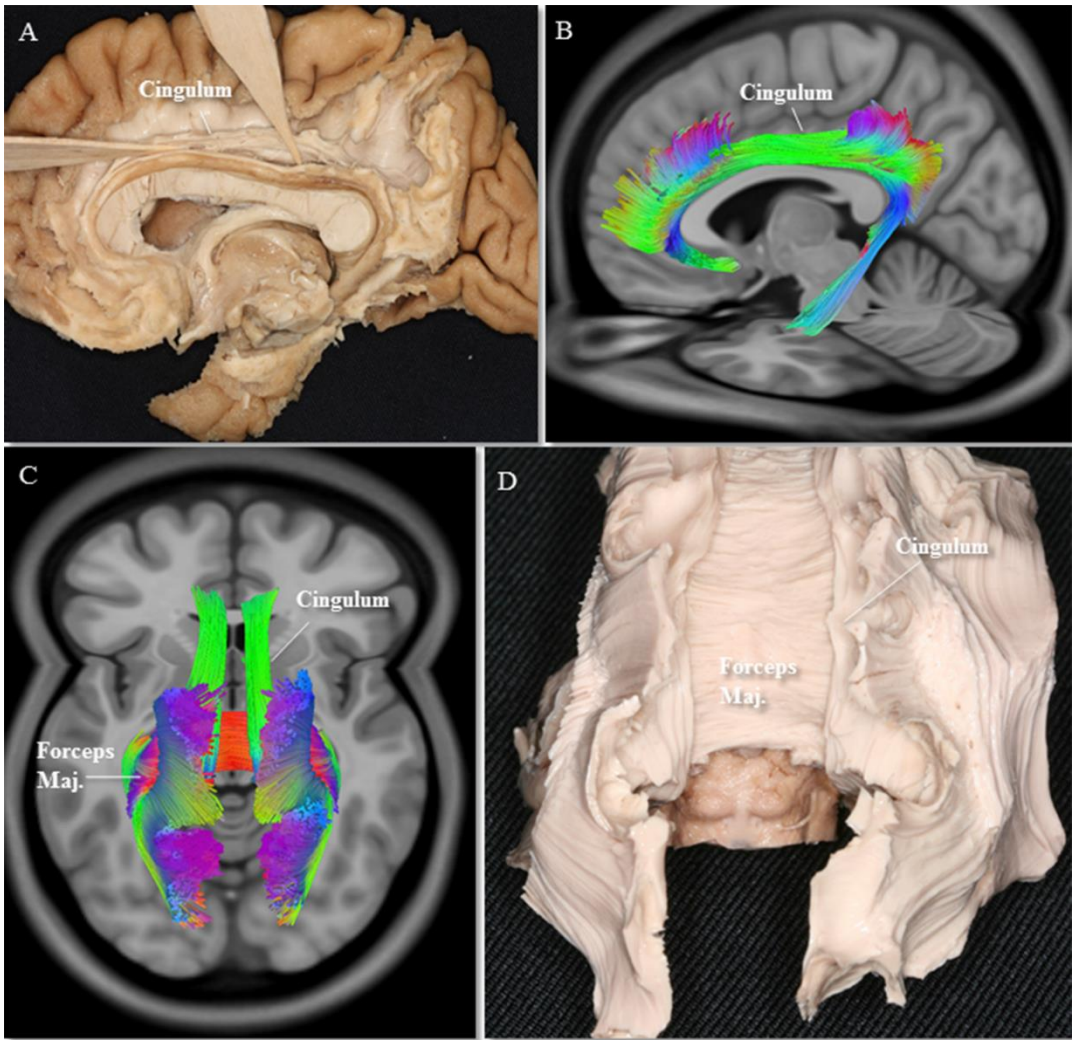

FIGURE S4. (A) Fiber-microdissection of the medial cerebral hemisphere demonstrates the location of the cingulum above the corpus callosum. (B) A corresponding HDFT reconstruction of the cingulum shows its continuation towards the parahippocampal gyrus. (C) HDFT reconstruction (superior view) accurately demonstrates the location of cingulum above the corpus callosum. Forceps major (Forceps Maj.) is also shown radiating from the splenium of the corpus callosum. (D) A corresponding fiber-microdissection demonstrates these anatomical features.

Chapter 7: Visualisation of cranial nerves using High-definition fiber tractography

Paper 6: Yoshino M, **Abhinav K**, Yeh FC, Pathak S Gardner PA, Fernandez-Miranda JC. Visualization of cranial nerves using High-definition fiber tractography. *Neurosurgery* 2016; 79(1):146-65

7.1 Declaration

I was the second author on this manuscript and was instrumental in the initial application of high definition fiber tractography (HDFT) in depiction of cranial nerves (CNs) both in normal and at a more preliminary level, in patients with complex skull base tumours. Overall, I contributed extensively towards the writing, literature search, figures, study design, data analysis and interpretation.

7.2 Introduction to and brief summary of the manuscript and relation to previous work

Like the previous study (Chapter 6), this study represented a switch in the direction from quantitative aspects of the advanced WM imaging towards evaluating its use in a qualitative fashion in the depiction of CNs. Diffusion tensor imaging (DTI) tractography imaging has been used for depiction of CNs. Spatial and angular resolution is however, limited with this modality as discussed. As demonstrated in the preceding chapters, a substantial improvement in image resolution can be achieved using high-angle diffusion MRI and atlas-based fiber tracking and our aim therefore, was to use HDFT or advanced white matter (WM) imaging modality to identify and depict CNs in healthy subjects and patients with brain tumours. Five neurologically healthy adults and three patients with brain tumours were scanned using diffusion spectrum imaging (DSI) that allowed for high angular resolution fiber tracking. In addition, a 488-subject diffusion MRI template constructed from the Human Connectome Project data was used to conduct atlas space fiber tracking of CNs. The cisternal portion of most CNs were successfully tracked and visualized in each healthy subject and in atlas fiber tracking. The entire optic radiation, medial longitudinal fasciculus, spinal trigeminal nucleus/tract, petroclival portion of the

abducens nerve, and the intra-brainstem portion of the facial nerve from the root exit zone to adjacent abducens nucleus were identified. High angular resolution fiber tracking was able to distinguish the facial nerve from the vestibulocochlear nerve complex. The tractography also clearly visualized CNs displaced by brain tumours. These tractography findings were confirmed intraoperatively with electrical stimulation.

Using high angular resolution fiber tracking and atlas-based fiber tracking, in a preliminary fashion, we were able to identify all CNs in significant detail. This has implications for localization of CNs during surgical planning and will be an important component of our future endeavours and direction.

7.3 Introduction

Conventional structural magnetic resonance imaging (MRI), such as T1-weighted images, T2-weighted images, and steady-state acquisition MRI, may allow localization of CNs (CNs) in the clinical setting.[1-11] Tracking CN trajectory in a three-dimensional fashion, however, may require advanced diffusion MRI, which allows resolution of complicated axonal direction in vivo.

Conventional diffusion tensor imaging (DTI) has been applied to track CNs with limited angular resolution (i.e. it cannot resolve crossing fibers).[12-18] Moreover, DTI tractography failed to identify the intra-brainstem portions of these nerves. In addition, DTI suffers from susceptibility artifacts and partial volume averaging of complex fiber architecture. Both of these can lead to poor tracking results during CNs identification.[19, 20]

To overcome these limitations, high-angular resolution diffusion MRI methods,[21-24] as well as new fiber tracking algorithms[21] have been developed. These advanced white matter imaging techniques can accurately reproduce multiple crossing fibers in a three-dimensional manner.[25] Our group has demonstrated the use of one such high angular resolution approach called high-definition fiber tractography (HDFT) which addresses the limitations of DTI. HDFT can provide accurate reconstruction of white matter fiber tracts, within normal subjects and in patients with intracranial masses.[26,

[27] HDFT uses diffusion spectrum imaging (DSI) for image acquisition,[24] generalised q-sampling imaging for fiber orientation estimation,[28] and a generalised deterministic fiber-tracking method for tracking the trajectories of fiber pathways.[29] We have reported its use in studies of several white matter tracts.[30-34]

We hypothesised that HDFT, in comparison with DTI, would provide better localization of CNs, by accurately solving and reproducing multiple crossing fibers within the brainstem. In this study, we investigated the feasibility of HDFT for tracking CNs in an atlas template of 488 healthy subjects from the Human Connectome Project. Additionally, in three patients with brain tumours, we examined the potential of HDFT to identify displaced CNs, a unique feature that may assist surgical planning.

7.4 Methods

7.4.1 Participants

Five neurologically healthy adults (4 males; age range: 21-36 years) and three patients with brain tumours participated in this study. Approval was granted by the internal review board at the University of Pittsburgh, and written consent was obtained from all participants prior to testing.

7.4.2 Image Acquisition and Reconstruction

The diffusion data were acquired on a 3-T Tim Trio System (Siemens) using a 32-channel coil. A multi-band (MB factor=3) spin-echo echo-planar imaging sequence was used to acquire 101-direction DSI in 15 minutes [repetition time (TR) = 9.916 ms, echo time (TE) = 157 ms, voxel size = 2.4 × 2.4 × 2.4 mm, field of view = 231 × 231 mm, 12 b-values (384, 769, 1153, 1538, 1923, 2307, 3076, 3461, 3846, 4230, 4615, 5000 s/mm2)]. For anatomical comparisons, we also included high-resolution anatomical imaging, employing a 9-min T1-weighted axial magnetization prepared rapid gradient echo sequence (TR = 2110 ms, TE = 2.63 ms, flip angle = 8°, 176 slices, field of view = 256 × 256 mm^2, voxel size = 0.5 × 0.5 × 1.0 mm^3). DSI data were reconstructed using a generalised q-sampling imaging approach[28]. The

orientation distribution functions (ODFs) were reconstructed to with a mean diffusion distance scaling parameter of 1.2.

7.4.3 488-subject high angular resolution atlas

We also conducted fiber tracking on the HCP 488 ODF atlas which is publically available at http://dsi-studio.labsolver.org. 488 subjects underwent diffusion scans (289 females, 199 males, average age 29.15, SD ±3.47) and Q-space diffeomorphic reconstruction[35] with a diffusion sampling length ratio of 1.25 was subsequently used to construct the atlas. The diffusion ODFs of the 488 individuals were averaged in the MNI space to obtain the population averaged diffusion ODF atlas that allows for fiber tracking.

7.4.4 Fiber Tracking and Analysis

All fiber tracking was performed with DSI-Studio (http://dsi-studio.labsolver.org). Tracts were constructed using a quantitative anisotropy (QA)-based generalised deterministic tracking algorithm.[28, 29] Fiber tracking was initiated from the selected regions of interest (ROIs) using all orientations present within a voxel until 1,000-10,000 streamlines were detected. ROIs were placed on the generalised fractional anisotropy map at the area of the CN that could best be identified[12-15, 17, 18, 36-38] or the area that the CN was found to run through[1, 10, 39-45] (Figure 1A, 2A, 2B, 3A, 3B, 4A, 5A, 6A, 6B, 7A, 8, Table 1). Fiber progression continued with a step size of 1.2 mm, a minimum fiber length of 2 to 20 mm, and a turning angle threshold of 60° to 70°. To smooth each tract, the next directional estimate of each voxel was weighted by 20% of the previous moving direction and by 80% of the incoming direction of the fiber. Tracking terminated when the relative QA for the incoming direction dropped below a preset threshold (0.02-0.50, depending on the subject) or exceeded a turning angle of 60° to 70°. All fibers that did not correspond to the CNs were manually deleted (Figure 4B, C).

Validation of fiber tracts was done by comparison with the previously identified nerves on the anatomical images over which reconstructed tracts were displayed (magnetization-prepared rapid gradient-echo imaging sequence). As for the nerves

that were difficult to identify on anatomical images, e.g. the trochlear nerve, optic radiations, medial longitudinal fasciculus, and spinal trigeminal nucleus/tract, we compared the tracts with known anatomical locations and pathways[39, 40, 42-44, 46] in order to validate our results.

Fiber tracking and validation was performed by a neurosurgeon (M.Y.) who had been engaged in fiber tracking analysis for four years. To address the issue of result reproducibility and inter-rater reliability, we tasked two co-authors (S.P. and D.F.C.) with reproducing the CN fiber tracts using the ROI placement guide outlined by the lead author (M.Y.). Both were medically trained research fellows, with one having 2 months of experience with HDFT/DSI studio (S.P.) and the other (D.F.C.) with 5 months of experience with the software and fiber tracking method. Fiber tracking was performed using the same tracking parameters as outlined in the methods section on 3 or 5 randomly selected normal subjects from the cohort used by the lead author, and additionally using the HCP 488 template.

7.5 Results

7.5.1 Cranial Nerves

The cisternal portion of all CNs, except for the trochlear nerve and lower CNs, were tracked bilaterally in all subjects.

Olfactory Nerve (CN I)

In all five healthy individuals, the olfactory tracts were successfully tracked (Figure 1B, C). The posterior division of the olfactory tract in medial and lateral olfactory striae could not be visualized.

Optic Nerve (CN II)

In all subjects, we were able to track the nasal and lateral portions of the optic nerve, optic chiasm, optic tracts, and the complete optic radiation including Meyer's loop, the central bundle, and the dorsal bundle (Figure 2C, D, E, F, G).

Oculomotor Nerve (CN III)

HDFT tracked CN III from the cavernous sinus to the brainstem in all subjects. For CN III, HDFT tracked both the cisternal and cavernous segments of the CN III and also the medial longitudinal fasciculus (MLF) (Figure 3C, D, E, F). Decussating fibers from the MLF to the contralateral abducens nucleus were not demonstrated in any subject.

Trochlear Nerve (CN IV)

We tracked CN IV from the ipsilateral inferior colliculus to the cavernous sinus in six of ten hemispheres (Figure 4C, D, E, F). Remarkably, we could observe the well-known crossing of CNs III and IV at the cavernous sinus – superior orbital fissure transition (Figure 4E, F).

Trigeminal Nerve (CN V)

The cisternal portion of CN V was tracked in all subjects (Figure 5B, C, D). However, the ophthalmic nerve was tracked in nine of ten hemispheres; the maxillary nerve was tracked in seven of ten hemispheres, and the mandibular nerve was tracked in six of ten hemispheres. HDFT also tracked the intra-brainstem portion of CN V in eight of ten hemispheres (Figure 5B, E, F). In six of eight hemispheres, tracking of the tract stopped at the pons. In two of eight hemispheres, fiber tracts descending in the brainstem were visualized. The location of these tracts were consistent with the spinal trigeminal nucleus/tract (Figure 5F).

Abducens Nerve (CN VI)

HDFT tracked the cisternal portion of CN VI in all subjects. The petroclival portion of CN VI was tracked in two of ten hemispheres (Figure 6C, D, E, F). The intra-brainstem portion of CN VI could not be tracked in any subject.

Facial-Vestibulocochlear Nerve complex (CN VII/VIII)

HDFT tracked the cisternal portion of the CN VII/VIII complex in all subjects (Figure 7B). Subsequently, we added an ROI adjacent to the facial colliculus in order to distinguish CN VII (Figure 7C). As a result, in nine of ten hemispheres, HDFT showed a distinct tract that passed through the anterior portion of the CN VII/VIII

complex. According to its location, this tract was considered to represent CN VII (Figure 7D, E, F, G).

Lower CNs (CN IX, X, XI, XII)

We obtained diffusion data for CNs IX and X in only two subjects, and for CNs XI and XII in one subject only. This was due to lack of ODF representation of the lower brainstem region. This was a consequence of the initial scanning procedure, as detailed in Methods section. Although distinguishing CN IX from CN X was difficult, HDFT also tracked CNs IX, X, XI, and XII in these two cases (Figure 8C, E, G, H, I).

7.5.2 HCP-488 "Template" Tractography Findings

HDFT using the 488-subject atlas produced similar results as for subject-specific tractography except for CNs I, V, VI, XI, and XII (Figure 9). For CNs I and VI, no diffusion signals were present at the olfactory tracts and prepontine cistern. Consequently these could not be tracked. Only the cisternal portion of CN V was tracked, while its divisions and the intra-brainstem portion could not be tracked. As the ODF atlas does not include data below the mid-portion of the medulla, we were unable to investigate lower CNs, XI and XII.

7.5.3 Reproducibility and Reliability (Table 2)

Fellow 1 (S.P.) was able to reproduce bilaterally CNs I, II, the optic radiations, III and the medial-longitudinal fasciculus (MLF), V and VII/VIII in all three selected normal subjects. CN VI was found bilaterally in one of three subjects. CN IV was found bilaterally in two of three subjects and unilaterally in one subject. Likewise, CN IX/X was reproduced bilaterally in two of three subjects and unilaterally in one subject. Fellow 1 was unable to reproduce any nerves lower than CN IX/X due to ODF mapping ending at the level of the medulla in all three subjects. On the HCP 488 template S.P. was able to reproduce bilaterally CNs II, the optic radiations, III and the MLF, IV, V, VII/VIII, IX/X using the ROIs described by the lead author.

D.F.C. was able to replicate bilaterally CNs I-XII in two of five real subjects; CNs I-XI in one subject; CNs I-X in two subjects. In the HCP 488 template, he was able to reproduce all CNs aside from CN VI and XII (Table2).

7.5.4 Illustrative Cases

Case 1

A 35-year-old woman with a known history of optic-hypothalamic glioma presented with worsening visual deterioration of the left visual field and associated cystic change in the lesion, as revealed by surveillance MRI imaging (Figure 10A, B). A decision was made to perform cyst fenestration and partial tumour debulking aimed towards optic pathway decompression and neuropathological reassessment. Two surgical approaches were considered: an endoscopic endonasal approach and a supraorbital approach. A pre-surgical HDFT study showed clear visualization of optic nerves, optic chiasm, and optic tracts with predominant inferior displacement of the optic apparatus, obvious infiltration and damage of the right optic nerve and lateral displacement of the left optic nerve (Figure 10C, D, E). These imaging findings were considered critical in choosing the supraorbital over endonasal approach, given the inferior displacement of the optic chiasm. All imaging findings were consistent with intraoperative findings (Figure 10E, F). Subtotal debulking and biopsy was successfully obtained with improved visual field examination on the left side.

Case 2

A 61-year-old woman with headache underwent an MRI which revealed a 2.5 x 3 cm petroclival meningioma compressing the midbrain and the upper pons. One year after initial diagnosis, follow-up imaging showed a slight increase in the tumour size, which prompted surgical intervention (Figure 11A, B). Both an extended middle fossa approach with anterior petrosectomy and an endoscopic endonasal approach were considered. We opted for an endoscopic endonasal transclival approach with transcavernous posterior clinoidectomy, as recently described.[47] Pre-operative HDFT

tracked CN III, IV, V, and VI on both affected and unaffected sides (Figure 11C). On the tumour side, CN III was severely displaced superiorly and medially, while CN VI was displaced inferiorly. The location of reconstructed nerves was consistent with the intraoperative findings (Figure 11D, E, F). Gross total resection was achieved. Postoperatively, the patient developed transient CN III and VI palsies, both of which had resolved by 3 months follow-up.

Case 3

A 39-year-old male patient presented with visual changes. On examination, he had obvious acromegalic features and a complete bitemporal hemianopsia (Figure 12A). MRI was compatible with a giant adenoma with large suprasellar extension and bilateral cavernous sinus invasion (Knosp grade 4) (Figure 12B). Preoperative HDFT showed severe displacement of the optic chiasm in superior and posterior directions (Figure 12C). Tracking of both the cisternal and cavernous segments of CN V bilaterally, demonstrated significant lateral displacement with no tumour encasement (Figure 12D). The right CN III was identified at the cisternal and cavernous segments, with lateral and superior displacement and no tumour encasement (Figure 12D). The left CN III was also identified at the cisternal and cavernous segments, but the tumour had extending lateral and superior to it, with complete encasement at the proximal cavernous sinus (Figure 12D, E). We could not reliably reconstruct CN IV or VI, probably due to their small caliber and the amount of cavernous sinus invasion. Intraoperative findings confirmed the location of the optic apparatus and cisternal portion of the left CN III as depicted by the HDFT (Figure 12E, F). Subtotal resection of the tumour was achieved with complete resection of the sellar and suprasellar portions, near-total resection of the right cavernous sinus component, and partial resection of the left cavernous sinus component (Figure 12G).

7.6 Discussion

In the present study, we demonstrated that HDFT was able to identify the cisternal portions of all CNs and additionally, the optic radiations, MLF, spinal trigeminal nucleus/tract, petroclival portion of CN VI, and part of the brainstem portion of CN

VII. Compared with the previous DTI studies,[14, 17, 36] HDFT identified the CNs and their course more precisely in their correct anatomical orientation (Table 3).

7.6.1 DTI versus HDFT (Table 3)

Only one previous report has described reconstruction of CN I.[36] In this study, a single-shot echo planar imaging sequence was optimized to reduce the susceptibility artifacts at the frontal base leading to reconstruction of CN I bilaterally in all five subjects. Although our results for CN I with the HDFT were comparable with the previously published report, our imaging sequence did not need any optimization for its visualization. For CN II, several studies about Meyer's loop have been reported,[14, 37, 38, 48-51] but there has only been one detailed analysis of the optic chiasm.[37] In this DTI-based fiber tracking study the optic chiasm was fully reconstructed in just one of six cases (16.7%) and partly reconstructed in four of six cases (66.7%). In our study, we were able to fully reconstruct the optic chiasm in both subject-specific investigation (all sides and subjects) and in the HCP 488 template. This result suggests that the HDFT can be used to reconstruct the crossing fibers of the optic chiasm more precisely than the DTI-based methods, which are unable to accurately track crossing fiber systems.[26, 27] Although reconstruction of Meyer's loop was challenging because of its pronounced curvature, recent advanced white matter techniques such as HDFT have successfully reconstructed Meyer's loop more precisely than the DTI-based methods.[51-54] Likewise, we were able to use HDFT to reconstruct the optic radiations more precisely than DTI-based reconstructions.

Two previous DTI-based studies have reported successful reconstruction of the cisternal portion of CN III,[14, 17] but no previous studies have reported reconstruction of the cisternal portion of CN IV. Reconstruction of CN IV was not possible in all subjects however, probably secondary to its small diameter. Similarly, a previous DTI-based study was able to reconstruct both only the cisternal portion of CN VI,[14] while in this study we were able to reconstruct both the cisternal and the petroclival portion of CN VI in some cases.

DTI-based methods are able to reconstruct branches of CN V arising from the Gasserian ganglion and its cisternal portion, but are unable to reconstruct its intra-brainstem portion.[13, 14] DTI with probabilistic tractography is able to reconstruct both

the branches and cisternal portion of CN V and also its intra-brainstem portion.[55] We were able to use HDFT to reconstruct both the cisternal and intra-brainstem portions of CN V in our subject-specific investigation. A plausible explanation is the potential ability of the HDFT to precisely differentiate the intra-brainstem portion of CN V from other crossing fibers within the brainstem such as, those belonging to the cerebellar peduncles.

Regarding CN VII/VIII, DTI has been applied to investigate both the normal CN VII/VIII complex,[12-14, 18] and pathologically-compressed CN VII.[12, 16, 56] According to these studies, the reconstruction ratio of the normal CN VII/VIII complex was increased to almost 100%. Currently however, there are no DTI-based methods that allow distinction of the CN VII specifically within the normal CN VII/VIII complex. As a result, it is impossible to judge whether reconstructed tracts represent the facial nerve, cochlear nerve, vestibular nerve, or noise. In this report, we showed that the HDFT was further able to distinguish CN VII specifically within the CN VII/VIII complex. This was due to addition of an ROI adjacent to the facial colliculus thereby generating a distinct tract.

There has only been one prior reported study using DTI to reconstruct the lower CNs.[14] According to this study, only the cisternal portion of CN X could be reconstructed using DTI. In our study, distinguishing CN IX from CN X was difficult, and thus, we considered CN IX and X as a CN IX/X complex. Furthermore, we were able to use the HDFT to reconstruct CN XI and CN XII. This is the first known instance of tractographic reconstruction of any of these CNs using a fiber tracking modality.

7.6.2 Differences between "subject-specific" tracking and "atlas-based" tracking

We used the HCP 488 atlas to compensate for the reliability and reproducibility issues found with subject-specific tractography applied to a small sample size. We confirmed the results of the subject-specific tractography except for CN I, V, VI, XI, and XII. It is likely that the incomplete tracking of CN I, V, and VI was due to the masks that were used to select the facial and ear regions and because of susceptibility artifact near these regions. These masks lead to removal of noise as well as the data

from the frontal base, middle fossa, and prepontine cistern. For CN XI and XII, the HCP 488 atlas did not include data under the mid-portion of the medulla, and thus failed to provide a sufficient ODF map to select seed or ROIs to initiate the fiber tracking.

7.6.3 Preoperative HDFT CN reconstruction

The main goal of our study was to demonstrate the accuracy of HDFT in tracking CNs in normal subjects. We illustrated the potential and feasibility of using HDFT in preoperative skull-base surgical planning. The translation of this imaging technique into routine clinical practice is still in its infancy. The interpretation of the derived data therefore, needs to be done with extreme caution and expert neuroanatomical knowledge. Limitations and potential artifacts associated with the technique can provide false and misleading information.

7.6.4 Limitations and Future Directions

Despite the advanced visualization of the intracranial portions of the CNs as demonstrated here, diffusion MRI suffers with prominent susceptibility artifact near the tissue interface. This makes mapping of the extracranial course (including the branches) of CNs challenging. These branches pass through the tissue interface at the skull base and currently there is no effective approach to resolve the artifact problem in diffusion MRI.

A significant concern with the HDFT and any other fiber tractography study is the reliability and reproducibility of results. Manual tractographic segmentation results are well known to rely on the user related settings for the reconstruction of fiber tracts including: the location and size of the ROIs; turning angle; anisotropy thresholds, and segmentation methods. Despite the reliability and reproducibility of our results, detailed neuroanatomical knowledge and diffusion software training is essential towards accurate reconstruction and interpretation of the data. Further optimization of the condition settings and automatization of fiber tractography are a focus of ongoing and future studies.

An important limitation in this study was the small sample of clinical cases. Of note however, our primary aim was to demonstrate the feasibility for clinical application of HDFT with respect to reconstruction of CNs in normal and pathological subjects. This will provide the impetus to stimulate further research in this field and thereby, lead to further evolution and integration of fiber tracking of CNs in the clinical setting. Further studies involving larger sample sizes are needed to evaluate the clinical usefulness of the proposed technique.

Finally, diffusion MRI can provide anisotropy and diffusivity measurements to characterise tissue integrity. Previous HDFT studies have shown that measuring quantitative anisotropy (QA) can be used to study axonal integrity values of fiber tracts.[25, 27, 57] This approach can potentially be utilized for quantitative assessment of CN integrity in patients and therefore warrants further investigation.

7.7 Conclusions

In the present study, we demonstrated that HDFT successfully identified the cisternal portion of most CNs in normal subjects. This approach provided a superior ability to solve complex fiber crossings and exhibits substantial improvement over DTI with respect to accurate depiction of the CNs. Preoperative HDFT for surgical planning for skull base lesions is a highly anticipated method for potentially predicting the location of the CNs displaced by tumour.

7.8 References

1. Sheth S, Branstetter BFt, Escott EJ. Appearance of normal cranial nerves on steady-state free precession MR images. *Radiographics.* Jul-Aug 2009;29(4):1045-1055.

2. Zhang Z, Meng Q, Chen Y, et al. 3-T imaging of the cranial nerves using three-dimensional reversed FISP with diffusion-weighted MR sequence. *J Magn Reson Imaging.* Mar 2008;27(3):454-458.

3. Linn J, Moriggl B, Schwarz F, et al. Cisternal segments of the glossopharyngeal, vagus, and accessory nerves: detailed magnetic resonance imaging-demonstrated anatomy and neurovascular relationships. *J Neurosurg.* May 2009;110(5):1026-1041.

4. Linn J, Peters F, Moriggl B, Naidich TP, Bruckmann H, Yousry I. The jugular foramen: imaging strategy and detailed anatomy at 3T. *AJNR Am J Neuroradiol.* Jan 2009;30(1):34-41.

5. Moon WJ, Roh HG, Chung EC. Detailed MR imaging anatomy of the cisternal segments of the glossopharyngeal, vagus, and spinal accessory nerves in the posterior fossa: the use of 3D balanced fast-field echo MR imaging. *AJNR Am J Neuroradiol.* Jun 2009;30(6):1116-1120.

6. Mikami T, Minamida Y, Yamaki T, Koyanagi I, Nonaka T, Houkin K. Cranial nerve assessment in posterior fossa tumours with fast imaging employing steady-state acquisition (FIESTA). *Neurosurg Rev.* Oct 2005;28(4):261-266.

7. Amemiya S, Aoki S, Ohtomo K. Cranial nerve assessment in cavernous sinus tumours with contrast-enhanced 3D fast-imaging employing steady-state acquisition MR imaging. *Neuroradiology.* Jul 2009;51(7):467-470.

8. Nakai T, Yamamoto H, Tanaka K, et al. Preoperative detection of the facial nerve by high-field magnetic resonance imaging in patients with vestibular schwannoma. *Neuroradiology.* May 2013;55(5):615-620.

9. Mitsuoka H, Tsunoda A, Okuda O, Sato K, Makita J. Delineation of small nerves and blood vessels with three-dimensional fast spin-echo MR imaging: comparison of presurgical and surgical findings in patients with hemifacial spasm. *AJNR Am J Neuroradiol.* Nov-Dec 1998;19(10):1823-1829.

10. Choi BS, Kim JH, Jung C, Hwang JM. High-resolution 3D MR imaging of the trochlear nerve. *AJNR Am J Neuroradiol.* Jun 2010;31(6):1076-1079.

11. Hong HS, Yi BH, Cha JG, et al. Enhancement pattern of the normal facial nerve at 3.0 T temporal MRI. *Br J Radiol.* Feb 2010;83(986):118-121.

12. Taoka T, Hirabayashi H, Nakagawa H, et al. Displacement of the facial nerve course by vestibular schwannoma: preoperative visualization using diffusion tensor tractography. *J Magn Reson Imaging.* Nov 2006;24(5):1005-1010.

13. Kabasawa H, Masutani Y, Aoki S, et al. 3T PROPELLER diffusion tensor fiber tractography: a feasibility study for cranial nerve fiber tracking. *Radiat Med.* Nov 2007;25(9):462-466.

14. Hodaie M, Quan J, Chen DQ. In vivo visualization of cranial nerve pathways in humans using diffusion-based tractography. *Neurosurgery.* Apr 2010;66(4):788-795; discussion 795-786.

15. Gerganov VM, Giordano M, Samii M, Samii A. Diffusion tensor imaging-based fiber tracking for prediction of the position of the facial nerve in relation to large vestibular schwannomas. *J Neurosurg.* Dec 2011;115(6):1087-1093.

16. Roundy N, Delashaw JB, Cetas JS. Preoperative identification of the facial nerve in patients with large cerebellopontine angle tumours using high-density diffusion tensor imaging: Clinical article. *J Neurosurg.* 2012;116(4):697-702.

17. Kwon HG, Kim MS, Kim SH, Jang SH. Neurological picture. Injury of the oculomotor nerve in a patient with traumatic brain injury: diffusion tensor tractography study. *J Neurol Neurosurg Psychiatry.* Oct 2013;84(10):1073-1074.

18. Yoshino M, Kin T, Ito A, et al. Diffusion tensor tractography of normal facial and vestibulocochlear nerves. *Int J Comput Assist Radiol Surg.* Nov 20 2014.

19. Mori S, van Zijl PC. Fiber tracking: principles and strategies - a technical review. *NMR Biomed.* Nov-Dec 2002;15(7-8):468-480.

20. Mukherjee P, Chung SW, Berman JI, Hess CP, Henry RG. Diffusion tensor MR imaging and fiber tractography: technical considerations. *AJNR Am J Neuroradiol.* May 2008;29(5):843-852.

21. Behrens TE, Woolrich MW, Jenkinson M, et al. Characterisation and propagation of uncertainty in diffusion-weighted MR imaging. *Magn Reson Med.* Nov 2003;50(5):1077-1088.

22. Jensen JH, Helpern JA, Ramani A, Lu H, Kaczynski K. Diffusional kurtosis imaging: the quantification of non-gaussian water diffusion by means of magnetic resonance imaging. *Magn Reson Med.* Jun 2005;53(6):1432-1440.

23. Tuch DS, Reese TG, Wiegell MR, Makris N, Belliveau JW, Wedeen VJ. High angular resolution diffusion imaging reveals intravoxel white matter fiber heterogeneity. *Magn Reson Med.* Oct 2002;48(4):577-582.

24. Wedeen VJ, Hagmann P, Tseng WY, Reese TG, Weisskoff RM. Mapping complex tissue architecture with diffusion spectrum magnetic resonance imaging. *Magn Reson Med.* Dec 2005;54(6):1377-1386.

25. Abhinav K, Yeh FC, Pathak S, et al. Advanced diffusion MRI fiber tracking in neurosurgical and neurodegenerative disorders and neuroanatomical studies: A review. *Biochimica et biophysica acta.* Aug 12 2014;1842(11):2286-2297.

26. Fernandez-Miranda JC, Pathak S, Engh J, et al. High-definition fiber tractography of the human brain: neuroanatomical validation and neurosurgical applications. *Neurosurgery.* Aug 2012;71(2):430-453.

27. Abhinav K, Pathak S, Richardson RM, et al. Application of high-definition fiber tractography in the management of supratentorial cavernous

malformations: a combined qualitative and quantitative approach. *Neurosurgery.* Jun 2014;74(6):668-681.

28. Yeh FC, Wedeen VJ, Tseng WY. Generalised q-sampling imaging. *IEEE Trans Med Imaging.* Sep 2010;29(9):1626-1635.

29. Yeh FC, Verstynen TD, Wang Y, Fernandez-Miranda JC, Tseng WY. Deterministic diffusion fiber tracking improved by quantitative anisotropy. *PLoS One.* 2013;8(11):e80713.

30. Wang Y, Fernandez-Miranda JC, Verstynen T, Pathak S, Schneider W, Yeh FC. Rethinking the role of the middle longitudinal fascicle in language and auditory pathways. *Cereb Cortex.* Oct 2013;23(10):2347-2356.

31. Jarbo K, Verstynen T, Schneider W. In vivo quantification of global connectivity in the human corpus callosum. *Neuroimage.* Feb 1 2012;59(3):1988-1996.

32. Greenberg AS, Verstynen T, Chiu YC, Yantis S, Schneider W, Behrmann M. Visuotopic cortical connectivity underlying attention revealed with white-matter tractography. *J Neurosci.* Feb 22 2012;32(8):2773-2782.

33. Verstynen TD, Badre D, Jarbo K, Schneider W. Microstructural organisational patterns in the human corticostriatal system. *J Neurophysiol.* Jun 2012;107(11):2984-2995.

34. Fernandez-Miranda JC, Wang Y, Pathak S, Stefaneau L, Verstynen T, Yeh FC. Asymmetry, connectivity, and segmentation of the arcuate fascicle in the human brain. *Brain structure & function.* Mar 17 2014.

35. Yeh FC, Tseng WY. NTU-90: a high angular resolution brain atlas constructed by q-space diffeomorphic reconstruction. *Neuroimage.* Sep 1 2011;58(1):91-99.

36. Skorpil M, Rolheiser T, Robertson H, Sundin A, Svenningsson P. Diffusion tensor fiber tractography of the olfactory tract. *Magn Reson Imaging.* Feb 2011;29(2):289-292.

37. Hofer S, Karaus A, Frahm J. Reconstruction and dissection of the entire human visual pathway using diffusion tensor MRI. *Frontiers in neuroanatomy.* 2010;4:15.

38. Benjamin CF, Singh JM, Prabhu SP, Warfield SK. Optimization of tractography of the optic radiations. *Human brain mapping.* Feb 2014;35(2):683-697.

39. Rhoton AL, Jr. The cerebellopontine angle and posterior fossa cranial nerves by the retrosigmoid approach. *Neurosurgery.* Sep 2000;47(3 Suppl):S93-129.

40. Haines DE. *Neuroanatomy: An atlas of structures, sections, and systems.* Vol 153: Lippincott Williams & Wilkins; 2004.

41. Bae YJ, Kim JH, Choi BS, Jung C, Kim E. Brainstem pathways for horizontal eye movement: pathologic correlation with MR imaging. *Radiographics.* Jan-Feb 2013;33(1):47-59.

42. Rhoton AL, Jr. Tentorial incisura. *Neurosurgery.* Sep 2000;47(3 Suppl):S131-153.

43. Rhoton AL, Jr. The sellar region. *Neurosurgery.* Oct 2002;51(4 Suppl):S335-374.

44. Rhoton AL, Jr. The cavernous sinus, the cavernous venous plexus, and the carotid collar. *Neurosurgery.* Oct 2002;51(4 Suppl):S375-410.

45. Yagmurlu K, Rhoton AL, Jr., Tanriover N, Bennett JA. Three-dimensional microsurgical anatomy and the safe entry zones of the brainstem. *Neurosurgery.* Dec 2014;10 Suppl 4:602-620.

46. Rubino PA, Rhoton AL, Jr., Tong X, Oliveira E. Three-dimensional relationships of the optic radiation. *Neurosurgery.* Oct 2005;57(4 Suppl):219-227; discussion 219-227.

47. Fernandez-Miranda JC, Gardner PA, Rastelli MM, Jr., et al. Endoscopic endonasal transcavernous posterior clinoidectomy with interdural pituitary transposition. *J Neurosurg.* Jul 2014;121(1):91-99.

48. Wu W, Rigolo L, O'Donnell LJ, Norton I, Shriver S, Golby AJ. Visual pathway study using in vivo diffusion tensor imaging tractography to complement classic anatomy. *Neurosurgery.* Mar 2012;70(1 Suppl Operative):145-156; discussion 156.

49. Kamada K, Todo T, Morita A, et al. Functional monitoring for visual pathway using real-time visual evoked potentials and optic-radiation tractography. *Neurosurgery.* 2005;57(1):121.

50. Staempfli P, Rienmueller A, Reischauer C, Valavanis A, Boesiger P, Kollias S. Reconstruction of the human visual system based on DTI fiber tracking. *J Magn Reson Imaging.* Oct 2007;26(4):886-893.

51. Lilja Y, Ljungberg M, Starck G, Malmgren K, Rydenhag B, Nilsson DT. Visualizing Meyer's loop: A comparison of deterministic and probabilistic tractography. *Epilepsy research.* Mar 2014;108(3):481-490.

52. Ehricke HH, Otto KM, Klose U. Regularization of bending and crossing white matter fibers in MRI Q-ball fields. *Magn Reson Imaging.* Sep 2011;29(7):916-926.

53. Kuhnt D, Bauer MH, Sommer J, Merhof D, Nimsky C. Optic radiation fiber tractography in glioma patients based on high angular resolution diffusion imaging with compressed sensing compared with diffusion tensor imaging - initial experience. *PLoS One.* 2013;8(7):e70973.

54. Tax CM, Duits R, Vilanova A, et al. Evaluating contextual processing in diffusion MRI: application to optic radiation reconstruction for epilepsy surgery. *PLoS One.* 2014;9(7):e101524.

55. Upadhyay J, Knudsen J, Anderson J, Becerra L, Borsook D. Noninvasive mapping of human trigeminal brainstem pathways. *Magn Reson Med.* Nov 2008;60(5):1037-1046.

56. Chen DQ, Quan J, Guha A, Tymianski M, Mikulis D, Hodaie M. Three-dimensional in vivo modeling of vestibular schwannomas and surrounding cranial nerves with diffusion imaging tractography. *Neurosurgery.* Apr 2011;68(4):1077-1083.

57. Zhang H, Wang Y, Lu T, et al. Differences between generalised q-sampling imaging and diffusion tensor imaging in the preoperative visualization of the nerve fiber tracts within peritumoral oedema in brain. *Neurosurgery.* 2013;73(6):1044-1053.

7.9.1 Figures

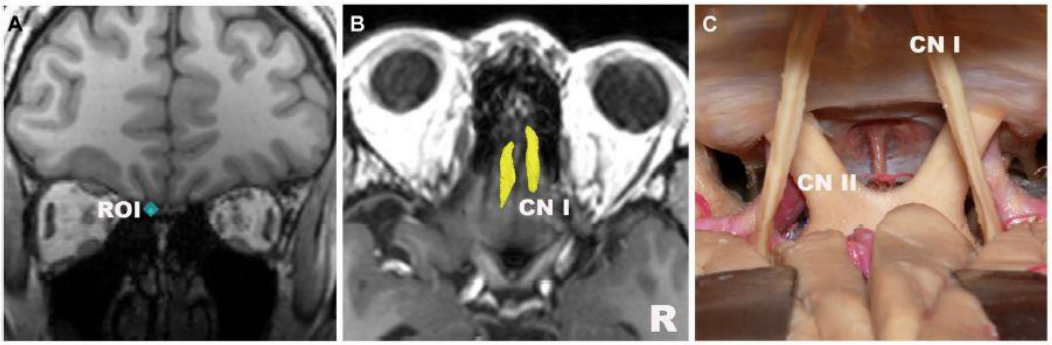

FIGURE 1. Olfactory Nerve **A, a** region of interest (ROI) is placed in the olfactory tract on the coronal section. **B,** high-definition fiber tractography of the olfactory nerve. **C,** anatomical dissection to correlate with B; superior view [R: right].

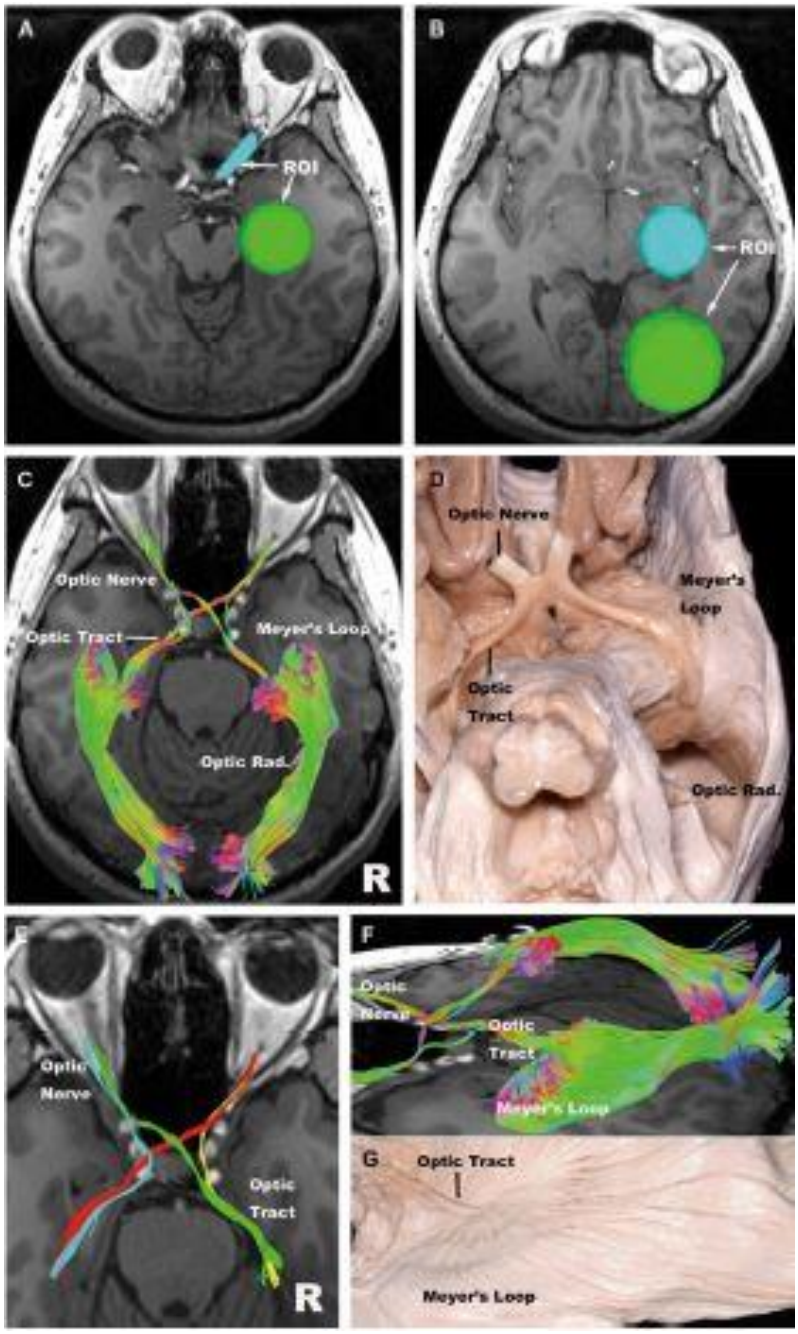

FIGURE 2. Optic Nerve **A,** regions of interest (ROIs) for the optic nerve; one is placed at the optic nerve and the other placed in the lateral geniculate body. **B,** ROI's for the optic radiation, one placed in the lateral geniculate body and another placed within the occipital lobe. **C,** high-definition fiber tractography (HDFT) of the visual pathways. In all subjects, we were able to reconstruct the nasal portion of the optic nerve, lateral portion of the optic nerve, optic chiasm, optic tracts, and the complete optic radiation including Meyer's loop, the central bundle, and the dorsal bundle. **D,** anatomical dissection to correlate with C; inferior view. **E,** close-up view of optic chiasm. Blue and yellow tracts represent the lateral portion of the optic nerve. Green

and red tracts represent the nasal portion of the optic tracts. The lateral portion of the optic nerve was reconstructed by combining an ROI in the optic nerve and a ROI in the same side of the lateral geniculate body. The nasal portion of the optic nerve was reconstructed by combining a ROI in the optic nerve and a ROI in the opposite side of the lateral geniculate body. **F,** close view of the optic radiation. **G,** anatomical dissection to correlate with F; lateral view [R: right].

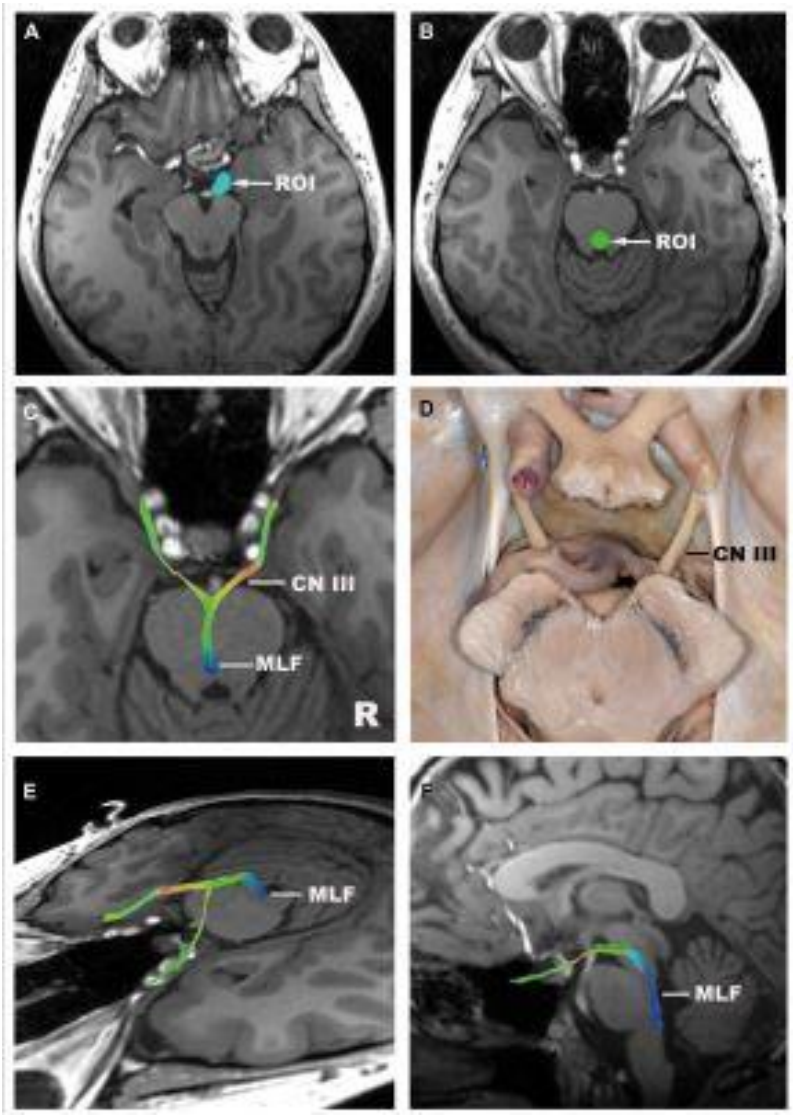

FIGURE 3 Oculomotor Nerve. **A,B,** regions of interest (ROIs) for the oculomotor nerve (CN III), one is placed at the cisternal portion of the oculomotor nerve (A), the other is placed in front of the fourth ventricle at the level of the upper pons (B). **C,** high-definition fiber tractography (HDFT) of CN III. Axial view. Fiber tracts enter from the interpeduncular cistern into the brainstem and then descend near the midline of the brainstem. **D,** anatomical dissection to correlate with C; superior view. **E,** HDFT of CN III. Oblique view. **F,** HDFT of CN III. Sagittal view [MLF: medial longitudinal fasciculus; R: right].

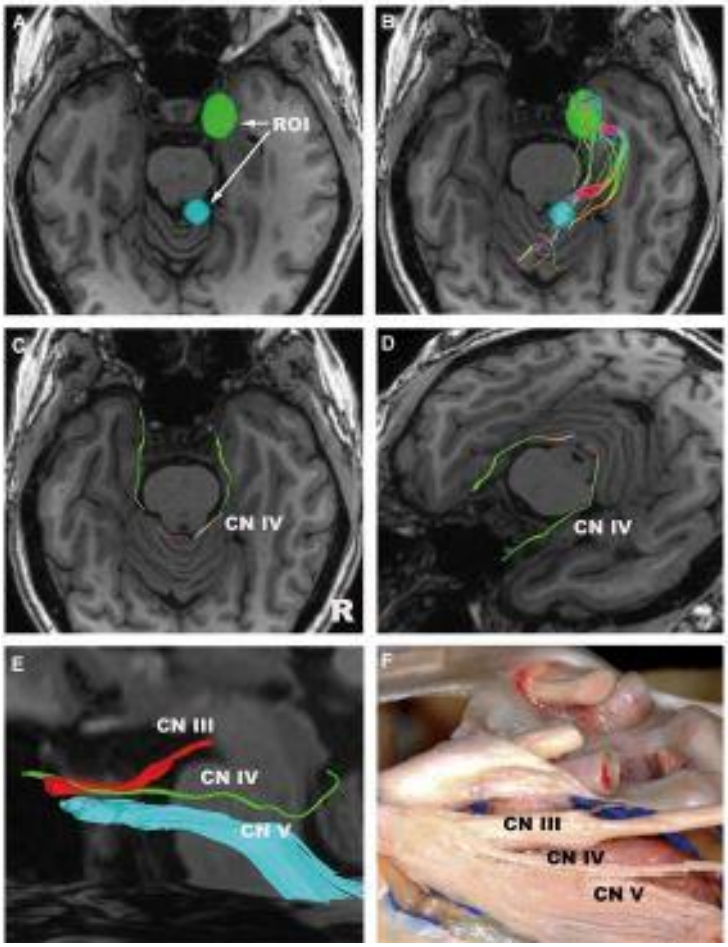

FIGURE 4. Trochlear Nerve. **A,** regions of interest (ROIs) for the trochlear nerve (CN IV), one is placed adjacent to the inferior colliculus, and the other is placed at the cavernous sinus. **B,** high-definition fiber tractography (HDFT) of CN IV. Pre-segmentation. Axial view. **C,** HDFT of CN IV. After segmentation. Axial view. **D,** HDFT of CN IV. After segmentation. Oblique view. **E,** close-up and lateral view of HDFT of the oculomotor (CN III), trochlear, and trigeminal (CN V) nerves. We could observe the well-known crossing of CNs III and IV at the cavernous sinus. **F,** anatomical dissection to correlate with E [R: right].

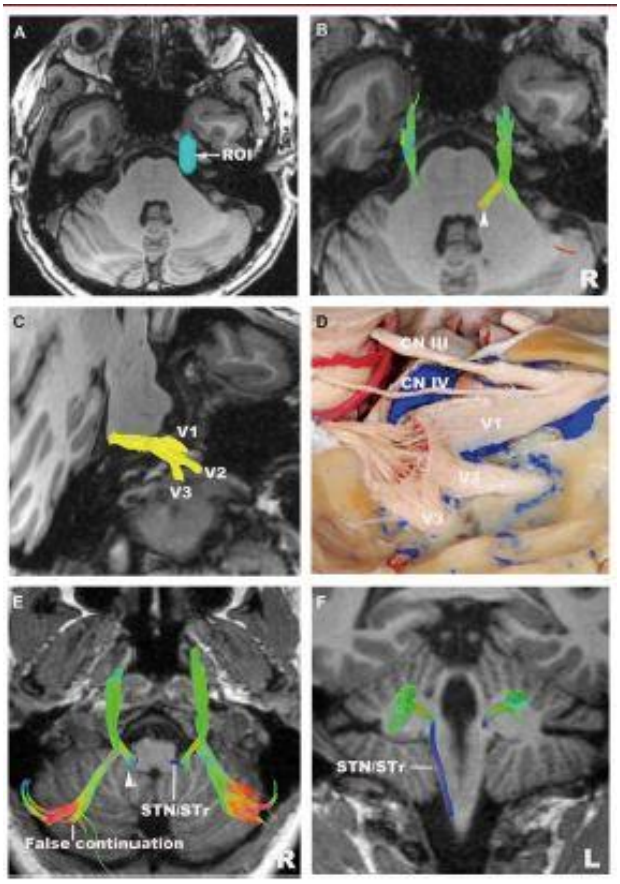

FIGURE 5. Trigeminal Nerve. **A,** region of interest (ROI) for the trigeminal nerve (CN V). A ROI is placed at the cisternal portion of CN V. **B,** high-definition fiber tractography (HDFT) of CN V. Reconstruction of CN V stopped at the pons (arrowhead). Whether these fibers went through the motor nucleus of CN V, the spinal nucleus of CN V, or the main sensory nucleus of CN V was difficult to ascertain, because these nuclei are anatomically very close to each other. **C,** HDFT of CN V, oblique view. The ophthalmic nerve (V1), the maxillary nerve (V2), and the mandibular nerve (V3) were reconstructed. V1 was reconstructed in nine out of 10 hemispheres, V2 was reconstructed in seven out of 10 hemispheres, and V3 was reconstructed in six out of 10 hemispheres **D,** anatomical dissection to correlate with C; lateral view. **E (axial), F (coronal),** HDFT of CN V (other case). Reconstruction of the left CN V stopped at the pons (arrowhead). Reconstruction of the right CN V descended in the brainstem. HDFT also reconstructed fibers into the cerebellum. However, these fibers did not correspond to normal structures, and thus, these fibers into the cerebellum were considered to be false continuations into the middle cerebellar peduncle [STN: spinal trigeminal nucleus, STr: spinal trigeminal tract, R: right, L: left].

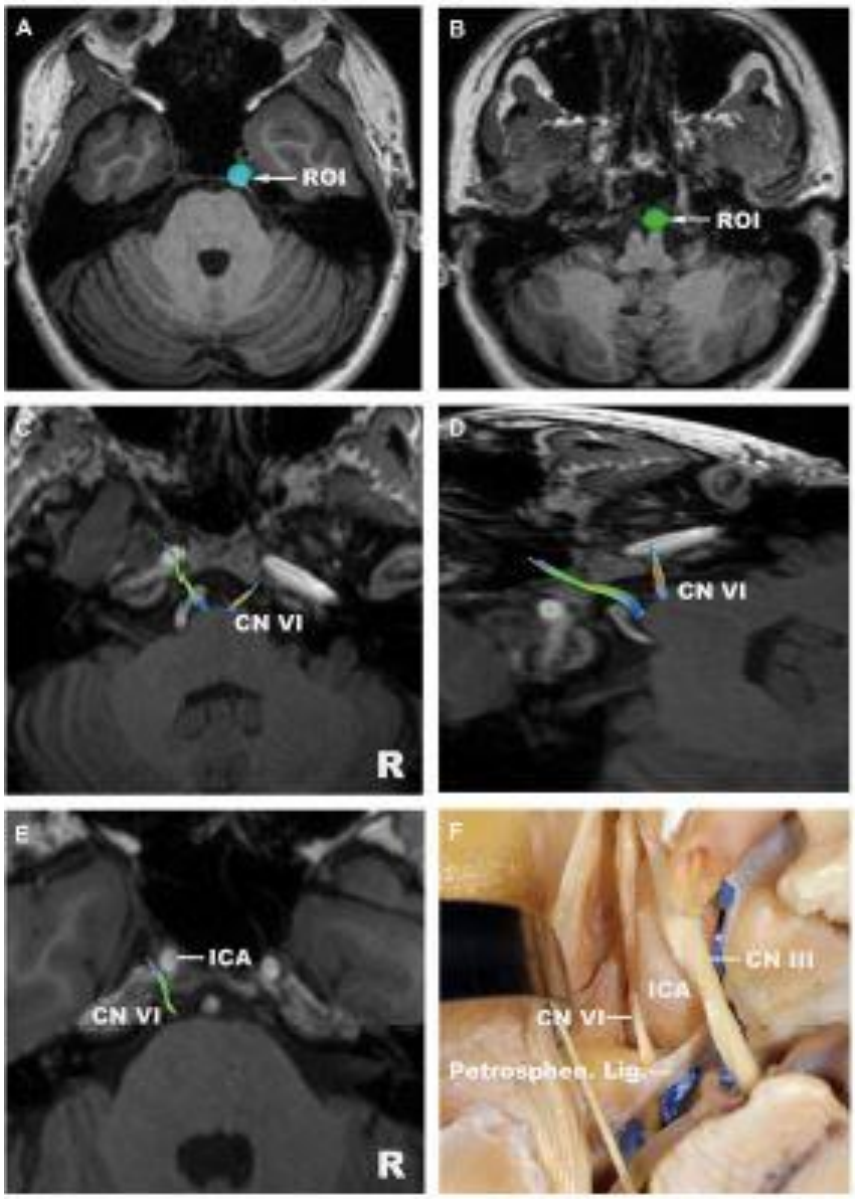

FIGURE 6. Abducens Nerve. **A,B,** regions of interest (ROIs) for the abducens nerve (CN VI). One is placed at the entrance of Dorello's canal (A), the other is placed at adjacent to the pontomedullary sulcus (B). **C,** high-definition fiber tractography (HDFT) of CN VI. Axial view. **D,** HDFT of CN V. Oblique view. **E,** close-up view of HDFT. The petroclival portion of CN VI was reconstructed in two out of 10 hemispheres. **F,** anatomical dissection to correlate with E; superior view [ICA: internal carotid artery, Petrosphen. Lig.: petrosphenoid ligament, R: right].

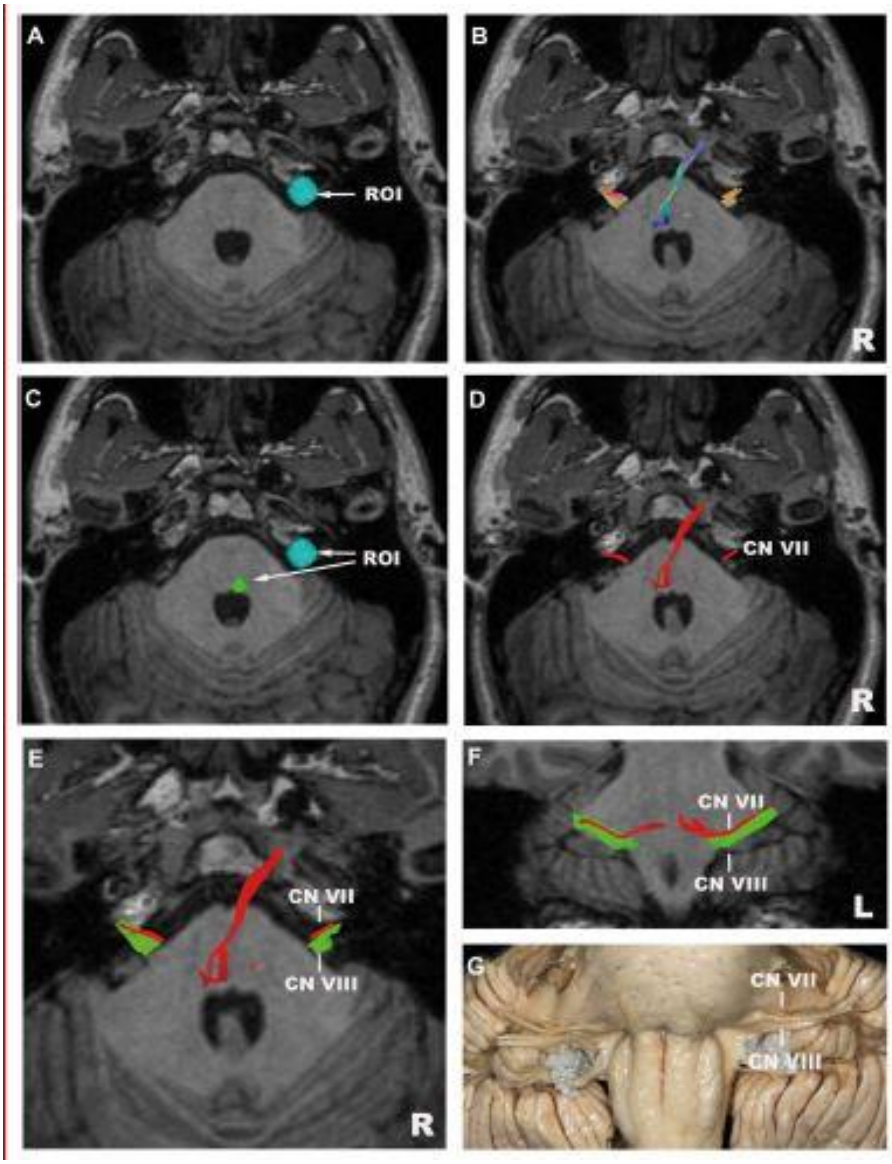

FIGURE 7. Facial-vestibulocochlear Nerve**. A,** region of interest (ROI) for the facial-vestibulocochlear nerve (CN VII/VIII) complex. One ROI is placed at the internal auditory meatus with the central focus on the porus of the internal auditory meatus. **B,** high-definition fiber tractography (HDFT) of CN VII/VIII complex, axial view. HDFT reconstructed the cisternal portion of the CN VII/VIII complex in all subjects. HDFT also demonstrated fibers above the pons. However, these tracts did not correspond to normal structures, and thus, these fibers above the pons were considered to be false continuations. **C,** ROI for the facial nerve (CN VII). One ROI is added adjacent to the facial colliculus. **D,** HDFT of CN VII, axial view. **E,** HDFT of CN VII and CN VIII, axial view. The red tract represents CN VII, and the green tract represents CN VIII. **F,** HDFT of CN VII and CN VIII, coronal view. **G,** anatomical dissection to correlate with F; frontal view **[**R: right, L: left].

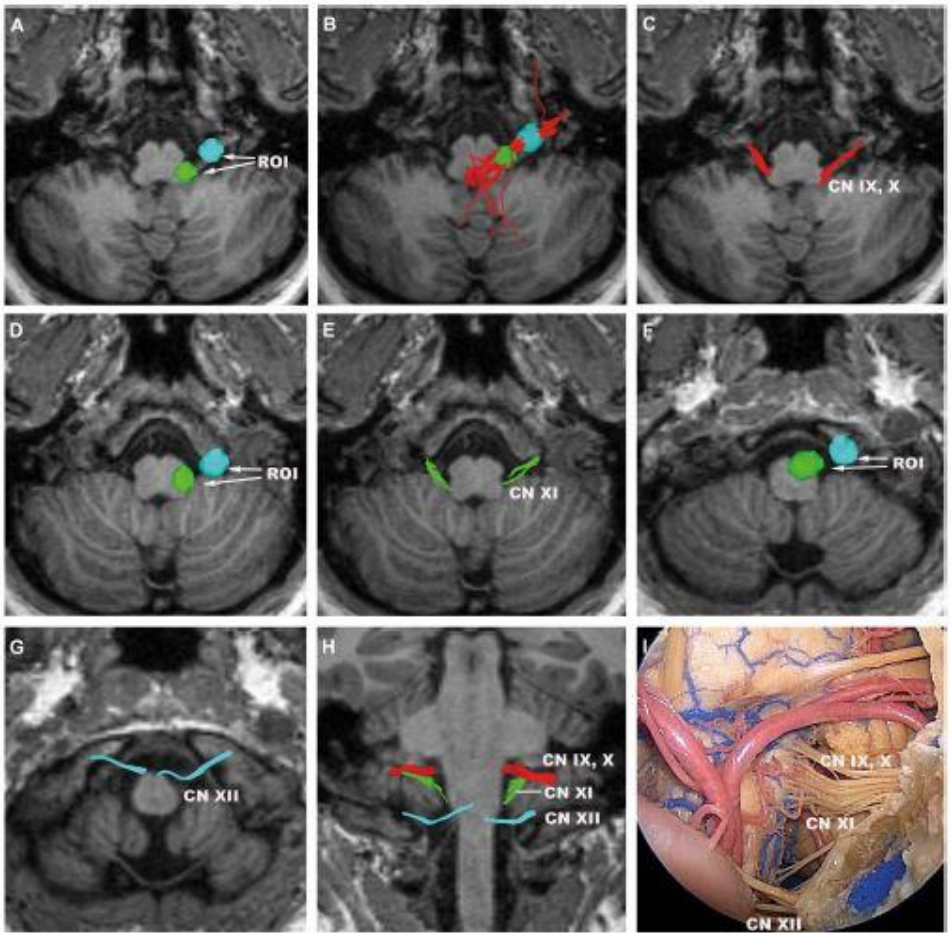

FIGURE 8. Lower Cranial nerves. **A,** regions of interest (ROIs) for the glossopharyngeal (CN IX), vagus (CN X) nerves. One ROI is placed at the jugular foramen and the other is placed adjacent to the superior one-third of the post-olivary sulcus. **B,** high-definition fiber tractography (HDFT) of CN IX, X. Pre-segmentation. Axial view. **C,** HDFT of CN IX, X. After segmentation. Axial view. **D,** ROIs for the accessory nerve (CN XI). One ROI is placed at the jugular foramen and the other is placed adjacent to the inferior two-thirds of the post-olivary sulcus. **E,** HDFT of CN XI, axial view. **F,** ROIs for the hypoglossal nerve (CN XII). One ROI is placed at the hypoglossal canal and the other is placed at the inferior two-thirds of the pre-olivary sulcus. **G,** HDFT of CN XII, axial view. **H,** HDFT of CN IX, X, XI, and XII. Coronal view. **I,** anatomical dissection to correlate with H; frontal view.

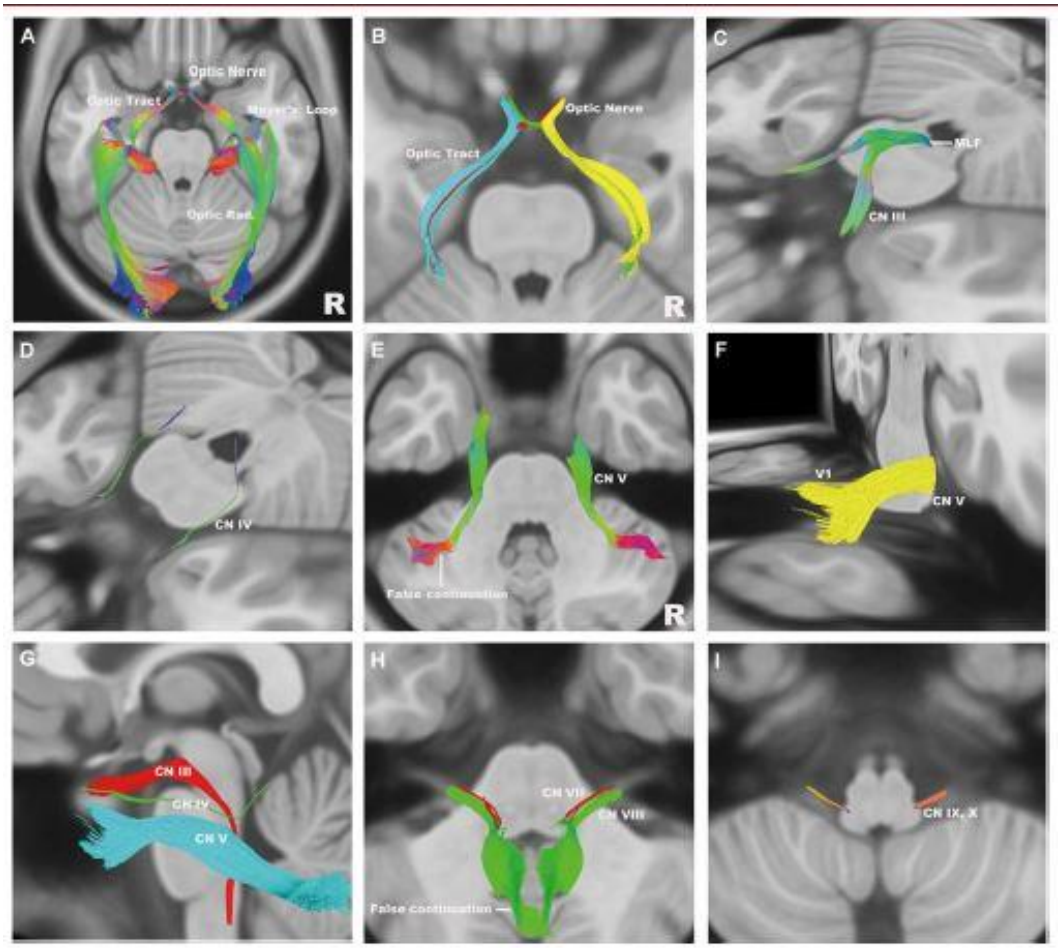

FIGURE 9. High-definition fiber tractography (HDFT) using HCP-488 "Template". **A,** HDFT of the visual pathways, axial view. **B,** close-up view of HDFT of optic chiasm, axial view. Blue and yellow tracts represent the lateral portion of the optic nerve. Green and red tracts represent the nasal portion of the optic tracts. **C,** HDFT of the oculomotor nerve (CN III), oblique view. **D,** HDFT of the trochlear nerve (CN IV), oblique view. **E,** HDFT of the trigeminal nerve (CN V), axial view. The intra-brainstem portion of CN V was not reconstructed. **F,** HDFT of CN V, oblique view. The branches of CN V were reconstructed incompletely. **G,** close-up and lateral view of HDFT of CN III, CN IV, and CN V **H,** HDFT of the facial nerve (CN VII), axial view. **I,** HDFT of the facial and vestibulocochlear nerve (CN VII/VIII). **J,** HDFT of the he glossopharyngeal (CN IX), vagus (CN X) nerves [R: right].

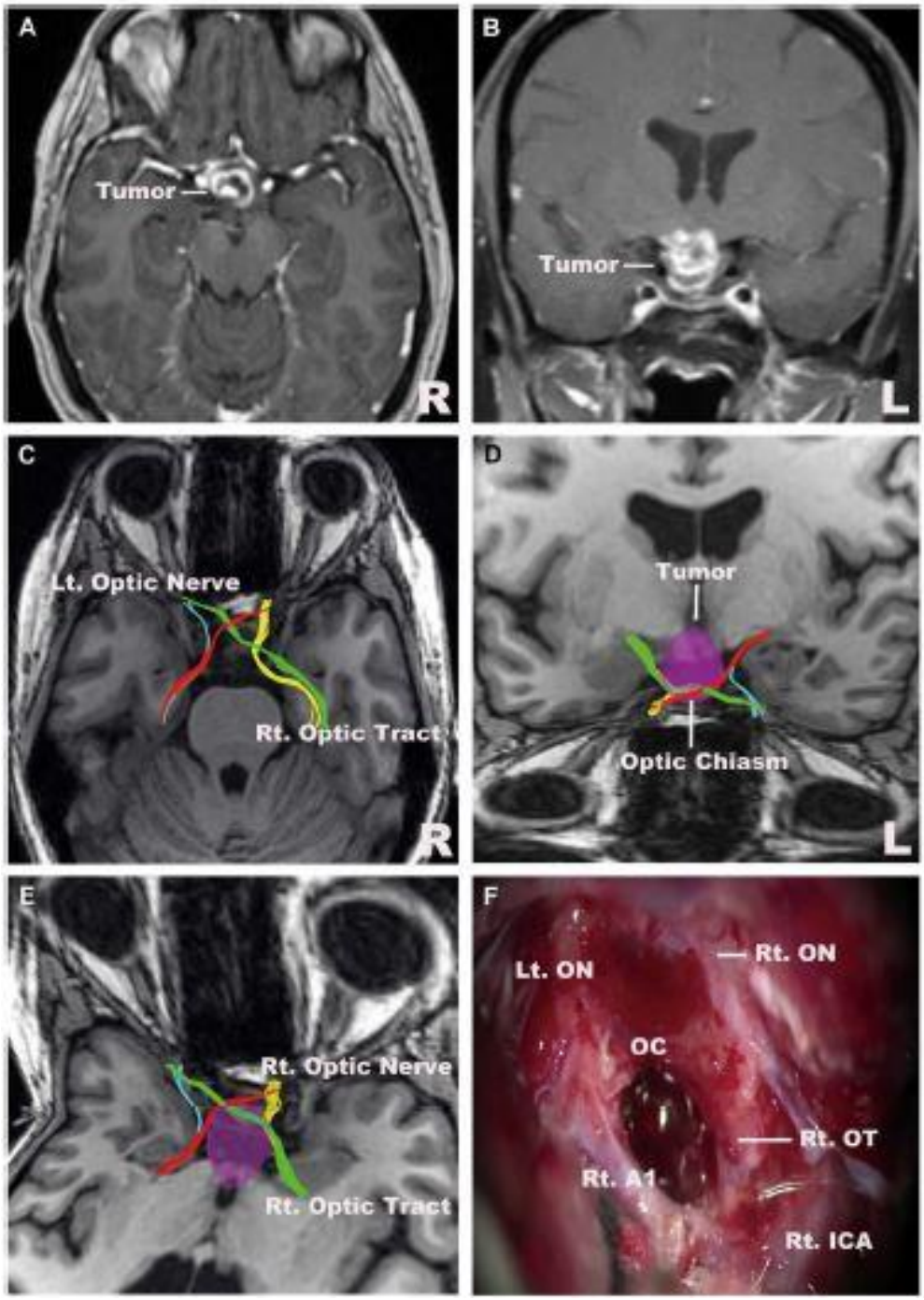

FIGURE 10. Illustrative case 1. Hypothalamic glioma. **A (axial), B (coronal),** structural MRI. **C,** high-definition fiber tractography (HDFT) of the optic nerve, chiasm, and tract. **D, E,** HDFT shows clear relationship between optic chiasm and tumour. D; frontal view. E; simulation view of the right supraorbital approach. **F,** intraoperative picture. The locations of reconstructed nerves were consistent with intraoperative findings [OC: optic chiasm, ON: optic nerve, OT: optic tract, ICA: internal carotid artery, A1: horizontal portion of the anterior cerebral artery, R: right, L: left].

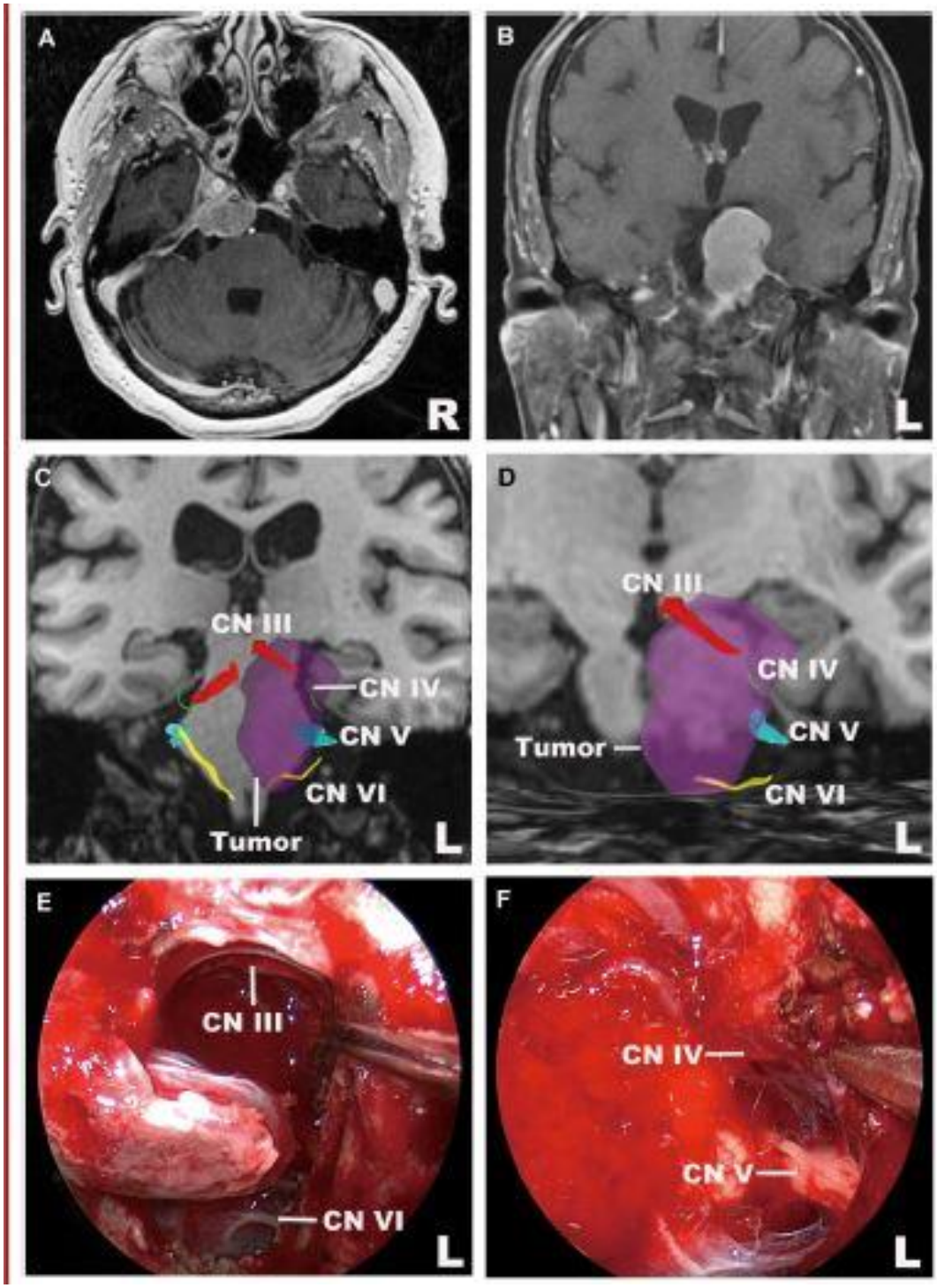

FIGURE 11. Illustrative case 2. Petroclival meningioma. **A (axial), B (coronal),** structural MRI images. A; axial view. B; coronal view. **C,** high-definition fiber tractography (HDFT) of the oculomotor nerve (CN III), trochlear nerve (CN IV), trigeminal nerve (CN V), and abducens nerve (CN VI). Coronal view. HDFT shows a clear relationship between CN's III – VI and the tumour. **D,** magnified views of left CN's III – VI. Coronal view. **E, F,** intraoperative pictures. The locations of reconstructed nerves were consistent with intraoperative findings [R: right, L: left].

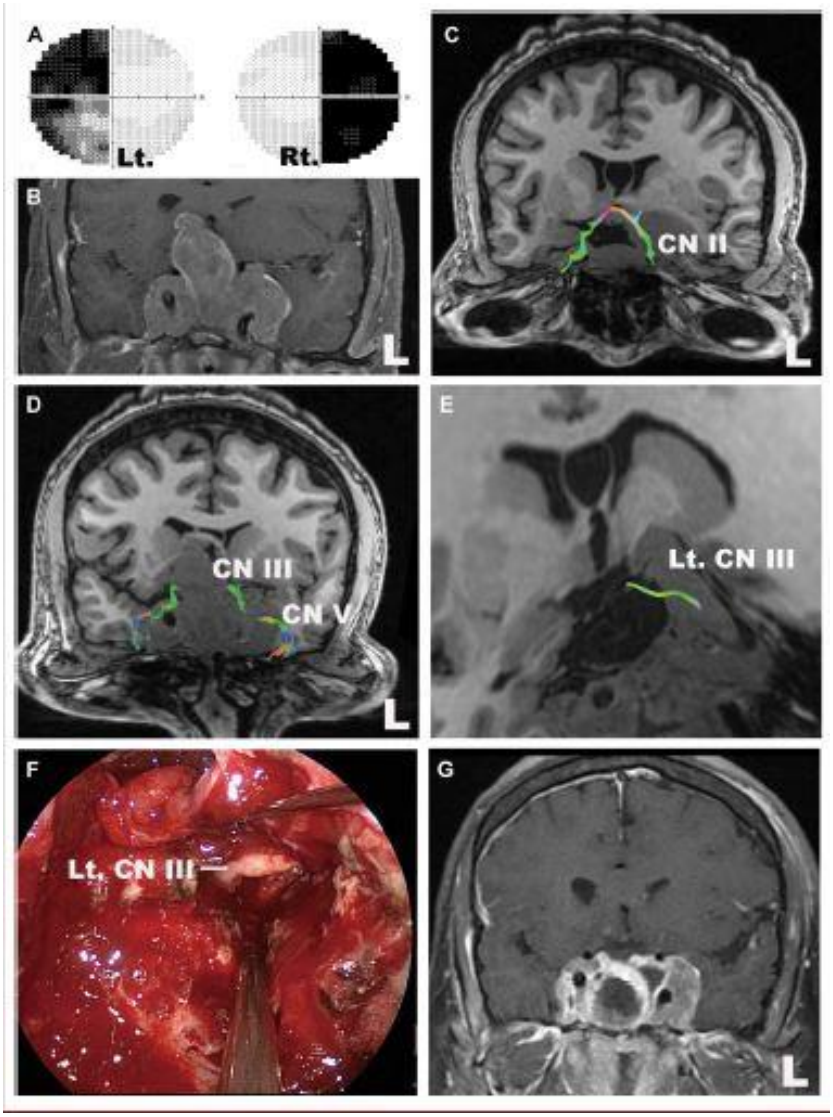

FIGURE 12. Illustrative case 3. Giant adenoma. **A,** visual field test showed a complete bitemporal hemianopsia. **B,** pre-operative structural magnetic resonance image. Coronal view. **C,** high-definition fiber tractography (HDFT) of the optic nerve (CN II) and chiasm. Coronal view. **D,** HDFT of the oculomotor nerve (CN III) and the trigeminal nerve (CN V). Coronal view. **E,** HDFT of left CN III. Oblique view. **F,** intraoperative picture. CN III is completely encased by tumour at the proximal cavernous sinus. The location of reconstructed CN III was consistent with intraoperative findings. **G,** post-operative structural magnetic resonance image. Coronal view [L: left].

7.9.2 Tables

TABLE 1: Definition of region of interest

Cranial Nerve	ROI
Olfactory nerve (CN I)	Similar to a previous report,[36] 1 ROI was placed in the olfactory tract on the coronal section (Figure 1A).
Optic nerve (CN II)	CN II was accomplished by combining an ROI in the optic nerve with an ROI in the lateral geniculate body (Figure 2A). Specifically, the lateral portion of the optic nerve was reconstructed by combining an ROI in the optic nerve and an ROI in the same side of the lateral geniculate body. The nasal portion of the optic nerve was reconstructed by combining an ROI in the optic nerve and an ROI in the opposite side of the lateral geniculate body. Fiber tracking of the optic radiation was accomplished by combining an ROI in the lateral geniculate body with an ROI in the occipital lobe adjacent to the visual cortex (Figure 2B).
Oculomotor nerve (CN III)	2 ROIs were placed on the axial section. One was placed at the cisternal portion of the oculomotor nerve (Figure 3A). The other was placed in front of the fourth ventricle at the level of the upper pons (Figure 3B) because CN III is connected to the medial longitudinal fasciculus.[17,41]
Trochlear nerve (CN IV)	2 ROIs were placed on the axial section. One was placed adjacent to the inferior colliculus, and the other was placed at the cavernous sinus (Figure 4A) because CN IV arises below the inferior colliculus and projects forward to the cavernous sinus.[42]
Trigeminal nerve (CN V)	Similar to previous reports,[14] 1 ROI was placed at the cisternal portion of the trigeminal nerve, and a target ROI was not used (Figure 5A).
Abducens nerve (CN VI)	We placed 1 ROI at the entrance of the Dorello canal and added an ROI adjacent to the pontomedullary sulcus (Figures 6A and 6B) because CN VI emerges from the pontomedullary sulcus, projects upward in the prepontine cistern, and enters the Dorello canal to enter the cavernous sinus.[43,44]
Facial-vestibulocochlear nerve complex (CN VII/VIII)	1 ROI was placed at the internal auditory meatus with the central focus on the porus of the internal auditory meatus (Figure 7A) because placing the ROI at the porus of the meatus improves the rate of successful reconstruction of the CN VII/VIII complex.[18] To distinguish CN VII, we added 1 ROI adjacent to the facial colliculus (Figure 7C) because the motor fibers of the facial nerve loop project posteriorly over the nucleus of CN VI and form the facial colliculus on the floor of the fourth ventricle.[45]
The glossopharyngeal (CN IX), vagus (CN X), accessory (CN XI), and hypoglossal nerve (CN XII)	To reconstruct CNs IX and X, we placed 1 ROI at the jugular foramen and the other adjacent to the superior one-third of the postolivary sulcus (Figure 8A) because CNs IX and X arise at the level of the superior one-third of the olive and reach the jugular foramen.[39] To reconstruct CN XI, we placed 1 ROI at the jugular foramen and the other adjacent to the inferior two-thirds of the postolivary sulcus (Figure 8D) because CN XI arises at the lower two-thirds of the olive and below and reaches the jugular foramen.[39] For CN XII, we placed 1 ROI at the hypoglossal canal and the other at the inferior two-thirds of the preolivary sulcus (Figure 8F) because CN XII arises along the anterior margin of the caudal two-thirds of the olive and reaches the hypoglossal canal.[39]

(CN: cranial nerve; ROI: region of interest)

TABLE 2: Reconstruction rate of cranial nerves performed by two fellows

Cranial Nerve	Fellow1		Fellow2	
	Normal subjects (%) N=6 sides	HCP 488 template (%)	Normal subjects (%) N=10 sides	HCP 488 template (%)
Olfactory Nerve (CN I)	100%	0%	100%	100%
Optic Radiation	100%	100%	100%	100%
Optic Nerve (CN II)	100%	100%	100%	100%
Oculomotor Nerve (CN III)	100%	100%	100%	100%
Medial-Longitudinal Fasciculus	100%	100%	100%	100%
Trochlear Nerve (CN IV)	83.3%	100%	100%	100%
Trigeminal Nerve (CN V)	100%	100%	100%	100%
Abducens Nerve (CN VI)	33.3%	0%	100%	0%
Facial-Vestibulocochlear Nerve complex(CN VII/VIII)	100%	100%	100%	100%
Glossopharyngeal and vagus Nerves (CN IX/X)	83.3%	100%	100%	100%
Accessory Nerve (CN XI)	0%	0%	60%	100%
Hypoglossal nerve (CN XII)	0%	0%	40%	0%

(CN: cranial nerve; HCP: human connectome project)

TABLE 3: Comparison with Diffusion Tensor Imaging

Cranial Nerve	Reconstructed Nerve (Reconstruction Rate)	
	HDFT	**Tractography With DTI**
Olfactory nerve (CN I)	Olfactory tract (100%), medial and lateral olfactory striae (0%)	Olfactory tract (100%), medial and lateral olfactory striae (0%)[36]
Optic nerve (CN II)	Nasal portion of the optic nerve (100%), lateral portion of the optic nerve (100%), optic chiasm (100%), optic tracts (100%), Meyer loop (100%), central bundle (100%), dorsal bundle (100%)	Nasal portion of the optic nerve (33.3%), lateral portion of the optic nerve (83.3%), optic chiasm (16.7%), optic tracts (100%), Meyer loop (50%), central bundle (66.7%), dorsal bundle (66.7%)[37]
Oculomotor nerve (CN III)	Cavernous portion of CN III (100%), cisternal portions of CN III (100%), MLF (100%)	Cavernous portion of CN III (63.6%), cisternal portions of CN III (63.6%), medial longitudinal fasciculus (63.6%)[14]
Trochlear nerve (CN IV)	Cavernous portion of CN IV (60%), cisternal portion of CN IV (60%), intrabrainstem portion of CN IV (60%)	No reconstruction
Trigeminal nerve (CN V)	Ophthalmic nerve (90%), maxillary nerve (70%), mandibular nerve (60%), cisternal portion of CN V (100%), intrabrainstem portion of CN V (80%)	Ophthalmic nerve (63.6%), maxillary nerve (63.6%), mandibular nerve (63.6%), cisternal portion of CN V (63.6%), intrabrainstem portion of CN V (0%)[14]
Abducens nerve (CN VI)	Petroclival portion of CN VI (20%), cisternal portion of CN VI (100%), intrabrainstem portion of CN IV (0%)	Petroclival portion of CN VI (0%), cisternal portion of CN VI (63.6%), intrabrainstem portion of CN IV (0%)[14]
Facial-vestibulocochlear nerve complex (CN VII/VIII)	Cisternal portion of CN VII/VIII (100%), intrabrainstem portion of CN VII/VIII (90%)	Cisternal portion of CN VII/VIII (63.6%), intrabrainstem portion of CN VII/VIII (0%)[14]
Glossopharyngeal and vagus nerves (CN IX/X)	Cisternal portion of CN IX/X (100%), intrabrainstem portion of CN IX/X (0%)	Cisternal portion of CN IX/X (63.6%), intrabrainstem portion of CN IX/X (0%)[14]
Accessory nerve (CN XI)	Cisternal portion of CN XI (100%), intrabrainstem portion of CN XI (0%)	No reconstruction
Hypoglossal nerve (CN XII)	Cisternal portion of CN XII (100%), intrabrainstem portion of CN XII (0%)	No reconstruction

(CN, cranial nerve; DTI, diffusion tensor imaging; HDFT, high-definition fiber tractography; MLF, medial longitudinal fasciculus)

Chapter 8: General limitations and future directions and conclusions

Limitations, future directions and conclusions have been discussed in the individual chapters (2-7) as pertinent to the specific research studies. In this chapter, the general overall limitations are presented in addition to a brief conclusion.

8.1 General limitations and future directions

All tractography-based techniques are susceptible to missing affected fiber tracts. This is related to the regions of interest (ROI) being chosen based on a known pathology or the location of a lesion. Diffusion connectometry, as discussed in Chapters 3 and 5, is a better approach in this respect, as no manual selection of ROIs is involved. Qualitative data from tractography-based studies with diffusion tensor imaging (DTI) or advanced white matter imaging techniques should be interpreted with a sound knowledge of the perilesional or loco-regional anatomy. In the setting of mass lesions, this problem is accentuated further as an abnormal trajectory of a fiber may be either technical in origin or be real. Good neuroanatomical knowledge therefore, may help with an accurate interpretation of the data. In order to reduce the subjectivity of the interpretation of qualitative data, particularly in the setting of mass lesions, the use of a combined qualitative and quantitative approach as demonstrated initially with the supratentorial (Chapter 2) cavernous malformations (CMs) is better. This approach can be adapted depending upon the relevant application and potentially provide information on the integrity of a fiber tract of interest with implications for prognostication and neurological recovery as demonstrated in the study on the deep seated CMs (Chapter 4). Of particular importance in longitudinal studies, is the variability in the quantitative parameters that can occur across scan sessions irrespective of the pathology. In order to ascertain this and also the normal range of differences in anisotropy values and/or volumes for tracts of interest that can exist between sides (left versus right) related to hemisphere dominance, one strategy is to scan several normal subjects on multiple occasions. Establishing these

parameters will assist with interpretation of the findings in both longitudinal studies and studies involving mass lesions in the brain.

Another issue pertains to the phantom studies. Recently solid fiber-based phantoms are being used to verify the issues concerning anisotropy and direction of the fibers. One solution involves building of a textile based *hollow fiber phantom,* which can potentially simulate restricted diffusion. Restricted water diffusion can quantify axonal bundle, which may therefore lead to a more robust quantitative metric reflecting changes in the morphology and integrity of the fibers.

One of the criticisms of the use of advanced imaging algorithms has been the long scanning time. Although this has not been prohibitive in our experience, it can cause difficulty in scanning patients with mass lesions, particularly those with altered mental status. One trend in diffusion field is to use fast scanning sequences at half their original length. This leads to a substantial reduction of scanning time to 10 to 15 minutes and improved patient comfort during clinical studies without compromising accuracy. It is noteworthy that experience with the advanced white matter imaging techniques is preliminary in research and clinical areas. Much of the experience has been acquired with DTI and with its applications in clinical research studies due to its wider availability. Even with conventional DTI, guidelines for its use in the clinical setting, for example in the resection of a neoplasm, are not completely clear. Use of the DTI is guided by its availability, institutional and surgeons' preference.

8.1.1 Quantitative indices with intracranial mass lesions

The anisotropy index, derived from the advanced white matter imaging technique, could be potentially affected by the susceptibility artifact due to the presence of blood products with mass lesions. This could give rise to *artifactual* disruption. With lack of histopathological data, using any quantitative index including fractional anisotropy, to support tract disruption may therefore be considered speculative. One solution is to undertake pre- and postoperative scans in patients. This will allow both qualitative and anisotropy data to be recorded and checked for consistency with the preoperative results after a potential lesionectomy. One will expect a potentially disrupted tract and its associated qualitative and quantitative characteristics (and

related deficits) to remain mostly unchanged after the lesionectomy. The reverse will be true for the displaced tracts. This has been explored in greater detail in Chapters 3 and 4 and particularly in Chapter 4 on the use of DTI in patients with deep seated CMs where in addition to the preoperative imaging, postoperative imaging was available in 50% of the patients.

A further limitation pertains to detecting minor degrees of change in the integrity of fiber tracts, where an overall or even a perilesional segment's anisotropy index in relation to the contralateral side may not be sensitive enough to provide the information. An 'automated' anisotropy profile, using multiple points in the perilesional and contralateral white matter tracts, will provide a better picture of the craniocaudal integrity of the tract. This approach may be useful towards prognostication. In view of the preliminary accuracy of cortical termination points from tractography, its correlation with the fMRI data and with results from the intraoperative white matter stimulation for cerebral lesions, is being examined. This may also assist with future anatomical studies. In these studies, integration of tractography with functional modalities like fMRI or magnetoencephalogram may allow a more reliable speculation regarding the role of a specific tract.

8.1.2 Neurodegenerative disorders

One current issue is to establish the normal variability in the quantitative parameters to allow meaningful interpretation of observed changes in these values across scan sessions in patients with neurological disorders like amyotrophic lateral sclerosis (ALS) or Huntington's disease (HD). A further issue pertains to the heterogeneity of the disease population, enrolled in the studies and its potential impact on the results. The control population are sex and age-matched to the patient population. It remains to be elucidated as to how the heterogeneity of both control and disease population may impact the variability in the measurement of the quantitative parameters. In the ALS study (Chapter 5), this was partially accounted for by enrolling patients with ALS, as defined according to the El-Escorial criteria before potentially focusing in the future on other phenotypes. In the group of patients with HD, the ongoing focus is on the early manifest and premanifest patients. Despite these measures, patients

with similar clinical disease burden or phenotype may have pathological heterogeneity making the data interpretation challenging.

8.1.3 Neuroanatomical studies

Well-established knowledge on white matter human neuroanatomy has largely relied upon the translational studies in monkeys' brains. Neuroanatomical studies, however using in-vivo tractography techniques, have revealed that there are multiple discrepancies between the microstructural connectivity features of human and animal brains. In fact, the precise structural connectivity of the brain remains largely unknown. Some of the endeavours in this direction as part of this thesis have been presented in the chapters 6 and 7. With the advancements in the white matter mapping techniques, one now has the opportunity to unravel many of the mysteries surrounding the structure and function of the human brain, as intended in the *Human Connectome Project*.

8.2 Conclusions

8.2.1 Specific conclusions

At a qualitative level, advanced white matter imaging techniques like HDFT can illustrate the precise spatial relationship of intracranial mass lesions like supra- and infratentorial CMs and high grade brain tumours to multiple perilesional tracts in a three dimensional fashion, thereby optimising surgical planning by minimising injury to these tracts. This was particularly relevant in patients with high grade brain tumours where using advanced white matter imaging technique, perilesional tracts were accurately depicted in the surrounding oedematous zone, an area susceptible to partial volume effects using DTI. Supratentorial CMs can displace and disrupt the perilesional white matter tracts with these changes being supported by the quantitative marker, quantitative anisotropy (QA). For the quantitative evaluation, mean QA values for the perilesional segments were used in a novel fashion with contralateral homologous tracts used for comparison leading to the recommendation

for using a combined qualitative and quantitative approach towards assessment of perilesional white matter tracts. Infratentorial or brainstem CMs can also disrupt and displace perilesional white matter tracts with the latter occurring in unpredictable directions. In a highly eloquent location such as, brainstem this requires the use of tractography to accurately define their orientation to optimise surgical entry point, minimise morbidity, and enhance neurological outcomes. Analogous to the supratentorial CMs, observed anisotropy decreases in the perilesional segments are consistent with neural injury or disruption following haemorrhagic insults as validated by postoperative imaging in a cohort of patients with brainstem CMs. Quantitative indices like QA or fractional anisotropy (FA) vales can be used for prognostication regarding neurological and functional outcomes for patients undergoing resection of brainstem CMs; for example, the higher FA value for the *distal ipsilateral* corticospinal tract (CST) was associated with better postoperative functional outcomes over the follow-up interval. Diffusion connectometry is a complementary automated approach overcoming some of the limitations associated with the conventional tractography approach and DTI and can be used to provide longitudinal information on the rostrocaudal involvement or integrity of the CST as in the study on brainstem CMs.

Combination of the connectometry approach with a more conventional tractography approach can used for devising imaging biomarkers in neurodegenerative disorders like ALS to identify the affected white matter tracts and track associated patterns of disease progression longitudinally with potential for correlation with clinical progression. Using this methodology, a number of changes bilaterally and asymmetrically in motoric and extramotoric white matter pathways could be demonstrated in patients with ALS, including progression in those with longitudinal data.

A sound neuroanatomical knowledge is a prerequisite for interpretation of data derived from advanced white matter imaging techniques. Use of these imaging techniques will also contribute to dedicate neuroanatomical studies, as demonstrated in our study on CNs, where we were able to identify all CNs in unprecedented detail. The localization of CNs will have implications for operative approach planning to complex skull base tumours or other pathologies distorting the normal course of these nerves.

8.2.2 Overall conclusion

The use of an advanced white matter imaging technique to obtain superior qualitative data in terms of accurate demonstration of multiple crossing fibers in a three dimensional manner around intracranial lesions is clearly useful in neurosurgery for decision making and surgical approach planning and in neuroanatomical studies for depicting course of white matter tracts and CNs in great detail. Quantitative indices can further characterise the change in the perilesional white matter tracts and assess potential injury with implications for prognostication in terms of long term postoperative neurological recovery and functional outcomes. Adaptation of the analytical approaches, for example the diffusion connectometry and its subsequent use in conjunction with the data from tractography, has enabled longitudinal studies in the neurodegenerative disorders, like ALS. These have provided us with preliminary, yet encouraging results which could also be potentially applied in patients with HD. Apart from ongoing technical advancements towards improvement of the advanced white matter imaging techniques and its ongoing use in neurosurgical, neuroanatomical and neurological disorders, future studies will need to be combined with functional imaging modalities.

Acknowledgements

I would like to express my deepest gratitude to the Ellison Cliffe travelling fellowship, Royal Society of Medicine; Fine foundation; Society of British Neurosurgeons and University of Pittsburgh Brain foundation for supporting me during my research time at the Skull Base and Fiber Tractography Laboratory, Centre for Cranial Base Surgery, Department of Neurological Surgery, University of Pittsburgh Medical Center (UPMC), University of Pittsburgh, Pittsburgh, USA where majority of the research work contributing to the thesis was carried out.

I would also like to express my sincerest gratitude to the following foundations and organisations for supporting the research work laid out in this thesis: Live Like Lou; The Copeland Fund of the Pittsburgh Foundation, University of Pittsburgh Brain Institute and the Fine Foundation.

This work was carried out in collaboration with a medical engineering scientist, Dr Fang-Cheng Yeh, Assistant Professor, University of Pittsburgh Medical Centre, Pittsburgh who is a co-author on several of the manuscripts and an on-going collaborator. I was also guided and mentored hugely by Dr Juan C Fernandez-Miranda, an excellent neuroanatomist and neurosurgeon who is the corresponding author on the publications. During the course of my study, he was an Assistant Professor at the UPMC Presbyterian, Pittsburgh. I also owe a debt of gratitude to Dr R Friedlander, Chairman, Department of Neurosurgery, UPMC, Pittsburgh and Dr Gary K Steinberg, Chairman, Department of Neurosurgery, Stanford University, Stanford for their guidance and assisting with data in patients, particularly those undergoing surgery for cavernous malformations. I am also thankful to Deepa Krishnaswamy and Emily Braun for helping with collection of imaging files. I am finally immensely thankful to my wife, Melanie and two children (Ava and Leon) who have tolerated my years of transatlantic adventure in my quest to improve as a scientist and as a neurosurgeon first over a two-year duration at the UPMC Presbyterian, University of Pittsburgh, Pittsburgh and then for another two years at the Department of Neurosurgery, Stanford University, Stanford; without their support this body of work would not be possible.

Appendix (PDF copies of published manuscripts relating to white matter imaging)

1. **Abhinav K**, Pathak S, Richardson RM, Engh J, Gardner P, Yeh FC, Friedlander RM, Fernandez-Miranda JC. Application of High Definition Fiber Tractography (HDFT) in Management of Supratentorial Cavernous malformations: a combined qualitative and quantitative approach. *Neurosurgery* 2014; **74(6):**668-81.
2. Faraji A*, **Abhinav K***, Jarbo K, Yeh FC, Shin SS, Pathak SK, Hirsch B, Schneider W, Fernandez-Miranda JC, Friedlander RM. Longitudinal evaluation of corticospinal tract in patients with resected brainstem cavernous malformations using high definition fiber tractography and diffusion connectometry analysis: preliminary experience. *Journal of Neurosurgery* 2015; **123(5):**1133-44. (*: equal contributors)
3. **Abhinav K**, Nielsen TH, Singh R, Weng Y, Han SS, Iv M, Steinberg GK. Utility of a quantitative approach using diffusion tensor imaging for prognostication regarding motor and functional outcomes in patients with surgically resected deep intracranial cavernous malformations. *Neurosurgery* 2019 July 30 [Epub ahead of print].
4. **Abhinav K**, Yeh FC, Mansouri A, Zadeh G, Fernandez-Miranda JC. High Definition Fiber Tractography for the evaluation of perilesional white matter tracts in high grade glioma surgery. *Neuro-Oncology* 2015; **17(9)**:1199-209.
5. **Abhinav K**, Yeh FC, El-Dokla A, Ferrando LM, Chang YF, Lacomis D, Friedlander RM, Fernandez-Miranda JC. Use of diffusion spectrum imaging in longitudinal evaluation of amyotrophic lateral sclerosis: development of an imaging biomarker. *Frontiers in Human Neuroscience* 2014; 29(**8):**270.
6. Yoshino M, **Abhinav K**, Yeh FC, Pathak S Gardner PA, Fernandez-Miranda JC. Visualization of cranial nerves using High-definition fiber tractography. *Neurosurgery* 2016; **79(1)**:146-65.
7. **Abhinav K**, Yeh FC, Pathak S, Suski V, Lacomis D, Friedlander RM, Fernandez-Miranda JC. Advanced diffusion MRI fiber tracking in neurosurgical and neurodegenerative disorders and neuroanatomical studies: A review. *BBA: Molecular Basis of Disease* 2014; **1842(11):**2286-97
8. Panesar S, **Abhinav K**, Yeh FC, Jacquesson T, Collins M, Fernandez-Miranda

JC. Tractography for surgical neuro-oncology planning: towards a gold standard. *Neurotherapeutics* 2019; **16(1):**36-51.